DEVELOPMENT OF CELLULOSE-REINFORCED ALGINATE MICROBEADS FOR OPTIMAL ENCAPSULATION AND DELIVERY OF PALM-BASED VITAMIN E

GOH KAR YIN

FACULTY OF SCIENCE
UNIVERSITI MALAYA
KUALA LUMPUR

2021

DEVELOPMENT OF CELLULOSE-REINFORCED ALGINATE MICROBEADS FOR OPTIMAL ENCAPSULATION AND DELIVERY OF PALM-BASED VITAMIN E

GOH KAR YIN

THESIS SUBMITTED IN FULFILMENT OF THE REQUIREMENTS FOR THE DEGREE OF DOCTOR OF PHILOSOPHY

DEPARTMENT OF CHEMISTRY
FACULTY OF SCIENCE
UNIVERSITI MALAYA
KUALA LUMPUR

2021

UNIVERSITI MALAYA

ORIGINAL LITERARY WORK DECLARATION

Name of Candidate: **GOH KAR YIN**

Matric No: **17042186/1**

Name of Degree: **DOCTOR OF PHILOSOPHY**

Title of Thesis ("this Work"):

DEVELOPMENT OF CELLULOSE-REINFORCED ALGINATE MICROBEADS FOR OPTIMAL ENCAPSULATION AND DELIVERY OF PALM-BASED VITAMIN E

Field of Study: **MATERIAL CHEMISTRY**

I do solemnly and sincerely declare that:

(1) I am the sole author/writer of this Work;
(2) This Work is original;
(3) Any use of any work in which copyright exists was done by way of fair dealing and for permitted purposes and any excerpt or extract from, or reference to or reproduction of any copyright work has been disclosed expressly and sufficiently and the title of the Work and its authorship have been acknowledged in this Work;
(4) I do not have any actual knowledge nor do I ought reasonably to know that the making of this work constitutes an infringement of any copyright work;
(5) I hereby assign all and every rights in the copyright to this Work to the University of Malaya ("UM"), who henceforth shall be owner of the copyright in this Work and that any reproduction or use in any form or by any means whatsoever is prohibited without the written consent of UM having been first had and obtained;
(6) I am fully aware that if in the course of making this Work I have infringed any copyright whether intentionally or otherwise, I may be subject to legal action or any other action as may be determined by UM.

Candidate's Signature Date: 18/8/2021

Subscribed and solemnly declared before,

Witness's Signature Date: 18/8/2021

Name:

Designation:

DEVELOPMENT OF CELLULOSE-REINFORCED ALGINATE MICROBEADS FOR OPTIMAL ENCAPSULATION AND DELIVERY OF PALM-BASED VITAMIN E

ABSTRACT

In this study, pH sensitive microfibrillated cellulose-reinforced alginate microbeads were synthesized for oral administration of vitamin E. Long and network-like hydrophilic microfibrillated celluloses with widths ranging from 8 to 40 nm, having −COOH functional groups were isolated from oil palm empty fruit bunches via ammonium persulfate (APS) oxidation. Cellulose derivatives, hydrophobic trimethylsilyl celluloses with the functional groups of $-Si(CH_3)_3$ were also produced via silylation. Palm-based vitamin E was loaded into the oil-in-water emulsions prior to the immobilization into calcium-crosslinked alginate microbeads. The vitamin E-loaded emulsions were first characterized and the influence of the emulsions' properties on the microbeads were evaluated. Two parameters were manipulated in the production of oil-in-water emulsions: type of cellulose and type of surface-active agents employed in the emulsion stabilization. Oil-in-water emulsions for loading vitamin E were produced using polyoxyethylene glycol sorbitan monooleate (Tween 80):polyoxyethylene lauryl ether (Brij® 35) or 1-butyl-3-methylimidazolium octyl sulfate as surface-active agents with the addition of various concentrations of celluloses (0.0, 0.0125, 0.025, 0.05, 0.1, 0.175, 0.25, 0.5 and 1.0 %w/v). Two distinct natures of celluloses were utilized in this study, which are hydrophilic APS-oxidized celluloses or hydrophobic trimethylsilyl celluloses. The emulsions were evaluated for the average droplet diameter, viscosity and rheological behaviors. Emulsions stabilized by Tween 80:Brij 35, using hydrophilic APS-oxidized celluloses as nanofillers were observed to exhibit the smallest average droplet sizes with moderate rheological properties. Whereas, emulsions stabilized by hydrophobic

trimethylsilyl cellulose, employing 1.5 % w/v Tween 80:Brij 35 (0.5:0.5 w/w ratio) as surface active agents exhibited nanometer scale droplet diameters with most remarkable rheological behaviors. In the contrary, the emulsions employing 1-butyl-3-methylimidazolium octyl sulfate as emulsifier showed micron range droplet sizes with poor rheological behavior regardless the concentration of APS-oxidized cellulose. Alginate microbeads were then fabricated by dripping vitamin E-loaded emulsions into crosslinking solution. Results showed that highest compressive strength of 58.8 kPa was obtained for microbeads containing Tween 80:Brij 35-stabilized emulsions with 0.25% w/v hydrophilic oxidized celluloses. This indicated that APS-oxidized celluloses participate in the formation of densely packed and three-dimensional matrix structures of microbeads by interacting with calcium ions via their -COO^- groups. Likewise, the highest encapsulation efficiency of 98.7% was also achieved by the 0.25% APS-oxidized cellulose reinforced alginate microbeads containing Tween 80:Brij 35-stabilized emulsion. In addition, the alginate/cellulose microbeads were more resistant against swelling in low pH condition because of the enhanced stability promoted by the bio-based celluloses. The microbeads showed slow release of vitamin E in the simulated gastric pH fluid but tend to release in the simulated intestinal pH fluid to allow the absorption of the drug. However, APS-oxidized cellulose-reinforced alginate microbeads containing 1-butyl-3-methylimidazolium octyl sulfate-stabilized emulsions exhibited lower encapsulation efficiency with unusual high *in vitro* release of vitamin E. *In vitro* drug release data of all the evaluated microbeads were fitted well into Ritger-Peppas model. ^{1}H NMR spectra showed that vitamin E retained its chemical structure after encapsulation into alginate-based microbeads.

Keywords: Alginate microbeads, Microfibrillated celluloses, Vitamin E, Emulsion

PERKEMBANGAN MANIK MIKRO ALGINAT YANG DIPERKUKUHKAN OLEH SELULOSA UNTUK OPTIMAL PENGKAPSULAN DAN PENGHANTARAN VITAMIN E YANG BERASASKAN DARIPADA KELAPA SAWIT

ABSTRAK

Dalam kajian ini, manik mikro alginat yang diperkukuh oleh selulosa mikrofibrilasi yang sensitif terhadap pH telah dihasilkan untuk pengkapsulan vitamin E dan diambil secara oral. Selulosa mikrofibrilasi hidrofilik dengan kumpulan −COOH yang panjang dan berangkai-rangkai dan mempunyai kelebaran antara 8 to 40 nm telah diekstrakan daripada tandan buah kosong kelapa sawit melalui pengoksidaan oleh amulium persulfat (APS). Selulosa trimetililil hidrofobik merupakan derivatif selulosa dengan kumpulan $-Si(CH_3)_3$ telah dihasilkan melalui silylation. Emulsi yang mengandungi vitamin E berasaskan daripada kelapa sawit dienkapsulasikan kedalam manik mikro alginat yang diperkukuh oleh nanoselulosa. Sebelum penghasilan manik mikro alginat, emulsi minyak-dalam-air telah dikarakterisasikan terlebih dahulu dan kesan sifat-sifat emulsi terhadap manik mikro telah dinilai. Dua parameter dimanipulasikan dalam penyediaan emulsi minyak-dalam-air iaitu jenis selulosa dan jenis agen aktif permukaan yang digunakan dalam penstabilan emulsi. Emulsi minyak-dalam-air untuk pemuatan vitamin E dihasilkan dengan menggunakan Tween 80:Brij 35 atau 1-butil-3-methylimidazolium oktyl sulfate sebagai agen aktif permukaan dan pelbagai kepekatan nanoselulosa juga ditambahkan (0.0, 0.0125, 0.025, 0.05, 0.1, 0.175, 0.25, 0.5 and 1.0 %w/v). Dua jenis selulosa yang berbeza digunakan dalam kajian ini adalah selulosa hidrofilik yang dioksidakan oleh APS atau selulosa trimetililil hidrofobik. Emulsi dikarakterisasikan untuk diameter titisan purata, kelikatan dan perilaku rheologi. Emulsi yang distabilkan oleh Tween 80:Brij 35 dan menggunakan selulosa APS-teroksida yang hidrofilik sebagai nanofiller menunjukkan diameter titisan yang paling kecil dengan perilaku rheologi yang

sederhana. Emulsi yang distabilkan oleh selulose trimetililil hidrofobik, dengan menggunakan Tween 80:Brij 35 sebagai agen aktif permukaan yang mempunyai diameter titisan berskala nanometer dengan kelakuan rheologi yang paling baik. Sebaliknya, emulsi yang menggunakan 1-butil-3-methylimidazolium oktil sulfat sebagai pengemulsi menunjukkan micron saiz titisan dengan kelakuan rheologi yang tidak memuaskan hati tanpa mengambil kira kepekatan selulosa APS-teroksida. Manik mikro alginat kemudiannya dihasilkan dengan menitiskan emulsi yang mengandungi vitamin E ke dalam larutan kalsium. Keputusan menunjukkan kekuatan mampatan yang tertinggi iaitu 58.8 kPa diperolehi oleh manik mikro yang mengandungi emulsi yang distabilkan oleh Tween 80: Brij 35 dan 0.25% w/v selulosa teroksidasi hidrofilik. Ini menunjukkan bahawa selulosa APS-teroksida mengambil bahagian dalam pembentukan tiga dimensi struktur matriks manik mikro yang padat dengan berinteraksi dengan ion-ion kalsium melalui kumpulan -COO^- mereka. Kecekapan enkapsulasi tertinggi sebanyak 98.7% juga dicapai oleh manik mikro yang diperkukuhkan oleh 0.25% selulosa APS-teroksida yang mengandungi emulsi distabilkan oleh Tween 80:Brij 35. Di samping itu, manik mikro alginate/selulosa lebih tahan terhadap pembengkakan dalam keadaan pH yang rendah disebabkan oleh peningkatan kestabilan yang dipromosikan oleh selulosa. Manik mikro melepaskan vitamin E secara perlahan dalam cairan gastrik pH simulasi tetapi mempunyai cenderung untuk melepaskan vitamin E dalam cairan usus simulasi untuk membolehkan penyerapan ubat. Walau bagaimanapun, manik mikro yang mengandungi emulsi yang distabilkan oleh 1-butil-3-methylimidazolium oktil sulfat menunjukkan kecekapan enkapsulasi yang lebih rendah dengan pelepasan vitamin E *in vitro* yang tinggi. Data pelepasan ubat *in vitro* untuk semua manik mikro yang dinilai menunjukkan kesesuai yang baik untuk model Ritger-Peppas. Spektrum ^{1}H NMR menunjukkan bahawa vitamin E mengekalkan struktur kimianya selepas enkapsulasi ke dalam manik alginat.

Kata kunci: Mikrob alginat, Selulosa mikrofibrilasi, Vitamin E, Emulsi

ACKNOWLEDGEMENTS

First and foremost, I would like to express my greatest gratitude to my highly-respected supervisors, Professor Dr. Chuah Cheng Hock and Associate Professor Dr. Ching Yern Chee as well as my project consultant, Dr. Ng Mei Han who had shown much patience and effort in guiding me throughout the entire project. In addition, I also would like to show my appreciation to my care taker, Dr. Teo Yin Yin who gave me motivation and unconditional support whenever I faced difficulties and obstacles.

Next, I would like to convey special thanks to my beloved laboratory mates for their assistance, discussion and encouragement. I was able to complete this project without much hindrance due to their precious advices. Furthermore, I also greatly appreciate the assistance from the laboratory officers, who were willing to guide me in performing the characterization tests.

In addition, my utmost thanks to University of Malaya and Malaysian Palm Oil Board for providing facilities and all the funding to conduct this project. Last but not least, my appreciation goes to my parents for their endless support and love.

TABLE OF CONTENTS

LIST OF FIGURES

LIST OF TABLES

LIST OF SYMBOLS AND ABBREVIATIONS

ε_c	:	Critical stain
G''	:	Loss modulus
G'	:	Storage modulus
ALG	:	Alginate
α-TTP	:	α-tocopherol transfer protein
APS	:	Ammonium persulfate
Brij 35	:	Polyoxyethylene lauryl ether
Ca^{2+}	:	Calcium ion
$C_4mimC_8SO_4$	:	1-butyl-3-methylimidazolium chloride
CNC	:	Cellulose nanocrystal
DS	:	Degree of substitution
ECM	:	Extracellular matrix
EE	:	Encapsulation efficiency
EMIMAc	:	1-ethyl-3-methylimidazolium acetate
EMIMCl	:	1-ethyl-3-methylimidazolium chloride
FTIR	:	Fourier transform infrared
GIT	:	Gastrointestinal tract
HLB	:	Hydrophilic-lipophilic balance
HMDS	:	1,1,1,3,3,3-hexamethyldisilazane
HPLC	:	High performance liquid chromatography
IL	:	Ionic liquid
LVR	:	Linear viscoelastic region
MFC	:	Microfibrillated cellulose
NCC	:	Nanocrystalline cellulose

NMR	:	Nuclear magnetic resonance
OPEFB	:	Oil palm empty fruit bunch
O/W	:	Oil-in-water
PBS	:	Phosphate buffered saline
PEO	:	Poly(ethylene glycol)
PVA	:	Poly(vinyl alcohol)
RT	:	Room temperature
SA	:	Sodium alginate
SDS	:	Sodium dodecyl sulfate
SGF	:	Simulated gastric fluid
SIF	:	Simulated intestinal fluid
TEMPO	:	2,2,6,6-tetramethylpiperidine-1-oxyl radical
TRF-70	:	Vitamin E, carotino natural palm tocotrienols
TMSC	:	Trimethylsilyl cellulose
TMSCl	:	Trimethylchlorosilane
Tween 20	:	Polyoxyethylene glycol sorbitan monolaurate
Tween 40	:	Polyoxyethylene glycol sorbitan monopalmitate
Tween 60	:	Polyoxyethylene glycol sorbitan monostearate
Tween 80	:	Polyoxyethylene glycol sorbitan monooleate
W/O	:	Water-in-oil
WPI	:	Whey protein isolate
XRD	:	X-ray diffraction

CHAPTER 1: INTRODUCTION

1.1 Research background

Bioactive ingredients with various therapeutic properties spark tremendous attentions in pharmaceutical industry. Basically, the oral intake of drug is a typical administration route in which this approach is user-friendly due to its ease of administration. Nevertheless, most of these active pharmaceutical ingredients are of hydrophobic nature, exhibiting poor water solubility. Non-polar character of the drugs restricted their incorporations in food formulations (C. Tan & Nakajima, 2005) as well as in classic pharmaceutical forms, resulting in low bioavailability especially after oral or parenteral/intravenous administrations (Khayata et al., 2012). Biocompatible materials that are able to load sufficiently high amount of bioactive agent with diverse therapeutic properties are in high demand in pharmaceutical industry (Eral et al., 2014). Considerable efforts have to be implemented to incorporate these lipophilic active compounds into aqueous media that suitable for oral administration.

Emulsification is one of the well-known techniques to improve the solubility of sparingly soluble drugs (Odriozola-Serrano et al., 2014). In addition, extensive attempts have also been carried out to modify polymers that capable of entrapping hydrophobic bioactive molecules because loading them via equilibrium partitioning is inefficient (Gou et al., 2008). Modification of polymers can be achieved by copolymerizing or grafting hydrophobic moieties to hydrophilic polymeric backbone network for improving encapsulation efficiency and sustainability of lipophilic drugs (Jeong et al., 2000). However, these approaches are ineffective because the modified polymers could not carry large amount of hydrophobic drug.

In the recent years, immobilization of nano-emulsions (Mason et al., 2006) or microemulsions (David Julian McClements, 2012a, 2012b) containing hydrophobic drugs

within polymeric matrix was observed to be appropriate method for achieving high drug loading (An et al., 2012; Jagadeesan et al., 2011). Previous study demonstrated that the ability to protect highly labile bioactive therapeutics from harsh processing and acidic condition was improved appreciably when entrapping them within polymeric structure as compared to loading them in nano-emulsion forms (Xiao et al., 2017). The crosslinked network of polymer can restrain the penetration of digestive enzymes, thus, protecting the therapeutic agents from degradation by inwardly diffusing enzymes. With this reason, the plasma half-life of drug can be extended by prolonging the time of drug retained in the body. Owing to its tunable physical properties, polymer serves as a versatile platform to facilitate various chemical interactions between polymers and drugs. This oral dosage form would enhance patient compliance as repeated administration of drugs to stimulate the therapeutic effect is not required (J. Li & Mooney, 2016).

Alginate is an appealing natural polymer that being employed as drug delivery system (Agüero et al., 2017). Drug-loaded emulsions can be dispersed in alginate solution followed by the formation of alginate gel upon reacting with divalent cations, such as calcium ions (Ca^{2+}) in calcium chloride ($CaCl_2$) crosslinking solution (Chuang et al., 2017). Alginate gels can be formulated in diverse physical forms such as microbeads, microcapsules, films and sponges (Hoare & Kohane, 2008). They are usually produced as small spherical beads (0.2-1.0 mm in diameter). Spherical microbeads are preferable because they provide larger surface to volume ratio that facilitates the sustained and controlled drug release with enhanced stability (Robitaille et al., 2000). Besides, porous structures of alginate microbeads also permit the loading of bioactive materials within gel matrix and subsequent elution of drugs at the site of absorption under controlled rate. The porosity of gel matrix depends mainly on the density of cross-links (Hoare & Kohane, 2008).

Alginate also exhibits pH-responsive and tunable swelling properties that make it an excellent biomaterial as drug carrier (Hariyadi & Islam, 2020). At low pH condition, carboxyl groups of alginates will be protonated, leading to minimal swelling of alginate microbeads in gastric fluids and limit the release of drugs. However, deprotonation of carboxyl groups as well as ion exchange process between Ca^{2+} ions and sodium (Na^{+}) or potassium ions (K^{+}) (present in phosphate buffer dissolution medium) occur at alkaline intestinal environment. These enhances the swelling of alginate microbeads, resulting in rapid drug release (Wong, 2011).

Previous studies demonstrate that alginate-based microbeads with improved functionalities and physicochemical properties can be achieved by blending with other biopolymers or nanoparticles. Incorporation of nanocelluloses into drug carrier is an effective approach to improve the encapsulation efficiency and its efficacy (Gheorghita Puscaselu et al., 2020). Nanocelluloses can be extracted from various sources of lignocellulosic biomass materials and can be generally categorized into three groups: microfibrillated celluloses (MFCs), cellulose nanocrystals (CNCs) and bacterial CNCs (BCNCs). MFCs have garnered considerable attentions due to their high aspect ratio (Ning Lin et al., 2012). MFCs exhibit long and network-like structures with diameters ranging from 10 to a few hundred nanometers and up to several micrometers in lengths (Sheikhi et al., 2019). In this study, MFCs extracted from oil palm empty fruit brunches were obtained via mechanical disintegration by homogenizer. MFCs were added into alginate-based microbeads as reinforcing materials due to their mechanically strong crystalline structures.

Chemical modification of nanocelluloses is crucial in order to facilitate the effective interaction with alginate matrix for controlled release of drugs. Oxidation is recognized to be one of the most common modification techniques in which nanocelluloses with

carboxyl functional groups can be achieved (Habibi, 2014). Hence, carboxylated MFCs were produced in this study via ammonium persulfate (APS) oxidation. Both anionic carboxylic groups of alginates and MFCs involved in the formation of three-dimensional network structure. MFCs can also from hydrogen bonds with alginate molecules that further strengthen the polymeric matrix (Agarwal et al., 2015). Previous studies also reported that chitosan-based delivery systems with enhanced mechanical strength can be achieved by incorporation of celluloses (HPS et al., 2016; Sampath et al., 2017).

In the present study, MFCs-reinforced alginate microbeads were developed to encapsulate vitamin E. Vitamin is a hydrophobic natural therapeutic with essential nutritional benefits. The effects of various concentrations of MFCs on the mechanical properties, swelling behaviors, encapsulation efficiency as well as the release profile of the alginate microbeads were studied.

1.2 Problem statements

Emulsification is one of the well-established approaches that generally enhanced the solubility of the lipophilic bioactive compounds in aqueous solution (Odriozola-Serrano et al., 2014). However, conventional emulsions are susceptible to physical instability due to the environmental stresses such as heat and light. These emulsions also subject to chemical degradation when they encounter digestive enzymes and harsh gastric conditions in the stomach region of gastrointestinal tract (GIT). Furthermore, the formulated emulsions exhibit limited controlled release because of the relatively small droplet size, implying that the diffusion rate of substances out of the emulsion droplets is extremely high (D. J. McClements et al., 2009).

Hence, microencapsulation of lipophilic drug-loaded emulsions within polymeric matrix is a favorable to enhance delivery and improve efficacy. Polymer serves as a protective structure that facilitates the delivery of lipophilic bioactive materials at the site of action under regulated release rate (Benavides et al., 2016). Alginate appears as one of the natural polymers that often employed as drug carrier due to its unique sol-gel transition behaviour that enables the loading of drug followed by subsequent release at site of action. Alginate exhibits numerous promising characteristics such as biocompatibility, biodegradability, non-toxicity and simple in preparation, rendering it as an attractive drug delivery system (Hariyadi & Islam, 2020). Moreover, alginate is readily available and is relatively low cost. However, alginate demonstrates poor mechanical properties that restricted its efficacy as drug delivery system (Gheorghita Puscaselu et al., 2020). Thus, alginate must be reinforced by other materials in order to be practically valuable (Roff & Scott, 2013). Cellulose has emerged as a prominent reinforcing agent due to its appealing mechanical properties to reinforce drug systems with poor mechanical performance (Anghel et al., 2021; Ooi et al., 2016; Treesuppharat et al., 2017).

Cellulose is the most abundant naturally occurring polysaccharides in the world that garnered considerable attentions due to its intriguing properties which include high mechanical strength, biocompatibility, renewability and non-toxicity. Nanocelluloses are commonly synthesized via sulfuric acid (H_2SO_4) hydrolysis. However, this chemical treatment involves multiple pretreatment steps prior to the production of nanocelluloses with relatively low yield. Therefore, we extracted microfibrillated celluloses (MFCs) from oil palm empty fruit bunches via ammonium persulfate (APS) oxidation in this study. With this APS oxidation, microfibrillated celluloses with carboxyl functional groups can be easily isolated in a one-step procedure.

In the present study, we incorporated APS-oxidized MFCs into vitamin E-loaded alginate-based microspheres to enhance the mechanical integrity of the three-dimensional polymeric matrix, which eventually reduce the leaking of vitamin E (Lin et al., 2011). Electrostatic interactions between the anionic carboxylic groups of alginate and APS-MFCs with bivalent calcium ions strengthen the three-dimensional network structure (Agarwal et al., 2015). Furthermore, formation of hydrogen bonds between oxidized MFCs and alginate results in the development of reinforced framework of beads. All these contribute to the improvement of the mechanical strength of the microbeads and subsequently improve the encapsulation efficiency of microbeads (N. Lin et al., 2012).

1.3 Research objectives

The main objective of this research is to synthesize alginate-based microbeads reinforced by microfibrillated celluloses for potential delivery of vitamin E. In order to achieve this main objective, the present study aims:

1. To extract, modify and characterize microfibrillated celluloses from oil palm empty fruit bunches.
2. To investigate the influence of emulsion properties on the formation of cellulose-reinforced alginate microbeads.
3. To evaluate the effect of the type and concentration of microfibrillated cellulose on the mechanical strength, encapsulation efficiency, physicochemical properties as well as the release profile of the alginate-based microbeads.

1.4 Organization of dissertation

This thesis has been organized into five chapters.

Chapter 1 introduced the research background on hydrogels and their advantages as drug delivery systems. The problem statements also mentioned in this chapter followed by the objectives of the research.

Chapter 2 presented the literature reviews on the hydrogels derived from natural polymers and their application as drug delivery system. Previous studies on the encapsulations of lipophilic therapeutic agents within hydrogels were reviewed. Besides, the importance of emulsification techniques and the uses of celluloses as reinforcements were also highlighted. Lastly, overview on the vitamin E was addressed.

Chapter 3 described the detailed materials and research methodologies in the extraction of microfibrillated celluloses from oil palm empty fruit bunches, the production of oil-in-water emulsions as well as the preparation of microfibrillated cellulose-reinforced alginate microbeads. In addition, the detailed experimental procedures to perform the characterization tests were also discussed.

Chapter 4 reported the results obtained and discussion on the characterization tests. The chemical and physical properties of microfibrillated celluloses and hydrophobic trimethylsilyl celluloses were first described. Furthermore, the droplet size, viscosity and the rheological behaviors of oil-in-water emulsions were discussed. This was followed by the discussion on the properties of cellulose-reinforced alginate microbeads. Lastly, *in vitro* release profile, release kinetics and the encapsulation efficiency of alginate-based microbeads were also studied.

Chapter 5 summarized the research work and made conclusive statements based on the results obtained from the characterization tests. The contributions of the present study were mentioned. In addition, suggestions on the future research directions related to this study were also described.

CHAPTER 2: LITERATURE REVIEW

2.1 Hydrogels

Hydrogels can be defined as three-dimensional, compact cross-linked polymeric networks that can be synthesized from any water-soluble polymers. Hydrogels can be produced from both naturally occurring (eg. collagen, chitosan and alginate) and synthetic polymers (eg. polyvinyl Alcohol (PVA), poly(lactic acid) (PLA), poly (2-hydroxyethyl methacrylate) (PHEMA) and poly(ethylene glycol) (PEG)) (Salmieri et al., 2015). Hydrogels exhibit numerous intriguing properties such as biocompatibility, biodegradability and bio-adhesive (Hoare & Kohane, 2008). The key determinant of their biocompatibility is the high water content in hydrogels due to their hydrophilic character. Besides, hydrogels also resemble the native extracellular matrix chemically and physically (Anuj Kumar & Han, 2017). In addition, they also capable of swelling and de-swelling reversibly in water, which stems from the presence of the hydrophilic functional groups on the polymeric backbone. However, hydrogels are resistant to dissolution which is attributed to the high density of cross-links between network chains (Peppas et al., 2000). Degradability of hydrogels can be achieved via enzymatic, hydrolytic, or environmental (e.g. pH, temperature, or electric field) approaches. Some of the hydrogels also display bio-adhesive properties whereby it could be favorable to adhere them at the targeted site (Hoare & Kohane, 2008).

The promising characteristics of hydrogels have sparked substantial interests in drug delivery systems. Besides, hydrogels with highly porous structures accommodate the entrapment of active pharmaceutical ingredients and allows the subsequent release of drugs from the gel matrix at the rate based on the diffusion coefficient. The porosity of hydrogels can be tailored by manipulating the cross-link density as well as the fabrication conditions (Caló & Khutoryanskiy, 2015). Hydrogels can be formulated in diverse physical forms such as slabs, micro- or nano-beads, films and sponges (Hoare & Kohane,

2008). Tablets and capsule are two conventional dosage forms that employed in treating acute and chronic diseases but they are not favorable forms for patients as these have to be administrated several times daily in order to maintain optimum plasma concentration. Recently, hydrogels in spherical microbeads with sizes range from 1 to 1000 μm are well-known to be effective dosage form in simulating the sustained and controlled drug release with enhanced stability due to their small particle size (Badwaik et al., 2019; N. Sharma et al., 2015). The drugs can be encapsulated within microbeads and to be delivered to targeted site of the body with prolonged drug release (Joshi & Joshi, 2019). Generally, the hydrophilic microbeads are efficient in encapsulating high content of hydrophilic drugs (Hoare & Kohane, 2008).

They offer numerous advantages over conventional dosage form which include the protection of the entrapped drugs from harsh condition of the stomach and increases the residence time at absorption site. Therefore, better therapeutic effect for short half-life of drugs can also be achieved (Sahil et al., 2011). Since microbeads can provide constant therapeutic effect in which frequent administration of drugs is not required, thus, improve the patient compliance (Patil et al., 2017). In addition, surfactant-stabilized emulsion droplets can also be immobilized within microbeads to improve the bioavailability of hydrophobic therapeutic agents (H. Yan et al., 2019).

Despite of numerous superior properties, the low mechanical strength and large pore sizes of most hydrogels restrain their application in drug encapsulation. Premature dissolution of the hydrogels might be observed and it might result in the burst release of drugs prior to the arrival at the absorption site. Furthermore, the loading of hydrophobic bioactive compounds into hydrophilic gel matrix is relatively inefficient due to their inherent incompatibility, leading to the inhomogeneity of drug distribution (Ullah et al., 2015).

2.2 Alginate and its chemical structure

Alginates are regarded as a family of natural polysaccharides that biosynthesized in the marine brown seaweeds whereby they comprise up to 40% of the dry matter (Haug & Smidsrød, 1967) as well as in the soil bacteria such as *Pseudomonas* and *Azotobacter* (Christensen, 2011; Haug et al., 1974). Alginates have also been found in the intercellular matrix of brown algae such as *Mycrocystis pyrifera*, *Laminaria hyperborean, Fucus vesiculosus, Ascophyllum nodosum* and so on as gels (L. Pereira & Cotas, 2020). According to Donati and Paoletti (2009), the annual industrial production of alginates is estimated to be about 30,000 tons worldwide. Alginates with different chemical compositions could be easily available by microbial fermentation and post-polymerization modification (Donati & Paoletti, 2009). However, the major source of commercially available alginates is commonly isolated from algae (P. X. Ma & Elisseeff, 2005). Bacterial-derived alginate production is not famous due to the significant higher production cost (Donati & Paoletti, 2009; P. X. Ma & Elisseeff, 2005).

Stanford (1881) was the first researcher who successfully discovered and patented the alginate molecule in 1881, this was then followed by intensive investigations by other researchers. In 1926, the backbone of alginate polymers was found to consist of uronic acids, which are mannuronic acids (Atsuki & Tomoda, 1926; Schmidt & Vocke, 1926). The mannuronic units are connected by 1,4-β-glycosidic bonds (Donati & Paoletti, 2009), thus, alginates were believed to be a strictly long polymer of (1,4)-linked β-D-mannuronate until Fischer and Dörfel (1955) found an enzyme called C5-epimerase. C5-epimerase converted β-D-mannuronate (M) to α-L-guluronate (G). Thus, alginate should be a complex structure containing homopolymeric G blocks (GGGGG), homopolymeric M blocks (MMMMM) and heteropolymeric M and G blocks (MGMGMG) in the presence of C5 epimerase (Christensen, 2011; Haug & Larsen, 1966; Tønnesen & Karlsen, 2002). Thus, alginate is known to be linear block co-polymers constitute of M

and G units with the ratio of G to M varies relying on the alginate sources (Haug & Larsen, 1966). It is obvious that alginate demonstrated an inhomogeneity in term of chemical structure (Donati & Paoletti, 2009). It was believed that only the G-blocks of alginate participate in the formation of hydrogels through intermolecular cross-linking with divalent cations (K. Y. Lee & Mooney, 2012).

The alginate molecule exhibits a notable sol-gel transition behavior in the presence of gelling ions such as magnesium (Mg^{2+}), barium (Ba^{2+}), strontium (Sr^{2+}), calcium (Ca^{2+}), which almost independent on temperature (Montanucci et al., 2015). Gelation of alginate can be explained by "Egg-box" model (Figure 2.1). "Egg-box" model is demonstrated based on the mechanism where cavities function as binding sites for ions, which are formed due to the diaxially linked G-residues. A gel network is created when molecular junctions are formed with the correct sequences of G-blocks (Braccini & Pérez, 2001; Sikorski et al., 2007). This feature makes alginate unique compared to other gelling polysaccharides. This outstanding behavior allows materials such as drugs and gelling ions to be added and dispersed in a liquid (a sol), then agglomerate together to form a continuous three-dimensional network extending throughout the liquid (a gel). Due to the excellent biocompatibility and sol-gel feature of alginates, they have also been involved in a broad range of applications (J. Sun & Tan, 2013), with drug delivery being the highly emphasized strategy (Tønnesen & Karlsen, 2002). Thus, alginate gel is used as wall material, encapsulating drugs, small proteins and antibodies in pharmaceutical industry (K. Y. Lee & Mooney, 2012).

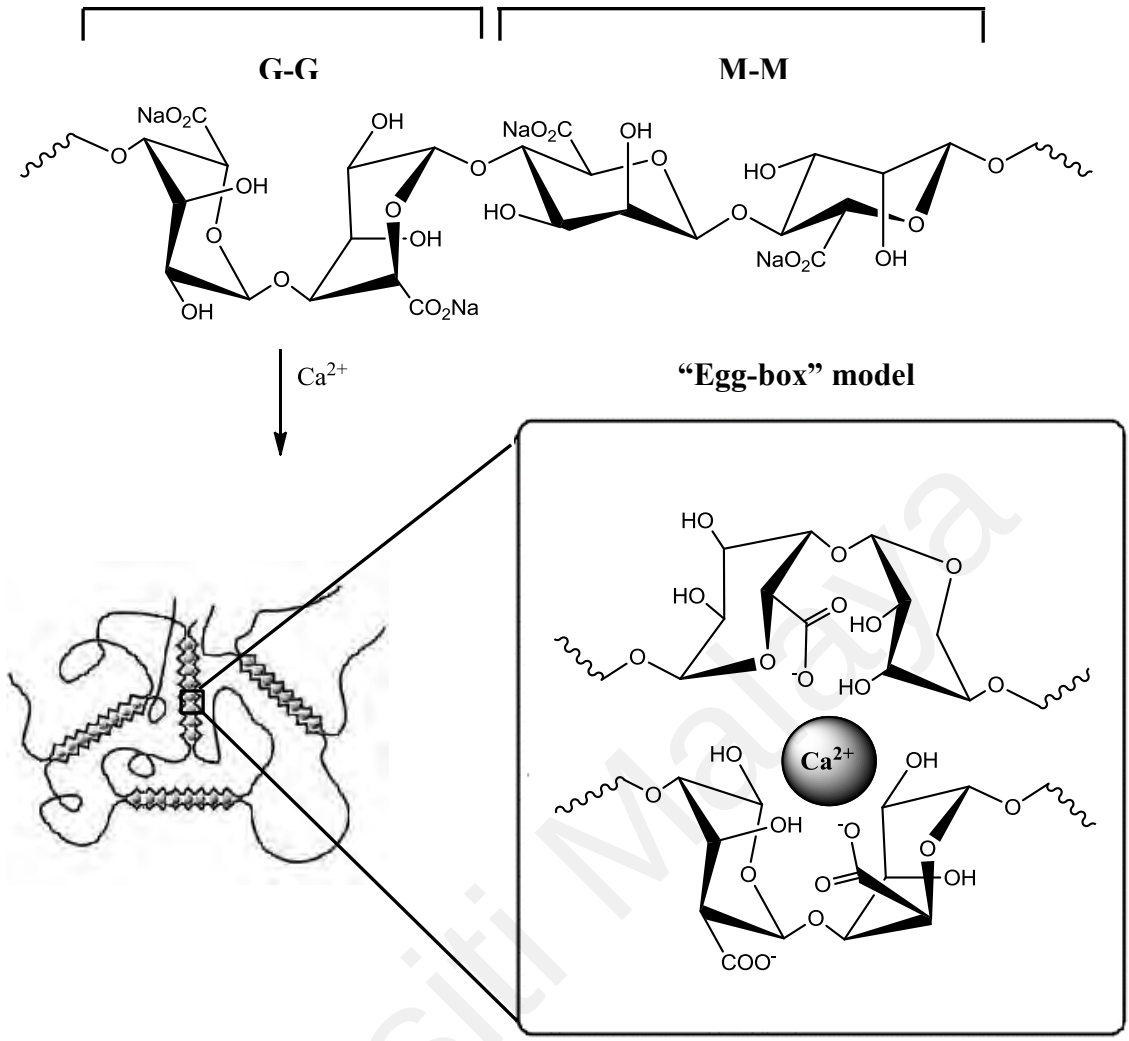

Figure 2.1: "Egg-box" structure of sodium alginate formed in the presence of Ca^{2+} (Paques et al., 2014).

It is vital to control the ways of introducing the cross-linking ions in alginate gelation process because it will directly affect the gel uniformity and the strength (J. Sun & Tan, 2013). Two fundamental methods that employed in the preparation of alginate gels by ionic cross-linking which are internal setting method and diffusion method (Draget, 2009). The diffusion method is a means in which alginate solution is allowed to drip from an outer reservoir into solution containing gelling ions such as Ca^{2+} (Draget, 2009). This rapid gelation process results in inhomogeneous alginate gels production. However, the degree of homogeneity can be governed by the concentration of gelling ions and the molecular weight of alginate molecules. In order to form more homogenous alginate gels

using diffusion setting, high concentration of gelling ions and non-gelling ions should be added into high molecular weight alginate. Diffusion method is well-known method for immobilization purposes with every single gel bead entrapping the living cells and growth factors (Draget, 2009).

Meanwhile, calcium-alginate gels can be prepared by means of internal setting as well (Christensen, 2011). In the internal setting method, $CaCl_2$ can be replaced by less soluble $CaSO_4$ or insoluble $CaCO_3$ to achieve more controllable and slower gelation process (Kuo & Ma, 2001; Ruvinov et al., 2010). In this technique, slightly soluble $CaSO_4$, insoluble $CaCO_3$ (inert calcium source) as well sequestering agent or chelating agent (EDTA, citrate etc.) could be used as agents to control the released of Ca^{2+} for the gelation purposes (Christensen, 2011; Draget, 2009). The leaking of Ca^{2+} ions from inactive source is controlled by changing the pH using organic acids or lactones. By lowering the pH to 4.0, Ca^{2+} can be readily released from chelating agents. Solubility of inert calcium source also affects the speed of Ca^{2+} ions released to the solution (Draget, 2009).

2.3 Cellulose and its chemical structure

Natural fibers comprise of celluloses as major components that embedded in non-cellulosic matrixes, which are lignin and hemicelluloses (Alemdar & Sain, 2008). Hemicelluloses are branched polysaccharides composed of several sugar units. Hemicelluloses are believed to be responsible in maintaining the structural integrity of fiber cell as they act as cementing matrix by forming hydrogen bonds with cellulose microfibrils. Lignin is a complex, three-dimensional copolymer with both aliphatic and aromatic constituents (Maya Jacob John & Rajesh D. Anandjiwala, 2008). The hydrophobic lignin network is positioned primarily at the exterior of microfibrils in which it covalently bonds to hemicellulose, contributing to the inherent rigidity of the fibers (Y. H. Zhang & L. R. Lynd, 2004).

Cellulose is the primary building material of photosynthetic green plants such as reeds, stalks, grasses and woody vegetation (Siró & Plackett, 2010). In addition, the presence of celluloses in marine invertebrates (tunicate), several species of algae and bacteria, fungi, slime molds and amoebae have also been documented (Lynd et al., 2002; Pathak, 2018). Cellulose is characterized as high molecular weight homopolymer of D-anhydroglucopyranose linked together by β-1,4-glycosidic bonds in a linear chain (Habibi et al., 2010; Siqueira et al., 2010) with a degree of polymerization (DP) of approximately 10,000 (KaliaKaith et al., 2011).

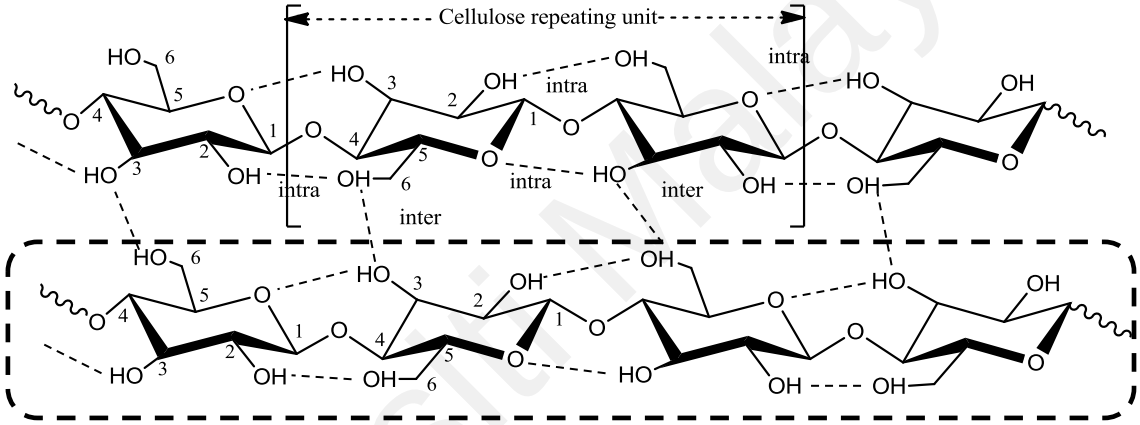

Figure 2.2: Chemical structure of cellulose (del Valle et al., 2017).

The basic chemical structure of cellulose is well illustrated schematically in Figure 2.2 demonstrating cellobiose as dimer that appears as a repeated segment. Anhydroglucose unit carries three hydroxyl groups located at C2, C3 and C6 positions that are responsible for the formation of intra- and intermolecular hydrogen bonds (del Valle et al., 2017). Pairing cellulose molecules was achieved via *van der Waals* forces as well as hydrogen bonding between hydroxyl groups and oxygen of adjacent molecules, forming multiple cellulose chains that alligned in parallel manner, containing both crystalline and amorphous domains (Azizi Samir et al., 2005; Hubbe et al., 2008). Multiple cellulose chains are assembled into elementary fibrils that further aggregate to form larger microfibrils (Moon et al., 2011; Y. H. Zhang & L. R. Lynd, 2004).

Generally, cellulose can be classified into four different polymorphs: cellulose I, II, III, and IV. Cellulose I occurs naturally and two allomorphs, I_α and I_β are found. Other cellulose polymorphs are formed after physical modifications. Cellulose II is recognized to be the most stable crystalline form, which can be obtained after re-crystallization or mercerization in the presence of aqueous sodium hydroxide (Aulin et al., 2009; Siqueira et al., 2010). Cellulose I and II are distinguished from each other in term of the structural arrangement whereby cellulose I alligned in a parallel direction while cellulose II has an antiparallel packing (Aulin et al., 2009). Cellulose III_I and III_{II} can be produced via ammonium treatment of cellulose I and II, respectively. Whereas cellulose IV is formed from the modification of cellulose III (Lavoine et al., 2012).

Celluloses have been extracted from numerous sources of lignocellulosic biomass materials, which include kenaf (Kargarzadeh et al., 2012), oil palm (Fahma et al. 2010), banana (Cherian et al., 2008; Elanthikkal et al., 2010) and bamboo (Wenshuai ChenHaipeng Yu & Yixing Liu, 2011), wheat straw (Alemdar & Sain, 2008), mulberry (R. Li et al., 2009), pineapple (Cherian et al., 2010), bacterial cellulose (Olsson et al., 2010) and cotton (Satyamurthy et al., 2011). Malaysia has now become the largest palm oil producer that contributes to 51% of the worldwide production of palm oil. Thus, this industry plays a vital role in contributing to economic resources of Malaysia (Ferrer et al., 2012). During periodically pruning and replanting of palm trees, the fruits or nuts are first stripped from fruit bunches, leaving behind the empty-fruit bunches as wastes (Abdullah & Sulaiman, 2013). Malaysia produces about 280,000 tons of oil palm empty fruit bunches (OPEFBs) annually, generating large amounts of lignocellulosic biomass. OPEFB comprises of 30.9 % hemicelluloses and 14.2 % lignin with 44.4 % celluloses being the major components (Rosazley et al., 2016). These abundant cellulose enriched biomasses create adverse environmental issues such as fouling and attraction of pests.

The utilization of these undesirable wastes in value-added products is an indubitable advantage in order to mitigate environmental impacts (Law et al., 2007).

2.4 Alginate/cellulose microbeads as drug delivery system

Due to the excellent mechanical performance of nanocelluloses, they have been extensively employed as reinforcements in various applications. In the recent years, there are many studies reported that the incorporation of nanocelluloses into polymer matrix improved the mechanical strength and encapsulation efficiency of microbeads as drug carriers with controlled release profile.

Bacterial cellulose nanofiber (nf-BC)/sodium alginate (SA) composites were produced as dual-stimuli responsive release systems for delivery of Ibuprofen (X. Shi et al., 2014). These nf-BC/SA composites are pH-responsive in which the swelling ratio increases with the increasing of pH. Hence, the slow release of Ibuprofen was observed at low pH condition because of the minimal swelling ratio of composites due to the protonation of calcium alginate. However, rapid release of drug occurred at alkaline environment attributed to the deprotonation of alginate that led to high swelling ratio. Besides, the swelling ratio can also be manipulated by electric field stimulus. When the applied electric field increased from 0 to 0.5 V, there was a rise in swelling ratio from 8 times to 14 times. Elevation in the applied electric field promotes the ionization of carboxyl groups of alginates, resulting in great electrostatic repulsions. In addition, the presence of nf-BC also enhanced the mechanical properties of the composites.

H. Yan et al. (2019) synthesized alginate composite beads entrapping hydrophobic alfacalcidol-loaded bacterial cellulose nanocrystals (BCNs) Pickering emulsions. Stable Pickering emulsions against re-coalescence were produced as BCNs adsorbed irreversibly at freshly formed oil-water interfaces. Drug-loaded Pickering emulsions were immobilized into alginate hydrogel beads via external gelation using $CaCl_2$ crosslinking

solution. The formation of Pickering emulsions enhanced the compatibility between sodium alginate (SA) and hydrophobic alfacalcidol, resulting in higher encapsulation efficiency. SA beads, SA/BCNs-0.3, SA/BCNs-0.6 and SA/BCNs-0.9 exhibited encapsulation efficiency of 54.2%, 80.3%, 89.6% and 91.4%, respectively. Outstanding drug-loading capacity of SA/BCNs composite beads can be ascribed to the formation of electrostatic forces and intermolecular hydrogen bonds between BCNs and alginate. This subsequently enhanced the mechanical performance of hydrogel beads, facilitating the sustained released of alfacalcidol.

Furthermore, alginate/cellulose nanocrystal hybrid nanoparticles (ALG-CNC NPs) were developed for the encapsulation of rifampicin (RIF) (Thomas et al., 2018). The bioavailability of RIF is restricted because it is sparingly soluble in water, thus, the administration of high doses of the drug is required in order to maintain desired plasma drug concentration. The results obtained in this study showed that sustained release of RIF can be achieved after entrapping into alginate polymer carrier. With this reason, the need for frequent administration of drugs can be effectively minimized, thus preventing overdosage and adverse side effects. In acidic gastric juice, ALG-CNC NPs demonstrated low release rate with only 10–15% of the RIF eluted in the first 2 h. Rapid release of drug was observed at alkaline environment (pH 7.4) in which 90% of the RIF was released in 12 h. CNCs serve as reinforcements to improve the encapsulation efficiency, to increase the stability as well as to prolong the release of drugs due to the three-dimensional network of the CNCs.

2.5 Alginate-based microbeads as drug delivery system

In recent years, various types of natural polysaccharides have been incorporated into alginate-based microbeads in order to enhance the functionalities and the physicochemical properties of the microbeads. Starch/alginate beads were fabricated as novel drug carriers for the controlled release of a model peptide drug, L-phenylalanine (Y. J. Kim et al., 2005). The addition of starch in the formation of alginate composite beads can retain the original bead shape after drying process. Preparation of beads in dried form is vital for commercial purpose to ease the storage and transportation process. Furthermore, the swelling degree of beads enhanced after the incorporation of starch into beads which is essential for the release of the drugs. After 15 mins of incubation in pH 7.4 phosphate buffer solution, only 0.0025 mg/ml of L-phenylalanine was released from alginate beads and remained almost the same until 120 mins. This was contributed by the limited swelling properties of alginate beads. In addition, the release rate also decreased with increasing concentration of starch in alginate composite beads.

Alginate/chitosan beads with enhanced mechanical performance were produced for the delivery of celecoxib (Segale et al., 2016). Alginate solution was first blended with celecoxib-loaded self-emulsifying phase, followed by dripping the emulsion into a calcium chloride or in a calcium chloride-chitosan crosslinking solution using hypodermic needles. The gelation of alginate/chitosan was attributed to the formation of polyelectrolyte complex between the carboxyl moieties of alginate and the amino moieties of chitosan. The formulated beads were able to remain intact and to protect the drug from harsh gastric condition, while promoting the elution of drug in the intestinal condition which is the absorption site of celecoxib. Maximum swelling degree of all the formulations in hydrochloric acid at pH 1.0 was less than 60%. Carboxylate groups of alginates was protonated in this acidic condition, which restricted the swelling of the beads due to the reduced repulsive forces. Although the amine units of chitosan were

converted into NH^{3+} soluble form, the interaction of amino group and protonated carboxylic groups is not strong enough to facilitate swelling. High swelling profile was observed at pH 7.4 in which the weight of beads was increased drastically. The weight was then diminished abruptly after reaching maximum swelling peak due to the disintegration of the beads. This was ascribed to the ion exchange reaction between Na^{+} that is present in the phosphate buffer and Ca^{2+}. However, the experimental results showed that the incorporation of chitosan improved the mechanical strength of the beads whereby the maximum swelling degree of chitosan-alginate beads is lower than that of the alginate beads. Alginate-chitosan systems achieved a swelling equilibrium in about 30 mins and their weights were remained constant until the end of the *in vitro* release study. In addition, complete release of celecoxib from alginate beads was observed in about 8 hours. In the contrary, less than 75% of the drug was eluted from alginate-chitosan beads within the same time frame. This could be probably due to the ionic interactions between alginate and chitosan.

Pectin is recognized to be promising colonic drug carrier due to the specific degradation mechanism by the bacterial flora of human colon (Rajpurohit et al., 2010). Nevertheless, high concentration of pectin is required in the formation of microbeads for encapsulation of drugs because of the limited carboxyl functional groups. In the previous study, alginate was added to fabricate pectin/alginate microbeads in order to reduce the concentration of pectin used (Tsai et al., 2013). The structure of galacturonic acid is similar to the guluronic and mannuronic acids of alginate. The microbeads were subsequently coated with Eudragit S100 to minimize the burst release of drugs in harsh gastric condition. Eudragit S100-coated pectinate/alginate microbeads (PAMs) were employed as colon-targeting carriers for delivering hyaluronan–cisplatin conjugate nanoparticles (HCNPs) via an electrospray method and a polyelectrolyte multilayer-coating technique in aqueous solution. The *in vitro* release studies demonstrated that only

25.1% of HCNPs was eluted within 24 hours in pH 1.2 medium. However, the drug release rate increased drastically to 75.6% at pH 7.4 dissolution medium. In addition, the entrapment efficiencies of HCNP-PAMs and Eudragit S100-coated HCNP-PAMs were found to be 89.0% ± 2.3% and 80.6% ± 3.8%, respectively. The incorporation of hyaluronan was also observed to be able to mitigate the adverse sides effects of cisplatin, which include acute nephrotoxicity and chronic neurotoxicity (Xie et al., 2010).

2.6 Criteria as an effective drug delivery system

2.6.1 High encapsulation efficiency

Encapsulation efficiency is one of the significant parameters in fabricating an effective delivery system because it is a measure of loading efficiency of the therapeutic agents. Small drug loading capacity was observed in conventional drug delivery systems due to their small reservoir size. The weak interactions between the hydrophobic drug and the hydrophobic polymer resulted in low encapsulation efficiency of 20% - 30% (Çalış et al., 2019). Encapsulation efficiency can be determined by the properties of the delivery systems as well the nature of the drugs such as their solubilities and the interactions between the active molecules with the carriers (Panyam et al., 2004). In general, it is believed that increased encapsulation efficiency can enhance the stability of the polymeric matrix. Nevertheless, excessive drug loading was noticed to alter the pharmacokinetic and pharmacodynamic properties of carrier, resulting in adverse impact to its activity/therapy efficacy (Callari et al., 2017).

2.6.2 Biocompatibility and porosity

It is essential that the material used for developing a drug delivery system to be non-toxic, biocompatible and immunogenicity (O. Pillai & Panchagnula, 2001). Transportation of any material such as drugs to the body will potentially evoke a certain immune response from the host as they are being recognized as foreign substances by the host immune system (Lacík, 2006). Therefore, construction of drug carrier is a general concept of immune-isolation, whereby it acts as an immune barrier to prevent direct interconnection between the encapsulated drugs and the hostile immunological environment (Thakur & Thakur, 2018). The drug carrier and the delivered drugs are dependence on each other as the immune rejection towards the drug carrier itself can have great impact on the inflammatory response towards the encapsulated drugs (de Vos et al., 2006). Hydrogels are well-known for their promising biocompatibility as reflected by

numerous successful *in vivo* experiments. The main key contributed to this biocompatibility is the large amount of water in hydrogels and their ability to resemble the native extracellular matrix (Hoare & Kohane, 2008).

In addition, there is another striking property of hydrogels which is their highly porous structures that offer great advantage in drug delivery applications especially in the sustained release system (Bacelar et al., 2017). Hydrogel can be employed as a depot from which drugs slowly elute, retaining a high local concentration of active pharmaceutical ingredients in the surrounding tissues over an extended period (Hoare & Kohane, 2008). The porosity of hydrogels accommodate the loading of drugs, subsequently allowing the migration of drugs through the gel network at a rate dependent on the diffusion coefficient of the bioactive compounds (Muñoz-Bonilla et al., 2019). The porosity can be tailored by adjusting the density of cross-links in the gel matrix as well as the gelling conditions, which will subsequently affect the release rate of the entrapped drug particles (Kharkwal & Janaswamy, 2016).

2.6.3 High mechanical strength

The drug carrier acts as a platform to protect the drugs and release them at the desired absorption site. The mechanical strengths of hydrogels used as drug carriers must be sufficient to maintain the physical integrity in order to prevent the leakage of the drugs prior to the arrival at the site of action (Amin et al., 2009). The molecular weight distributions of polymers, cross-linking density and the type of cross-linker are important elements in determining the mechanical properties (eg. stiffness and swelling) of hydrogels as drug carriers (Ratner et al., 2004). There are two types of alginates which are low molecular weight and high molecular weight alginates. In case of high molecular weight alginate, elevation of stiffness occurred upon increasing the concentration of polymer (Aarstad et al., 2017). Nevertheless, the viscosity of the gelling solution was

promoted which in turn increased the difficulty of processing and degradation of polymer by high shear mechanical forces (H. J. Kong et al., 2003). However, this problem can be minimized by merging high- and low-MW alginates in the formulations. With this approach, the elastic modulus of gels can be improved considerably while the viscosity of the pre-gel solution minimally raises in the case of mixed molecular weights alginates. Gelling conditions also affect the mechanical properties whereby the diffusion rate of Ca^{2+} ions will be reduced at low temperatures, resulting in slower cross-linking process. A more ordered network structure with enhanced mechanical strength can be formed (Augst et al., 2006).

The mechanical properties of gels at small transformation can be evaluated by Young's modulus, which largely depend on the cross-link density (Draget et al., 2006). The composition, the molecular weight and the concentration of polymers as well as the cross-linker type are the key determinants for the gel strengths (Morch et al., 2007). Besides, rupture strength is also frequently used to describe the gel strength, providing the information about the gel behavior at large deformation. Although both the Young's modulus and rupture strength are correlated to the number of crosslinks in the network but they are not directly proportional. The compressive test of gel cylinders allows the measurement of Young's modulus and rupture strength of hydrogels (Johnson et al., 2004).

2.6.4 Excellent stability

Stability is one of the essential criteria in the development of effective delivery system. During the storage period, hydrogels might experience syneresis whereby shrinkage of gels occur with concomitant exudation of liquids. This will subsequently lead to the loss of bioactive molecules from the polymeric structure. In addition, change in the physicochemical properties of drugs or degradation process might take place. The

presence of impurities also affects the shelf life of the drugs. Hence, the drug-loaded hydrogels must be stored under appropriate conditions for maintaining the shelf life (Çalış et al., 2019; Edlund & Albertsson, 2003).

2.7 Therapeutic agents/drugs

2.7.1 Classification of drugs

Drugs can be generally classified into two types: hydrophilic and hydrophobic drugs. Based on Biopharmaceutics Classification System (BCS), hydrophilic drugs are categorized in class III compounds whereby they are highly soluble in water with low cell permeability. These compounds are mainly larger and charged molecules (Martin et al., 2016; Papich & Martinez, 2015). For instance, ascorbic acid, cobalamin, folic acid, riboflavin and water-soluble vitamins (Vitamin B & C). Whereas, hydrophobic drugs are belong to class II drugs substances in which they have low water solubility but high cell permeability (Martin et al., 2016; Papich & Martinez, 2015). Griseofulvin, acyclovir, flufenamic acid, aceclofenac, diazepam, glipizide and fat-soluble vitamins (vitamin A, D, E and K) are some of the examples of lipophilic therapeutic agents (Bhowmik et al., 2013).

Over 70% of the drugs in the current market as well as the newly discovered chemical entities are predominantly poor water-soluble or lipophilic compounds but exhibiting wide variety of physiological functions. This poses challenges in pharmaceutical industry as high doses of lipophilic drugs are required to achieve therapeutic plasma concentrations after oral administration. Hence, extensive researches are required to improve their bioavailability and subsequently contribute to dose reduction (TD Tran & HL Tran, 2017). Various strategies such as solid dispersions and emulsifications have been developed to improve the therapeutic index of lipophilic compounds (T. N. Nguyen et al., 2017; Tran et al., 2009).

2.7.2 Chemical structure and sources of vitamin E

In 1922, vitamin E was extracted from green leafy vegetables by Herbert Evans and Katherine Bishop and has been described as an essential fertility factor (Evans & Bishop, 1922). Vitamin E consists of two predominant groups which are tocopherols and tocotrienols. They exhibited similar chemical structures as shown in Figure 2.3. Tocopherols consist of a chromanol ring with a saturated C_{16} tail and the tocotrienols are structurally different from the tocopherols in which three trans double bonds are located at positions 3', 7' and 11' in the hydrocarbon chain (Sen et al., 2006). Both tocopherols and tocotrienols contain four chemically distinct analogues: alpha (α), beta (β), gamma (γ) and delta (δ)-tocopherols and α, β, γ and δ-tocotrienols, that are distinguished based on the number and the position of methyl groups attached to their chromanol rings (Aggarwal et al., 2010). Vitamin E appears as a crucial lipid-soluble nutrient with antioxidative property, which could not be produced by the body but instead to obtain from food and supplement (Sen et al., 2006).

Tocopherols

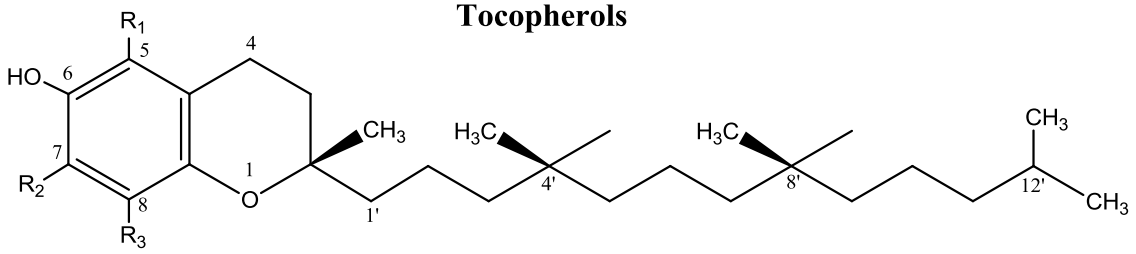

Tocotrienols

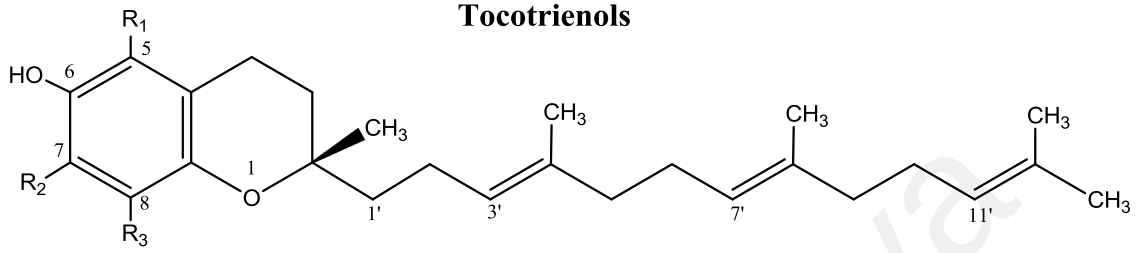

Isomers	R_1	R_2	R_3
α	CH_3	CH_3	CH_3
β	CH_3	H	CH_3
γ	H	CH_3	CH_3
δ	H	H	CH_3

Figure 2.3: Chemical structures of tocopherols and tocotrienols and their isomers.

2.7.3 Clinical benefits of tocopherols and tocotrienols

Vitamin E emerged as one of the prominent natural resources that plays numerous essential roles beyond that of its antioxidant function (Ying Yang & McClements, 2013). Vitamin E is widely consumed due to its multiple health benefits and it has been shown to be effective against several chronic diseases that associated with oxidative stress such as cardiovascular diseases (Jialal & Devaraj, 2005), atherosclerosis (Upston et al., 2003), and cancer (I.-M. Lee et al., 2005). However, only α-tocopherol was intensively studied because the hepatic α-tocopherol transfer protein (α-TTP) in human body is preferentially bind to α-tocopherol (Irías-Mata et al., 2018). The half-life of RRR-α-tocopherol (57 ± 19 hours) was found to be 3-fold greater than the half-lives of SRR-α-tocopherol (Traber & Atkinson, 2007) or γ-tocopherol (Leonard et al., 2005), evidencing the favorable binding of α-TTP with RRR-α-tocopherol. In addition, various non-α-tocopherol forms are metabolized in preference to α-tocopherol (Traber & Atkinson, 2007). With these reasons, D-α-tocopherol or RRR-α-tocopherol exhibited the highest bioavailability and their health potentials have often been discovered against the other forms of vitamin E (Sen et al., 2006).

Oxidative degradation of low-density lipoprotein was believed to be the key factor causing atherosclerosis (Sen et al., 2006). α-tocopherol is well known as the major peroxyl radical scavenger present in human lipoproteins, which effectively suppresses the biological oxidation processes in tissues (Terentis et al., 2002; Traber & Stevens, 2011). The importance of human α-TTP in maintaining the plasma α-tocopherol concentrations was reflected in the experiments conducted by Yokota et al. (2001) and Terasawa et al. (2000). They observed severe vitamin E deficiency in mice after removing the α-TTP gene, which resulted in increased level of oxidative lipid damage and erythrocyte hemolysis. α-tocopherol plays numerous essential roles beyond that of its antioxidant function. α-tocopherol is responsible in avoiding the platelet adhesion. Steiner (1993)

investigated the antiadhesive effect of α-tocopherol, in which 400 IU/day of α-tocopherol aided in inhibiting more than 75% platelet adhesion to adhesive proteins when carried out in a laminar flow chamber at low shear rate. α-tocopherol was believed to decrease the number and size of pseudopodia upon platelet activation.

Tocotrienols attracted minimal attentions due to the favorable recognition of α-tocopherol by α-TTP as well as the preferential metabolism of non-α-tocopherol forms (Traber & Atkinson, 2007). Tocotrienols were identified to possess unique nutritional functions such as cholesterol-lowering (Sen et al., 2006), anticancer (Ahsan et al., 2014) and neuroprotective properties (Khanna et al., 2003). For instance, oral administration of palm oil-based α-tocotrienol at nanomolar concentrations was reported to be able to attenuate the stroke-mediated neuropathy. This is because α-tocotrienol exhibits distinctive neuroprotective properties in which it can reduce both enzymatic and non-enzymatic mediators of polyunsaturated fatty acids metabolism and neurodegeneration in the central nervous system. Figure 2.4 illustrated some of the physiological functions of tocotrienols. All these health functions are often not exhibited by tocopherols. In addition, the antioxidant properties of tocotrienols are found to be more potent than tocopherols (Sen et al., 2006).

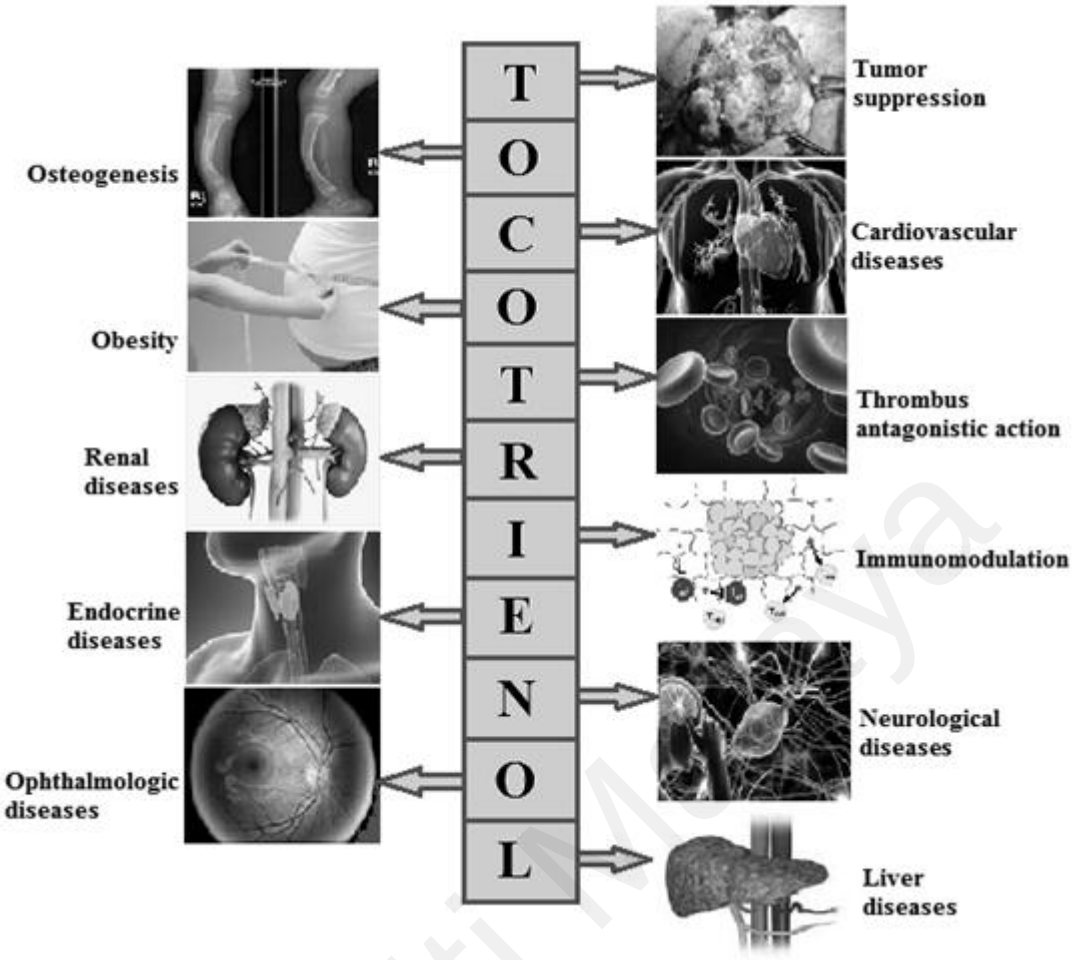

Figure 2.4: Physiological functions of tocotrienols in controlling some of the health problems and diseases (Aggarwal et al., 2010).

Lack of research carried out on tocotrienol predominantly because of its inferior bioavailability as compared to α-tocopherol because α-TTP in human body has higher affinity towards natural α-tocopherols than tocotrienols (Sen et al., 2006). Despite of this, oral administration of tocotrienols resulted in plasma tocotrienol concentration of 1μM as reported in the previous study (O'Byrne et al., 2000), which is sufficient to prevent inducible neurodegeneration (Khanna et al., 2003). Figure 2.5 displays the tocotrienol contents in some of the natural sources. Palm oil is the richest natural source of the lesser characterized vitamin E, α-tocotrienol, thus, palm oil-derived tocotrienol rich fraction was selected in this study.

Figure 2.5: The contents of tocotrienols in various natural sources.

2.8 Techniques for the encapsulation of lipophilic therapeutic agents using hydrogel-based carrier

Hydrogel is an ideal material for delivery of therapeutic moieties due to its highly porous structure. The degree of porosity is governed by the cross-link density in the gel matrix. Owing to this unique structure, it allows the bioactive materials to be encapsulated within the gel matrix and followed by the release of drugs at the targeted local site via the diffusion of drugs through the gel matrix (Hoare & Kohane, 2008). Although there are numerous advantageous properties of hydrogels, the application of hydrogel as drug carrier is limited when it comes to transdermal delivery of lipophilic drugs. Due to the hydrophilic nature of the polymer matrix, integration of hydrophobic drugs into hydrogels becomes a major challenge (J. J. Pillai et al., 2014). Inhomogeneity of encapsulated hydrophobic compound and the hydrogel may reduce the stability of the system and result in relatively rapid drug release (J. Li & Mooney, 2016). This limitation has encouraged the modification of hydrogels to make it possible to deliver the hydrophobic compounds. Hydrophobically modification of hydrogels is one of the approaches to enhance the compatibility of hydrophobic drugs with hydrogels. The hydrophobic domain can be coupled to a hydrophilic polymer segment by copolymerizing hydrophobic monomers into hydrogel matrix (Hoare & Kohane, 2008). However, the inclusion of drug-loaded lipid nanoparticles within hydrogel scaffold is a more sophisticated system with higher encapsulation efficiency (Larrañeta et al., 2018). Water insoluble drugs can first be efficiently encapsulated into lipid nanoparticles via emulsification, which then they are immobilized into the hydrogel matrix by cross-linking method. This double encapsulation strategy can control over the release of the drug, while benefiting from the biological properties of the hydrogel (Desfrançois et al., 2018).

2.8.1 Hydrophobically modified hydrogels for encapsulation of lipophilic drugs

Due to the hydrophilicity of hydrogels, the encapsulation efficiency and the homogeneity of lipophilic drugs loading into hydrogels remain as great challenges for hydrogels to be effective drug vehicles (Pourjavadi et al., 2018). Besides, rapid or burst release of hydrogels is another concern in the development of drug delivery system (Kang-Mieler et al., 2017). Hence, various strategies have been explored to facilitate the application of hydrogels as drug carriers with prolonged drug release and able to load various types of drugs. Hydrophobically modification of hydrogels is one of the well-known approaches to improve the interactions between lipophilic drugs and hydrogel matrix as well as to enhance the encapsulation efficiency of hydrogels (Gu et al., 2017; Takei et al., 2020). Hydrogels can be modified via copolymerization of polymers with hydrophobic segments to hydrophilic polymeric matrix, introducing the binding sites for lipophilic drugs. Alternatively, polymer amphiphile can also be achieved by grafting of hydrophobic side chains (Hoare & Kohane, 2008).

For instance, hydrophobically modified N,O6-partially acetylated chitosan hydrogels were synthesized for achieving sustained release of vitamin E (Quiñones et al., 2013). DL-α-tocopherol was conjugated to N,O6-partially acetylated chitosan via reaction with 1-ethyl-3-(3-dimethylaminopropyl) carbodiimide hydrochloride (EDC) and N-hydroxysuccinimide. The release profile of tocopheryl-modified N,O6-partially acetylated chitosan followed zero order kinetics during the first 6–7 h, reaching cumulative release of 39% after 96 h. The antioxidant activities of the resultant nanoparticles were evaluated through the *in vitro* test of DPPH (1,1'-diphenyl-2-picrylhydrazyl) at 2, 4, 6, 8 and 96 h in pH 6.0 phosphate buffer saline. % radical scavenging activities of tocopheryl-modified N,O6-partially acetylated chitosan gels were monitored to be 35%, 44%, 61%, 75% and 81%, respectively.

In addition, M. Wu et al. (2013) modified alginate hydrogels via esterification process using 1,10-decanediol as both cross-linker and hydrophobic component. Covalently crosslinked and hydrophobically modified alginate hydrogels were employed as delivery systems for the hydrophobic drug, ibuprofen. Covalently crosslinked alginate hydrogels showed enhanced stability in salt solutions. Using unmodified Ca-alginate hydrogel as a control, the encapsulation efficiency was improved from 20.6% to 49.8% after the esterification of alginate with 1,10-decanediol at molar ratio [COOH] : [OH] of 1 : 2. Highly modified and stable alginate hydrogels demonstrated remarkable programmed release profiles with the cumulative release of drug decreased from 78.0% to 52.6% in 8h with the increasing of the amount of 1,10-decanediol added from 0.25 g to 0.99 g. Hence, the drug loading was significantly improved after the incorporation of hydrophobic segments onto the alginate matrix.

Other type of hydrophobic modified alginate has been synthesized by incorporating hydrophobic octylamine chains onto alginate through a carbodiimide-facilitated reaction under low pH condition. This hydrophobically modified alginate was used to encapsulate the anti-inflammatory drug, sulindac. Hydrophobically modified hydrogels were produced with two different degree of substitution, 0.14 and 0.18 using pure alginate hydrogel as control sample. The maximum solubility of drug in both pure alginate and hydrophobically modified alginate solutions were found to be 0.15 wt% and 1.5 wt%, respectively, indicating that modified alginate has better drug loading capacity. It was observed that sulindac was fully released from the pure alginate gels after 2 days in dissolution medium. However, the complete release of sulindac from hydrophobically modified alginate gels was extended up to 5 days. Different degree of substitution showed insignificant effect on the release studies (Choudhary et al., 2018).

Alternatively, Pourjavadi et al. (2018) fabricated hydrophobic hydrazine oleate grafted alginate dialdehyde (AlgOA) coated with MNP/OA as magnetic nanocarrier to carry lipophilic anticancer drugs, doxorubicin hydrochloride (DOX) and paclitaxel (PTX) by allowing the drug molecules to adsorb physically to its surface. The results showed that a large amount of anticancer cells was encapsulated into nanocarriers, in which maximum loadings of DOX and PTX were 282.3 ± 11 mg/g and 316.4 ± 30 mg/g, respectively. The *in vitro* cytotoxicity assay was carried out on MCF-7 human breast carcinoma and HeLa cells. They observed that the cell viability of drug-laden delivery systems was lower than the free drugs. This indicate that the anticancer drugs were highly toxic to cancerous cells when they are encapsulated within nanocarriers.

2.8.2 Immobilization of drug-laden emulsions within hydrogels

Formation of composite hydrogels is another remarkable technique to overcome the inherent pharmacological limitations of hydrogel as potential drug carrier. This technique involves the encapsulation of drug-loaded surfactant-stabilized emulsions into hydrogels which normally produced in the form of microspheres. Production of emulsions increases the solubility of poorly soluble drugs (GR, 2015) and subsequent encapsulation of drug-loaded emulsions into hydrogels serves as protective barrier for moderating the burst release of drugs (Jacob et al., 2021). This method can be achieved by mixing emulsions with hydrous sol prior to the formation of hydrogels in the presence of cross-linkers (Chaemsawang et al., 2018). Table 2.1 shows the maximum encapsulation efficiency of different polymeric matrix for loading various drugs.

Table 2.1: Highest encapsulation efficiency of different polymeric matrix for loading of drugs.

Polymeric matrix	Bioactive molecules	Highest encapsulation efficiency (%)	Reference
Xanthan gum/starch	Vitamin E	66.8	M. Jiang et al. (2019)
Pectin/alginate	α-tocopherol	52.11	Singh et al. (2018)
Alginate	Curcumin	90.3	Xiao et al. (2015)
Chitosan/alginate	Sudan orange G	80	Ribeiro et al. (1999)
Alginate	Thyme essential oil	85	Benavides et al. (2016)
Chitosan/alginate	Tocotrienol	84.9	P. Y. Tan et al. (2018)
Gum acacia-galactomannan	Tocotrienol	70	Tarigan et al. (2018)
Maltodextrin-sodium caseinate	Vitamin E	71.5	Selamat et al. (2018)

M. Jiang et al. (2019) fabricated starch-based microcapsule for the delivery of vitamin E via spray-drying microencapsulation with the incorporation of xanthan gum (XG) as acid-resistant and anti-enzymolysis material to slow down the *in vitro* drug release in the stomach (Newton et al., 2014). Degree of substation (DS) of acid-hydrolyzed carboxymethyl starch (H-CMS) is one of the key determinants for the encapsulation efficiency whereby H-CMS with higher DS tends to improve the encapsulation efficiency of the microcapsules as emulsions with enhanced stability can be produced. Microcapsules produced from H-CMS with DS of 0.4382 and the ratio of XG-H-CMS at 1:20 attained the minimum release (38.32%) in the simulated gastric fluid but desirable release (61.68%) in the simulated intestinal fluid. This was favorable because upper part of small intestine is the desirable site of action.

In addition, Singh et al. (2018) fabricated pectin/alginate microcapsules via ionic gelation for loading α-tocopherol. α-tocopherol-loaded emulsions stabilized by Tween 80

were first produced and subsequently immobilized into pectin/alginate microcapsules. Optimum formulation using 1.5% w/v of sodium alginate and 2.0% w/v pectin resulted in the highest encapsulation efficiency of 52.11%. The encapsulation efficiency of microcapsules also increased upon increasing the core and wall ratio from 0.6 to 1.0. This indicated that the thin layers of materials are insufficient to load increasing amount of the oils, leading to the instability of the oil droplets in the emulsion (Hogan et al., 2001). The % yield for each formulation of pectin/pectin alginate microencapsules were determined to be above 90%. Furthermore, Xiao et al. (2015) observed that kafirin protein nanoparticles-stabilized Pickering emulsion failed to withstand high temperature (i.e., 60 ^{o}C) and alkaline (i.e., pH = 8.5) treatments. The emulsion droplets are also susceptible to proteolysis in gastric digestive fluid. Thereafter, the researchers immobilized kafirin nanoparticles-stabilized Pickering emulsions (KPEs) within alginate hydrogel strips via ionic crosslinking in $CaCl_2$ solutions (Xiao et al., 2017). The emulsion embedded hydrogels (EGs) allowed them to entrap curcumin, a lipophilic drug with enhanced storage and sustained release behavior.

Benavides et al. (2016) encapsulated thyme essential oil (TEO) into alginate microspheres via ionotropic gelation technique. The effect of dispersion degree/homogeneity of TEO on the encapsulation efficiency (EE%) of resultant microspheres were studied. The results showed that higher EE% was achieved for the microspheres containing 18000 rpm agitated-emulsions. High degree of dispersion indicated the formation of highly homogenous emulsions and allowed them to be well distributed within the alginate matrix. In addition, concentration of TEO (1%, 2% and 3% v/v) added is also one of the key determinants for the EE% of the resultant alginate microspheres whereby the increased in TEO content showed an adverse effect on the EE% of the microspheres. According to the results, highest EE% (>85%) was achieved

for microspheres loading with emulsions that prepared from 2% v/v TEO blended at 18000 rpm.

Moreover, Ribeiro et al. (1999) fabricated chitosan-coated alginate microbeads encapsulating Sudan orange G-loaded oil-in-water-in-oil (O/W/O) emulsions. The EE% was enhanced after the chitosan coating with the highest EE (80%) observed for the microspheres coated with highest molecular weight chitosan. In addition, the release of Sudan orange G from the uncoated alginate microspheres was higher as compared to chitosan-coated alginate microspheres and decreased with the increasing of chitosan molecular weight. P. Y. Tan et al. (2018) also produced chitosan-coated alginate microcapsule but for the loading of tocotrienol-containing emulsions. Resultant tocotrienol microcapsules exhibited considerably high encapsulation efficiency of 84.9 ± 2.2%. Chitosan-alginate microcapsules serve as protective walls to reduce the deterioration of loaded tocotrienols by decreasing the exposure of compounds to oxidation stimulants.

Tarigan et al. (2018) immobilized tocotrienol-rich fraction extracted from palm fatty acid distillate into gum acacia-galactomannan microcapsules by applying spray drying method. The final yield of microcapsules with and without galactomannan was observed to be 64.1% and 53.2%, respectively. Besides, the incorporation of galactomannan into microcapsules increased the encapsulation efficiency by 9.3%. The findings demonstrated that the p-anisidine value of the tocotrienols that loaded into microcapsules with the addition of galactomannan was lower, indicating that the combination of galactomannan and gum acacia served as an excellent protective wall for the tocotrienol-rich fraction.

Selamat et al. (2018) employed the spray drying method to encapsulate palm mixed tocotrienols and tocopherol concentrate within maltodextrin/sodium caseinate matrix.

Maltodextrin functions to prevent the oxidation of vitamin E concentrate whereas sodium caseinate was used to be a stabilizer in the encapsulation process. The core retention was significantly correlated by the oil content in the microcapsules as it increased with an increasing of core/wall ratio. Moreover, the antioxidant activity was greatly influenced by the total content of tocopherol and tocotrienol. The optimum formulation that possessed highest core retention (71.5%) with moderate radical–scavenging activity (43%) was observed to be the microcapsules that made up from 18.5 w/w% of maltodextrin, 7 w/w% of sodium caseinate and 24.5 w/w% of vitamin E concentrate. The optimum formulated blend was selected for further storage stability test at 5 ^{o}C, 28 ^{o}C and 50 ^{o}C using non-encapsulated sample as a control over 4 weeks of storage period. It was observed that more than 80% of encapsulated vitamin E concentrate was retained after storage period for whole range of temperature. Regardless the temperature, less than 50% of non-encapsulated vitamin E was remained after 4 weeks.

2.9 Emulsification

Emulsification is one of the well-established steps in the microencapsulation of oils. This approach generally enhanced the solubility of lipophilic bioactive compounds in aqueous solution (Odriozola-Serrano et al., 2014).

2.9.1 Type of emulsion

An emulsion is a heterogeneous system comprising of two or more immiscible liquids whereby a liquid medium (disperse phase) is dispersed in another liquid medium (continuous phase) in the form of droplets (Adams et al., 2007). Emulsion can be generally classified into two types: oil-in-water (O/W) or water-in-oil (W/O) based on the volume ratio of the two liquids, the sequence of addition and the nature of the emulsifier. However, these systems demonstrate a minimal stability that can be accentuated by third components, namely, the emulsifiers such as surfactants and finely divided solid particles (Maphosa & Jideani, 2018).

Both W/O and O/W emulsions can be produced in different sizes, which are macroemulsions (1–2 μm), micellar emulsions (5-50 nm) and nano-emulsions (20-200 nm) (T. F. Tadros, 2013). The key determinant for the final droplet diameters of emulsions is the rate of droplet break-up and droplet re-coalescence during emulsification (Zafeiri et al., 2017). Nano-emulsions with small droplet sizes can be optically translucent to slightly milky. Owing to their small sizes, the Brownian motions of nano-emulsions are sufficiently high to overcome the sedimentation or creaming. Thus, nano-emulsions with prolonged physical stability can be achieved (Laouini et al., 2012). Nano-emulsions are kinetically stable but they are thermodynamically unstable, which indicates that they tend to breakdown during storage (Rao & McClements, 2012).

Nano-emulsions have garnered considerable attentions in researches due to their inherent high colloidal stability. They also demonstrated several advantages over

conventional emulsions such as low concentration of surfactant (less than 10% surfactant) is required for the preparation. In addition, nano-emulsion systems with large surface area accommodate the efficient delivery of bioactive molecules. The striking properties of this system makes it a potential candidate in diverse fields, which include pharmaceutical, food and cosmetic industries (Laouini et al., 2012).

Furthermore, there is another complex system called multiple emulsion whereby both W/O and O/W emulsions exist simultaneously. Basically, there are two types of multiple emulsions: water-in-oil-in-water (W/O/W) emulsion and oil-in-water-in-oil (O/W/O) emulsion. Conventional homogenization technology involves two-steps procedure in synthesizing multiple emulsions. In order to prepare O/W/O emulsions, O/W emulsions are first produced in which the small oil droplets dispersed in larger water droplets. This is followed by re-emulsified the resultant O/W emulsions in an oil continuous phase. A pair of hydrophilic and lipophilic emulsifiers is required in this process to stabilize O/W and W/O emulsions, respectively (Niknam et al., 2020). Mechanical-induced stresses during second homogenization stage are undesirable because it leads to disruption of primary O/W emulsion droplets that consequently reduce the yield of multiple emulsions (Phillips & Williams, 2009). This can be solved by employing a low-shear mixer for the second step of emulsification. Nevertheless, this approach usually synthesizes highly polydisperse and coarse emulsion droplets with poor creaming stability.

2.9.2 Emulsifications using high energy approaches

Emulsification technique is a key determinant for the droplet diameter of the resultant emulsions (Laouini et al., 2012). Conventional methods such as low-shear mixing and rotor-stator homogenization tend to produce polydisperse emulsions because the dissipated energy is uncontrollable and inefficient, influencing the stability of the emulsions (Urban et al., 2006). Typically, production of nano-emulsions can be achieved by energy-intensive shearing processes such as homogenization, ultrasonication and microfluidization (Mahdi Jafari et al., 2006).

2.9.2.1 Homogenization

Homogenization is the most common technique to produce micron size emulsions. High pressure homogenization works with a simple principle whereby a coarse emulsion passes through a narrow valve in which the breakdown of emulsion droplets occurs due to the intense shear and cavitation (David Julian McClements, 2015). The droplet diameter of the resultant emulsion can be manipulated by tuning the pressure of the homogenizer and the gap size of the valve. Smaller emulsion droplets can be obtained by increasing the pressure and decreasing the gap size (Desrumaux & Marcand, 2002).

2.9.2.2 Microfluidization

Microfluidizer has been recognized to be the most powerful homogenizer, employing in the production of nano-emulsions (Jafari et al., 2007b; Leong et al., 2009; Wooster et al., 2008). In microfluidization, coarse emulsions pass through an intensifier pump followed by Y- or Z-type geometry interaction chamber in which deformation of emulsion droplets can be achieved by high shearing action and impacts against the channel walls and colliding streams (Spence et al., 2011; Zimmermann et al., 2010). Emulsification by microfluidization is more effective as compared to the other types of conventional homogenizations. This energy extensive device produces exceptionally fine

emulsion droplets with a narrower size distribution and improved long-term stability (Mahdi Jafari et al., 2006).

However, microfluidization is a high cost production approach and high maintenance is required for the instrument. Ultrasonic homogenizer is an alternative to the microfluidizer for practical purpose. Contamination of samples can be avoided because the ultrasonic probe can be cleaned easily and this device capable of achieving similar local power densities through cavitation (Leong et al., 2009). Although microfluidization is superior than ultrasonication in terms of the resultant emulsion droplet size and energy efficiency, but the high production cost and equipment contamination issue are the constraints for the usage of microfluidizer (Kentish et al., 2008).

2.9.2.3 Ultrasonication

Compared to mechanical agitation by low-shear mixer, ultrasonic emulsification can produce less polydisperse and more stable emulsions. It works on the principle of acoustic cavitation. Cavitation is a mechanism accountable for ultrasonically generated effects (Leong et al., 2009). Cavitation involves the formation, growth and subsequent collapse of vapor cavities in a flowing liquid due to the pressure fluctuations of the acoustic wave (Leong et al., 2009). Such microbubbles formed when the atmospheric pressure is reduced to that of the bubbles (Mahdi Jafari et al., 2006), expanding through a few acoustic cycles into larger size before collapsing violently when the collapse pressure of cavitation bubbles is dominated (Kaltsa et al., 2014). The collapse of these microbubbles causes the propagation of powerful shock waves throughout the solution in proximity to the sonotrode tip, resulting in the implosion and finally breaking the dispersed liquid (Canselier et al., 2002). This cavitation is proportional to the ultrasonic intensity as expressed through the amplitude applied (Gaikwad & Pandit, 2008).

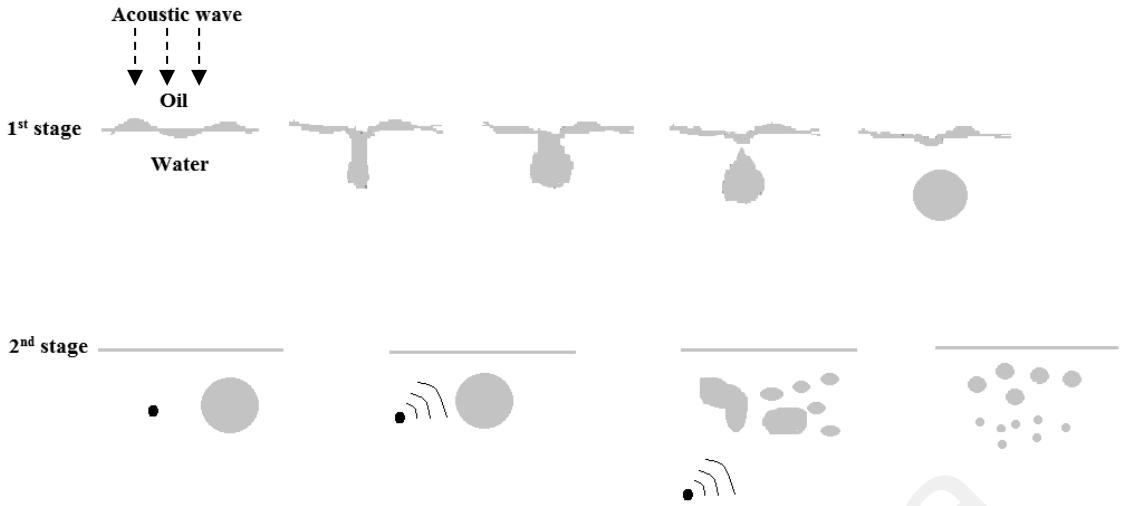

Figure 2.6: Ultrasound emulsification – Formation and break down of droplets.

In some previous studies, higher ultrasonic amplitude induced droplet coalescence as evidenced by the increased droplet size. This phenomenon is known as "over-processing" (Jafari et al., 2007a). The frequency of droplet collision increased due to its high kinetic energy at elevated ultrasonic amplitude, favoring droplet coalescence (Ng et al., 2017). Since the droplet disruption and recoalescence occur simultaneously during the emulsification, the competition between these two opposite processes can affect the droplet size of the resultant emulsions (Jafari et al., 2008b). During droplet disruption, a rapid casing of the oil-water interfaces of the newly formed droplets by surfactant is required to impede the immediate recoalescence of droplets. Upon increasing of the sonication intensities, the droplets move faster and diffuse with each other, leading to recoalescence before the surfactant can completely cover the interfaces. Therefore, droplet recoalescence is inevitable when the relative rate of drop collision is greater than the surfactant adsorption (Mahdi Jafari et al., 2006). Above the optimum amplitude, chemical degradation of the surfactant by H• and •OH radicals that formed during the thermal decomposition of water molecules can be possible .

2.9.3 Emulsion instability

Various breakdown processes may occur on storage and can be distinguished as illustrated in Figure 2.7.

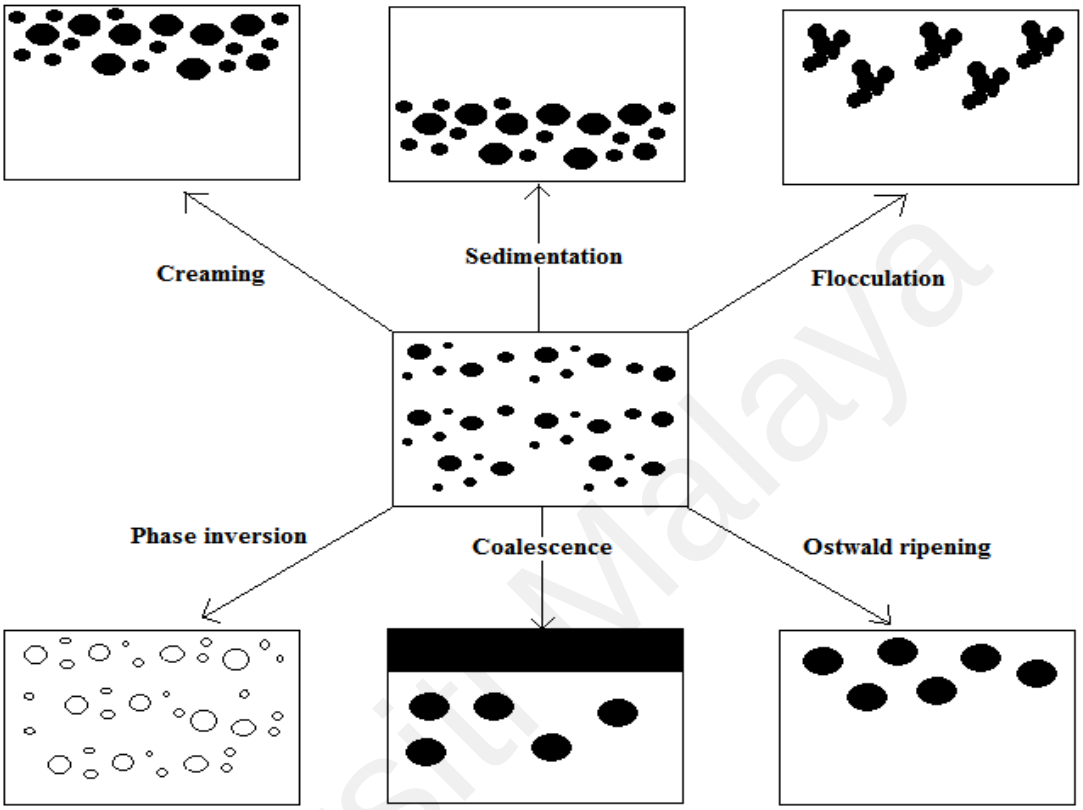

Figure 2.7 Various breakdown processes of emulsions.

2.9.3.1 Creaming and Sedimentation

Creaming or sedimentation occurs when the gravitational or centrifugal forces surpass the Brownian motion of the droplets. Creaming or sedimentation is greatly influenced by the relative densities of dispersed and continuous phase. Creaming takes place when dispersed droplets with lower density array on top of the emulsion system. Conversely, the dispersed droplets will tend to move downward when its density is higher than the continuous phase, forming a separate layer at the bottom of the system. This phenomenon is known as sedimentation. Emulsions with tiny droplets can reduce the gravitational separation because Brownian motion will be dominated in this case (T. F. Tadros, 2013).

David Julian McClements (2011) observed that emulsion droplet size less than 10 nm inhibited the occurrence of creaming.

2.9.3.2 Flocculation

Flocculation is resulted from the aggregation of droplets, whereby the *van der Waals* attractive forces exceed the repulsive forces while remaining their physical properties. This process may be reversible or irreversible, relying on the magnitude of the attractive forces (T. Tadros, 2013). The rate of flocculation can be tailored by regulating the colloidal interactions between droplets such as steric stabilization by utilizing nonionic surfactants or polymers, electrostatic stabilization by employing ionic surfactants and electrosteric by using mixed emulsifier systems of ionic and nonionic surfactants (Roman Pichot, 2012).

2.9.3.3 Ostwald Ripening (Disproportionation)

Ostwald ripening is a common phenomenon that takes place in the emulsion systems whereby the energetically unstable surface particles have the affinity to shrink over time in the emulsions, increasing the number of free particles in the system. These free particles will merge with each other to form larger droplets. On the other hand, the tiny particles tend to decrease in size and eventually disappeared from the emulsion system. Shrinking and growing of particles will result in the emulsions with high polydispersity (T. Tadros, 2013).

2.9.3.4 Coalescence

There is a layer of thin film exists between the droplets in the continuous phase, serving as a barrier to impede the merging of two droplets (Sanfeld & Steinchen, 2008). Coalescence is the process of fusion of two or more droplets to form larger single droplet and subsequently resulting in the complete separation of emulsions into two distinct layers. The rupture of the thin films between the droplets leads to the aggregation of

droplets and initiates the occurrence of this process (Walstra, 2002). However, emulsifier molecules can protect the thin film from rupture by adhering at the oil-water interface and forming an interfacial membrane around the droplets (T. F. Tadros, 2013). For instance, the presence of ionic surfactants with positive or negative charges in the emulsions induces electrostatic repulsions between the droplets, hindering the close approach of droplets. Whereas, solid particles irreversibly adhere at the oil-water that hinder the coalescence of droplets (Roman Pichot, 2012).

2.9.3.5 Phase Inversion

Phase inversion is another undesirable condition in emulsification whereby it involved the transition of disperse phase to continuous phase and vice versa. For instance, O/W emulsion can be inverted to W/O emulsion or in another way round, which might be driven by composition or temperature changes . There are several ways to prevent the phase inversion such as (a) by lowering the volume fraction of the disperse phase; (b) coating with polymer to promote the viscosity of the emulsions and (c) by employing the appropriate surfactants (T. Tadros, 2013).

2.9.4 Optimization of the formation of emulsions

2.9.4.1 Droplet charge

The surface charges of droplets can be determined by zeta-potential measurement that provides information about the physical stability of emulsions (J. Jiang et al., 2009). In general, the zeta-potential of emulsions should be either less that −30 mV or more than +30 mV in order to achieve an excellent electrostatic stabilization due to the strong repulsive forces of droplets (Uchegbu et al., 2013). Dispersions with insufficient zeta-potential values will eventually result in particle agglomeration and flocculation attributed to the interparticle interactions such as *van der Waals* attractive forces, hydrogen bonding and hydrophobic interactions (Hunter, 2013; Shah et al., 2014). However, droplet size, dispersed phase volume fraction and continuous phase characteristic are also the key determinants for the stability of the emulsions.

2.9.4.2 Droplet size

The emulsion stability as well as the release rate of drugs are significantly influenced by droplet diameter. Nano-emulsions with mean diameter less than 100 nm are often favorable to attain outstanding physical stability (Ding et al., 2018). The presence of surfactant, oil content and homogenization pressure and cycle are essential parameters that determine the emulsion droplet diameters. With constant homogenization pressure and cycle, the rise in emulsion droplet size can be resulted upon increasing of oil content or in the presence of low concentration of surfactant. During the homogenization process, shear forces are applied to disintegrate the larger droplets into smaller ones and sufficient amount of surfactants must be present in order to quickly and completely cover the freshly formed oil droplets. With this reason, surfactant molecules can impede the immediate re-coalescence of droplets that will subsequently result in the of droplet broadening. The droplet diameter of emulsions can also be tuned by adjusting the homogenization parameters. Elevation of homogenization pressure can minimize the average droplet

diameter. Upon increasing of the homogenization pressure, relative rate of drop collision is greater than the surfactant adsorption, leading to droplet recoalescence (Mahdi Jafari et al., 2006). Hence, several parameters such as homogenization time, number of cycles and pressure have to be optimized to obtain small droplets with remarkable stability.

2.9.4.3 Dispersed phase volume fraction

The dispersed phase (oil phase) volume fraction also contributes to the stability of the emulsions (Mollakhalili Meybodi et al., 2014). The formation of smaller size droplets could be possible at low oil content. However, the emulsion stability reduces with the increasing of the oil concentration ascribed to the elevated viscosity that affects the homogenization efficacy, facilitating the droplet broadening. In addition, the enlargement of droplet size occurs in the presence of higher oil concentration mainly due to the emulsifiers available for assembling at the newly formed oil-water interfaces are insufficient (Derkach, 2009). This was evidenced by the previous study (Baloch & Hameed, 2005) whereby the turbidity of emulsion increased upon increasing the concentration of oil. This is a good indication for the enlargement of droplet size because the turbidity is very sensitive to size. At low emulsifier concentration and less intense homogenization, it was observed that increased in the dispersed phase volume fraction tend to reduce the droplet surface area as well as promote the polydispersity of the emulsion (Dapčević Hadnađev et al., 2013).

2.9.4.4 Continuous phase characteristics

Rheological properties of emulsions provide clues on the stability of emulsions. The viscosity of the continuous phase plays a vital role in the formation of highly stable emulsions (Mollakhalili Meybodi et al., 2014). Hydrocolloids such as chitosan, alginate and starch are commonly employed as thickening agents that enhance the viscosity of emulsions. This will eventually improve the shelf stability of emulsions by reducing the

creaming and sedimentation rate via steric hindrance, electrostatic interactions and viscosity effect (David Julian McClements, 2015). Nevertheless, excess hydrocolloid concentrations could enhance the emulsion stability via depletion flocculation (D. McClements, 2000).

2.9.5 Surfactant as surface-active agent for emulsion formation

The surfactant is a crucial element in emulsion system whereby it rapidly covers the freshly formed oil-water interface prior to the droplet re-coalescence. It further promotes the droplet break-up during emulsification by lowering the interfacial tension. Surfactants have both hydrophilic and hydrophobic segments and the inherent amphiphilic character allows them to act as surface active agents (R Pichot et al., 2009). The surfactant molecule orients itself so that the hydrophobic domain attaches to the hydrophobic part and the hydrophilic domain adheres to the hydrophilic part (T. F. Tadros, 2013). The selection of surfactants with different hydrophilic-lipophilic balance (HLB) determined the type of emulsion produced. The selection of surfactant for specific purposes can based on the guideline as shown in Table 2.2 (T. F. Tadros, 2013). Hydrophilic surfactants with high HLB facilitate the formation of O/W emulsions as they curve towards the oil phase, while lipophilic surfactants with low HLB values tend to stabilize W/O emulsions, in the opposite way (R Pichot et al., 2009).

Table 2.2: HLB range and its application (T. F. Tadros, 2013).

HLB range	Application
3-6	W/O emulsifier
7-9	Wetting agent
8-18	O/W emulsifier
13-15	Detergent
15-18	Solubilizer

The mixed emulsifier systems have been long appreciated to induce long-term emulsion stability against coalescence (R Pichot et al., 2009). HLB values for the mixed emulsifier systems were determined using the equation 2.1 established by Griffin (1949) as shown below:

$$HLB_{mix} = HLB_A\ A\% + HLB_B\ B\% \quad (2.1)$$

where HLB_{mix}, HLB_A and HLB_B are the HLB values of mixed surfactants, individual surfactant A and individual surfactant B, respectively. A% and B% are mass percentages of surfactant A and B in the mixed systems.

Food grade emulsifiers such as whey protein isolate (WPI) and gum Arabic are widely used in producing edible nano-emulsions. Nevertheless, food grade emulsifiers exhibit low mobility and adsorption rate at freshly formed droplet interfaces due to their large molecular weight, leading to re-coalescence of emulsion droplets (Jafari et al., 2006). Small molecular weight nonionic emulsifiers are promising alternative surfactant that aid in the emulsion stabilization. They can diffuse quickly and adhere onto a newly formed O/W interface, producing emulsions with high stability. In addition, nonionic emulsifiers have well documented low toxicity that suitable for oral administration (G. P. Kumar & Rajeshwarrao, 2011). Moreover, ionic surfactant such as sodium dodecyl sulfate (SDS) is another well recognized surface-active agent but this type of emulsifier is sensitive to the presence of electrolytes (T. F. Tadros, 2013).

Generally, surfactants are classified based on the nature of the hydrophilic portion. These can be distinguished by the charges they carried and namely, amphoteric, nonionic, anionic and cationic that accompanied by counterions in the latter two cases (Rosen & Kunjappu, 2012).

2.9.5.1 Anionic surfactants

Anionic surfactants ionize and form negative charges upon dissolution in water. Anionic surfactants are effective in removing positively charged dirt, clay, particulate soils and some oily stains. Consequently, anionic surfactants are broadly used in laundering, dishwashing liquids and shampoos due to their outstanding cleaning properties (Dave & Joshi, 2017). Most of the anionic surfactants are carboxylates, $C_nH_{2n+1}COO^-X$; sulfonates, $C_nH_{2n+1}SO^{3-}X$; sulfates, $C_nH_{2n+}OSO^{3-}X$; and phosphates, $C_nH_{2n+1}OPO(OH)O^-X$, with n being the range 8–16 atoms and the counterion X is usually Na^+. Anionic surfactants are often introduced with ether groups by treating with polyethylene oxide in order to improve the chemical stability and water solubility of the molecules (Kronberg & Lindman, 2003).

2.9.5.2 Cationic surfactants

Cationic surfactants possess a positively charged hydrophilic head and found to be compatible with non-ionic and amphoteric surfactants (Tadros, 2005). The most common cationic surfactants are the quaternary ammonium compounds with the general formula R'R"R"'R""N^+X^-, where X^- is usually chloride ion and R represents alkyl groups (T. Tadros, 2013). Cationic surfactants are widely used in bactericides (benzalkonium chloride), detergents as fabric softeners (dialkyl dimethyl ammonium chloride) and in some antiseptics. Besides, they also exhibited germicidal properties making them particularly suited for use in bathroom and hand sanitizers (Dave & Joshi, 2017).

2.9.5.3 Amphoteric surfactants

Amphoteric surfactants also known as zwitterionic surfactants, which comprised of both positive and negative charges. The cationic moieties are almost always ammonium ions and the anionic parts can be carboxylate, sulphate and sulphonate ions (Dave & Joshi, 2017). Amphoteric surfactants behave differently at different pH conditions, which make

them unique as compared to other surfactants. The surfactant molecules become positively charged and behave like a cationic in low pH solutions. While in high pH solutions, the molecules acquire negative charges and act like an anionic (T. Tadros, 2013). Amphoteric surfactants are not sensitive to high concentrations acid, alkalis and electrolytes as well they are compatible with all other classes of surfactants. These surfactants are very mild with outstanding dermatological properties that make them useful in personal care, cosmetic and household cleaning products (Dave & Joshi, 2017).

2.9.5.4 Non-ionic surfactants

Non-ionic surfactants are not ionizable in water ascribed to the presence of the non-dissociable hydrophilic groups such as alcohol, ether, phenol, amide, or ester. These surfactants are neutral without any charge that makes them resistant to the deactivation by the ions in the hard water. Non-ionic surfactants are commonly served as emulsifiers in drug delivery system for water insoluble therapeutic agents (Dave & Joshi, 2017). Ethoxylated surfactants are most common nonionic surfactant in which they are prepared via ethoxylation of a fatty chain alcohol. The solubility of the alcohol ethoxylates determined by the alkyl chain length and the number of ethylene oxide units in the molecules. Molecules with an average 12 C chains and more than 5 ethylene oxide units are often soluble in aqueous solution at room temperature. Nevertheless, sorbitan esters and their derivatives (Spans and Tweens) are commercially available that serve as the most vital class of nonionic surfactants. The most common Spans series are sorbitan monolaurate (Span 20), sorbitan monopalmitate (Span 40), sorbitan tristearate (Span 65) sorbitan monostearate (Span 60), sorbitan monooleate (Span 80) and sorbitan trioleate (Span 85). Whereas, the commercially available Tweens series are polyoxyethylene (20) sorbitan monolaurate (Tween 20), polyoxyethylene (20) sorbitan monopalmitate (Tween 40), polyoxyethylene (20) sorbitan monostearate (Tween 60), polyoxyethylene (20) sorbitan monooleate (Tween 80), polyoxyethylene (20) sorbitan tristearate (Tween 65)

and polyoxyethylene (20) sorbitan trioleate (Tween 85). The sorbitan esters are synthesized via treatment of sorbitol with a fatty acid at a high temperature (> 200 C) (T. Tadros, 2013).

In the previous study, Laouini et al. (2012) developed nano-emulsion loaded with vitamin E as a lung targeted drug delivery system via SPG membrane emulsification. Solubilities of vitamin E in different oils and different surfactants were conducted. Numerous oils were tested, which include medium chain triglyceride (MCT), ethylhexyl caprilate/caprate, ethylhexyl laurate, ethylhexyl ethylhexanoate, ethylhexyl stearate, diethylhexyl adipate and isononyl isononanoate. Among all these oils, vitamin E showed the highest solubility in MCT (241.22 mg/ml). Furthermore, it was also vital to investigate the solubility of drug in various surfactants. The surfactants tested in this study were Tween 20 (polyoxyethylene glycol sorbitan monolaurate), Tween 60 (polyoxyethylene glycol sorbitan monostearate), Tween 80 (polyoxyethylene glycol sorbitan monooleate), Span 40 (Sorbitan monopalmitate), Span 60 (Sorbitan monostearate), Brij 35 (polyoxyethylene glycol dodecyl ether), Brij 98 (Polyoxyethylene glycol monooleyl ether) and Labrafil (Oleoyl macrogol-6 glycerides). Some of the structures of non-ionic surfactants are shown in Figure 2.8. They observed that vitamin E demonstrated considerable high solubility in Tween 80 and Brij 35, which were 87.25 mg/ml and 74.32 mg/ml, respectively. Since vitamin E-loaded nano-emulsion consisted of water, MCT as oil phase and Tween 80 or Brij 35 or a mixture Tween 80–Brij 35 50:50 w/w as the surfactants, ternary phase diagram was constructed to determine the ratio for the individual components of the system. Mixed emulsifiers system displayed smaller mean droplet diameter and enhanced physical stability with increased encapsulation efficiency (99.7 ± 0.4%). Hence, the optimum formulation consisted of water, MCT oil and 50:50 w/w Tween 80–Brij 35 at weight ratio of 80:14:6 was obtained. Under optimal conditions, monodispersed nano-emulsion with a span factor of 0.25 ± 0.01 and mean droplet size of

78 ± 3 nm was produced. The occurrence of droplet recoalescence was diminished due to the high negative zeta potential of −22.9 ± 0.9 mV.

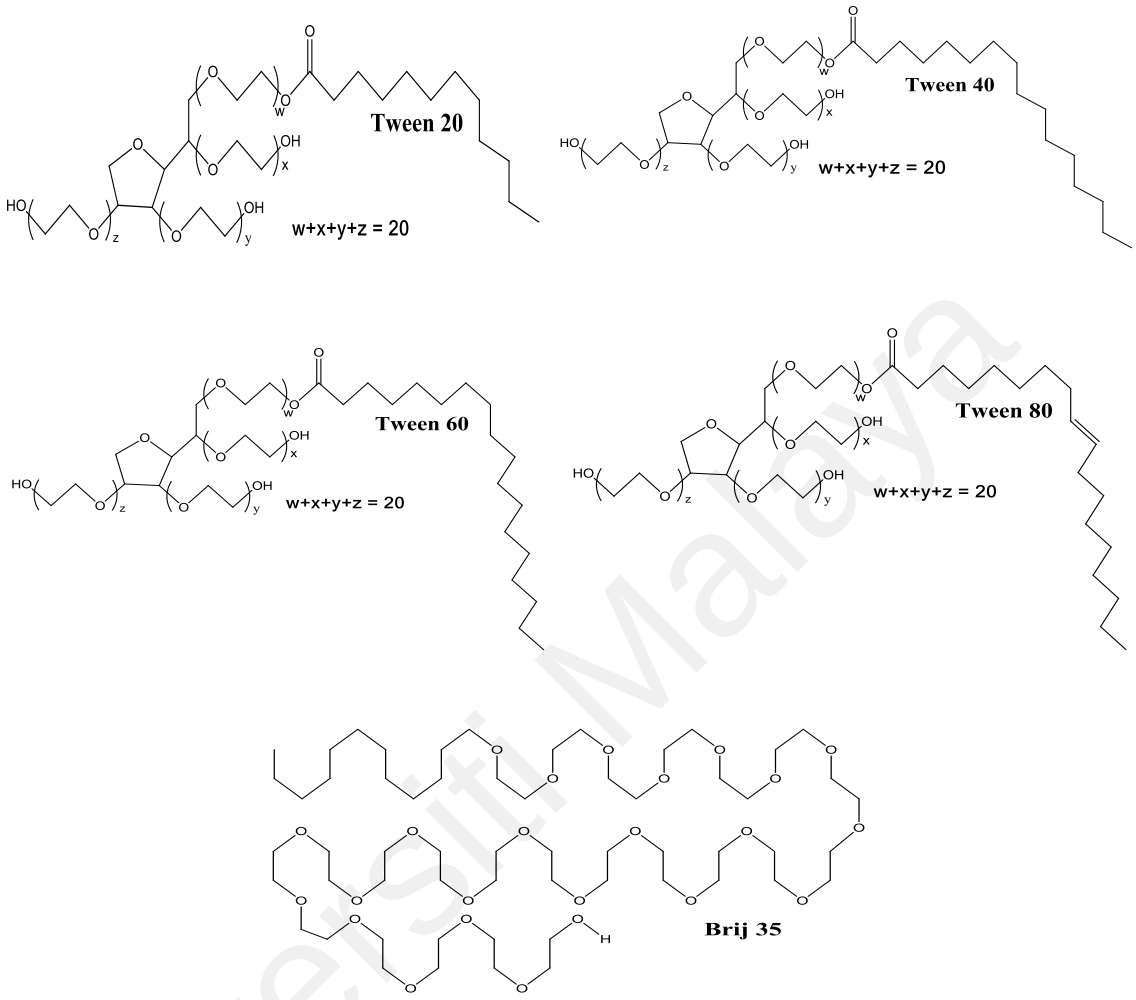

Figure 2.8: Chemical structures of Tween 20, Tween 40, Tween 60, Tween 80 and Brij 35.

In addition, palm-based tocotrienol rich fraction encapsulated nano-emulsions were synthesized via microfluidic-assisted technique by P. S. Goh et al. (2015). The homogenization pressure and the number of cycles were parameters manipulated in this study. Based on the findings, smallest particles were synthesized at the optimum condition of 10 homogenization cycles with the pressure of 25,000 psi. Therefore, these conditions were selected for further studies to investigate the effect of the emulsifier type on the nano-emulsions properties. Various individual emulsifier and blend emulsifiers systems were investigated in this study: Tween 20, Tween 40, Tween 60, Tween 80, Brij

35, Span 80:Tween 20, Span 80:Tween 40, Span 80:Tween 60, Span 80:Tween 80 and Span 80:Brij 35. They reported that systems that stabilized by sole emulsifier displayed mean droplet diameter less than 100 nm, while the systems containing mixed emulsifiers showed mean droplet diameter larger than 200 nm except for the nano-emulsion stabilized by Span 80:Brij 35. The droplet size of emulsion stabilized by Span 80:Brij 35 was centered around 66.0 ± 1.9 nm with PDI of 0.173 ± 0.029. Although the emulsions stabilized solely by Brij 35 possessed smallest droplet particles, but high PDI value pf 0.561 was obtained with bimodal distribution. Highly polydispersed emulsion was unfavorable due to its instability and the susceptibility to Ostwald ripening process (David Julian McClements, 2015). The synergistic effect between Span 80 and Brij 35 reduced the interfacial tension and facilitated the droplet deformation. The stability of nano-emulsions was evaluated by monitoring the droplet size, PDI and the zeta-potential of the systems over a month at 25 ^{o}C and 4 ^{o}C and the resulted showed that all the parameters remained unchanged throughout the storage period regardless of storage temperature. However, the nano-emulsions stabilized by Span 80:Brij 35 were noticed to be suffered great loss of 25% of tocotrienols during processing.

Moreover, Koroleva et al. (2018) prepared oil-in-water nano-emulsions using non-ionic Brij 30 or blend of Tween 80 and Span 80 as emulsifiers via the phase inversion temperature approach. Average droplet diameters range from 42 to 50 nm were obtained for Brij 30 stabilized nano-emulsions with oil fractions of 0.17 – 0.37. In the contrary, a significant reduction of droplet size was noticed upon increasing the oil fraction up to 0.3 for the systems stabilized by Tween 80 and Span 80. The mean droplet size decreased to approximately 20 nm and remained almost unchanged with the rise in the oil fraction up to 0.45. When the oil fraction was less than 0.3, larger droplet size was observed because of the insufficient amount of Span 80 to stabilize the emulsion. Nevertheless, the zeta-potential values for systems stabilized by Brij 30 or by mixture of Tween 80 and Span 80

were found to be −4 ± 1 mV and −2 ± 1 mV, respectively. With this reason, the resultant nano-emulsions were subjected to flocculation over time.

2.9.6 Ionic liquid as surface-active agent for emulsion formation

Recently, there is a significant growth of interest in employing ionic liquids in the formation of emulsions. Ionic liquids are versatile substances whereby they can function as oil phase, aqueous phase or surfactant in the formation of emulsions (Kunz et al., 2012). Ionic liquids with a long hydrophobic tail and a hydrophilic imidazolium head group are amphiphilic in which they have the capability to self-aggregate and form micelles that is pre-requisite for optimizing the partitioning behaviors in the emulsion systems (Łuczak et al., 2008). Ionic liquids exhibit several advantages over the conventional surfactants. First, the imidazolium headgroup can interact strongly with co-surfactants or additives that facilitates their adsorptions at the oil-water interfaces, enhancing the stability of the oil droplets. Next, the broad imidazolium ring can also accommodate more solutes than the tert-ammonium cationic system of conventional surfactants (Z. Qiu & Texter, 2008). Ionic liquids with long-chain alkylsulfates such as 1-butyl-3-methylimidazolium octyl sulfate and 1-butyl-3-methylimidazolium dodecyl sulfate were observed to exhibit amphiphilic properties that can behave as a surface active agent (Paul & Moulik, 2015). However, there are several drawbacks of ionic liquids such as high viscosity, low biodegradability and non-negligible toxicity. It is also difficult to obtain fully purified ionic liquids due to the tedious and costly purification process (Kunz et al., 2012).

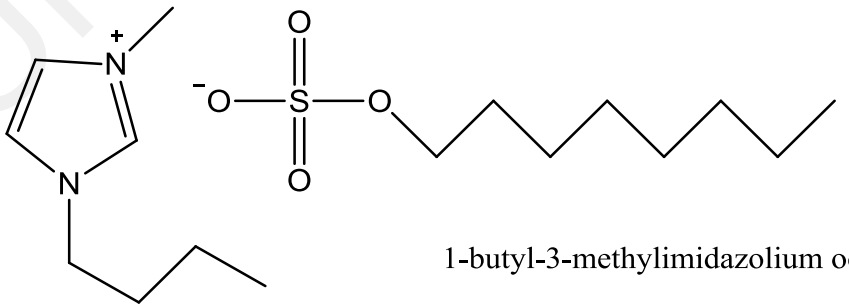

1-butyl-3-methylimidazolium octyl sulfate

Figure 2.9: Chemical structure of 1-butyl-3-methylimidazolium octyl sulfate ($C_4mimC_8SO_4$).

Since ionic liquids exhibited various remarkable properties such as the ability to dissolve the poorly soluble drugs, high thermal stability and negligible vapor pressure, they have been widely employed in pharmaceutical industry. According to the previous study, oil-in-water (O/W) emulsions were produced by employing hydrophilic 1-hexyl-3-methylimidazolium chloride ([HMIM][Cl]) and the hydrophobic 1-butyl-3-methylimidazolium hexafluorophosphate ([BMIM][PF6]). The effect of ionic liquid type on the emulsion properties was investigated (Dobler et al., 2013). The viscosity and the droplet diameter of emulsions reduced after the addition of the ionic liquids. However, the formulations containing ionic liquids exhibited long term stability, while remaining the consistent pH value. [HMIM][Cl] demonstrated amphiphilic character because it consists of both the hydrophilic and hydrophobic moieties. With this reason, [HMIM][Cl] can produce smaller emulsion droplets by effectively decreasing the surface tension. Conversely, the pH of the system without the incorporation of ionic liquid decreased significantly over the same time period. Dropped in pH values can be ascribed to the microbial contamination. However, O/W emulsions stabilized by hydrophobic [BMIM][PF6] tends to increase the droplet diameter because [BMIM][PF6] is immiscible with oil. Hence, the oil and ionic liquid droplets can exist simultaneously and the mean droplet diameter increased proportionally with the ionic liquid content due to the significant differences between oil and [BMIM][PF6] droplets. Antimicrobial activities of the emulsions are determined by the alkyl chain length of the ionic liquids. Previous report determined that ionic liquids with short substituents are relatively inactive against bacteria and fungi and both the ionic liquids used in the present study possess fairly short alkyl chains (4 or 6 carbon atoms, respectively) (Pernak et al., 2003). Nevertheless, [BMIM][PF6] and [HMIM][Cl] used in this study were effective against bacterial and fungi because the concentrations of ionic liquids are about 30 times higher than the required limits. The minimum inhibitory concentrations and minimum bactericidal or

fungicidal concentrations were reported to be between 4300 and 8600 μM for [HMIM][Cl] and >5800 μM for [BMIM] [PF6] (Pernak et al., 2003).

N. Zhang et al. (2017) investigated the properties of bovine serum albumin interfacial molecularly imprinted microspheres, which prepared using two different types of emulsifiers: 1-dodecyl-3-methylimidazolium chloride ([DMM]Cl) and sodium dodecyl sulfate. Molecularly imprinted polymers are synthetic polymers with functionally artificial recognition sites that have affinity towards predetermined target molecules (Ramanavicius et al., 2021). Taking the advantage of the superior interactions between the surfactants and template protein molecules as well as the emulsifying ability of the proteins, the oil soluble monomers and cross-linkers can be incorporated onto the template protein via copolymerization process. Molecularly imprinted nanospheres can then be obtained by removing the template molecules. In this study, the authors fabricated an amphiphilic ionic liquid, 1-dodecyl-3-methylimidazolium chloride ([DMM]Cl) with an imidazolium cation and chloride anions to stabilize bovine serum albumin. The findings demonstrated the destructive effect of sodium dodecyl sulfate on bovine serum albumin was higher than that of ionic liquid [DMM]Cl. This is because the kosmotropic anion, Cl^- of [DMM]Cl can excellently stabilize bovine serum albumin. The specific recognition characters of molecularly imprinted polymers were determined by the imprinting factor. By comparing the kinetic curves of the interfacial molecularly imprinted microspheres (IMIMs) and interfacial non-imprinted microspheres (INIMs), the results revealed that IMIMs-[DMM]Cl can adsorb higher quantities of BSA, indicating that there are more specific recognition sites available on IMIMs-[DMM]Cl for adsorption of protein as compared to INIMs-[DMM]Cl. IMIMs-[DMM]Cl demonstrated stronger stabilizing capacity on BSA conformational integrity as evidenced by the higher adsorption rate during the initial phase. The imprinting factor of IMIMs-[DMM]Cl was 2.15, while the adsorption capacity of IMIMs-SDS was similar to that of

INIMs-SDS. This implies that [DMM]Cl exhibited higher imprinting efficiency as compared to bovine serum albumin.

Ionic liquids are organic salts with cationic and anionic moieties. The emulsion systems containing ionic liquids are greatly affected by the complex interactions between the ionic liquids and other constituents. The intermolecular interactions and self-organization of ionic liquids can be manipulated by varying the chemical structures of ions (Smirnova & Safonova, 2010). Ionic liquid-assisted nonaqueous emulsions could serve as excellent candidate for the efficient delivery of lipophilic compounds. Ionic liquids with different polarities can be obtained by tuning the anionic/cationic moieties using pharmaceutical grade organic cations and inorganic anions (Brennecke & Maginn, 2001). According to the previous study, sparingly soluble acyclovir (ACV) was used as a drug model and modified hydrophilic ionic liquids with anions were found to be very effective in the dissolution of ACV (MoniruzzamanTahara et al., 2010). Extraordinarily high amount of ACV can be loaded into microemulsions, in which ionic liquid functions as dispersed phase because ACV is highly soluble in ionic liquid. ACV-containing microemulsions consisted of a mixture of polyoxyethylenesorbitan monooleate (Tween-80) and sorbitan laurate (Span-20), isopropyl myristate (IPM) as an oil phase, and ionic liquid $[C_1mim][(CH_3O)_2PO_2]$ (dimethylimidazolium dimethylphosphate) as a pseudophase. The weight ratios of Tween 80:Span 20 were varied and it was observed that the formulation with the ratio of 3:2 Tween 80:Span 20 demonstrated remarkable solubility and skin permeation enhancing effect for ACV. Since it is essential to investigate the cytotoxicity of a new carrier, *in vitro* studies were conducted to evaluate the relative safety of microemulsions using the reconstructed human epidermal model LabCyte^{TM} EPI-MODEL12. Ionic liquid-containing microemulsions were observed to show over 80% in cell viability as compared to Dulbecco's Phosphate-Buffered Salines, indicating low cytotoxicity of the carrier. The clarity and the phase separation of the

emulsions provide information on the stability of ACV-laden emulsions. Besides, the emulsion stability can also be evaluated based on the droplet size after the storage at 25 ºC for 2 months. Based on the results obtained, the droplet diameters of microemulsions 1 (ME1) containing 4 mg mL^{-1} ACV stabilized by 3:1 Tween 80:Span 20 & 4 wt% ionic liquid and microemulsions 2 (ME2) containing 4 mg mL^{-1} ACV stabilized by 3:2 Tween 80:Span 20 & 4 wt% ionic liquid was slightly increased from 19.3 to 22.4 nm and from 18.6 to 20.1 nm, respectively after 2 months of storage at 25 ºC. The encapsulation efficiencies of ME1 and ME2 with same amount of ACV were determined to be 95.3% and 97.6%, respectively after 60 days of storage, implying that there was no degradation.

Ionic liquids such as ethylammonium nitrate are polar and have been utilized to replace the polar phase of emulsions, creating non-aqueous emulsion system. In the previous study, Rojas et al. (2010) produced emulsions using halogen-free ionic liquids as both aqueous phase as well as surface-active agent. MoniruzzamanKamiya et al. (2010) proposed a toxicologically acceptable system containing a short chain imidazolium-based ionic liquid as aqueous phase, isopropyl myristate as oil phase and Tween–Span mixture as emulsifiers. Both cytotoxicity and transdermal drug delivery tests were conducted in these studies and the results showed that these systems are potential candidates for immobilizing lipophilic bioactive substances (Kunz et al., 2012).

2.9.7 Solid particle as stabilizer for emulsion formation

In 1907, finely divided solid particles were examined to be able in stabilizing the emulsions and these emulsions are referred as Pickering emulsions (Pickering, 1907). Silica nanoparticles and several cellulose derivatives such as ethylcellulose and hydroxypropyl methylcellulose are commonly used in the stabilization of Pickering emulsions. Surface-active solid particles significantly enhanced the stability of the emulsion systems due to their high desorption energy at the oil-water interface that can be several thousand kT. They are unlikely to be displaced by other amphiphiles and significantly prevent the occurrence of Ostwald ripening (Murray et al., 2011).

The wettability of solid particles at both the oil and water phases of the emulsions can be determined by the contact angle θ. The contact angle act in the similar way as hydrophilic-lipophilic balance of surfactants in which it governs the positioning of solid particles at oil-water interface. Particles with contact angles $\theta < 90^{\circ}$ tend to form O/W emulsions, while particles with $\theta > 90^{\circ}$ facilitate the formation of W/O emulsions. Highly hydrophobic or hydrophilic particles prone to reside in the oil or aqueous phase rather than anchoring at an oil–water interface, thus yielding unstable emulsions (Xhanari et al., 2011). Moreover, solid particles are larger entities, which they could not diffuse and enclose the available oil/water interface as rapid as surfactants (Murray et al., 2011). Some food grade solid particles such as cellulose, hydroxyapatite, silica and clay are suitable to be function as Pickering emulsifiers due to their low toxicity. Consequently, these particle-stabilized emulsions can be loaded into functional materials such as composite microspheres.

Since both the surfactant and solid particles have specific advantageous features, it was suggested that both surfactant and solid particles shall involve together in the emulsion stabilization. When used in conjunction with colloidal particles, the coverage

of interface is likely to be dominated by low molecular weight surfactants to hinder droplet coalescence. This allows solid particles to have sufficient time to adhere at the interface and provides long-term stability (Murray et al., 2011; R Pichot et al., 2009). In addition, surfactants can also adsorb to the particles and adjust their wettability, which consequently tailoring the interfacial adsorption characteristics (Zafeiri et al., 2017). Synergistic stabilization of emulsions by a blend of surfactant and solid particles have been reported in many previous studies (BinksDesforges et al., 2007; BinksRodrigues et al., 2007).

2.9.7.1 Hydroxyapatite particles

Hydroxyapatite [$Ca_{10}(PO_4)_6(OH)_2$] (Hap) is the primary mineral of bones and teeth and Hap nanoparticles are commonly utilized as the particulate emulsifiers in the formation of Pickering emulsions due to their excellent adsorbability with numerous compounds (Yunqi Yang et al., 2017). However, a stable Pickering emulsion could not be obtained when stabilized solely by Hap nanoparticles (Fujii et al., 2009). Hap nanoparticle can only function as an effective surfactant in the presence of oils or polymers with an ester group (Fujii et al., 2007). This because of the strong interactions between the Hap nanoparticles and the ester groups of the polymers or oils at the oil-water interfaces, stabilizing the Pickering emulsions. Okada et al. (2012) studied the effect of polystyrene molecules with different end groups (like carboxyl groups, ester groups) and molecular weights on the formation of Hap nanoparticle-stabilized emulsions. They also successfully produced Hap nanoparticles-stabilized emulsions with biodegradable poly-L-lactide containing ester groups dissolved dichloromethane as an oil phase. The Hap-coated biodegradable microspheres can be obtained via the *in situ* evaporation of dichloromethane from Pickering emulsions. The resultant microspheres exhibited improved cell adhesion properties, which serve as potential candidates in tissue engineering applications. In addition, Song et al. (2018) fabricated stable Pickering

emulsions using mixed emulsifiers of hydroxyapatite nanoparticles and nonionic sorbitan monooleate (Span 80). The stability of the emulsion system relied on the formation of hydrogen bonds between hydroxyapatite and Span 80. Katepalli (2014) synthesized artemisia argyi oil (AAO)-loaded hydroxyapatite-stabilized oil-in-water emulsions without the addition of surfactants. In this study, the emulsions stabilized by spherical Hap nanoparticles (ie. widths ranging from 30 - 70 nm) were observed to be stable against coalescence for about 5 months with insignificant change in droplet size.

2.9.7.2 Silica particles

Silica is one of the well-known inorganic particles that widely used in the stabilization of the Pickering emulsions due to its biocompatibility, non-toxicity and accessibility (Katepalli, 2014). Hydrophilic silica without surface modification preferentially stabilizes oil-in-water Pickering emulsions, while hydrophobically modified silica tend to form water-in-oil Pickering emulsions (Yunqi Yang et al., 2017). However, highly hydrophilic silica particles are likely to aggregate at low pH condition due to their surface charges. Hence, numerous researches were conducted to fabricate modified silica in order to enhance the stability of the emulsions while remaining the modest surface charges (Yunqi Yang et al., 2017). Sullivan and Kilpatrick (2002) enhanced the hydrophobicity of the silica particles by embedding the oleic acid onto the particle surfaces. Oil-in-water Pickering emulsions with mean droplet size of 200 nm were obtained by using modified hydrophobic silica as stabilizer. Besides, hydrophobic SiO_2 can be easily obtained from outer shells, which is commonly used in emulsion formation (Wei et al., 2012). Furthermore, surface modification of silica can be achieved via the adsorption of surfactant molecules. Silica particles and surfactant molecules showed synergistic interactions in which they formed a mechanical barrier at oil-water interface against droplet coalescence (Salaün et al., 2018). Oil-in-water emulsions stabilized solely by conventional surfactants show poor thermal stability that restricted their applications at

high temperature conditions. Hence, the incorporation of silica particles produced surfactant-stabilized emulsions with higher thermal stability (Taherpour & Hashemi, 2018).

2.9.7.3 Clay particles

Clay minerals are phyllosilicates that could be classified as colloidal hydroxides of Al^{3+}, Si^{4+} or Mg^{2+}. Clay minerals have a sheet-like structure that composed of two tetrahedral silica sheets sandwiching an octahedral sheet. Aluminum and magnesium atoms are arranged in octahedral coordination. Diverse clays can be produced by varying the octahedral cations. For instance, montmorillonite can be formed by substituting Al^{3+} with Mg^{2+} and hectorite can be obtained by replacing Mg^{2+} with Li^{+} (Guillot et al., 2009). The commercial "Laponite" are known as synthetic hectorite nanoparticles, which often used in the literature and produced at an industrial scale due to their remarkable advantages such as ease of modification and excellent purity (Yunqi Yang et al., 2017). Clay has been extensively used as the particulate emulsifier in the production of Pickering emulsions due to its low cost, abundancy and also environmentally friendly. In order to improve the adsorptivity of clay particles at the oil-water interface, amphiphilic molecules are usually incorporated to the siloxane surfaces of clay particles (Guillot et al., 2009). Moreover, Reger et al. (2012) used blended laponite clays and surfactants to produce gel-like Pickering emulsions with enhanced stability. In the previous study, Brunier et al. (2016) studied the influence of various grades of Laponite clays on the stabilization of emulsions. Laponite clays with different compositions and adsorption isotherms exhibited different levels of stabilization efficiencies.

2.9.7.4 Carbon nanotubes

Among all the solid particles, carbon nanotubes have appealed tremendous interests in the formation of Pickering emulsion as emulsifiers due to their unique mechanical (J.-W.

Shin et al., 2009), electrical (Im et al., 2009) as well as optical (S. Tan et al., 2004) properties. The stabilization mechanism of cylindrical carbon nanotubes is unique as compared to other solid particles whereby carbon nanotubes can assemble at the oil-water interface parallelly while also having attractive forces between the tubes. Strong interactions between carbon nanotubes are responsible for hindering the droplet coalescence, unlike silica particles in which the electrostatic repulsive forces inhibit droplet coalescence (Cummins, 2007). Since carbon nanotubes are naturally hydrophobic, it will be a hurdle to disperse them homogeneously in the aqueous solutions. Incorporation of hydrophilic functional groups such as hydroxyl and carboxyl groups onto surfaces via oxygen plasma treatment is one of the most common techniques to enhance the hydrophilicity of carbon nanotubes. It was observed that the oxygen plasma-treated carbon nanotubes showed enhanced dispersity in water as well as in cyclohexane. The plasma-treated carbon nanotubes were self-assembled at the oil-water interface to form stable O/W Pickering emulsions (Wenbao Chen et al., 2011). However, it was inevitable that some of the carbon nanotubes will be disintegrated during the oxidation treatment. As compared with spherical particles, carbon nanotubes can effectively restrict the rotation of the microspheres at oil-water interface, forming highly stable emulsions (Liang et al., 2011). In the previous study, Brunier et al. (2016) employed the covalent and noncovalent approaches to increase the hydrophilicity of multiwalled carbon nanotubes. Furthermore, Pickering emulsions with high thermal stability can be produced by two-dimensional carbon nanotube architectures made up from layered double hydroxide coupled with carbon nanotubes. This unique two-dimensional structure renders carbon nanotubes with amphiphilicity as excellent emulsifiers that self-assemble at oil-water interface (Shan et al., 2015).

2.9.7.5 Cellulose particles

Cellulose is well-known bio-based materials that garnered substantial attentions in both industry and research lines because of its remarkable properties such as renewability, biocompatibility as well as biodegradability (Aaen et al., 2019). Besides, cellulose particles can be employed as novel eco-friendly emulsifying agents in the formation of surfactant-free Pickering emulsions due to its amphiphilic character (Rein et al., 2012). Jim nez Saelices and Capron (2018) had successfully produced oil-in-water nano-emulsions with mean droplet diameters range from 100 to 600 nm stabilized by TEMPO-oxidized cellulose nanofibrils via high pressure homogenization.

2.10 Cellulose as an emulsifying agent as well as a reinforcing agent

2.10.1 Characteristics of cellulose as an emulsifying agent

Emulsifiers play an essential role in maintaining the stability of the emulsions against Ostwald ripening, creaming, flocculation as well as phase inversion. Hence, the selection of emulsifier in the formation of emulsions is paramount importance. Cellulose is one of the solid particles with numerous outstanding properties that has been explored as remarkable surface-active agent. Native cellulose exhibits amphiphilic properties with both hydrophilic and hydrophobic moieties that are preferentially wetted by water and oil phases, respectively (Kalashnikova et al., 2012). Therefore, they are capable to self-assemble at the freshly formed oil-water interfaces and form a mechanical barrier around the emulsion droplets, hindering the droplet coalescence (Capron & Cathala, 2013). The adsorption of particles at the oil-water interface is irreversible due to the high adsorption energy and they will remarkably reduce the interfacial tension (Ankit Kumar et al., 2013). Besides, lipid oxidation can also be hampered in the presence of cellulose particles due to the formation of thick interfacial layers. This is one of the major concerns in food applications as well as in pharmaceutical industry (David Julian McClements & Gumus, 2016). In addition, celluloses garnered considerable attentions due to their biocompatibility and low toxicity that are particularly essential in food, cosmetics, biomedical and pharmaceutical industries. Most importantly, celluloses are abundant in nature and economically viable because they can be readily obtained from plants, biomass or bacteria (P. Bajpai, 2018).

2.10.2 Enhancement of properties as surface-active agents by modified celluloses

2.10.2.1 Generation of strong electrostatic repulsions by sulfated cellulose nanocrystals

Sulfuric acid (H_2SO_4) hydrolysis is a typical approach that preferentially depolymerizes the amorphous portions of the cellulose, yielding the highly crystalline cellulose nanoparticles which known as cellulose nanocrystals (CNCs) or nanocrystalline celluloses (NCCs) (Abraham et al., 2011). Amorphous fractions are more susceptible to acid attack due to their randomly oriented arrangement (H. D. Nguyen et al., 2013). CNCs have needle-like shape with typical widths of less than 100 nm and tens to hundreds of nanometers in length (E. Lam et al., 2013). Therefore, they possess a large surface-to-volume ratio (Huang et al., 2003).

The efficiency of this technique is determined by the acid concentration, the acid species, the reaction time and temperature (H. D. Nguyen et al., 2013). Hydrolysis by H_2SO_4 introduces negative charge bulky sulfate half ester groups onto surfaces of CNCs via esterification with surface hydroxyl groups and the electrostatic repulsion forces result in the formation of a stable colloidal suspension (Martínez-Sanz et al., 2011; Satyamurthy et al., 2011). Based on the previous study, stable oil-in-water emulsions containing high volume fractions of oil can be obtained at very low concentration of sulfated cellulose nanocrystals (0.1% w/w). The anionic charges on the surfaces of sulfated celluloses induce strong electrostatic forces that surpass the attractive interactions between the oil droplets, preventing the droplet coalescence (Capron & Cathala, 2013).

There are some drawbacks of sulfuric acid hydrolysis in term of productivity and thermal stability (Qua et al., 2011). According to Qua et al. (2011), approximately 30% in weigh basis of nanocelluloses can be isolated as final yield, which impedes the mass productions of nanocelluloses. The thermal stability of sulfuric acid hydrolyzed

nanocelluloses is also lowered by the presence of sulfate half ester groups (Roman & Winter, 2004).

2.10.2.2 Improved emulsion stability by microfibrillated celluloses with high aspect ratio

In some particular applications especially tissue engineering scaffolds, fine and long nanofibers are indispensable as they are required to emulate the native extracellular matrix (ECM) for nutrient transportation as well as for cell attachment (Coburn et al., 2011). Microfibrillated cellulose (MFC) is another type of nanofiber that elicits much interest, having similar features as CNC but with a higher aspect ratio (L/d) (Ning Lin et al., 2012). In 1983, Turbak et al. (1983) were first extracted MFCs from wood pulp employing high pressure homogenization. MFCs exhibit long and network-like structures (Ning Lin et al., 2012) with widths ranging from 10 to a few hundred nanometers with several micrometers in lengths (Fatah et al., 2014). Productions of MFCs are normally achieved by the means of mechanical disintegrations such as homogenization (Zhao et al., 2013), microfluidization (Ferrer et al., 2012) and ultrasonication (Wenshuai ChenHaipeng YuYixing Liu et al., 2011).

As compared to spherical celluloses, microfibrillated celluloses with irregular shape and higher aspect ratio can produce highly stable emulsions at lower concentrations (S. Lam et al., 2014). Microfibrillated celluloses formed a protective layer at oil-water interface to hinder droplet aggregation (Costa et al., 2019). Additionally, the excess non-adsorbed particles were observed to form three-dimensional network in the continuous phase, acting as rheology modifier to restrict the movement of the oil droplets. This contributes to the stability of emulsions by reducing the occurrence of creaming. Previous study also revealed that microfibrillated cellulose employed as surface-active agent in emulsions also able to reduce the lipid oxidation (Kargar et al., 2012). Furthermore,

Winuprasith and Suphantharika (2015) also prepared highly stable emulsions in the absence of droplet coalescence over 80 days by employing mangosteen rinds-extracted microfibrillated celluloses as emulsifying agents.

Regioselective conversion of C6 primary hydroxyls of cellulose to carboxylate groups can be possible via 2,2,6,6-tetramethylpiperidine-1-oxyl radical (TEMPO)-mediated oxidation. There are two systems: TEMPO/NaBr/NaClO and TEMPO/NaClO/$NaClO_2$ oxidation systems that carried out at pH 10-11 and pH 4.8-6.8, respectively (Haniffa et al., 2017; Isogai et al., 2011). The cellulose carboxylation is only restricted on the surface of the microfibrils (T Saito et al., 2005). Interestingly, the structural properties of the celluloses are not affected by TEMPO reaction because only the amorphous regions of celluloses been hydrolyzed but the crystalline regions remained unchanged after the treatment (Haniffa et al., 2017; Qin et al., 2011).

Recently, there is an exciting discovery on the isolation of carboxylated CNCs via ammonium persulfate (APS) oxidation (Figure 2.10) (Castro-Guerrero & Gray, 2014; E. Lam et al., 2012; Leung et al., 2011). Ammonium persulfate is a strong oxidant that performs versatile functions to generate nanocelluloses in a one-step procedure without any pretreatment. Removal of hemicellulose and lignin as well as the bleaching of fiber can be easily attained in a simple method. The *in situ* exclusion of these non-cellulosic components and amorphous regions can be explained by the postulated mechanism whereby $SO_4^{\bullet-}$, HSO_4^- and hydrogen peroxide are formed during the course of nanocellulose synthesis by APS (Leung et al., 2011). In contrast to sulfuric acid hydrolysis, this method generates some carboxyl groups on the surface of the nanocelluloses (Castro-Guerrero & Gray, 2014; Leung et al., 2011). Wen et al. (2014) produced D-limonene Pickering emulsions stabilized by ammonium persulfate oxidized-cellulose nanocrystals. Low concentration of ammonium persulfate oxidized-cellulose

nanocrystals of 0.2% w/w was sufficient to confer excellent emulsion stability against droplet coalescence attributed to strong electrostatic repulsions due to the presence of negatively charged carboxyl groups.

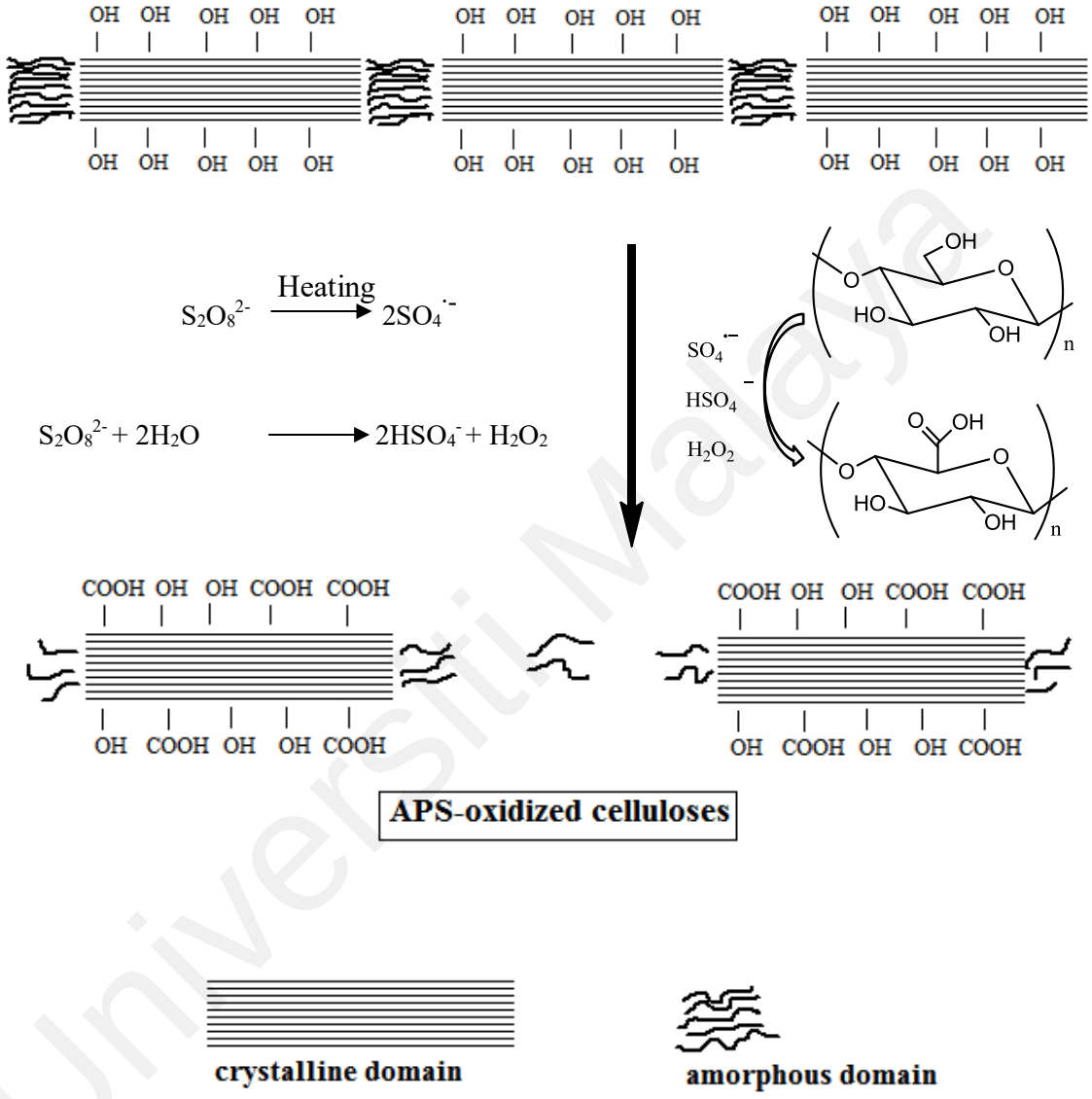

Figure 2.10: Oxidation of cellulose via ammonium persulfate (APS) treatment.

2.10.2.3 Enhanced solubility and increased interactions at oil-water interface by hydrophobically modified trimethylsilylated cellulose

The insolubility of celluloses in most organic solvents restricted their exploitations in diverse applications. Silylation of cellulose is one of the promising approaches for the preparation of soluble hydrophobically modified cellulose derivatives, which widens the spectrum of applications. In addition, silylated celluloses can also function as an intermediate for further chemical modifications such as esterification reaction (Köhler et al., 2008; Kostag et al., 2010). The most commonly used silylating agents include 1,1,1,3,3,3-hexamethyldisilazane (HMDS) (Jankauskaitė et al., 2020), chlorotrimethylsilane (Malekghasemi et al., 2016) and *N,O*-bis(trimethylsilyl)acetamide (Mormann & Wezstein, 2009). Trimethylsilylated cellulose (TMSC) can also be synthesized by employing ionic liquids such as 1-ethyl-3-methylimidazolium acetate (EMIMAc), 1-butyl-3-methylimidazolium chloride (BMIMCl) and 1-ethyl-3-methylimidazolium chloride (EMIMCl) (Köhler et al., 2008). TMSC shows good solubility in many organic solvents, for examples, *n*-hexane, acetone and chloroform (Puspasari et al., 2015). Due to its hydrophobicity, TMSC can disperse homogenously within polymer matrix to form thin films with improved properties. Besides, emulsion with enhanced stability can also be produced by using hydrophobic TMSCs as emulsifiers because of their strong adsorption at oil-water interface (Mormann & Wezstein, 2009).

2.10.3 Characteristics of cellulose as a reinforcement

Celluloses have elicited considerable attention in industry and research line due to their impressive mechanical strength, biocompatibility, biodegradability, renewability, low density as well as ease in surface modification (Azizi Samir et al., 2005; KaliaDufresne et al., 2011). Cellulose is an inexhaustible source of biopolymer (Cherian et al., 2011) that can be processed into nano-scale dimensions with a plethora of potential applications such as drug carrier (Jackson et al., 2011; Lavoine et al., 2014), paper additives (Sehaqui et al., 2011), reinforcements for nanocomposites (H. Dong et al., 2012; A. L. S. Pereira et al., 2014; Silvério et al., 2013) and enzyme immobilization (Mahmoud et al., 2009).

As compared to macroscopic fibers, nanocelluloses attained tremendous attraction in diverse applications because of their outstanding mechanical properties. Excellent mechanical performance of nanocelluloses is attributed to its high degree of crystallinity (Pääkkö et al., 2008). Literature reviews manifested that the modulus of a cellulose crystal is in the range of 100-200 GPa due to its compact three dimensional structure that physically coupled by multiple hydrogen bonds, which contributes to the high stiffness of nanofibers (Pääkkö et al., 2008; X. Wu et al., 2013). However, the tensile strength of the crystal structure is noticeably lower, which estimated to be in the range of 0.8–10 GPa (Satyamurthy et al., 2011).

Many previous studies employed celluloses as reinforcements to improve the mechanical strength of matrix. N. Lin et al. (2012) fabricated Ca-crosslinked alginate-based sponges, employing unmodified and oxidized celluloses as reinforcements. As compared to the neat alginate sponge, the mechanical strength of alginate sponges filled with unmodified nanocelluloses had been improved remarkably as evaluated by the compressive test. Nevertheless, the compressive test results demonstrated that alginate

sponges reinforced by oxidized celluloses were much stronger and more robust than unmodified cellulose-reinforced sponges. This indicated that the carboxyl groups of the oxidized celluloses involved in the crosslinking process by interacting with the Ca^{2+} ions. Oxidized celluloses also served as the coupling points with alginate structure and remarkably enhanced the structural and mechanical stability of the sponges.

As reported in the previous study, cellulose nanocrystals (CNCs) also used to reinforce chitosan hydrogel for oral delivery of curcumin. The incorporation of 0.5% CNCs increased the maximum compressive stress of chitosan hydrogel from 25.9 ± 1 kPa to 38.4 ± 1 kPa at constant concentration of crosslinker (0.2% v/v glutaraldehyde). The formation of semi-interpenetrating polymer networks (semi-IPNs) improved the strength of the hydrogels, implying the increased ability to withstand the pressure that might be *in vivo* (Udeni Gunathilake et al., 2017). In addition, Lin et al. (2011) also observed the mechanical reinforcement of alginate in the presence of cellulose nanocrystals (CNCs) by evaluating the storage modulus (G′) and the loss modulus (G″) of the nanocomposite sols. CNCs-stabilized alginate sols exhibited higher G′ and G″ values than neat alginate sols. This was attributed to the increased interactions between CNCs and alginate matrix via hydrogen bonding.

2.11 Summary

Chemical structures and properties of both alginate and cellulose have been reviewed and summarized. Alginate-based composite with enhanced functionalities and physicochemical properties can be achieved by blending of alginate with other polysaccharides such as chitosan, collagen, pectin, starch and cellulose. Immobilization of drug-loaded emulsions into alginate-based microbeads were reported by many researchers. Furthermore, nanocellulose has been extensively employed as reinforcing agents in drug delivery systems due to its appealing mechanical strength. Although there are many previous studies reported that various natural hydrogels could be potentially function as drug carriers, but there is no report on the development of cellulose-reinforced alginate microbeads for the encapsulation of palm-based vitamin E. As compared to direct oral administration of drugs, encapsulation of drugs within microbeads offers numerous advantages which include improved solubility of lipophilic drugs, controlled release feature, protection of drugs from harsh gastric condition as well as enhanced patient compliance. Several recent studies focused on the strategies to improve the swelling properties and the encapsulation efficiency of alginate-based composites in the drug delivery systems. Hydrophobically modification of polymeric matrix and incorporation of other polysaccharides and fillers into microbeads are remarkable techniques to enhance the properties of microbeads. In addition, the release profile of alginate-based microbeads can be evaluated by investigating the experimental conditions and limiting parameters towards the optimum encapsulation efficiency with favorable swelling properties, which subsequently affect the release profile of microbeads. The potential application of the cellulose-reinforced alginate microbeads as drug delivery system can be evaluated through swelling, encapsulation efficiency and *in vitro* release studies. There are few factors that govern the mechanical strength and the encapsulation efficiency of microbeads such as the concentration of filler, type of filler as well as the emulsion

properties. The effective application of a drug carrier implies its suitability for encapsulating other drugs with similar nature.

CHAPTER 3: MATERIALS AND METHODS

3.1 Individualization of microfibrillated celluloses (MFCs) from oil palm empty fruit bunches (OPEFBs)

3.1.1 Materials

The OPEFB fibers were provided by Sabutek Sdn. Bhd., Malaysia, and were used as the starting material. Sodium hydroxide (NaOH) pellets, glacial acetic acid, 65 % nitric acid (HNO_3), 95–97 % sulfuric acid (H_2SO_4) and ammonium persulfate (APS) were purchased from Friendemann Schmidt Chemicals. Sodium chlorite ($NaClO_2$) (80 %) and absolute ethanol were supplied by Sigma-Aldrich and Kollin Chemicals, respectively.

3.1.2 Extraction of microfibrillated celluloses via sulfuric acid hydrolysis

OPEFB fibers were passed through a 45 μm sieve. First, the resins, waxes and oil components of OPEFBs were removed by Soxhlet extraction using 250 mL of 70% (v/v) ethanol as solvent for 24 hr. The extractive-free fibers were washed with boiled water and allowed to dry. Next, 6 wt% of NaOH solution was prepared and added into the extracted samples for 4 h at 30 ºC, which resulted in the swelling of the fiber and subsequent increased in the moisture absorption (Abraham et al., 2011). For removal of hemicelluloses, swollen fibers were treated with a higher concentration of NaOH solution (17.5 wt% of NaOH). This was conducted at 80 ºC for 4 h under constant mechanical stirring. After the treatment, the fibers were subjected to centrifugation and washed with distilled water to remove the alkali-soluble components as well to neutralize the fibers. A subsequent bleaching process was carried out by adding equal parts of acetate buffer (solution of 2.7 g NaOH and 7.5 ml of glacial acetic acid in 100 ml of distilled water) and 1.7 wt% aqueous chlorite to the treated fibers for 4 h at 80 ºC. This process was repeated for a few times until the fibers had completely turned into white. After this, bleached fibers were washed with cold water. For purification of fibers, bleached fibers were soaked in a mixture of 10 ml of 65% HNO_3 and 100 ml of 80% acetic acid and then placed

in preheated oil bath (120 ºC) for 30 min. The acid hydrolysis was conducted by adding 64 wt% of H_2SO_4 into the purified sample with the ratio of 10:1 for 1 h at 45 ºC under vigorous agitation. The reaction was quenched by diluting it with cold water. The diluted suspension was centrifuged at 12,000 rpm for 10 min and this step was repeated several times until it turned into turbid suspension.

3.1.3 Preparation of carboxylated microfibrillated celluloses via ammonium persulfate oxidation

One liter of 1 M of ammonium persulfate (APS) was prepared and added to 10 g of OPEFB fibers, which were used as the starting biomass materials. The mixture was heated at 60 ºC for 16 h under constant mechanical stirring. Centrifugation of the treated suspension was carried out at 12, 000 rpm for 10 min. The washing process was repeated for four times until the pH of the suspension was close to 4. This was followed by homogenizing the cellulose suspension for 10 min at 10,000 rpm using a IKA T25 digital ultra turrax. Prior to the formation of emulsion, the cellulose suspension was sonicated (Digital ultrasonic cleaner, model ST-UB3300LDT) in an ice bath for 30 min.

3.1.4 Characterizations of microfibrillated celluloses

3.1.4.1 Fourier transform infrared spectroscopy (FTIR)

Fourier transform infrared (FTIR) spectroscopy studies were performed using a Perkin-Elmer FTIR spectrophotometer (FT-IR spectrometer frontier, Perkin Elmer) to determine the functional groups of all the raw fibers, pre-acid hydrolysis treated fibers, acid-hydrolyzed nanocelluloses as well as the APS-treated nanofibers. Effects of the treatments on the chemical compositions can be tracked from the IR spectra. Samples were ground and mixed well with KBr (1:100, w/w), then pressed into thin pellet prior to analysis. FTIR analysis was performed in the transmittance mode with the wavenumber range of 4000-400 cm^{-1} and a resolution of 4 cm^{-1} at an accumulation of 32 scans. The positions of the peaks were determined by the OriginPro software.

3.1.4.2 Morphological investigation

Bleached fibers and freeze-dried samples were mounted on aluminum stubs using double-sided adhesive carbon tapes, and the samples were sputter-coated with platinum using auto fine coater (Jeol JFC-1600). Morphological characteristics were observed using a FESEM (Jeol JSM-7600F), operated in high vacuum mode with a 5 kV accelerating voltage. Fiber diameters were analyzed using software imageJ.

3.1.4.3 X-ray diffraction (XRD) analysis

The crystallinities of raw OPEFB, acid-hydrolyzed MFCs and APS-oxidized MFCs were evaluated by X-ray diffraction study. Impacts of the treatments on the crystallinity index values of the celluloses can be investigated from the X-ray diffractograms. The X-ray diffraction patterns of the specimens were obtained from an X-ray diffractometer (PANalytical EMPYREAN) operated at 40 kV and 40 mA with Ni-filtered CuKα radiation. X-ray diffractograms were recorded from 10° to 60° at a scan rate of 2s/step with step size of 0.02°.

To conform with the required crystallographic conventions for cellulose, equation 3.1 is defined as follows:

$$\mathrm{CrI}\ (\%) = \frac{\mathrm{I_{002}} - \mathrm{I_{AM}}}{\mathrm{I_{002}}} \times 100 \qquad (3.1)$$

where CrI expresses crystallinity index, I_{200} is the maximum intensity of diffraction at 2θ = 22.4° and I_{AM} is the intensity for the amorphous phase. This is the intensity of diffraction at 2θ = 18°.

3.1.4.4 Thermostability analysis

Thermal properties of the samples were analyzed by a thermogravimetric analyzer (TGA) (TGA 4000, Perkin Elmer). Samples were placed into crucible and heated under nitrogen atmosphere from 35 ºC to 600 ºC with the heating rate of 10 ºC/min.

3.1.4.5 Optical transmittance

Bleached fiber and nanofiber suspensions were prepared and introduced into quartz cuvette. The optical transmittance was measured between 300 and 800 nm using a Shimadzu UV–Vis spectrophotometer (UV-2600, Shimadzu). A cuvette filled with distilled water was used as blank.

3.2 Synthesis of hydrophobic cellulose derivative

3.2.1 Materials

Trimethylchlorosilane (TMSCl), FTIR grade potassium bromide (KBr) and deuterated chloroform were supplied by Merck. Pyridine, toluene, methanol and sodium acetate were purchased from Friendemann Schmidt Chemicals.

3.2.2 Preparation of hydrophobic trimethylsilyl celluloses

Trimethylsilyl cellulose (TMSC) was derived from neutralized acid-hydrolyzed microfibrillated cellulose via silylation. A mixture of 13.4 mL pyridine, 60.8 mL toluene and 10.6 mL of trimethylchlorosilane (TMSCl) was added into 1.5 g neutralized acid-hydrolyzed cellulose. The mixture was heated at 110 ºC under constant mechanical stirring for 5 h. Approximately 60 mL toluene was added and the mixture was filtered. The filtrate was slowly added into 200 mL methanol containing 5 g sodium acetate. TMSC was obtained as white precipitate. The white precipitate formed was washed with methanol and oven dried at 40 ºC for overnight.

3.2.3 Characterizations of trimethylsilyl celluloses

3.2.3.1 Fourier transform infrared spectroscopy (FTIR)

Fourier transform infrared (FTIR) spectroscopy (FT-IR spectrometer frontier, Perkin Elmer) was used to identify the changes in the functional groups of celluloses after silylation. Samples were ground and mixed uniformly with KBr in the ratio of 1:100 (w/w), which then pressed to form thin pellet for analysis. FTIR analysis was performed in the transmittance mode with the wavenumber range of 4000-400 cm^{-1} and a resolution of 4 cm^{-1} at an accumulation of 32 scans.

3.2.3.2 ^{1}H nuclear magnetic resonance (NMR) spectroscopy

For determination of degree of substitution (DS), ^{1}H NMR spectroscopy study was performed by a Jeol ECA 400 NMR spectrometer running at 400 MHz using deuterated chloroform ($CDCl_3$) as a solvent. 16 scans were accumulated. DS of trimethylsilyl cellulose can be determined using equation 3.2 as follows:

$$DS = \frac{A_{TMS\ H}}{9} \times \frac{7}{A_{cellulose\ H}} \qquad (3.2)$$

where $A_{TMS\ H}$ and $A_{cellulose\ H}$ represent the peak areas of protons in the silyl groups (approximately 0 ppm) and cellulose (2.9–5.5 ppm), respectively (Puspasari et al., 2015).

3.3 Preparations of vitamin E-loaded alginate emulsions

3.3.1 Materials

Vitamin E, carotino natural palm tocotrienols (labelled as TRF-70) was supplied by Carotino Sdn. Bhd. (Johor, Malaysia). Polyoxyethylene glycol sorbitan monolaurate (Tween 20), polyoxyethylene glycol sorbitan monopalmitate (Tween 40), polyoxyethylene glycol sorbitan monostearate (Tween 60), polyoxyethylene glycol sorbitan monooleate (Tween 80) and sodium alginate were purchased from R & M Chemicals, United Kingdom. Polyoxyethylene lauryl ether (Brij® 35), hexane, heptane, ethyl acetate and iso-propanol were supplied by Merck (New Jersey, United States). Calcium chloride ($CaCl_2$) was obtained from Friendemann Schmidt Chemicals (Washington, USA). Phosphate buffered saline (PBS), 1-butyl-3-methylimidazolium octyl sulfate (C_4mim C_8SO_4) was supplied by Sigma (St Louis, Missouri United States), while absolute ethanol was purchased from Kollin Chemicals (Seoul, Korea).

3.3.2 Selection of emulsifiers: Solubility of vitamin E in different emulsifiers

The emulsifiers were selected based on the solubility of vitamin E in different emulsifier solutions using a method modified from Laouini et al. (2012). 1.5g vitamin E was added to 15 ml of 10% w/v emulsifier solution and allowed it to stir at 500 rpm for overnight. The solution was centrifuged for 10 min at 12,000 rpm and the supernatant (organic layer) was extracted with hexane/ethanol. The centrifugation and extraction process were repeated twice and the organic layer was collected. The organic layer was assayed for vitamin E using high performance liquid chromatography (HPLC) analytical method. The emulsifiers tested were: Brij 35, Tween 20, Tween 40, Tween 60, and Tween 80.

3.3.3 Effect of different parameters on the formation of oil-in-water (O/W) emulsion

Different concentrations of alginate solutions (1.5, 2.0 and 3.0 % w/v) were prepared by dissolving sodium alginate powder in 100 mL distilled water at 60ºC for 1 h. Tween 80:Brij 35 (0.5:0.5 w/w ratio) solutions at various concentrations (1.0, 1.5, 2.0 and 2.5 % w/v) was prepared by dissolving them in 100 mL distilled water at room temperature (21 ºC). The influence of vitamin E content on the emulsion properties was investigated by adding different concentrations of vitamin E, TRF-70 (2.5, 3.0 and 3.5% w/v) into 1.5 % w/v Tween 80:Brij 35 (0.5:0.5 w/w ratio) solution and homogenized using IKA T25 digital ultra turrax, at 10,000 rpm for 10 min to obtain coarse emulsion (ie. emulsion before subjecting to ultrasonification). The coarse emulsion was then subjected to ultrasonification (Hielscher Ultrasound Technology, Teltow, Germany) for 10 min. After sonication, alginate solution was added into the prepared vitamin E-loaded emulsion and mechanically stirred (IKA RW 20 digital, Germany) at 1,000 rpm for 1 h. The parameters tested include sonication amplitude (60, 80, 100%), concentration of emulsifier (1.0, 1.5, 2.0 & 2.5 %w/v), concentration of vitamin E (2.5, 3.0 & 3.5 %w/v), and concentration of alginate (1.0, 1.5 & 2.0 %w/v).

3.3.4 Preparation of primary oil-in-water emulsions

Emulsions were prepared by first homogenizing 2.5 % w/v of tocotrienol-rich fraction (TRF-70) with 1.5 % w/v Tween 80:Brij 35 (0.5:0.5 w/w ratio) using a IKA T25 digital ultra turrax, at 10,000 rpm for 10 min. Ammonium persulfate-derived MFC suspensions were dispersed in the preformed Tween 80:Brij 35 solution prior to the emulsification. This was followed by blending the emulsions using a UP100 Hielscher Ultrasonic Processor (Hielscher Ultrasound Technology, Teltow, Germany), with 100 W output power, amplitude 100% and a frequency of 30 kHz equipped with a 10 mm sonotrode for 10 min. Night different formulations of primary O/W emulsions were synthesized by

tuning the concentrations of MFCs (0, 0.0125, 0.25, 0.05, 0.1, 0.175, 0.25, 0.5 and 1.0 %w/v). Same procedure was repeated by replacing hydrophilic ammonium persulfate-derived MFC with hydrophobic TMSC as bio-based filler in order to investigate the effect of the cellulose type on the emulsion properties. Besides, we also aimed to study the influence of surface-active agent type on the emulsion properties. Hence, Tween 80:Brij 35 was replaced by ionic liquid (1-butyl-3-methylimidazolium octyl sulfate, $C_4mimC_8SO_4$) for this purpose.

3.3.5 Characterizations of primary oil-in-in-water emulsions

3.3.5.1 Emulsion droplet size & polydispersity index

Average droplet sizes and polydispersity index (PDI) of emulsions were determined by Zetasizer Nano ZS (Malvern Instruments, Cambridge, UK) based on dynamic light scattering method. Prior to measurement, the emulsions were diluted with distilled water in a ratio (1:100 v/v) and dispersed evenly to avoid the multiple scattering effects. Each sample was performed in triplicate.

3.3.6 Preparation of secondary oil-in-water emulsions

Alginate solution was prepared by dissolving 1.5 g sodium alginate powder with distilled water at 60 °C for 1 h. Alginate solution was added into the prepared primary O/W emulsions under constant mechanical stirring (IKA RW 20 digital, Germany), at 1,000 rpm for 1 h to produce secondary O/W emulsions. Different formulations of secondary O/W emulsions are shown in table 3.1.

Table 3.1: Compositions of secondary oil-in-water emulsions

Formulation code	Concentration (% w/v)			
	Tween 80:Brij 35	**APS-oxidized MFC**	**Vitamin E**	**Sodium Alginate**
SA/TB/OMFC0.0	1.5	–	2.5	1.5
SA/TB/OMFC0.0125	1.5	0.0125	2.5	1.5
SA/TB/OMFC0.025	1.5	0.0250	2.5	1.5
SA/TB/OMFC0.05	1.5	0.0500	2.5	1.5
SA/TB/OMFC0.1	1.5	0.1000	2.5	1.5
SA/TB/OMFC0.175	1.5	0.1750	2.5	1.5
SA/TB/OMFC0.25	1.5	0.2500	2.5	1.5
SA/TB/OMFC0.5	1.5	0.5000	2.5	1.5
SA/TB/OMFC1.0	1.5	1.0000	2.5	1.5
	Tween 80:Brij 35	**TMSC**	**Vitamin E**	**Sodium alginate**
SA/TB/TMSC0.0	1.5	–	2.5	1.5
SA/TB/TMSC0.0125	1.5	0.0125	2.5	1.5
SA/TB/TMSC0.025	1.5	0.0250	2.5	1.5
SA/TB/TMSC0.05	1.5	0.0500	2.5	1.5
SA/TB/TMSC0.1	1.5	0.1000	2.5	1.5
SA/TB/TMSC0.175	1.5	0.1750	2.5	1.5
SA/TB/TMSC0.25	1.5	0.2500	2.5	1.5
SA/TB/TMSC0.5	1.5	0.5000	2.5	1.5
SA/TB/TMSC1.0	1.5	1.0000	2.5	1.5
	C_4mim C_8SO_4	**APS-oxidized MFC**	**Vitamin E**	**Sodium alginate**
SA/IL/OMFC0.0	1.5	–	2.5	1.5
SA/IL/OMFC0.0125	1.5	0.0125	2.5	1.5
SA/IL/OMFC0.025	1.5	0.0250	2.5	1.5
SA/IL/OMFC0.05	1.5	0.0500	2.5	1.5
SA/IL/OMFC0.1	1.5	0.1000	2.5	1.5
SA/IL/OMFC0.175	1.5	0.1750	2.5	1.5
SA/IL/OMFC0.25	1.5	0.2500	2.5	1.5
SA/IL/OMFC0.5	1.5	0.5000	2.5	1.5
SA/IL/OMFC1.0	1.5	1.0000	2.5	1.5

3.3.7 Characterizations of secondary oil-in-water emulsions

3.3.7.1 Emulsion droplet size, polydispersity index & Zeta potential

Emulsion droplet sizes, polydispersity index (PDI) and Zeta potential (ζ-potential) were determined by Zetasizer Nano ZS (Malvern Instruments, UK) based on dynamic light scattering method. Prior to measurement, the emulsions were diluted with distilled water in a ratio (1:100 v/v) and dispersed evenly to avoid the multiple scattering effects. ζ-potential was calculated from the electrophoretic mobility using Smoluchowski equation as programmed in the instrument. Each sample was performed in triplicate. However, the droplet sizes of ionic liquid-emulsified secondary O/W emulsions were monitored using Mastersizer 3000 (Malvern Instruments, Cambridge, UK) because the mean droplet diameters for these emulsions were out of the analysis range of Zetasizer. In Mastersizer, the average droplet sizes are reported as surface area-weighted mean diameter, D[3,2]. The droplet size distribution (polydispersity) was measured in terms of span factor, which defined as span = (d90−d10)/d50, where d10, d50 and d90 are the droplet diameters at 10%, 50% and 90% of the cumulative volume, respectively. Since the secondary O/W emulsions were employed to produce the vitamin E-loaded alginate microbeads, thus, viscosity and the rheological behaviors of secondary O/W emulsions were also investigated.

3.3.7.2 Viscosity

The viscosity of secondary O/W emulsions was investigated with an increasing shear rate from 1 to 100 s^{-1} using a Modular Compact Rheometer (Physica MCR 300, Paar Physica, Germany) with a 25 mm diameter cone-plate geometry (Sharma et al., 2014).

3.3.7.3 Rheological behaviors

The rheological analysis of secondary O/W emulsions was carried out using a Modular Compact Rheometer (Physica MCR 300, Paar Physica, Germany) with a 25 mm diameter

cone-plate geometry. The gap distance between cone and plate was fixed at 0.05 mm. First, dynamic strain sweep test was conducted with the strain from 0.1 to 100% (at 1.6 Hz frequency, 10 rad s^{-1} angular frequency) to determine the linear viscoelastic region (LVR). A frequency sweep test was conducted to determine the storage modulus (G′) and loss modulus (G″) over the angular frequency (ω) range from 0.1 to 100 rad s^{-1} at γ = 0.2% (T. Sharma et al., 2015).

3.4 Preparation of alginate-based microbeads

3.4.1 Immobilization of vitamin E-loaded emulsions within alginate microbeads

The beads were formed by extruding vitamin E-loaded alginate emulsions dropwise from a hypodermic needle into 0.05 M $CaCl_2$ gelling solution with constant agitation at room temperature (21 ºC). The needle was placed approximately 15 cm above the surface of the gelling bath. The spherical beads were allowed to cure in $CaCl_2$ solution for 30 min. The beads were collected and rinsed with distilled water to remove excess calcium ions. The beads were freeze-dried (Labconco, Kansas City, MO, USA) and stored in the desiccator.

3.4.2 Characterizations of alginate microbeads encapsulating vitamin E-loaded emulsions

3.4.2.1 Fourier transform infrared spectroscopy (FTIR)

Fourier transform infrared (FTIR) spectroscopy analysis was performed using a PerkinElmer FTIR spectrophotometer (Massachusetts, United States) to determine the functional groups of vitamin E, sodium alginate (SA), APS-oxidized MFCs, TMSCs and vitamin E-loaded microbeads as well as to examine the possible interactions in the vitamin E-loaded alginate microbeads. Samples were ground and mixed well with KBr (1:100, w/w), then pressed into thin pellets prior to the analysis. FTIR spectra were scanned over a wavenumber range of 4000–400 cm^{-1} with a resolution of 4 cm^{-1} at an accumulation of 32 scans (Lin et al., 2011).

3.4.2.2 Syneresis test

Syneresis of vitamin E-loaded alginate microbeads was determined at room temperature (21 ºC) and at refrigerated condition (4 ºC) for day 1, 3 and 7 after the production of the beads. Syneresis was monitored as weight reduction of microbeads with respect to the initial weight as a function of time.

Syneresis degree (%) was expressed as:

$$\text{Syneresis degree (\%)} = \frac{W_0 - W}{W_0} \times 100\% \quad (3.3)$$

where W_0 is the weight of microbeads at day 0 and W is the weight of microbeads at day 1, 3 or 7 (Aarstad et al., 2017).

3.4.2.3 Compressive test

The mechanical properties of the vitamin E-loaded alginate microbeads were evaluated by a compression test, which performed using a universal testing machine (Shimadzu EZ tensile tester, Japan). Samples for compressive test were prepared by filling the hollow cylindrical sponge (Diameter: 2.3 cm; Height: 1.4 cm) with 160 microbeads. A load cell of 500 N was applied to the microbeads filled-sponges at a displacement rate of 0.5 mm/min. The compressive stress at 85% strain represents the compressive strength of the microbeads using empty hollow cylindrical sponge as a control. Three replicates were measured to obtain the average compressive strength of each sample and its standard deviation (Belscak-Cvitanovic et al., 2015).

3.4.2.4 Swelling test

Swelling studies of vitamin E-loaded alginate microbeads were conducted in two aqueous media: simulated gastric fluid (SGF, pH 1.2 HCl) and simulated intestinal fluid (SIF, pH 7.4 PBS). 100 mg of microbeads were immersed in 30 mL of SGF for 2 hours. At predetermined time intervals (every 15 mins up to 2 hours), microbeads were separated from the medium and weighed carefully after wiping off residual liquid with filter paper. Acid-treated microbeads were then transferred into SIF until the completion of degradation at 37 ºC.

The weight change of the microbeads was calculated as a function of time. Swelling ratio (SR) % was expressed as:

$$SR\ \% = \frac{(W_2 - W_1)}{W_1} \times 100\% \quad (3.4)$$

where W_2 is the weight of the wet beads and W_1 is the initial weight of the beads (J. P. Zhang et al., 2010).

3.4.2.5 Determination of encapsulation efficiency

The encapsulation efficiency (EE) was determined after vitamin E was extracted from the freeze-dried vitamin E-loaded alginate microbeads (El-Say, 2016). About 100 mg of vitamin E-loaded microbeads were dispersed in 30 mL pH 7.4 PBS and continuously stirred overnight to ensure complete release of the encapsulated vitamin E. Samples were centrifuged at 5,000 rpm for 15 min and the supernatant was extracted with hexane/ethanol. The extraction was repeated twice and the organic layer was collected. The collected organic layer was purged dry under a stream of nitrogen gas (N_2) using TurboVap Lv. A Waters high performance liquid chromatography (HPLC) equipped with Waters 2475 multi λ Fluorescence Detector was used to determine the concentration of the collected oil. The column used was Luna 5µ Silica 4.6 mm i.d. × 250 mm length. The mobile phase consists of heptane and ethyl acetate (94:6 *v*/*v*) at the flow rate of 0.6 mL/min. EE% was calculated as follows:

$$EE\% = \frac{\text{Actual vitamin E loading}}{\text{Theoretical vitamin E loading}} \times 100\% \quad (3.5)$$

3.4.2.6 *In vitro* drug release studies

In vitro drug release studies were conducted by first dispersing vitamin E-loaded microbeads in simulated gastric pH condition (pH 1.2 HCl) for 2 h and then in simulated intestinal pH condition (pH 7.4 PBS) at 37 ºC. At predetermined time intervals, 3 mL of solution was withdrawn and same amount of fresh dissolution medium was added in order to maintain the constant volume. The amount of the vitamin E released was determined using HPLC.

3.4.2.7 Analysis of release kinetics and mechanisms of microbeads

To study the release kinetics of vitamin E from alginate microbeads, the experimental release data were fitted into three different mathematic models: zero-order (% release versus time), first-order (log % drug remained versus time) and Higuchi (% drug release versus $\sqrt{t}$). The equations for the above-mentioned models are as follow:

$$\text{Zero-order model: } Q = k_o t \tag{3.6}$$

where Q is the cumulative amount of the drug release at time t, k_o is the zero-order rate constant and t is the time.

$$\text{First-order model: } \text{Log } O_o - \text{Log } Q_t = k_1/2.303\ t \tag{3.7}$$

where Q_t is the cumulative amount of drug released at time t, Q_o is the initial concentration of drug in the microbeads and k_1 is the first-order rate constant. Thus, a graph of log cumulative of % drug retained in the microbeads (Log O_0 – Log Q_t) versus time was plotted.

$$\text{Higuchi model: } Q_t = k_H \sqrt{t} \tag{3.8}$$

where Q_t is the cumulative amount of drug released at time t and k_H is the Higuchi constant.

In addition, the release mechanism of microbeads was determined by Ritger-Peppas model (Ritger & Peppas, 1987) and the equation is shown below:

$$\text{Ritger-Peppas model: } \frac{M_t}{M_\infty} = k_R t^n \tag{3.9}$$

where M_t and M_∞ are the cumulative drug release at time t and at infinite time, respectively; k_R is a release constant which depends on the structural and geometrical characteristics of the materials. The drug release manner is described by the diffusional exponent, n.

3.4.2.8 Drug activity

The chemical structure of tocotrienol-rich fraction before and after the encapsulation was examined by ^{1}H NMR spectroscopy study using a Jeol NMR 600 running at 600 MHz with deuterated chloroform ($CDCl_3$) as a solvent. The samples with concentration of 15 mg/500 µL were prepared for analysis. In addition, the drug profile was also determined by a Waters high performance liquid chromatography (HPLC) that equipped with Waters 2475 multi λ Fluorescence Detector. The column used was Luna 5µ Silica 4.6 mm i.d. × 250 mm length. The mobile phase consists of heptane and ethyl acetate (94:6 *v*/*v*) at the flow rate of 0.6 mL/min.

CHAPTER 4: RESULTS AND DISCUSSION

4.1 Characterizations of microfibrillated celluloses

4.1.1 Fourier transform infrared spectroscopy (FTIR)

FTIR spectroscopy is an appropriate technique to monitor the variations on the chemical compositions of the samples in response to different treatments. As presented in Figure 4.1 and Figure 4.2, all the treated and untreated OPEFBs exhibited two major absorbance regions which include the regions at high wavenumbers (2800–3500 cm^{-1}) as well as low wavenumbers (500–1700 cm^{-1}), which was in consistent with previous studies (Chee et al., 2013; Fahma et al., 2010). Figure 4.1 displays the FTIR spectra of all the pre-treated samples before the digestion by sulfuric acid. Based on the spectra obtained, there were slight changes in the chemical compositions after the alkaline treatment and the bleaching process.

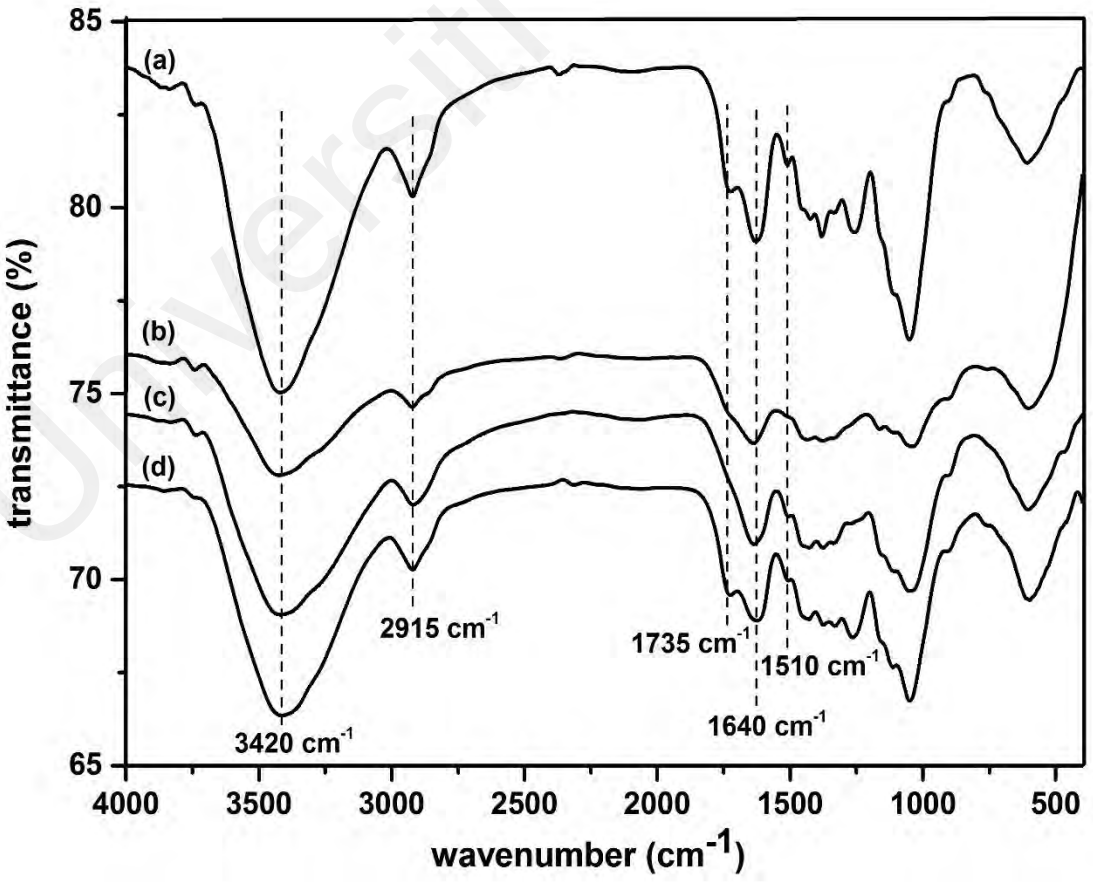

Figure 4.1: FTIR spectra of (a) raw OPEFB, (b) bleached OPEFB, (c) alkaline treated fibers, and (d) OPEFB after Soxhlet extraction.

The dominant and broad absorption band located from 3500-3400 cm^{-1} and the peak at approximately 2900 cm^{-1} were observed in the entire spectra, ascribed to the OH and CH stretching, respectively (Ching et al., 2015; Satyamurthy et al., 2011). The prominent peak at 1735 cm^{-1} could be observed in the spectra of raw OPEFBs, fibers after Soxhlet extraction and APS-treated MFCs, but it totally vanished in other spectra. The peak at 1735 cm^{-1} was associated to the presence of the acetyl and uronic ester groups of the hemicelluloses or to the ester linkage of the carboxylic groups of the ferulic and p-coumeric acids of lignin and/or hemicellulose (Sain & Panthapulakkal, 2006). The disappearance of this peak substantiated that most of the hemicelluloses and lignin were removed effectively after NaOH and $NaClO_2$ treatments (Cherian et al., 2008).

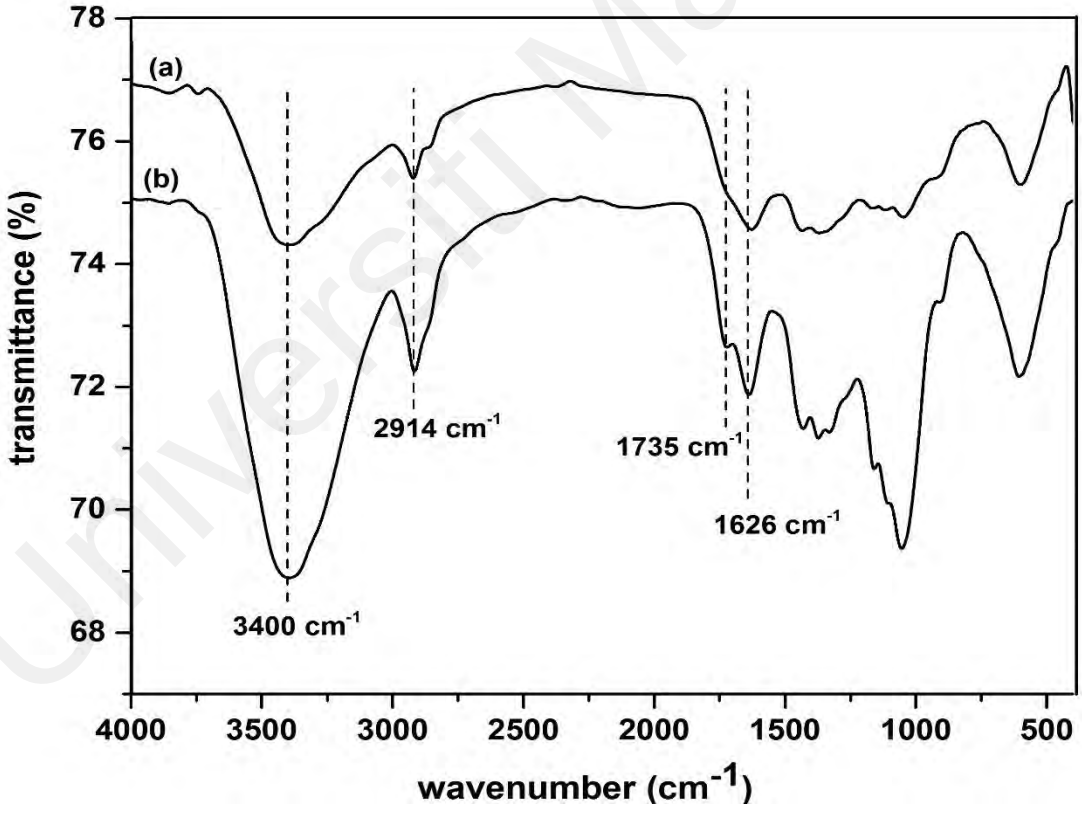

Figure 4.2: FTIR spectra of (a) sulfuric acid hydrolyzed MFCs, and (b) APS treated MFCs.

However, the IR spectrum of APS-derived nanocelluloses as shown in Figure 4.2(b) displayed a signal at 1735 cm^{-1}, indicating the presence of the C=O band that was the

most notable difference observed in respect to acid-hydrolyzed nanofibers. The APS-oxidized samples have peaks at 3400 cm^{-1} and at 1735 cm^{-1}, attesting the presence of carboxylic acid groups (Leung et al., 2011). In addition, the peak at approximately 1510 cm^{-1} was another significant signal for tracking the presence of the lignin as it represented the C=C stretching vibration in the aromatic ring of lignin (Wenshuai ChenHaipeng Yu & Yixing Liu, 2011; Wenshuai ChenHaipeng YuYixing Liu et al., 2011; R. Sun et al., 2000). This characteristic peak disappeared completely after the bleaching process, indicating that $NaClO_2$ had successfully dissolved the lignin components of OPEFB. Furthermore, the peak at approximately 1640 cm^{-1} observed in all the spectra corresponded to the H–O–H stretching vibration of the water molecules absorbed by the OPEFB fiber as OPEFB is hygroscopic in nature (Wenshuai ChenHaipeng YuYixing Liu et al., 2011).

4.1.2 Morphological investigation

Figure 4.3 depicted the FESEM micrographs of bleached fibers, acid-hydrolyzed MFCs and APS-derived MFCs. The pristine OPEFB fiber is composed of microfibril bundles tangled with massive non-fibrous components; namely hemicelluloses and lignin (Fatah et al. 2014; Alemdar and Sain 2008; Johar et al. 2012). However, Figure 4.3(a) showed individualized fibrils under FESEM observation, indicating the elimination of cementing materials after bleaching process which was in a strong agreement with spectroscopic result.

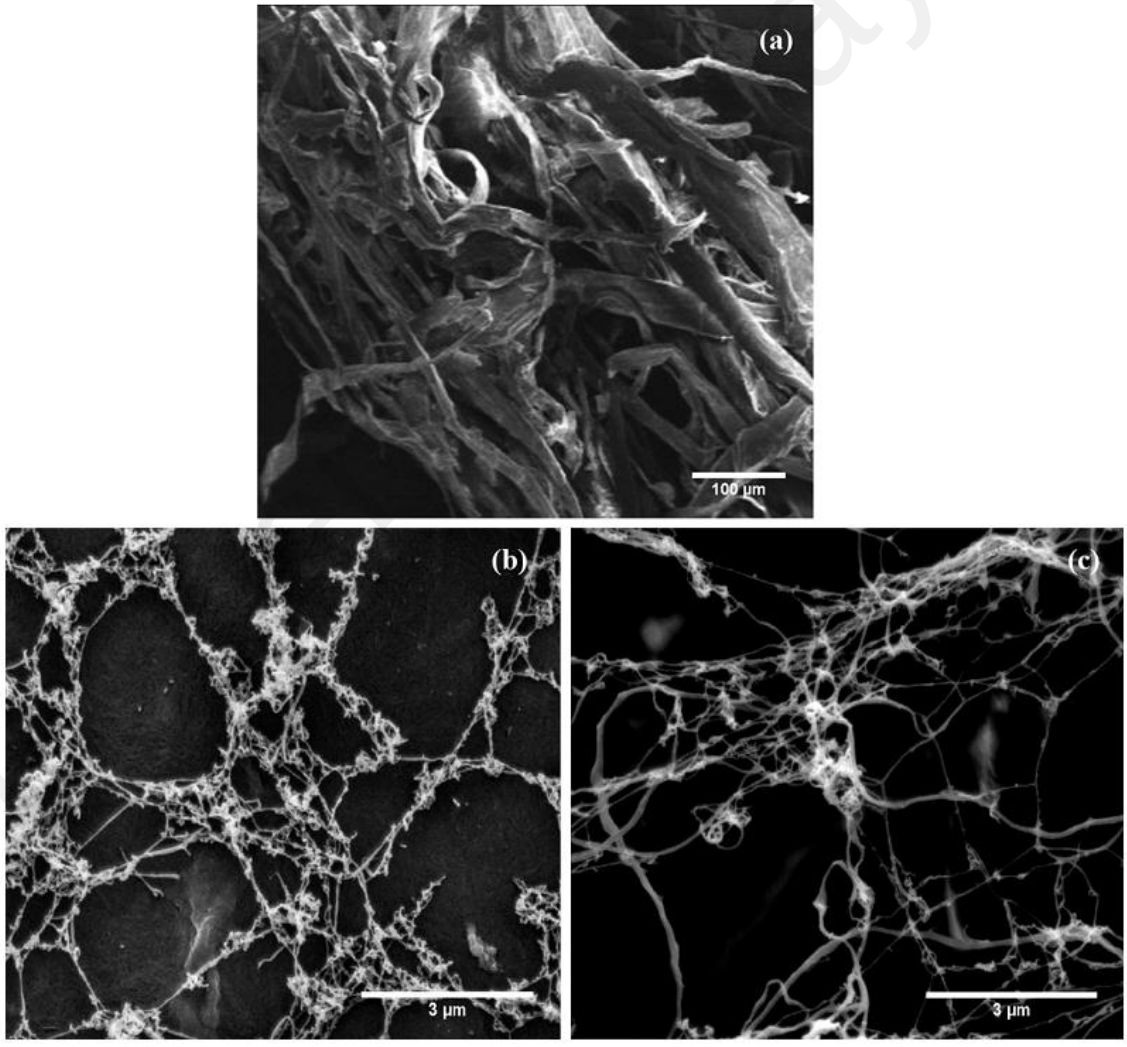

Figure 4.3: FESEM micrographs of (a) bleached fibers, (b) sulfuric acid hydrolyzed MFCs, and (c) APS derived MFCs.

As mentioned in the procedure description, OPEFB fibers were treated by NaOH prior to the bleaching using $NaClO_2$. NaOH treatment facilitated the dissolution of hemicelluloses and partial depolymerization of the lignin as well induced the segregation of fiber bundles into elementary fibers. Meanwhile, the bleaching process aided to exclude most of the lignin present in OPEFB fibers effectively, contributing to further defibrillation and reduction in the fiber diameter. The bleaching agent containing chlorine was able to oxidize the lignin and stimulate the formation of hydroxyl carbonyl and carboxylic groups, which in turn facilitated the solubilization of lignin in an alkaline medium (Cherian et al., 2010). The bleached fibers were found to have average mean of 14 μm.

The results revealed that the fiber diameter diminished to nanometer scale after sulfuric acid hydrolysis reaction and APS treatment. Both acid-hydrolyzed MFCs (Figure 4.3(b)) and APS-derived MFCs (Figure 4.3(c)) exhibited long and network-like fibrils, whereby the morphologies of both samples were similar to the morphologies of the MFCs obtained by Zimmermann et al. (2010). Aggregation of nanocellulose can be observed in Figure 4.3(b) and Figure 4.3(c), which is the common phenomenon that reported by many previous studies (Kargarzadeh et al., 2012; Lu & Hsieh, 2012; Rubentheren et al., 2015). Self-assembly of cellulose can be due to the hydrogen bonding and depends on the species as well as separation method of the nanofibers (Hult et al., 2001). Nanofibers hydrolyzed an hour in sulfuric acid have diameters ranging from 8 to 26 nm, with the majority at approximately 16 nm. Meanwhile, 16 hours APS treated nanofibers have mean diameter of 23 nm. Nevertheless, it was difficult to obtain an appropriate measurement of the length for both APS-oxidized and acid-hydrolyzed MFCs because of the difficulty in assigning the ends of the MFCs.

Fatah et al. (2014) also reported on the isolation of nanofibers from OPEFB by sulfuric acid hydrolysis but with the assistance of mechanical disintegration. They treated the bleached OPEFB with 30% of H_2SO_4 solution at 60 °C for 2 h with an acid to fiber ratio of 17.5:1 and successfully reduced the size of the fibers to 9 ± 1 μm, along with the shortened length of fibers. This revealed that the size of the resulting fibers after sulfuric acid hydrolysis was strongly dependent on the acid concentration as well as the acid-to-fiber ratio. Furthermore, X. M. Dong et al. (1998) showed that 45 ºC was more favorable for acid hydrolysis than higher temperatures such as 65 ºC because higher temperatures can potentially lead to dehydration reaction. For extraction of nanofibers by APS, E. Lam et al. (2013) prepared rod-shape nanowhiskers from microcrystalline cellulose (Avicel PH102 microcrystalline cellulose, FMC Corp.) using APS oxidation, and the final diameter of the fiber was found to be approximately 5 nm. This indicated that the morphology and width of the nanocelluloses formed from APS treatment depend on the raw material used.

The nanofiber yield after sulfuric acid hydrolysis and APS oxidation was determined by the weight difference. The yield percentage of the acid-hydrolyzed MFCs was approximately 25%. Meanwhile, extraction via APS treatment was determined to produce about 40% of MFCs in weigh basis. This result showed that APS oxidation can effectively synthesize nanofibers in larger quantities with only one-step treatment.

4.1.3 X-ray diffraction (XRD) analysis

XRD studies were conducted to evaluate the crystalline behaviors of raw OPEFB and chemical treated fibers. Celluloses are semi-crystalline biopolymers that well-known to comprise of both crystalline and amorphous domains in their molecular structure. Crystalline regions are well-organized parts because of the hydrogen bonding interactions and *van der Waals* forces between the molecules (Bakar et al., 2015; Y. H. P. Zhang & L. R. Lynd, 2004). On the contrary, amorphous regions are disordered parts within the cellulose structures due to the absence of the H-bonding (Jonoobi et al., 2011). The implications of different chemical treatments on the crystallinity index of the cellulose can be determined and compared from the XRD diffractogram profiles obtained.

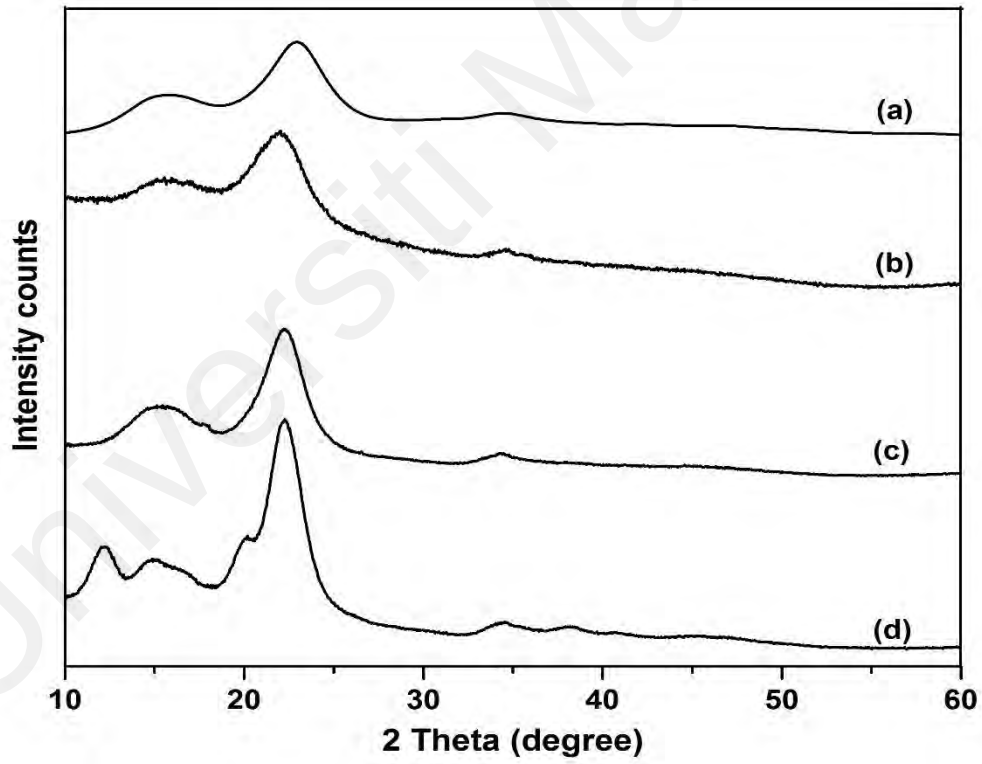

Figure 4.4: Powder diffraction pattern calculated based on (a) cellulose I structure (pwhm = 3.8°) using mercury software and the experimental powder diffraction patterns of (b) raw OPEFB, (c) APS oxidized MFCs and (d) sulfuric acid hydrolyzed MFCs.

Figure 4.4 displays the experimental and simulated diffraction patterns of cellulose. All the treated and untreated fibers exhibit typical X-ray diffraction patterns of cellulose

I. The crystallinity index values for raw OPEFB and APS-oxidized MFCs and acid-hydrolyzed MFCs were calculated to be 31, 64 and 72 %, respectively. A partial transformation to cellulose II is seen for the sulfuric acid-hydrolyzed MFCs. This is probably due to the treatment 17.5 % NaOH to remove hemicellulose. Leung et al. (2011) investigated the APS oxidation on different cellulosic sources including the flax, hemp, bacterial cellulose, commercial microcrystalline cellulose and fibrous cellulose powder (Whatman CF1). They reported that the crystallinity index for most of the nanofibers after the treatment was higher than for the parental counterparts except for the nanofibers isolated from commercial microcrystalline cellulose and Whatman CF1. The crystallinity index of nanofibers prepared from commercial microcrystalline cellulose increased only slightly after the APS oxidation and remained similar for Whatman CF1.

The crystallinity index of nanofibers after 60 min of sulfuric acid hydrolysis was anticipated to be higher as compared to raw fibers because of the removal of a substantial part of the amorphous non-cellulosic constituents including pectin, hemicelluloses and lignin during the pre-treatment steps (Alemdar & Sain, 2008; Wenshuai ChenHaipeng Yu & Yixing Liu, 2011; Wenshuai ChenHaipeng YuYixing Liu et al., 2011; R. Li et al., 2009). Both alkalization and bleaching processes can effectively alter the crystallographic structure of fibers as well to eliminate the surface impurities which are vital for the enhancement of the fiber-matrix interaction. This occurs because both of these treatment stages induce the exposure of the hydroxyl groups for the bonding reactions (Abraham et al., 2011).

After the sulfuric acid hydrolysis, it was postulated to have a further increment in crystallinity as the hydronium ions could penetrate into the more accessible amorphous domains of cellulose, promoting the hydrolytic cleavage of glycosidic bonds and eventually liberating the elementary crystallites (R. Li et al., 2009). Moreover, higher

crystallinity could be achieved during the self-assembling of nanocellulose as the realignment occurred in this nature phenomenon, enabling close packing and hydrogen bonds formation (Li et al. 2009; Lu and Hsieh 2012). However, the crystallinity index of nanofibers after 60 min of sulfuric acid hydrolysis was determined to decrease slightly, which possibly the consequence of excessive exposure to concentrated sulfuric acid. According to Fahma et al. (2010), the crystallinity of fibers tended to decline slightly after 60 min of sulfuric acid hydrolysis as well. They reported that the crystallinity index of nanofibers prepared from OPEFB by 60 min of sulfuric acid hydrolysis was about 54% with the raw OPEFB being 55%. Furthermore, alkaline treatment also believed to be able to consume the crystalline cellulose while increasing the amount of the amorphous cellulose, as shown in the XRD pattern of acid hydrolyzed nanofibers (Maya Jacob John & Rajesh D Anandjiwala, 2008).

Cellulose crystallinity is of prime importance as this is a key factor to determine the reinforcing capability and mechanical strength of cellulose to be utilized in composite application. The highly crystalline fibers are expected to be more effective in providing higher reinforcement for composite materials owing to the increased stiffness and rigidity, achieving a higher Young's modulus (Q. Cheng et al., 2007).

4.1.4 Thermostability analysis

Thermogravimetric analysis was used to investigate the thermal stability of the untreated and treated fibers. Determination of the thermal characteristics of the reinforcing materials is essential in order to evaluate the applicability of these materials in biocomposite applications at high temperatures. Both TG and dTG curves were plotted, as shown in Figure 4.5 and Figure 4.6, to track the thermal stability differences for all the samples. The dTG curves allowed for more precise assessment and comparison.

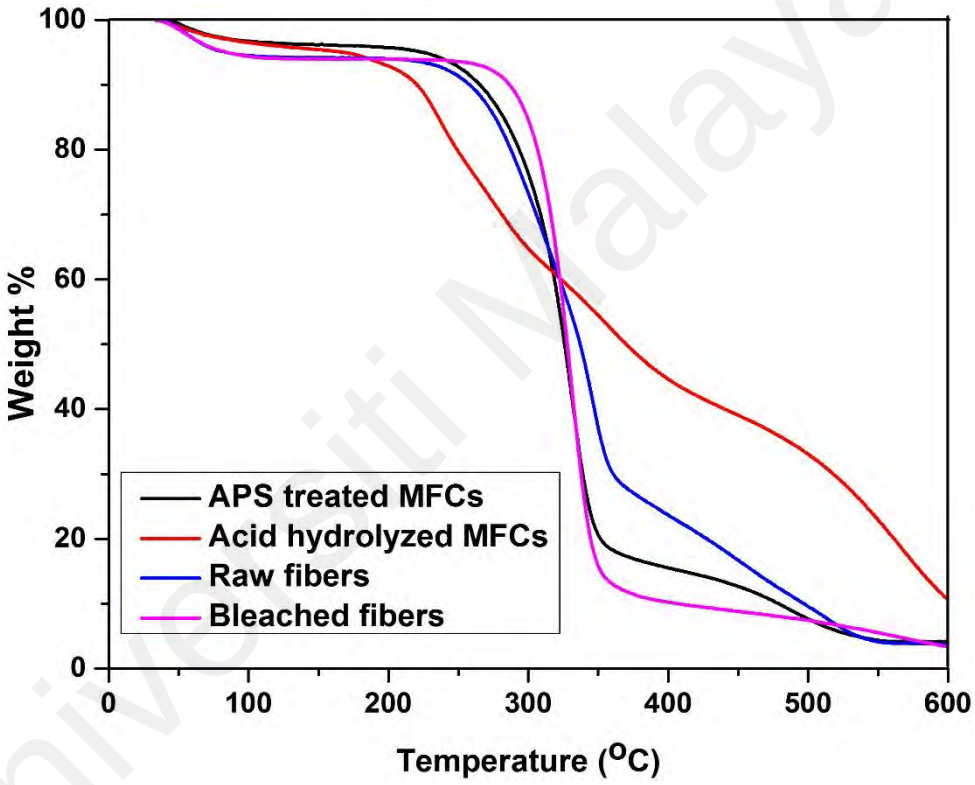

Figure 4.5: TG curves of APS-treated MFCs, sulfuric acid hydrolyzed MFCs, raw fibers and bleached fibers.

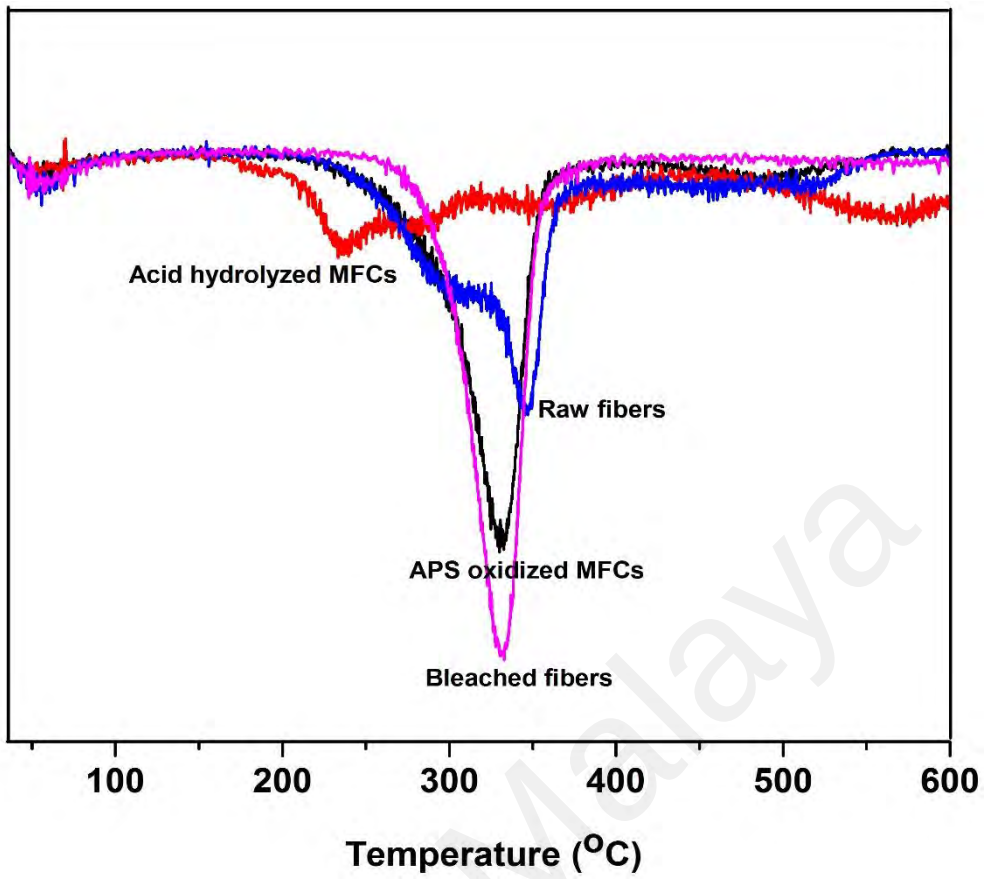

Figure 4.6: dTG curves of APS treated MFCs, sulfuric acid hydrolyzed MFCs, raw fibers and bleached fibers.

An initial weight loss was observed for all the samples upon heating to 100 ºC, resulting from the vaporization of the loosely bound moisture on the surface of the materials (Fahma et al., 2010; Kargarzadeh et al., 2012; Yong et al., 2015). According to Morán et al. (2007), another reason for this small weight loss was the degradation of the low molecular compounds remaining after various treatment stages. Raw OPEFB was detected to pyrolyze at different stages because it consists of various constituents, which include hemicelluloses, lignin and cellulose. This observation was expected because cellulosic and non-cellulosic components decompose at different temperatures (Morán et al., 2007; H. Yang et al., 2007). A low temperature shoulder was clearly observed in dTG curve of raw OPEFB that ascribed to the degradation of hemicellulose (Morán et al., 2007). Hemicellulose decomposed at lower temperature than lignin and cellulose, and this was attributed to the presence of acetyl groups in its structure. Meanwhile, there was

another noticeable peak at around 350 ºC that corresponded to the pyrolysis of cellulose (Kargarzadeh et al., 2012).

The findings revealed that there were two decomposition stages for acid-hydrolyzed nanofibers at approximately 235 ºC and 350 ºC, which in accordance with the previous study reported by Mandal and Chakrabarty (2011) (Figure 4.5). It was plausible to postulate that the early decomposition temperature is the consequence of the hydrolysis process, which results in a massive reduction of the molecular weight (Mohamad Haafiz et al., 2013). Furthermore, it was also believed that the sulfuric acid hydrolysis not only removes the non-crystalline segment, but could also potentially dissolve some crystalline segment, making it more susceptible to degradation in response to rising temperature (Mandal & Chakrabarty, 2011). Moreover, two different decomposition stages can also be explained by the presence of highly sulfated amorphous domains and unsulfated crystalline domains. The highly sulfated regions were more susceptible to degradation at lower temperature, whereas the higher temperature decomposition corresponded to the breakdown of unsulfated crystals (Kargarzadeh et al., 2012). While, both bleached fibers and APS-derived MFCs depicted major peak at 330 ºC, which represented the decomposition of cellulose.

Previous studies (D.-Y. Kim et al., 2001; Roman & Winter, 2004; Wang et al., 2007) reported that a longer hydrolysis period induced the incorporation of more negatively charge sulfate groups to cellulose surfaces and led to the reduction in the thermostability of treated nanofibers. Sulfate groups replaced the OH groups of celluloses, leading to dehydration reactions. Cellulose degradations can be catalyzed because the activation energies of cellulose chain degradations were lowered bey dehydration reactions (Roman & Winter, 2004; Wang et al., 2007). In addition, long hydrolysis time also cleaved celluloses into short chains, providing a large surface area and resulting in low degree of

polymerization that tended to degrade at low temperatures (Wang et al., 2007). The large surface area diminished the thermal stability of the cellulose because of the increased exposure to heat (Lu & Hsieh, 2010).

The low thermal properties of acid-hydrolyzed nanofibers can be solved by neutralization with NaOH (Martínez-Sanz et al., 2011; Wang et al., 2007) or by conducting the hydrolysis using different acid species such as hydrochloric acid (HCl) in replacement of H_2SO_4 (Mohamad Haafiz et al., 2013). After neutralization with NaOH, no acid sulfate groups remained and the thermal stability was shifted to a higher temperature but the crystallinity was similar. Therefore, sulfate group contents play a significant role in determining the thermal properties of the materials (Kargarzadeh et al., 2012). In addition, sulfated groups were recognized to be flame retardants. For this reason, the char fraction increased with an increasing amount of the sulfated groups. As a result, the amount char residues remained after 600 ºC was found to be higher for acid-hydrolyzed fibers (Roman & Winter, 2004).

4.1.5 Optical transmittance

UV-Vis spectroscopy was carried out to obtain information on the impacts of different treatments on the transparency of the MFC suspensions. The degree of the transparency also reflects the size of the fibers. The transmittance is strongly dependence on the wavelength in which it decreases with decreasing wavelength (Benhamou et al., 2014). Indeed, light will scatter when it passes through nanocellulose suspension containing randomly dispersed particles because the scattering occurs when there is a discontinuous in refractive index and eventually causing a reduction in transparency degree (Besbes et al., 2011). In addition, light will scatter more when the wavelength approaches the width of the dispersed particles (Tsuguyuki Saito et al., 2006). As observed from UV-Vis spectra in Figure 4.7, acid-hydrolyzed nanofibers were noted to have highest optical transmittance followed by APS-oxidized nanofibers and bleached fibers. This indicated that the nanofibers generated by sulfuric acid hydrolysis had smaller sizes than APS-derived nanofibers. These results were in accordance with the observations from FESEM.

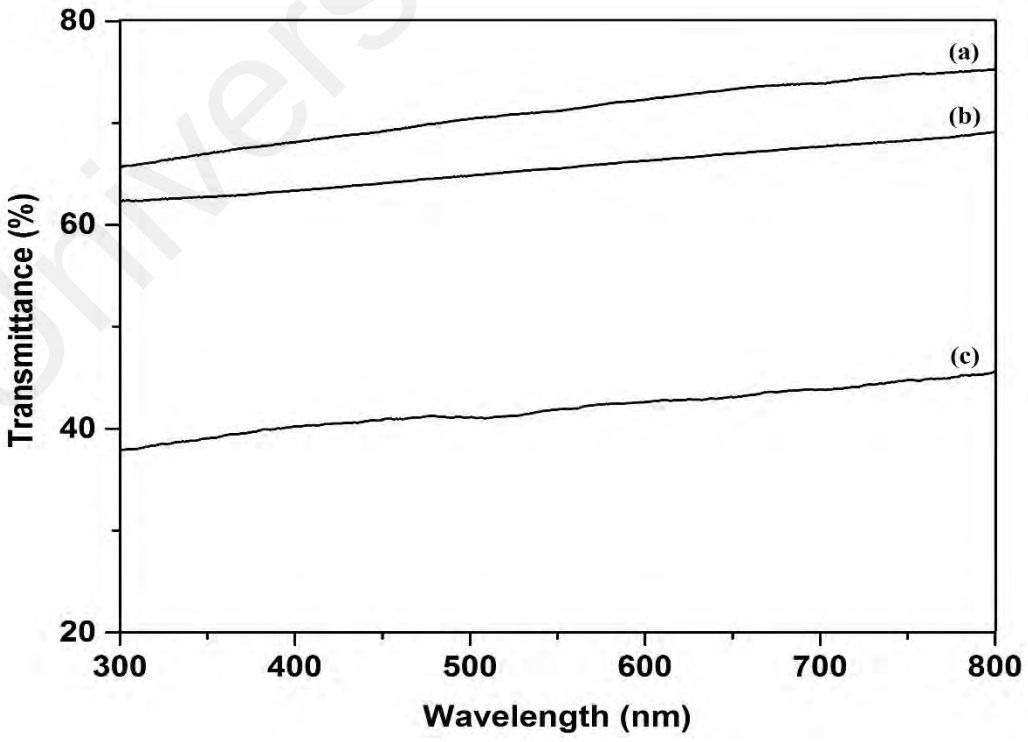

Figure 4.7: UV-Vis transmittance spectra of (a) sulfuric acid hydrolyzed nanofiber suspensions, (b) APS oxidized nanofiber suspensions, and (c) bleached OPEFB.

4.2 Characterizations of trimethylsilyl celluloses

4.2.1 Determination of characteristics functional groups of trimethylsilyl cellulose

Sample of TMSC was characterized by FTIR spectroscopy. The spectra for both TMSC and the corresponding acid-hydrolyzed MFCs were displayed in Figure 4.8. FTIR spectroscopy is an appropriate technique to monitor the substitution of -$Si(CH_3)_3$ groups onto cellulose backbone. Several characteristic peaks of the substituted groups, namely: 747 cm^{-1} and 1252 cm^{-1} ($Si(CH_3)_3$); 840 cm^{-1} (Si-C) and 1126 cm^{-1} (Si-O-C) were identified (Mormann & Wezstein, 2009) in the spectrum of TMSC. As compared to acid-hydrolyzed MFCs, it was observed that the pronounced OH-stretching band (3400-3500 cm^{-1}) was shifted to higher wavenumber and appeared contracted for TMCS sample. This was ascribed to the transformation of hydroxyl groups into $Si(CH_3)_3$ groups. It was supported by the decreased in the intensity of the OH-stretching band which is proportional to the degree of silylation (Puspasari et al., 2015).

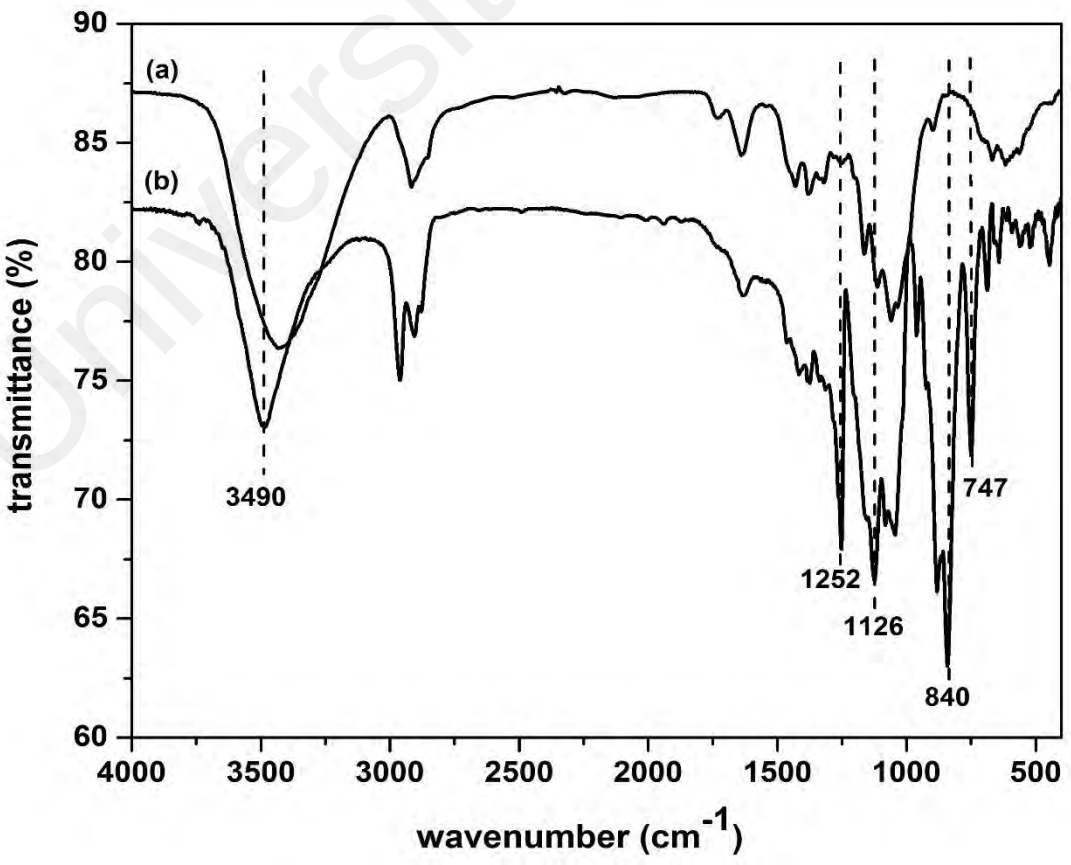

Figure 4.8: FTIR spectra (a) acid-hydrolyzed MFCs and (b) trimethylsilyl celluloses.

4.2.2 ^{1}H nuclear magnetic resonance spectroscopy

Figure 4.9 showed NMR spectrum of trimethylsilyl cellulose. Hydrogen atoms of trimethylsilyl groups show signals at approximately 0.09 ppm; whereas signals due to the resonances of the hydrogen atoms of the cellulose's CH groups appear between 2.9 and 5.5 ppm (Mormann & Wezstein, 2009; Puspasari et al., 2015). Degree of substitution (DS) was determined using ^{1}H NMR by dissolving the hydrophobic cellulose derivative in deuterated chloroform. Silylation of cellulose yielded highly functionalized TMSC with DS of 2.91. The solubility of TMSC in organic solvents depends on the degree of silylation. Mormann and Wezstein (2009) synthesized TMSCs with different DS and their solubility in different solvents were tested. TMSC with DS = 1.0 was soluble in dimethyl sulfoxide (DMSO) and dimethylacetamide (DMAc), while samples DS ≥ 2.3 were soluble in chloroform ($CHCl_3$), tetrahydrofuran (THF) and toluene.

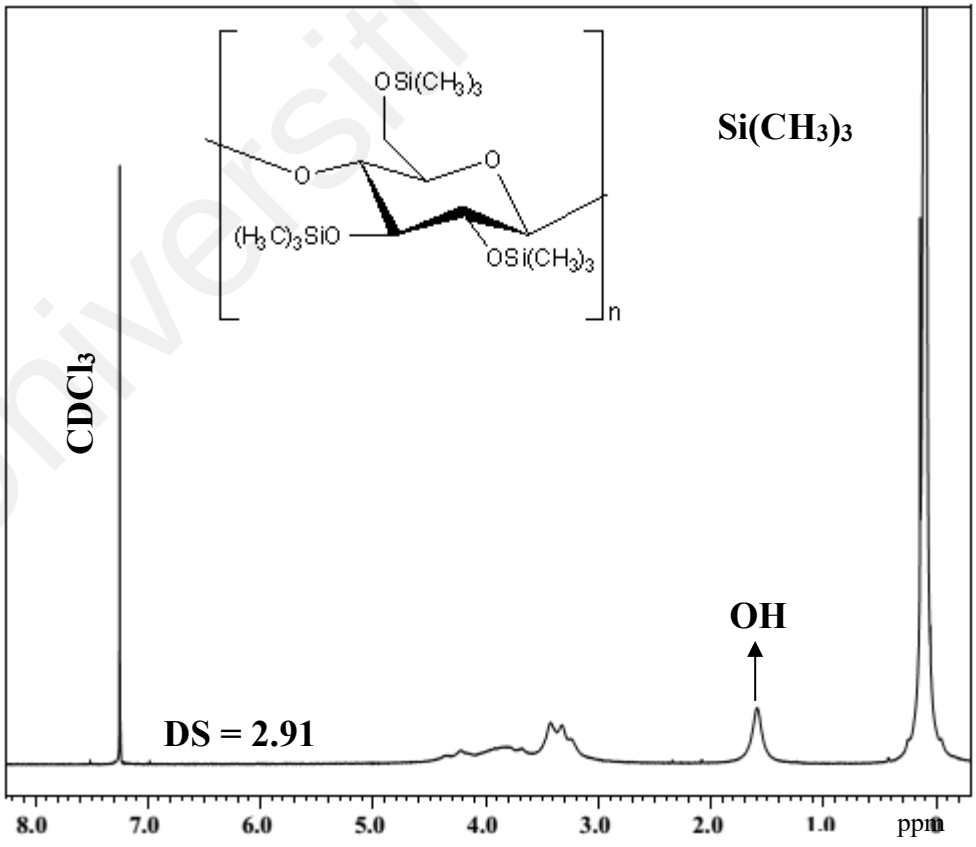

Figure 4.9: NMR spectrum of trimethylsilyl cellulose

4.3 Selection of emulsifiers: Solubility of vitamin E in different emulsifiers

Emulsion is a system that consists of two immiscible liquids, in which one liquid is dispersed in another with the aid of surface active agents (Branen et al., 2001). The presence of emulsifier is of paramount importance in the emulsification. Emulsifier plays an essential role in droplet stabilization by rapidly assembling at the bare oil/water interface to hinder the recoalescence of droplets. They further facilitate the droplet disruption by reducing the interfacial tension forces between oil and water (R. Pichot et al., 2010). The selection of suitable emulsifier is critical in the formation of a stable monodispersed system. Hence, the solubility of vitamin E in various emulsifier solutions was screened by HPLC and presented in Table 4.1.

Table 4.1: Solubility of vitamin E in different types of emulsifier solutions.

Emulsifier	HLB value	Lipophilic domain (Hydrocarbon chain length:unsaturation)	Solubility (mg/g)
Tween 20	16.7	monolaurate (C12:0)	530.4 ± 17.8
Tween 40	15.6	monopalmitate (C16:0)	596.3 ± 7.8
Tween 60	14.9	monostearate (C18:0)	598.6 ± 29.9
Tween 80	15.0	monooleate (C18:1)	707.6 ± 32.9
Brij 35	16.9	(C12:0)	690.2 ± 32.8
Tween 80:Brij 35	15.95	–	731.6 ± 39.4

The emulsifiers evaluated in this study are Tween series of non-ionic surfactants as well as Brij 35. Tween series and Brij 35 are hydrophilic emulsifying agents that widely used in stabilizing the O/W emulsion (P. S. Goh et al., 2015). The hydrophilic-lipophilic balance (HLB) of tested emulsifiers are stated in Table 4.1, and Tween series surfactants are distinguished by the chain length and unsaturation of their hydrocarbon tails. It was believed that the ability of the surfactants to solubilize oil-form vitamin E is greatly

influenced by their molecular structures (Ziani et al., 2012). This study revealed that the solubility of vitamin E in Tween 20 was lowest among all the tested emulsifiers, which might be attributed to its shorter hydrophobic chain. Among all the assessed emulsifiers, Tween 80 and Brij 35 exhibited higher vitamin E solubility that are 707.6 ± 32.9 and 690.2 ± 32.8 mg/g, respectively. With this result, we further studied the vitamin E solubility in the blend of Tween 80:Brij 35 and we observed that its solubility increased to 731.6 ± 39.4 mg/g. Selection of emulsifiers for stabilizing vitamin E nanoemulsions based on the solubility of vitamin E in different emulsifiers was also conducted in the previous study (Laouini et al., 2012). Several emulsifiers were tested in their study: Tween 20 (polyoxyethylene glycol sorbitan monolaurate), Tween 60 (polyoxyethylene glycol sorbitan monostearate), Tween 80 (polyoxyethylene glycol sorbitan monooleate), Span 40 (Sorbitan monopalmitate), Span 60 (Sorbitan monostearate), Brij 35 (polyoxyethylene glycol dodecyl ether), Brij 98 (Polyoxyethylene glycol monooleyl ether), Labrafil (Oleoyl macrogol-6 glycerides) and Phosphatidylcholine. They examined that vitamin E was more soluble in Tween 80 and Brij 35 among all the evaluated surfactants. Therefore, mixture of Tween 80–Brij 35 (50:50 w/w) was selected to be employed in their study to stabilize vitamin E containing nanoemulsions. Since the resultant vitamin E-loaded emulsions will then be immobilized within alginate microbeads, surfactants that can solubilize highest amount of vitamin E are desirable to produce microbeads with high drug entrapment efficiency (Jafari et al., 2008a). Thus, mixed emulsifiers (Tween 80:Brij 35) were selected for further experiments.

4.4 Effect of different parameters on the formation of oil-in-water (O/W) emulsion

Emulsification is a vital step prior to entrapping vitamin E into microbeads. Droplet size is a key determinant for the properties of the emulsions such as physical stability (Joscelyne & Trägårdh, 2000). Besides, the emulsion droplet diameter also shows great impact on the encapsulation efficiency and the release profile of the resultant microbeads (Mahdi Jafari et al., 2006). Therefore, the effect of various parameters such as sonication amplitude, emulsifier concentration, vitamin E concentration as well as the polymer concentration on the Z-average diameter and the polydispersity index of emulsion droplets were investigated. The results were presented in Table 4.2. Besides, we also studied the influence of sodium alginate concentration on the percentage loss of vitamin E by using HPLC and the results obtained were displayed in Table 4.3. The observations for all the parameters were discussed in the following sections.

Table 4.2: Influence of sonication amplitude, emulsifier concentration, vitamin E concentration and sodium alginate concentration on Z-average diameter and polydispersity index of emulsions.

Sonication amplitude (%)	Concentration (% w/v)			Z-average diameter (nm)	Polydispersity index (PDI)
	Tween 80:Brij 35	Vitamin E	Sodium alginate		
60	2.5	2.5	–	131.7 ± 7.1	0.488 ± 0.031
80	2.5	2.5	–	111.3 ± 2.0	0.386 ± 0.021
100	2.5	2.5	–	88.4 ± 0.7	0.342 ± 0.042
100	1.0	2.5	–	95.3 ± 1.7	0.402 ± 0.022
100	1.5	2.5	–	88.6 ± 1.3	0.212 ± 0.013
100	2.0	2.5	–	88.6 ± 0.8	0.293 ± 0.006
100	2.5	2.5	–	88.4 ± 0.7	0.342 ± 0.042
100	1.5	2.5	–	88.6 ± 1.3	0.212 ± 0.013
100	1.5	3.0	–	126.9 ± 22.3	0.407 ± 0.081
100	1.5	3.5	–	148.5 ± 38.5	0.479 ± 0.094
100	1.5	2.5	1.5	127.7 ± 4.9	0.468 ± 0.016
100	1.5	2.5	2.0	139.3 ± 4.4	0.485 ± 0.015
100	1.5	2.5	3.0	148.5 ± 38.5	0.479 ± 0.094

Table 4.3: Influence of sodium alginate concentration on the percentage loss of vitamin E after the addition of alginate solution into primary O/W emulsions with 1.5 %w/v Tween 80:Brij 35 and 2.5 %w/v vitamin E.

Concentration of sodium alginate (% w/v)	Concentration of vitamin E (mg/g)		Percentage loss of vitamin E (%)
	Before the addition of sodium alginate	After the addition of sodium alginate	
1.5	734.1 ± 11.3	731.0 ± 11.8	3.1 ± 1.7
2.0	736.5 ± 10.2	729.6 ± 9.1	6.9 ± 1.6
3.0	737.2 ± 5.8	728.4 ± 6.6	8.8 ± 1.9

4.4.1 Influence of sonication amplitude

Sonication amplitude is an influential factor that affects the properties of emulsions formed because more intensive cavitation can be achieved upon increasing the applied amplitude (Kaltsa et al., 2014). Hence, the influence of sonication amplitude (60, 80 and 100%) on the droplet Z-average diameter and polydispersity index (PDI) of nano-emulsions was investigated at constant reaction time of 10 min as shown in Table 4.2. Elevated sonication amplitude minimized the mean droplet diameter, achieving smallest droplet size of 88.4 ± 0.7 nm with lower PDI at maximum amplitude of 100%. The results were in agreement with the previous study by P. S. Goh et al. (2015) in which the droplet diameter of tocols emulsions were reduced from 136.1 ± 2.5 nm to 108.6 ± 0.4 nm upon increasing the sonication amplitude from 60% to 100%. The study also reported that increased in sonication amplitude resulted in the decreased of PDI from 0.369 ± 0.011 to 0.268 ± 0.015. This was also supported by the study of Kaltsa et al. (2014). They produced whey protein isolate/xanthan gum (WPI/XG) stabilized emulsions using ultrasonication and they investigated the influence of sonication amplitude on the emulsion droplet size. They also noticed that it is effective to reduce the average droplet sizes by elevating the sonication amplitude due to increased cavitation. The droplet diameter of WPI/XG stabilized emulsions decreased from 1.432 to 0.943 μm when the amplitude increased from 40 to 100 %. In addition, orange peel essential oil (OPEO) in water nanoemulsions were fabricated in the previous study (Hashtjin & Abbasi, 2015). Amplitude of sonication appears to be one of the essential parameters that affect the resultant emulsion droplet size. The sizes of emulsion droplets increased significantly upon increasing the sonication amplitude. However, “over-processing” phenomenon was observed in the research conducted by Sinsuebpol and Changsan (2020). When the sonication amplitude level was set higher than 60%, both the emulsion droplet size and PDI were proportional to the

sonication amplitude. This phenomenon is undesirable because emulsions with larger droplet diameters and higher PDI are less stable.

4.4.2 Influence of emulsifier concentration

The mean droplet diameter and polydispersity index are also governed by emulsifier concentration of the obtained emulsions. The rise in the emulsifier concentration from 1.0% to 1.5% w/v diminished the Z-average diameter of emulsion droplet from 95.3 ± 1.7 to 88.6 ± 1.3 nm. Additionally, PDI also reduced from 0.402 ± 0.022 to 0.212 ± 0.013, indicating more uniform emulsion system was obtained (Table 4.2). This suggests that 1% w/v Tween 80:Brij 35 was insufficient to adhere at the oil-water interfaces, leading to droplet recoalescence (Khayata et al., 2012; Laouini et al., 2012). By adding more emulsifier, the average droplet size of emulsion reduced with lower PDI, which attributed to the declined in interfacial tension (R. Pichot et al., 2010). Spyropoulosa et al. (2011) also investigated the influence of emulsifier concentration on the emulsion droplet size using membrane emulsification technique. Few emulsifiers were tested, including Tween 20, Tween 80, soy lecithin and sodium dodecyl sulphate at various concentrations (0.0, 0.1, 0.2, 0.4, 0.6, 0.8 & 1.0 %wt). Their findings showed that the droplet size reduced upon increasing of emulsifier concentration regardless of the emulsifier type. Besides, P. S. Goh et al. (2015) also produced tocotrienol rich fraction containing emulsions stabilized by 50:50 w/w Tween 80 and Brij 35. Positive correlation between the concentration of emulsifier (0.75% to 3% w/v) and the mean emulsion droplet diameter was observed. In addition, Sinsuebpol and Changsan (2020) also reported that the emulsifier concentration has paramount effect on emulsion droplet size. The average droplet size of emulsions was decreased upon increasing the emulsifier concentration from 1.5% to 5% w/v, which was ascribed to the reduction of interfacial tension.

Above 1.5% w/v Tween 80:Brij 35, the emulsion droplet size was independent on the emulsifier concentration and situated at approximately 88.0 nm, but the PDI was greatly affected. PDI expresses the uniformity of droplet diameters, which is also being one of the crucial emulsion properties. Similar observation was reported in the previous study (Sullivan & Kilpatrick, 2002), the emulsion droplet size did not change significantly at the emulsifier concentrations above 0.5 wt%. This indicates that 0.5 wt% Tween 80 or milk protein isolate (MPI) was sufficient to stabilize newly formed oil/water interfaces of emulsions in their study. Since the resultant vitamin E nano-emulsions will then be loaded into microbeads, it is often desirable to produce high stability nano-emulsions which will in turn result in the formation of microbeads with high encapsulation efficiency (Jafari et al., 2008a). Hence, 1.5 %w/v of Tween 80:Brij 35 was retained for further studies.

4.4.3 Influence of vitamin E concentration

The effect of the vitamin E content on the emulsion droplets size and polydispersity was investigated by preparing vitamin E-loaded emulsions with three different concentrations of vitamin E (2.5%, 3.0% and 3.5% w/v). Increasing concentration of Vitamin E demonstrated adverse effect as the emulsion droplet size shifted towards larger diameter and PDI also increased accordingly (Table 4.2). Large variations in average droplet size and PDI upon increasing the concentration of vitamin E, highlighting the importance of this variable in the emulsification process. The viscosity of the dispersed phase was promoted because of the increased of vitamin E concentration contributes to these unfavorable results. High viscosity of dispersed phase makes it difficult to break up, resulting in large droplet size (Laouini et al., 2012).

The study of Hatanaka et al. (2010) reported similar result, in which the emulsion mean droplet diameter and size distribution were greatly influenced by the concentration of α-tocopherol. The emulsion droplet size prepared using 10 %wt of α-tocopherol was observed to be approximately 85.0 nm and increased up to 381.0 nm when the α-tocopherol ratio in the emulsion composition changed to 50 %wt. With the increase of α-tocopherol amount, the uniformity was also decreased that represented by the span factor. Hence, 2.5 %w/v of vitamin E was selected for subsequent experiment.

4.4.4 Influence of sodium alginate concentration

Various concentration of alginate (1.0, 1.5 and 2.0 %w/v) was incorporated into vitamin E-loaded emulsions and its modulating effect on the droplet size, PDI and EE% of drug was examined. Upon increasing alginate concentration from 1.0 to 2.0 % w/v, enlargement of emulsion droplet size from 127.7 ± 4.9 to 148.5 ± 38.5 nm was observed, as displayed in Table 4.2. Likewise, Khayata et al. (2012) also investigated the effect of polymer amount (50, 100 125 and 200 mg polycaprolactone, PCL) on the vitamin E-loaded nanocapsule size and the mean droplet diameter was noticed to increase from 150 ± 7 nm to 195 ± 8 nm with an increasing of polymer amount. The authors reported that this variation could be associated with the growth of shell thickness encapsulating the oil droplets by polymer molecules (Cauchetier et al., 2003). This implies that the number of the vitamin E-loaded emulsion droplet produced will not be necessarily doubled even we increased the alginate concentration from 1.0 to 2.0 %w/v (Khayata et al., 2012). In addition, the percentage loss of vitamin E after the addition of ALG solution into primary O/W emulsions was also investigated. As shown in Table 4.3, the percentage loss of vitamin E after the formation of secondary O/W emulsions increased from 3.1 ± 1.7 to 8.8 ± 1.9 % when the concentration of polymer increased from 1.5 to 3.0 %w/v. It can be postulated that ALG molecules have affinity towards Tween 80:Brij 35 via hydrophilic interactions. There is a possibility that surfactants interact solely with ALG molecules without attaching to the oil molecules. Hence, increased amount of ALG increased the competition between ALG molecules and oil molecules to attach with surfactants (K. Y. Lee & Mooney, 2012). Hence, 1.5 % w/v ALG solution was employed for further experiment.

4.5 Characterizations of primary oil-in-water (O/W) emulsions

4.5.1 Emulsion droplet size & polydispersity index (PDI)

The emulsion droplet size and its polydispersity index (PDI) were measured immediately after the emulsification. Polydispersity index (PDI) defined as the broadness of the droplet size distribution, representing the uniformity of the system. The smaller the value of PDI, the narrower the size distribution (P. S. Goh et al., 2015). The droplet diameter of the primary O/W emulsion prepared using Tween 80:Brij 35 as emulsifiers without the incorporation of celluloses was first investigated. Their ability in oil droplet break-up during the emulsification was screened. As shown in Figure 4.10, we observed that the droplet size of emulsion stabilized solely by Tween 80:Brij 35 was centered around 87.4 ± 4.9 nm with PDI of 0.212 ± 0.013. Tween 80 and Brij 35 are responsible to impede the re-coalescence of the formed emulsion droplets by rapidly assembling at the bare interface. Simultaneously, surfactants also promote further droplet break-up by lowering the interfacial tension (R. Pichot et al., 2010).

The droplet diameters of a series of primary emulsions stabilized by 1.5 % w/v Tween 80:Brij 35 with various APS-oxidized MFC concentrations were also studied (Figure 4.10). The incorporation of oxidized cellulose nanofibrils into Tween 80:Brij 35-stabilized systems was examined to show an antagonistic effect on emulsion droplet sizes. The droplet sizes of the emulsions were monitored to have larger sizes than those stabilized exclusively by Tween 80:Brij 35, with both systems containing the same concentration of surfactants. The droplet diameters of the primary O/W systems were rising upon increasing the concentration of APS-treated MFCs. According to the previous study, tricaprylin-in-water emulsions were produced by employing hydrophilic silica particles or heptaethylene glycol monododecyl ether ($C_{12}E_7$) surfactant molecules as sole emulsifier. The droplet sizes of these emulsions were compared with those emulsions stabilized by mixed emulsifiers of conventional surfactant and surface active

nanoparticles (BinksDesforges et al., 2007). The droplet diameters of emulsion obtained using silica particles as stabilizer were larger than that of surfactant-stabilized emulsions. In mixed emulsifier systems, the droplet sizes increased with increasing concentration of nanoparticles while remaining the same amount of surfactant.

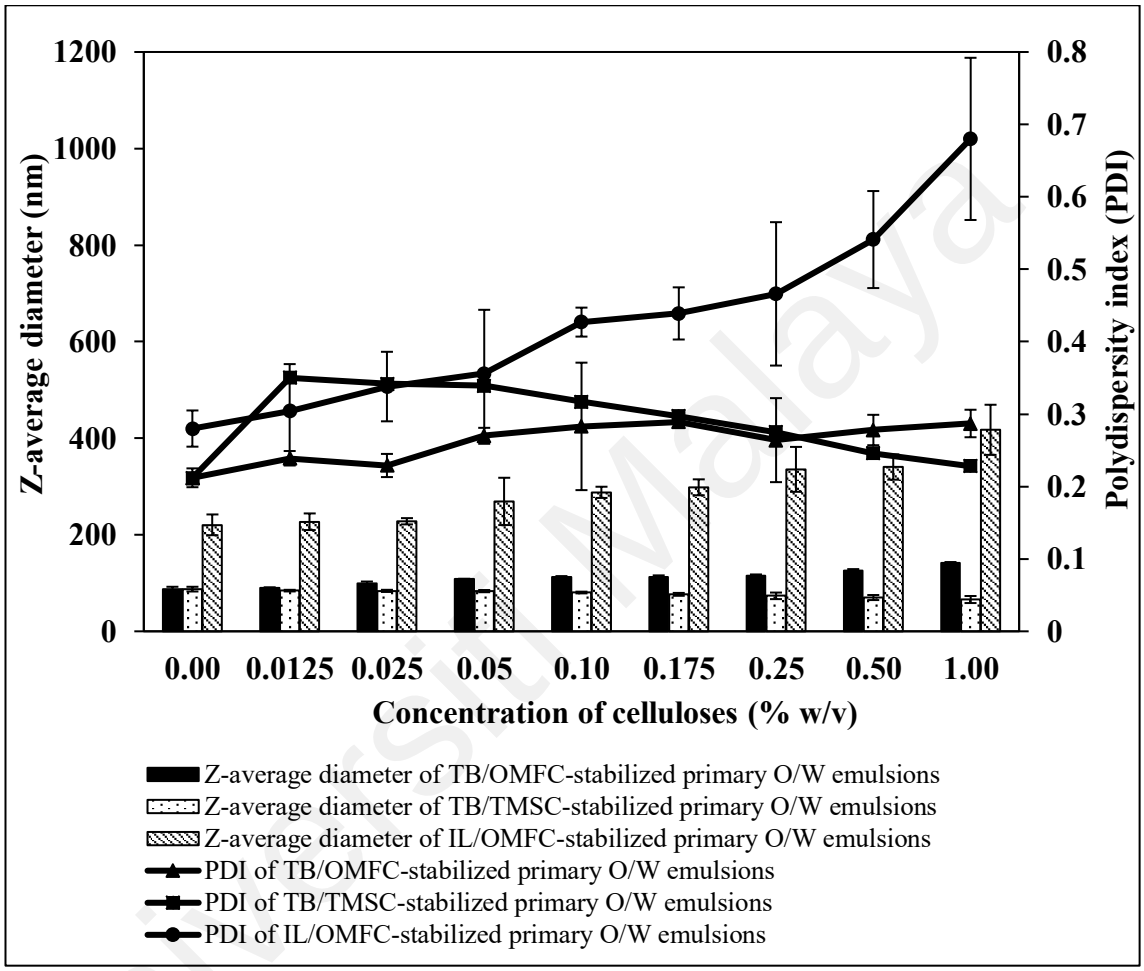

Figure 4.10: The effect of cellulose concentration on the Z-average diameter and polydispersity index (PDI) of TB/OMFC-stabilized, TB/TMSC-stabilized and IL/OMFC-stabilized primary O/W emulsions.

The rise of droplet diameters in Tween 80:Brij 35-stabilized systems after the addition of MFCs was due to the affinity of surfactants to attach to the cellulose particle surfaces, depleting surfactants from the oil-water interfaces (BinksRodrigues et al., 2007). As the cellulose particle concentration increases, more stabilizing amphiphiles loss to particle surfaces resulted in droplet coarsening (BinksDesforges et al., 2007). Nonionic surfactants with ethoxylated groups can form hydrogen bonds with carboxyl groups on

APS-oxidized cellulose surfaces (Abhay R. Ladhe & Bhattacharyya, 2009; Abhay R Ladhe et al., 2006; R. Zhang & Somasundaran, 2006). This is the possible reason accounts for the difference in the droplet size between the emulsions stabilized solely by Tween 80:Brij 35 and those stabilized by the mixture of surfactants and oxidized MFCs.

In the previous study, Katepalli and Bose (2014) studied the influence of the addition of negatively charged fumed silica particles on the properties of Triton X-100 (nonionic surfactant) stabilized dodecane-in-water emulsions. They obtained similar results whereby droplet coarsening was observed after the incorporation of fumed silica particles into Triton X-100 stabilized emulsions and the average droplet diameters increased with an increased in silica concentration. They also believed that the droplet broadening was probably resulted from the depletion of surfactants from the interfaces. This can be attributed to the formation of hydrogen bonds between ethoxylated groups of Triton X-100 with hydroxyl groups of silica. Furthermore, Angkuratipakorn et al. (2017) also investigated the droplet sizes of Pickering emulsions stabilized by both defatted rice bran (DRB)-extracted cellulose nanocrystals and non-ionic surfactant, poly(glycerol-succinate) oligoester (PGS oligoester). In their study, cellulose nanocrystals and PSG oligoester showed synergistic effect, as evidenced by the formation of stable Pickering emulsions. Emulsion produced by 2.5 wt% of PSG oligoester and 0.25 wt% cellulose nanocrystals showed highest stability with smallest droplet diameters and they were monodisperse droplets. However, the emulsion droplet sizes turned to be larger (more than 10 μm) and polydisperse after the addition of gum arabic. The absence of cellulose nanocrystals in the systems containing PSG oligoester and gum arabic led to the enlargement of droplet size. Droplets separation was observed from the confocal laser scanning microscopy images because of the repulsion between the droplets attributed to the same charged functional groups of cellulose nanocrystals and gum arabic. This is favorable in hindering the droplet aggregations. Although cellulose nanocrystals are

effective in stabilizing the emulsions, excess cellulose nanocrystals tend to increase the emulsion droplets due to the coalescence of cellulose nanocrystals.

In addition, we extended our studies by replacing hydrophilic APS-derived MFC with hydrophobic TMSC as stabilizer. Modification of cellulose via silylation produced hydrophobic TMSC by incorporating the silyl group, $-Si(CH_3)_3$ into cellulose backbone. Hydrophobic TMSCs aided in enhancing the emulsion stabilization by anchoring to the oil/water interfaces, together with non-ionic surfactants. This claim was supported by the reduction of mean droplet diameter upon increasing the amount of TMSC because more TMSC particles were available to adhere at the freshly formed interfaces (Figure 4.10). PDI of surfactant-TMSC emulsions declined slightly from 0.350 ± 0.041 to 0.228 ± 0.004 while increasing the concentration of TMSC from 0.0125 to 1.000 % w/v.

The influence of the type of emulsifier employed to stabilize the emulsion was also examined by substituting Tween 80:Brij 35 with ionic liquid, 1-butyl-3-methylimidazolium octylsulphate ($C_4mimC_8SO_4$) as surface-active agent. As illustrated in Figure 4.10, the droplet size of primary O/W emulsion stabilized solely by ionic liquid was approximately 220.6 ± 21.5 nm with PDI of 0.280 ± 0.025, and it increased after the addition of MFCs. Emulsions that using Tween 80:Brij 35 as emulsifier showed much smaller droplet diameters than the emulsions employing $C_4mimC_8SO_4$ as surface active agent at the corresponding concentration of cellulose. By referring to the chemical structures of Tween 80, Brij 35 (Figure 2.8) and $C_4mimC_8SO_4$ (Figure 2.9), we noticed that both Tween 80 & Brij 35 possess longer hydrophobic alkyl tails than $C_4mimC_8SO_4$. The hydrophobic interaction between non-polar alkyl groups and the oil was believed to be the driving force for the stability of emulsions and reduction of droplet size (Chandler, 2005). The longer the hydrophobic domain of the emulsifier, the stronger the hydrophobic

interaction with the oil. This led to minimization of the droplet size (Murshid & Wang, 2017).

4.6 Characterizations of secondary oil-in-water (O/W) emulsions

4.6.1 Emulsion droplet size, polydispersity index (PDI) & Zeta potential

The incorporation of ALG solution into primary emulsions imparted profound effect on the emulsion droplet size as well as PDI (Figure 4.11 and Figure 4.12). The enlargement of emulsion droplet diameter was observed for all the tested formulations that ascribed to the formation of the shell covering emulsion droplet by ALG (Pongsawatmanit et al., 2006). The mean droplet sizes of Tween 80:Brij 35-stabilized secondary O/W emulsions at various APS-oxidized MFC contents were noticeably smaller with more uniform systems as indicated by the lower PDI (Figure 4.11). It is noteworthy to mention that micron droplet sizes that range from 6.9 ± 0.1 to 9.5 ± 0.1 μm were obtained for secondary O/W emulsions stabilized by $C_4mimC_8SO_4$ at different amounts of APS-oxidized MFCs, which can only be detected by Mastersizer (Figure 4.12). However, the size distributions of $C_4mimC_8SO_4$-stablized systems were defined by span factor. Low span factor indicates narrow size distribution and more uniform the system is (Hatanaka et al., 2010).

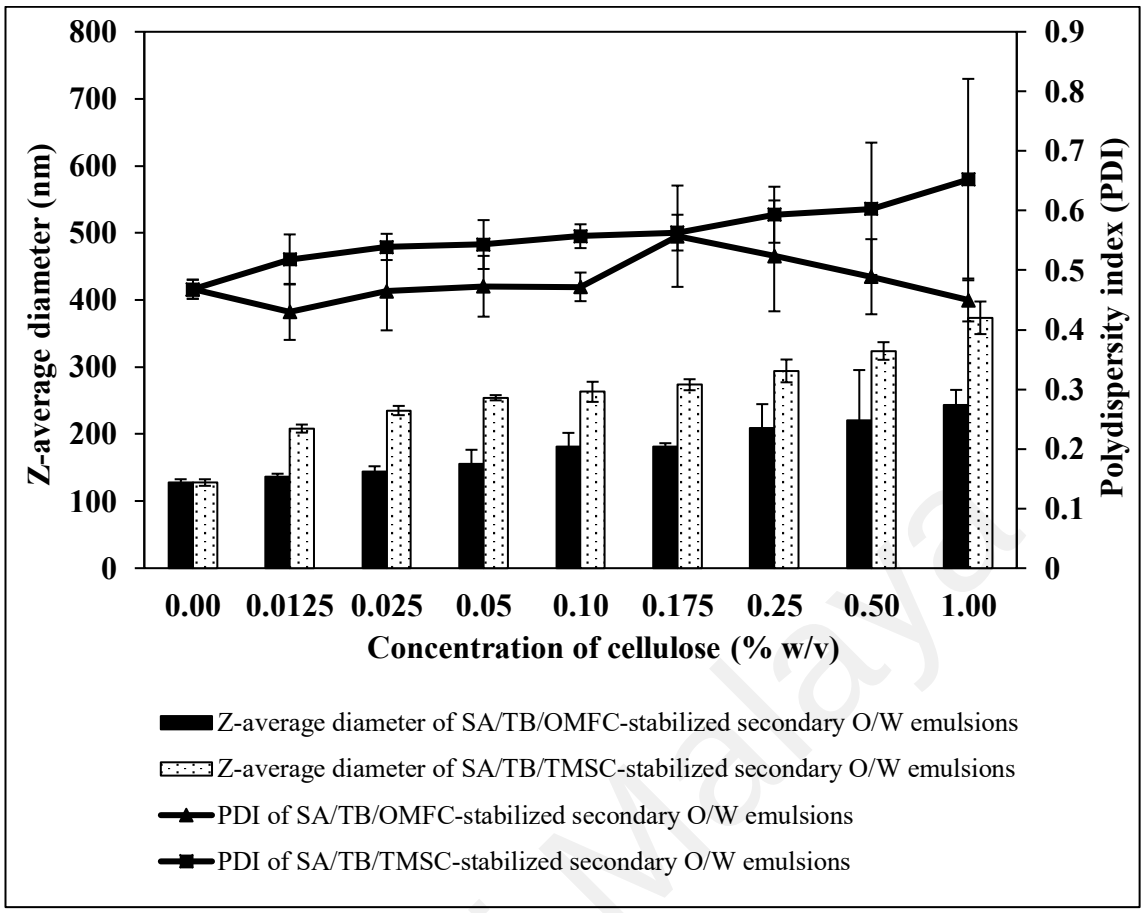

Figure 4.11: The effect of cellulose concentration on the Z-average diameter and polydispersity index (PDI) of SA/TB/OMFC and SA/TB/TMSC secondary O/W emulsions.

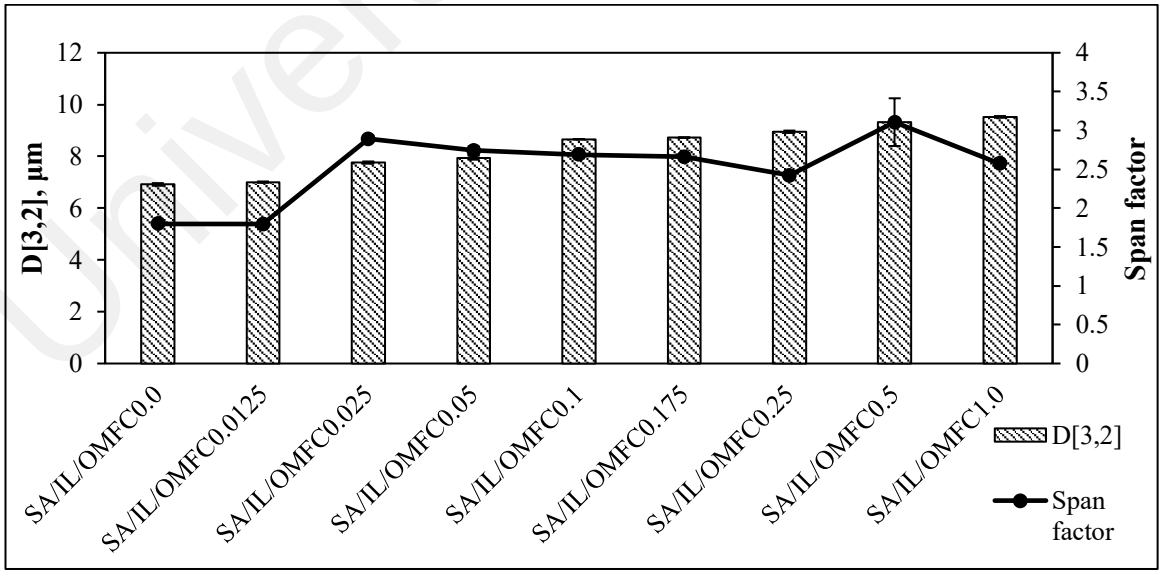

Figure 4.12: The mean droplet size and the span factor of SA/IL/OMFC secondary O/W emulsions at various concentrations of celluloses.

Zeta potential (ζ-potential) is another significant parameter that needs to be addressed as this factor predicts the stability of the emulsions (Yesiltas et al., 2017). ζ-potential of emulsions should be either less than −30 mV or more than +30 mV in order to attain a good electrostatic stabilization (Uchegbu et al., 2013). The adsorption of ALG molecules on the droplet surfaces was monitored by ζ-potential and the electrical charge on the emulsion droplets relies on the distribution of the ionized groups (Pongsawatmanit et al., 2006).

ζ-potential can be tailored by the type of the cellulose particles (hydrophilic APS-oxidized MFCs or hydrophobic TMSC) utilized in the emulsion stabilization. As for the formulations employing Tween 80:Brij 35 as emulsifiers, their ζ-potential values were noticed to be negative due to the presence of carboxylic terminals on the polymer backbones, knowing that Tween 80 & Brij 35 employed in the emulsion formation are non-ionic surface active agents (Khayata et al., 2012). By comparing the secondary O/W emulsion systems stabilized by Tween 80:Brij 35 with different types of cellulose particles, ζ-potential became less negative (Figure 4.13) after replacing hydrophilic MFC with hydrophobic TMSC as stabilizer for producing emulsions. This could be credited to the difference in the chemical structure of oxidized MFC and TMSC. APS oxidation rendered MFCs with carboxylate groups and silylation of cellulose produced TMSC by introducing -$Si(CH_3)_3$ groups. The adsorbed ALG layer generates electrostatic repulsive forces with APS-oxidized MFCs because both of them have free anionic carboxylate moieties (N. Lin et al., 2012). ALG molecules can also adhere to O/W emulsions via hydrophilic interaction with surfactants (K. Y. Lee & Mooney, 2012) and by hydrogen bonding with -OH groups of APS-oxidized MFCs (N. Lin et al., 2012).

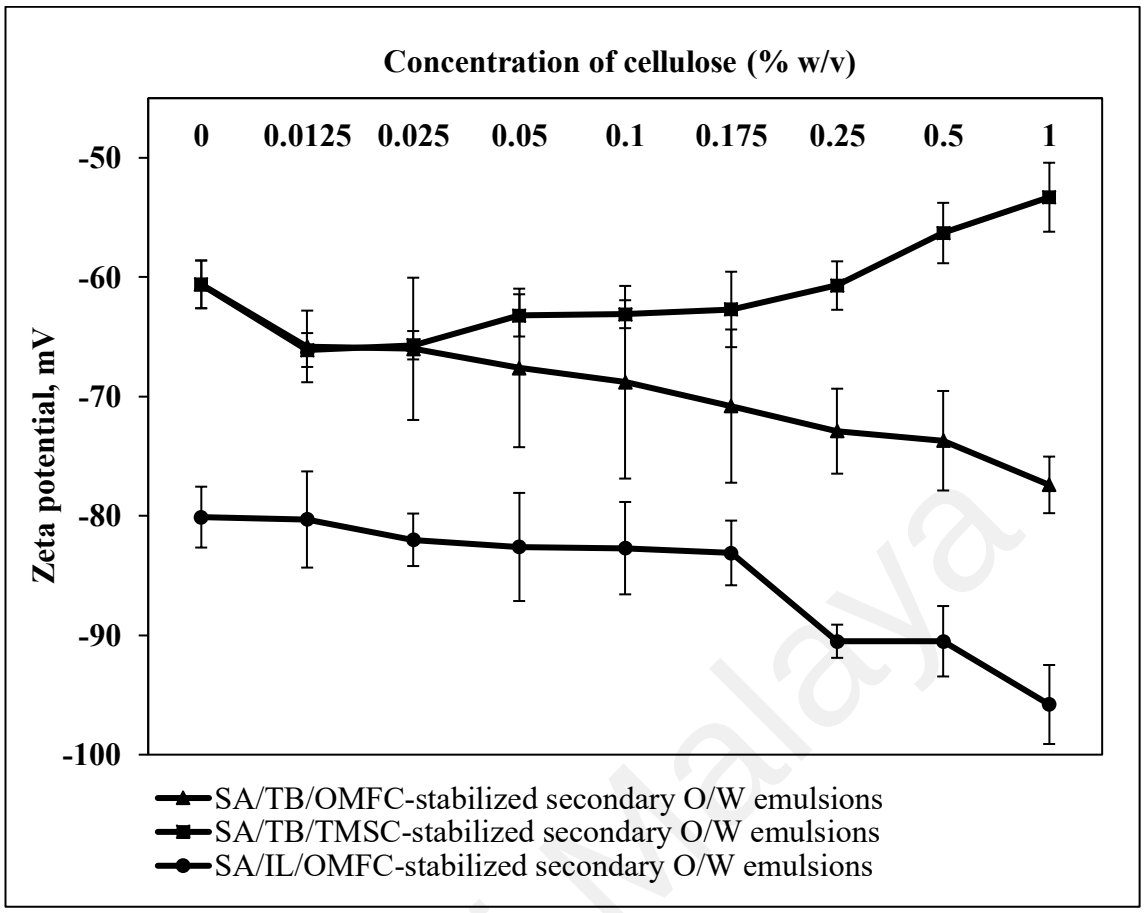

Figure 4.13: Zeta potential of SA/TB/OMFC, SA/TB/TMSC and SA/IL/OMFC secondary O/W emulsions at various concentrations of celluloses.

ALG could not form hydrogen bonds with TMSC due to the limited -OH groups on TMSC structure. Nevertheless, ALG can adsorb to the droplet surface through hydrophilic interaction with surfactants (K. Y. Lee & Mooney, 2012). Thus, the negative ζ-potential was contributed solely by the electrostatic repulsions among ALG molecules (Figure 4.13). The presence of non-adsorbed ALG molecules in the continuous phase generate osmotic attractive forces that bring droplets into close vicinity followed by the removal of the adsorbed polymer molecules around the oil droplets, in which this phenomenon known as depletion flocculation (David Julian McClements, 2004; Pallandre et al., 2007; Yesiltas et al., 2017). Subsequently, depletion flocculation facilitates the bridging flocculation whereby the structural rearrangement of adsorbed ALG molecules occurred, leading to sharing of one ALG molecule by more than one oil

droplet (Pallandre et al., 2007). This was reflected by the larger droplet sizes of secondary O/W emulsions stabilized by TMSC.

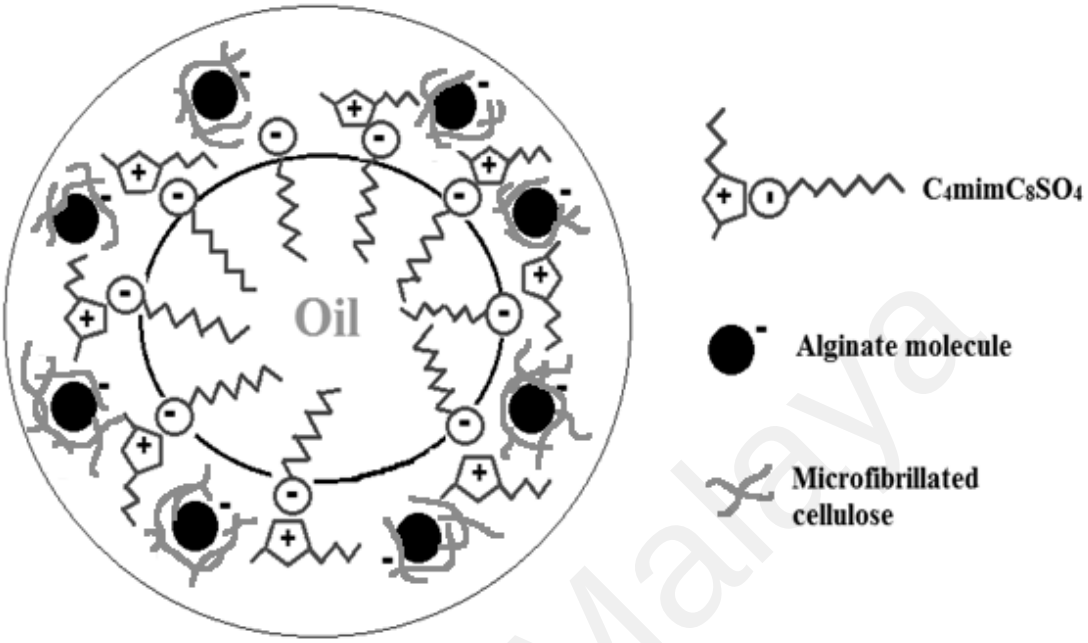

Figure 4.14: The possible $C_4mimC_8SO_4$-stabilized secondary O/W emulsion system.

A series of emulsion systems stabilized by $C_4mimC_8SO_4$ showed highly negative charged as signified by their ζ-potential (Figure 4.13). In this study, halogen-free amphiphilic ionic liquid, $C_4mimC_8SO_4$ with high surface activity (Barhoumi et al., 2016) was utilized as emulsifier to stabilize the palm based emulsions. Octylsulphate anion ($C_8SO_4^-$) is likely to penetrate in oil due to its sufficiently long hydrophobic alkyl chain that behaves like a surface active anionic ionic liquid while imidazolium cation (C_4mim^+) acts as counterion, forming O/W emulsions with negative charge (Thakkar et al., 2016). The incorporated anionic ALG molecules interact with anionic ionic liquid induced electrostatic repulsive forces. Besides, there are also substantial electrostatic repulsive forces between alginate molecules and APS-oxidized MFCs because both of them have anionic carboxylate moieties on their polymer backbones (N. Lin et al., 2012). The possible $C_4mimC_8SO_4$-stabilized secondary O/W emulsion system is shown in Figure 4.14. This explained the formation of $C_4mimC_8SO_4$-stabilized secondary O/W emulsions

with extraordinary high negative ζ-potential values. Owing to these strong electrostatic repulsive forces, alginate molecules were inhomogeneous distributed at the oil droplet surfaces, facilitating the droplet recoalescence. This was evidenced by the enlargement of emulsion droplet diameter from nano- to micron-sized after the addition of alginate molecules.

4.6.2 Viscosity

Viscosity is a measure of motion resistance of a fluid that reflects the molecular movement of a material (Nokhodchi et al., 2012). A system comprises of long chain molecules, forming highly twisted coils entangled with each other shows low tendency to flow, resulting in the increased viscosity (Belscak-Cvitanovic et al., 2015). The viscosity of emulsions is one of the crucial parameters that determine the stability of emulsions. The formation of highly viscous interfacial films enhances the emulsion stability by providing a mechanical barrier against droplet recoalescence. This is essential prior to the formation of alginate microbeads (J. Zhang et al., 2021).

Alginate is a hydrophilic polymer that incorporated into the primary O/W emulsions as a rheology modifier to enhance the viscosity of the continuous phase due to the formation of a gel network (Gombotz & Wee, 2012; Sachan et al., 2009). Viscosity of alginate is a result of polymer chain hydration via (1,4)-glucoside linkages joining β-D-mannuronate (M) and α-L-guluronate (G) units, forming extended and relatively open hydrated coils (Rehm, 2009). –OH groups of alginate further forming hydrogen bonds with water molecules in the system (K. Y. Lee & Mooney, 2012). In addition, APS-oxidized MFCs with high aspect ratio can also produce highly viscous dispersions at considerably low concentration (S. Shin et al., 2017).

The flow behaviors of the SA/TB/OMFC based secondary emulsions were examined (Figure 4.15). APS-oxidized MFCs involved in physically crosslinking with alginate via hydrogen bonding in the ether linkage (N. Lin et al., 2012) and also interacting with Tween 80:Brij 35 to create a mechanical barrier surrounds the oil-water interface, hindering coalescence (Chevalier & Bolzinger, 2013). APS-derived MFCs continue to form hydrogen bonds with water molecules in the continuous phase (Chami Khazraji & Robert, 2013). With these reasons, the viscosity was promoted upon increasing MFC

concentration as a consequence of the increased intermolecular interactions (Ahmadi-Dastgerdi et al., 2015). This observation was in line with the previous study whereby the O/W Pickering emulsions stabilized by mangosteen rind-extracted MFCs increasingly viscous when the MFC concentration increased from 0.05% to 0.70% w/w. The elevation in the apparent viscosity was due to the presence of surplus non-adsorbing MFCs in the continuous aqueous phase as evidenced by their microscopic observations. Their emulsions also exhibited shear-thinning behavior in which the viscosity of all the formulated emulsions decreased with the increasing of shear rate (Winuprasith & Suphantharika, 2015).

In addition, the study by Sharma et al. (2014) also obtained the similar results. In their research, nanoparticle-surfactant-polymer O/W emulsions were produced by adding various concentrations (1.0 to 5.0 wt%) of hydrophilic silicon dioxide (SiO_2) or partially hydrophobic clay into pre-formed polyacrylamide O/W emulsions stabilized by the surfactant, sodium dodecyl sulfate (SDS). At 0.1 MPa pressure, the viscosity of the system was enhanced from 0.19 Pa·s to 0.71 Pa·s and to 0.76 Pa·s after the incorporation of 1.0 wt% SiO_2 or 1.0 wt% clay, respectively into the surfactant-polymer emulsion. The increased in the viscosity was ascribed to the adsorption of particles at the oil-water interfaces. They also investigated the effect of the nanoparticle concentrations (1.0 to 5.0 wt%) on the viscosity of the emulsions. Their observation was consistent with our result whereby the emulsion viscosity increased marginally with the increasing of nanoparticle contents. They also believe that the enhanced viscosity was probably due to the presence of excess nanoparticles in the continuous phase. All the formulated emulsions also exhibited non-Newtonian shear thinning behavior. Hermes and Clegg (2013) reported that the bonds between silica particles used in stabilizing Pickering emulsions tend to break down in the increasing shear rate. However, bonds reformed at large strains, leading to the formation of emulsions with shear thickening behavior.

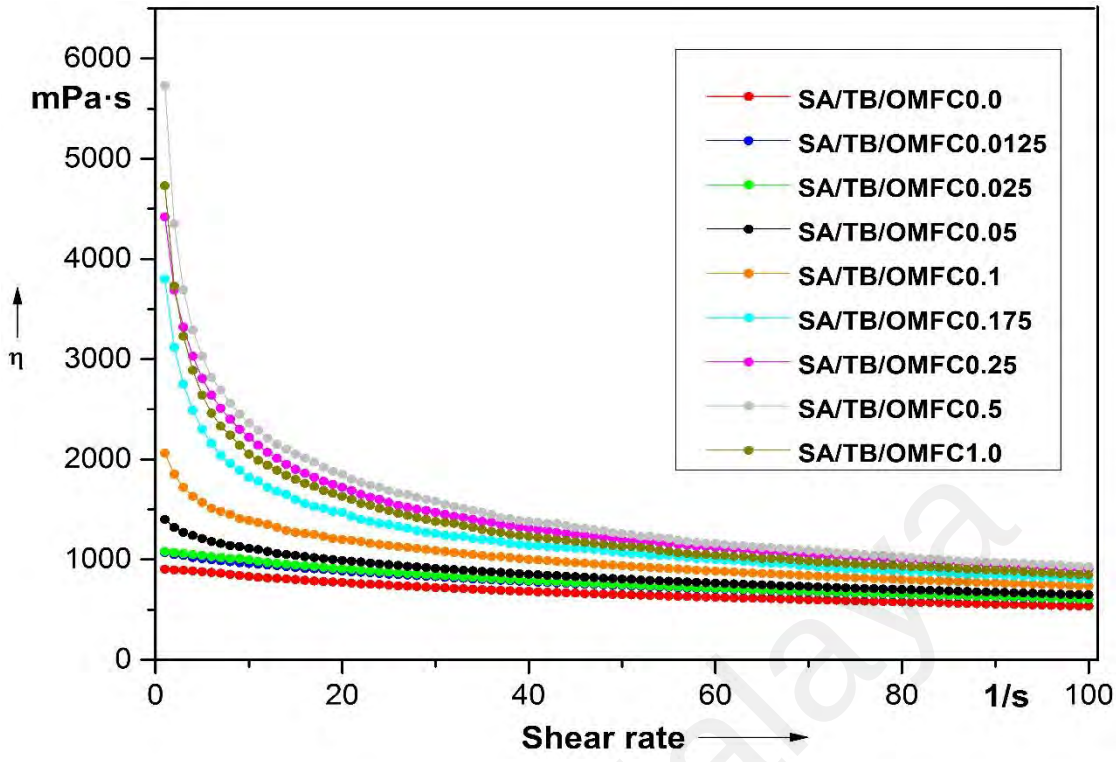

Figure 4.15: Viscosity of the SA/TB/OMFC based secondary emulsions at various concentrations of APS-oxidized MFCs.

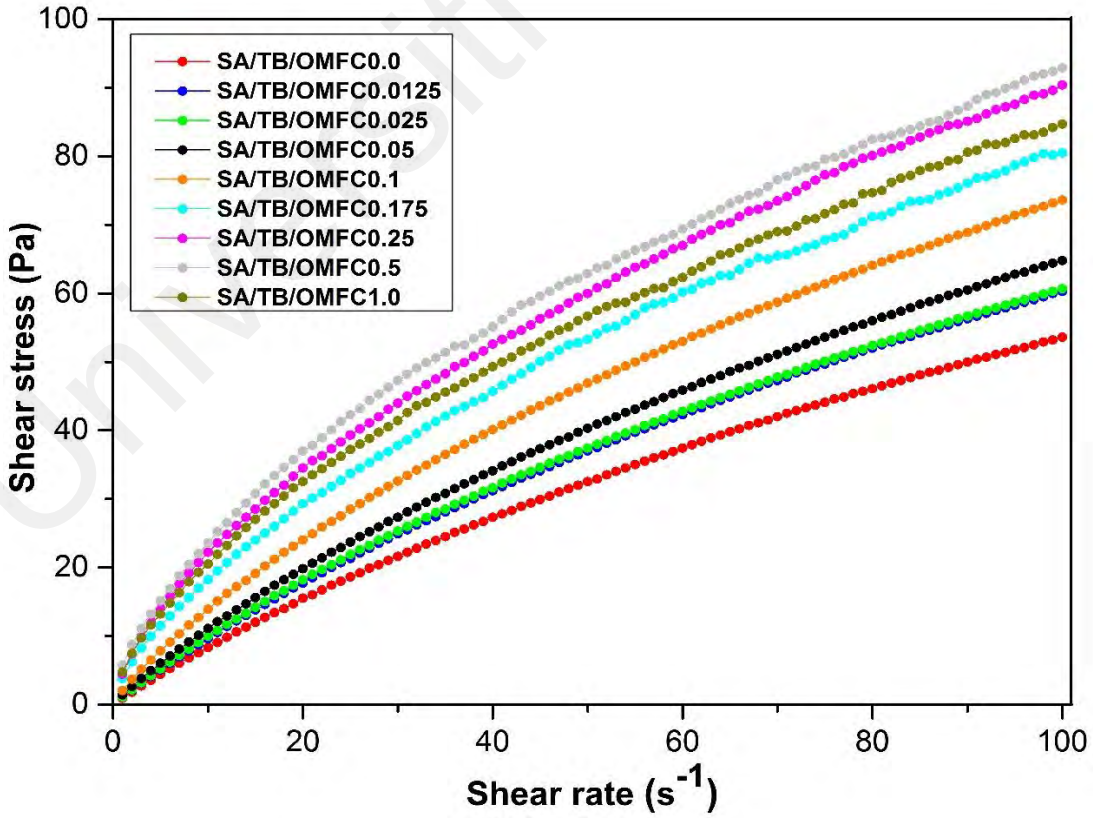

Figure 4.16: Shear stress-shear rate plots of SA/TB/OMFC based secondary O/W emulsions.

Figure 4.15 displays the viscosity (η) of SA/TB/OMFC based secondary emulsions as a function of shear rate (γ). At low shear rates, the viscosity for all the evaluated O/W emulsions decreased as the shear rate increased, approaching a constant value when the shear rate reduced above 60 s^{-1}. Increasing the shear rate causes progressive dissociation of the inter/intra molecular interactions among MFCs as well as the entanglement between ALG and MFCs, which in turn reduces its apparent viscosity and results in thinning of the emulsions (Ahmadi-Dastgerdi et al., 2015). As shown in Figure 4.16, the shear stress-shear strain plots revealed that the tested emulsions were categorized as non-Newtonian shear thinning fluids across the entire range of shear rate (Belscak-Cvitanovic et al., 2015).

The viscosity values of SA/TB/TMSC based secondary emulsions (Figure 4.17) were compared with the corresponding viscosity values of SA/TB/OMFC based secondary emulsions to investigate the effect of the cellulose type on the flow behavior of emulsions. Significant reduction in the viscosity was observed after replacing the hydrophilic MFC with hydrophobic TMSC while the concentration of non-ionic surfactants was held constant. It was argued that the hydrophobic TMSCs with limited −OH groups formed only weak hydrogen bonds with water molecules due to their non-polar character (Mormann & Wezstein, 2009). On the contrary, MFCs with more –OH groups formed stronger hydrogen bonds with water molecules in the continuous phase with relatively high dispersive forces, resulting in higher viscosity of samples (Chami Khazraji & Robert, 2013). Hence, the viscosity of SA/TB/TMSC based secondary emulsions reduced with the increasing of TMSC concentration. SA/TB/TMSC based secondary O/W emulsions with different concentrations of TMSC particles were being characterized as non-Newtonian shear thinning fluids due to the non-linear shear stress-shear rate relationship (Belscak-Cvitanovic et al., 2015) (Figure 4.18).

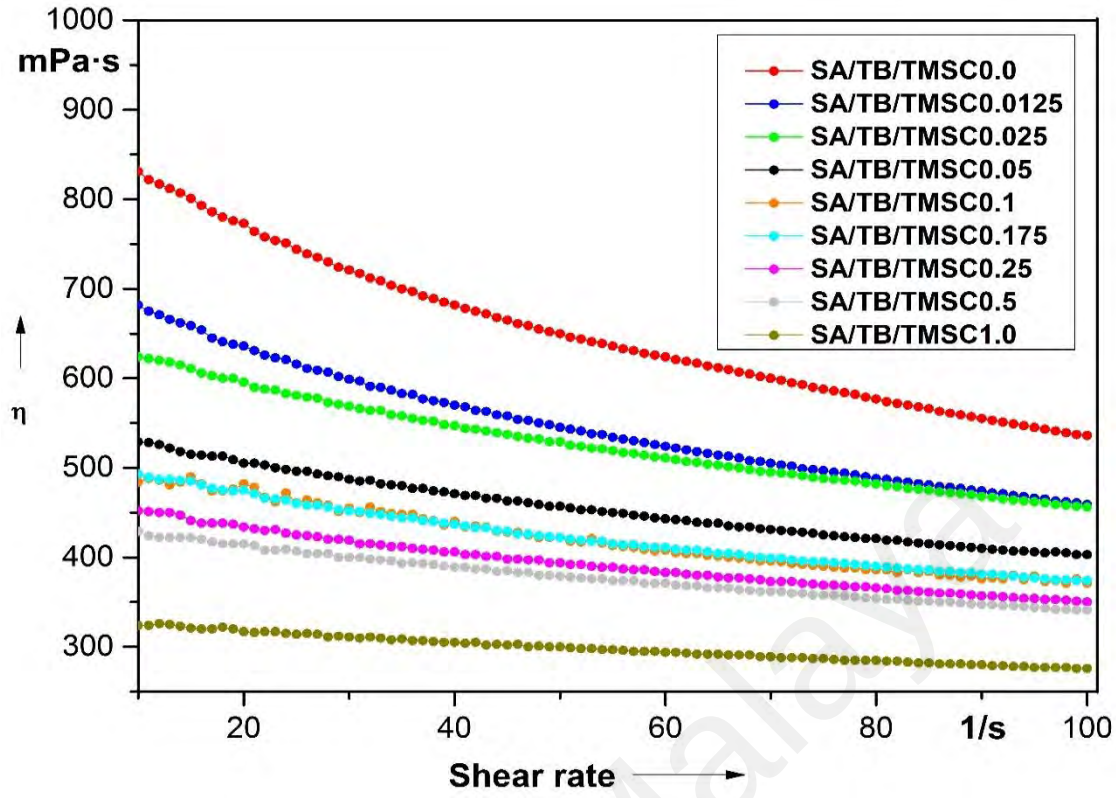

Figure 4.17: Viscosity of the SA/TB/TMSC based secondary emulsions at various concentrations of TMSCs.

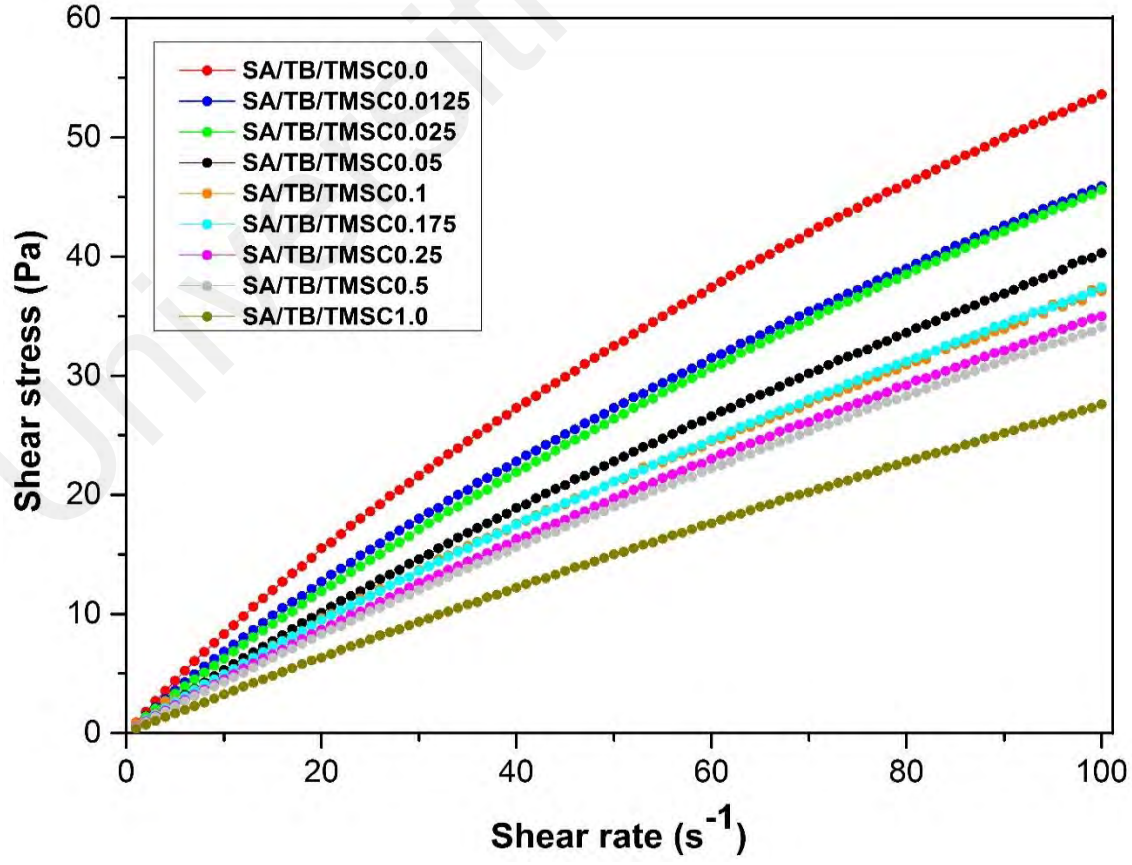

Figure 4.18: Shear stress-shear rate plots of SA/TB/TMSC based secondary O/W emulsions.

Moreover, the relative viscosities for SA/IL/OMFC based secondary emulsions were found to be significantly lower than the corresponding values for SA/TB/OMFC emulsions. It was suggested that the molecular weight of emulsifiers to be one of the essential factors that determine the flow behavior of the emulsions (Daik et al., 2007). Comparatively low viscosity of SA/IL/OMFC secondary emulsions can be credited to the lower molecular weight and lesser complexity of $C_4mimC_8SO_4$ structure (Figure 2.9) as compared to Tween 80 and Brij 35 (Figure 2.8). System flow behaviors for all the assessed SA/IL/OMFC O/W secondary emulsions demonstrated similar trend as presented in Figure 4.19. A transient shear thickening was observed as a resultant effect of jamming at very low shear rate (Moakes et al., 2015). This was followed by shear thinning when continued increase in the applied shear rate. The observed reduction of viscosity was owing to the weakening of particle interactions in the system (Peters et al., 2016). The shear stress-shear strain relationship of SA/IL/OMFC secondary emulsions was examined to be non-linear, indicating the emulsions behave as marked non-Newtonian shear thinning fluids (Figure 4.20) (Belscak-Cvitanovic et al., 2015).

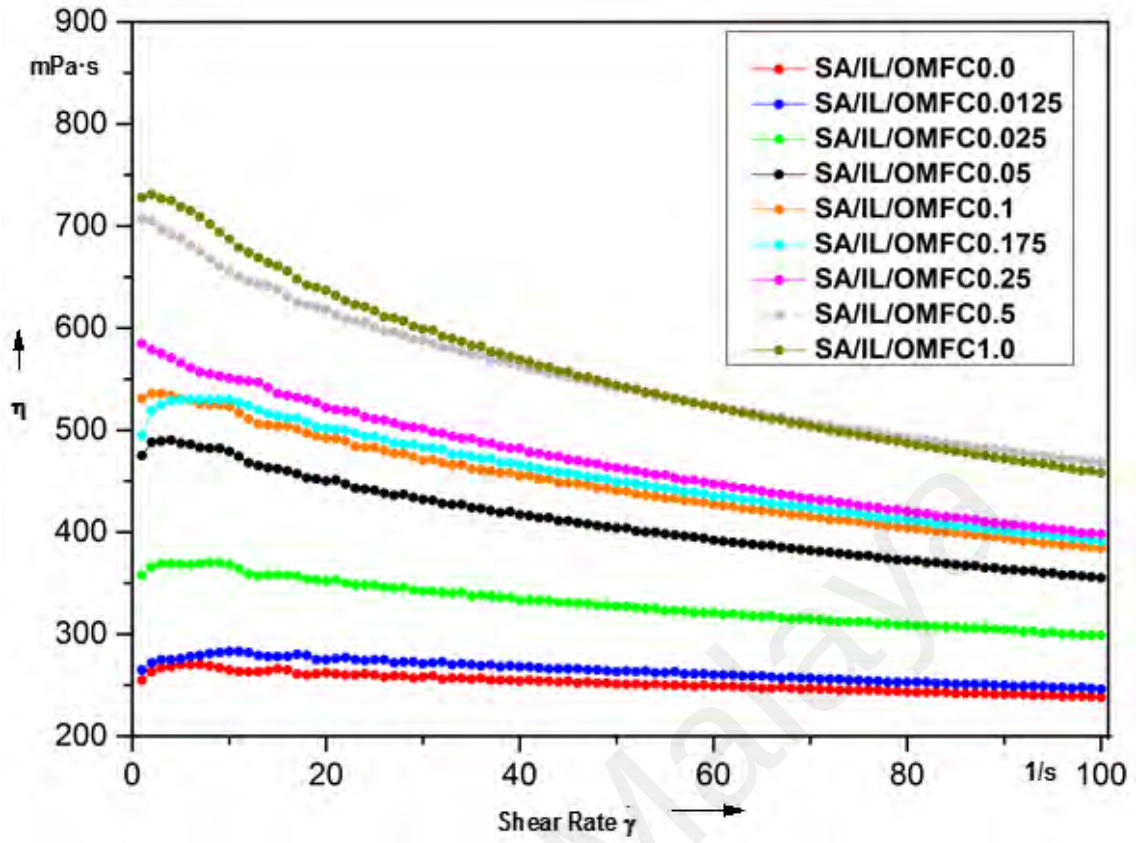

Figure 4.19: Viscosity of the SA/IL/OMFC based secondary emulsions at various concentrations of APS-oxidized MFCs.

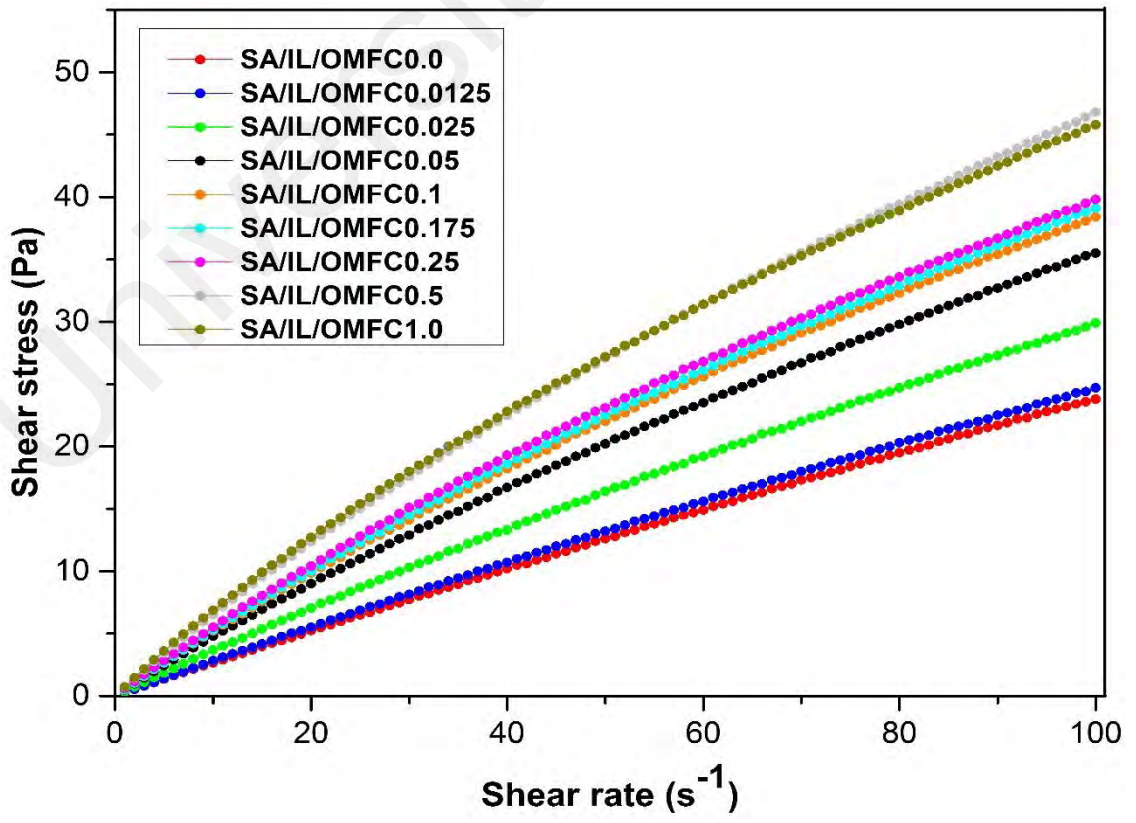

Figure 4.20: Shear stress-shear rate plots of SA/IL/OMFC based secondary emulsions.

4.6.3 Rheological behaviors

Rheological measurements provide several pieces of valuable information such as dynamic viscoelastic properties by investigating the evolution of storage modulus (G′) and loss modulus (G″) in different formulations (T. Sharma et al., 2015). This characterization provides crucial insight into the long-term stability of emulsions. First, dynamic strain sweep test was conducted to determine the linear viscoelastic region (LVR) for the evaluated O/W systems, in which G′ was basically independent of the applied strain and no dissociation of molecular interaction occurred. The end of LVR was identified as the critical strain (ε_c) (Benhamou et al., 2014) above which G′ demonstrates a decreasing trend (Aben et al., 2012). Hence, dynamic oscillatory measurements are important in determining the elasticity and the maximum strain that the material can withstand prior to the shear thinning (T. Sharma et al., 2015).

4.6.3.1 Viscoelastic properties of SA/TB/OMFC based secondary emulsions

Dynamic strain sweep plots for SA/TB/OMFC based secondary emulsions were presented in Figure 4.21. SA/TB/OMFC secondary emulsions with ≤ 0.1% w/v APS-oxidized MFCs exhibited liquid-like behavior with G″ dominance and absence of crossover points over the complete range of strain amplitude. Whereas, SA/TB/OMFC secondary emulsions with ≥ 0.175% w/v APS-oxidized MFCs behave like viscoelastic liquids. The LVR of these samples with diverse MFC concentrations (0.175-1.000 %w/v) are relatively short with a plateau in G′ for a small range of strain. G′ values were then decreased nonlinearly above the ε_c, that might be attributed to the relaxation and disentanglement of polymer molecules (T. Sharma et al., 2015). This implies that SA/TB/OMFC secondary emulsions containing ≥ 0.175 %w/v MFCs displays viscoelastic behavior with elasticity over a limited region of small strain followed by demonstration of liquid-like nature after the crossover point. When APS-treated MFCs added into the O/W secondary emulsions increased up to 0.175 %w/v, the systems

transforming from liquid-like nature into viscoelastic behavior. Thus, SA/TB/OMFC based emulsions stabilized by MFCs provided systems with improved rheological behavior. According to the previous study, the incorporation of silica nanoparticles enhanced the rheological properties of polymer solution by increasing the elastic modulus of the solution (Zhu et al., 2014).

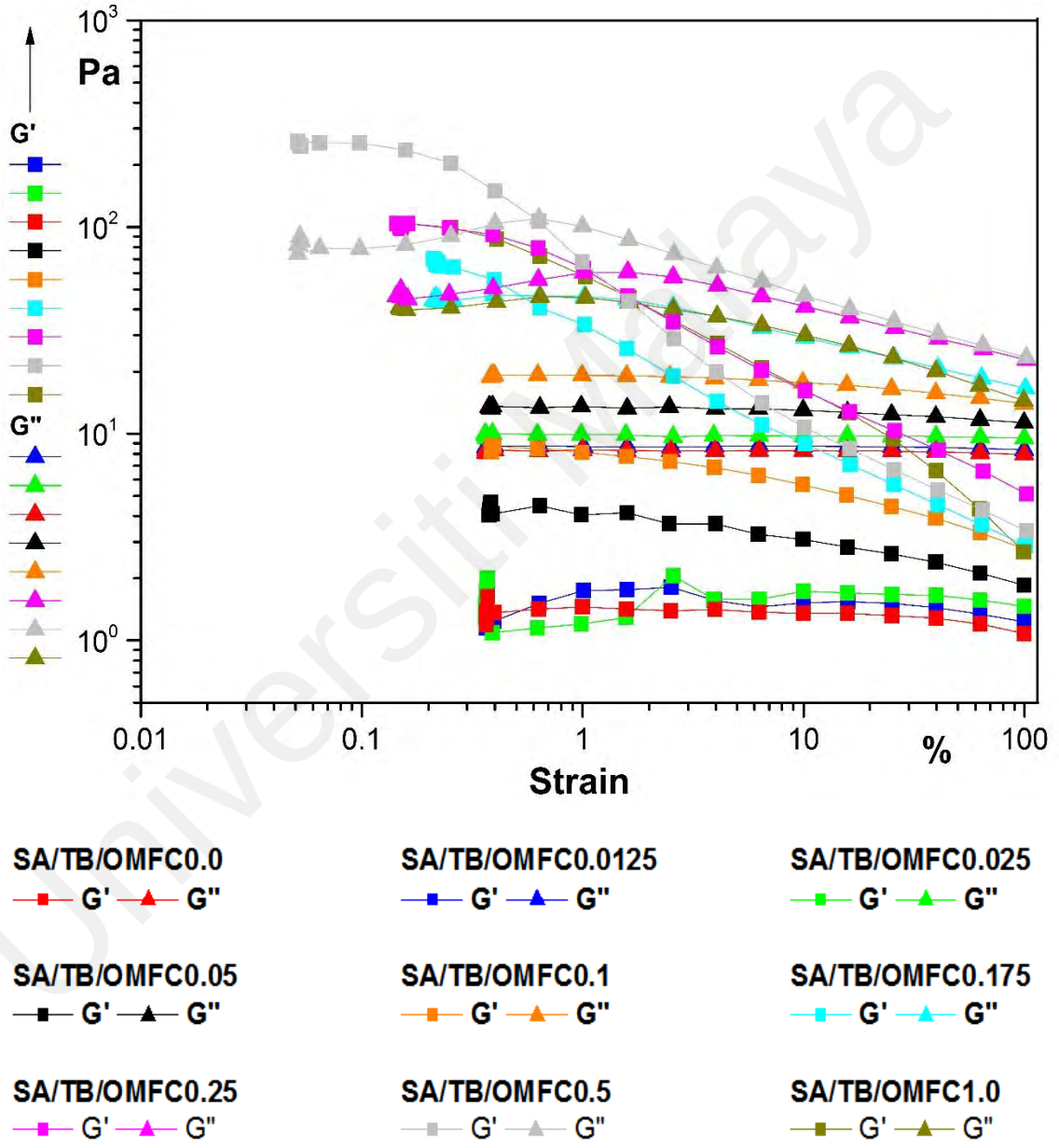

Figure 4.21: Dynamic strain sweep measurements for Tween 80:Brij 35-stabilized emulsions at various concentrations of APS-oxidized microfibrillated celluloses.

The measurement of storage modulus reflects molecular interactions within the systems, which indirectly provide information on the mechanical properties of the respective emulsions (Aben et al., 2012). For understanding the influence of various oxidized MFCs on the viscoelastic properties of SA/TB/OMFC based secondary emulsions, the frequency-sweep measurements were conducted at constant strain within the LVR (γ=0.2%) in order to measure dynamic moduli from 100 to 0.1 rad·s^{-1} (Figure 4.22). G′ and G″ for SA/TB/OMFC secondary emulsions with ≤ 0.1% w/v oxidized MFCs increased as ω increased. On the contrary, G′ of SA/TB/OMFC secondary emulsions with ≥ 0.25% w/v oxidized MFCs manifested near plateau below 1 rad·s^{-1} and increased marginally thereafter. The crossover point was not noticeable throughout the complete range of frequency for all the SA/TB/OMFC based emulsions except for sample SA/TB/OMFC0.175. Viscous behavior was dominating at low frequency regime for SA/TB/OMFC0.175 as G″ value was greater than G′. As ω proceeded, G′ approaching G″ until the crossover point was appeared at about 0.4 rad·s^{-1}, above which G′ dominant over G″, transforming into elastic behavior.

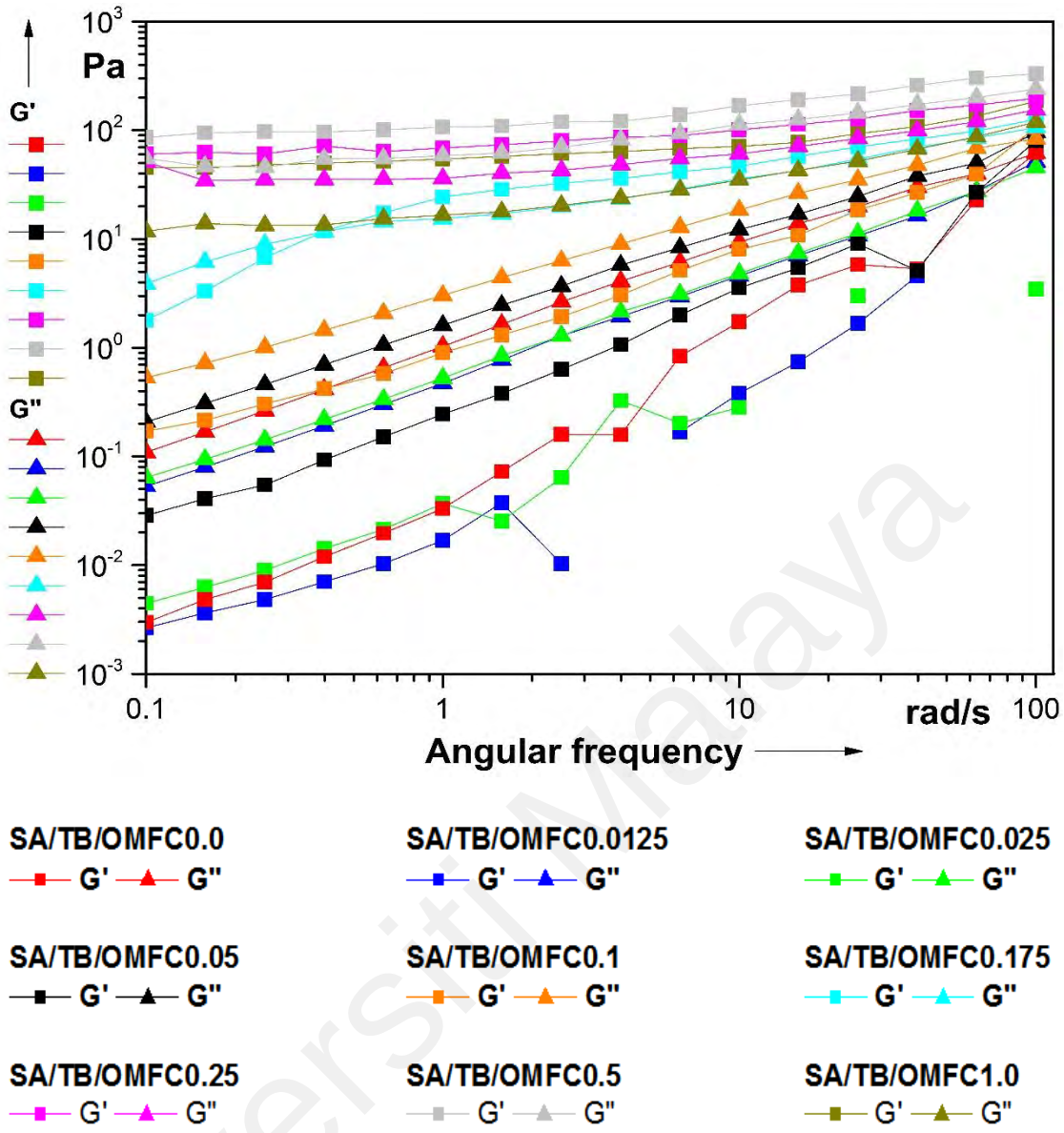

Figure 4.22: Frequency sweep measurements for Tween 80:Brij 35-stabilized oil-in-water emulsions at γ=0.2%.

The addition of oxidized MFC as stabilizer is sufficient to alter the rheological properties of SA/TB/OMFC based emulsions. Modest amount of MFCs (≥ 0.25% w/v) incorporated allows the transition in rheological behavior from liquid-like (G″ > G′) to gel-like (G′ > G″). Increased the amount of oxidized MFCs led to a higher possibility of hydrogen bonding among themselves as well to facilitate physical crosslinking with ALG, inducing the substantial increase in G′ (N. Lin et al., 2012). This finding was in concurring with literature study whereby they observed improvement in G′ after the addition of

cellulose nanofiber into gelatin methacrylamide (S. Shin et al., 2017). As ω increased, G" was gradually getting closer to G', suggesting the disruption and reestablishment of intra- and intermolecular hydrogen bonds of APS-oxidized MFCs and the entanglements between oxidized MFCs and ALG (Yue et al., 2016). Thus, MFCs can act as a viscosity enhancer and pronouncedly increase the rheological behaviors of emulsions at relatively small amount (S. Shin et al., 2017).

4.6.3.2 Viscoelastic properties of SA/TB/TMSC based secondary emulsions

The incorporation of hydrophobic TMSCs into the Tween 80:Brij 35-stabilized O/W emulsions altered the rheological behaviors of the emulsions from liquid-like to viscoelastic nature. Figure 4.23 showed that the distinct G′ and G″ crossover points are visible in the dynamic strain sweep plots for SA/TB/TMSC based secondary emulsions with ≥ 0.1% w/v of hydrophobic trimethylsilyl cellulose (TMSC), exhibiting typical viscoelastic behavior. Both G′ and G″ values increased upon increasing the concentration of TMSC. The pronounced improvement of rheological behaviors was presumably due to the synergistic interaction between hydrophobic TMSC and Tween 80:Brij 35 in emulsion stabilization by forming a strong membrane surrounds the droplets, providing long term stability of emulsions (Nciri et al., 2010; Reger et al., 2011; T. Sharma et al., 2015). The viscoelastic behavior of the emulsions was strongly affected by the type of the particles used in the emulsion stabilization. As reported in the previous study, T. Sharma et al. (2015) examined that nanoparticle-surfactant-polymer O/W emulsions stabilized by 1 wt% silica (SiO_2) or clay nanoparticles displayed distinct viscoelastic behaviors. Strain sweep measurements demonstrated that G′ of SiO_2-surfactant-polymer O/W emulsion was relatively higher than clay-surfactant-polymer O/W emulsion that ascribed to the stronger interaction of SiO_2 nanoparticle with surfactant as compared to clay. They also believed that the difference can be associated with the more elastic interfacial film was formed by SiO_2 nanoparticles at the oil-water interfaces.

Figure 4.24 represents the frequency sweep measurements for SA/TB/TMSC based secondary emulsions at various concentrations of TMSCs. G′ of emulsions increased marginally with increasing of frequency and the values greater than G″ without the appearance of crossover points for SA/TB/TMSC based secondary emulsions with ≥ 0.1% w/v of TMSCs. This evidenced that these systems exhibited characteristic gel behavior in accordance with the observations obtained from strain-sweep experiments.

The G′ and G″ values of SA/TB/TMSC based secondary emulsions with ≥ 0.1% w/v TMSCs are essentially higher than the corresponding values reported in SA/TB/OMFC based secondary emulsions. The noteworthy differences in rheological behavior of these emulsions can be ascribed to the stronger interaction of hydrophobic TMSC with surfactant than the emulsions stabilized by APS-oxidized MFCs, enhancing the attachment of TMSC particles at oil-water interface (T. Sharma et al., 2015).

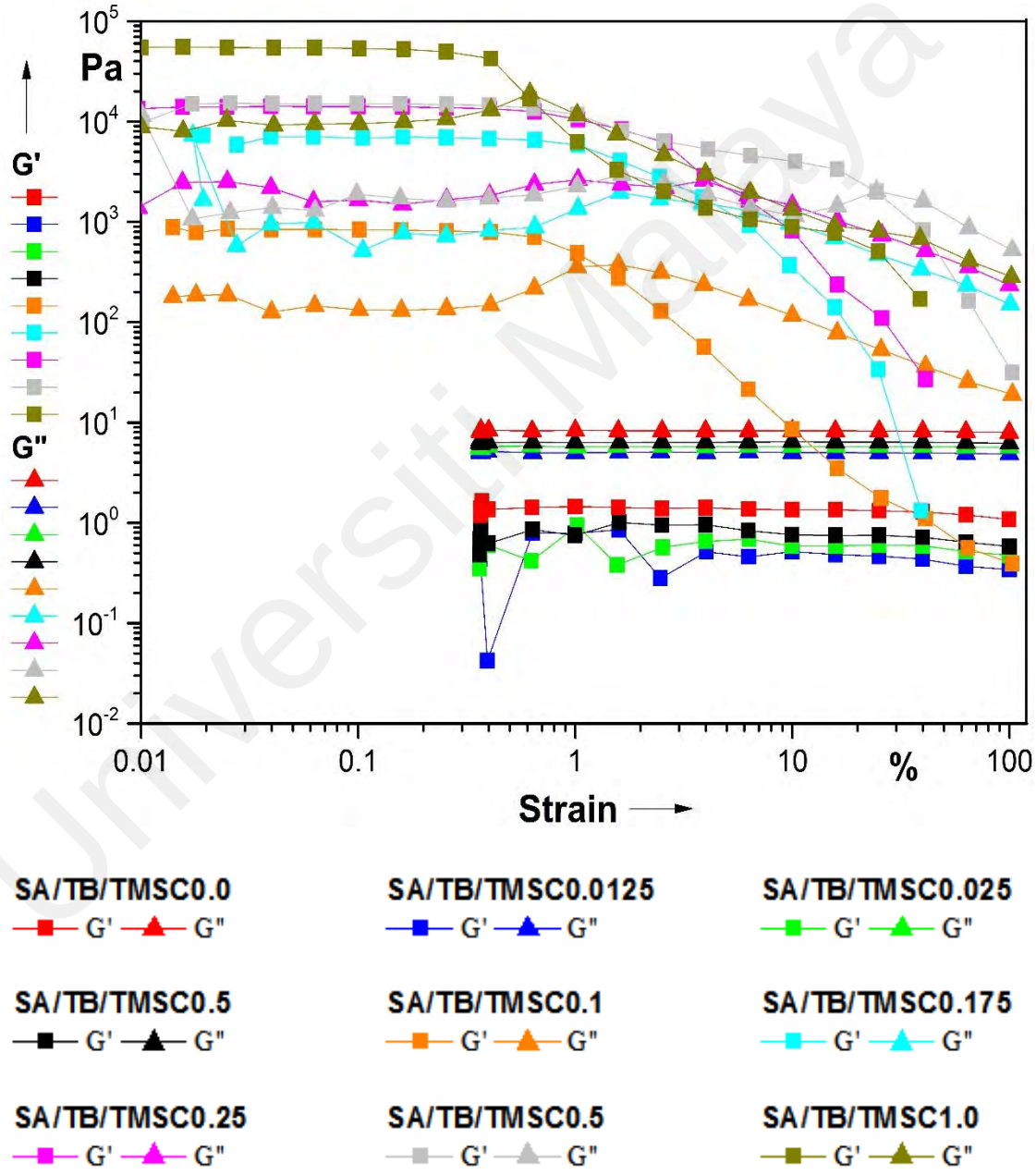

Figure 4.23: Dynamic strain sweep measurements for Tween 80:Brij 35-stabilized emulsions at various concentrations of TMSCs.

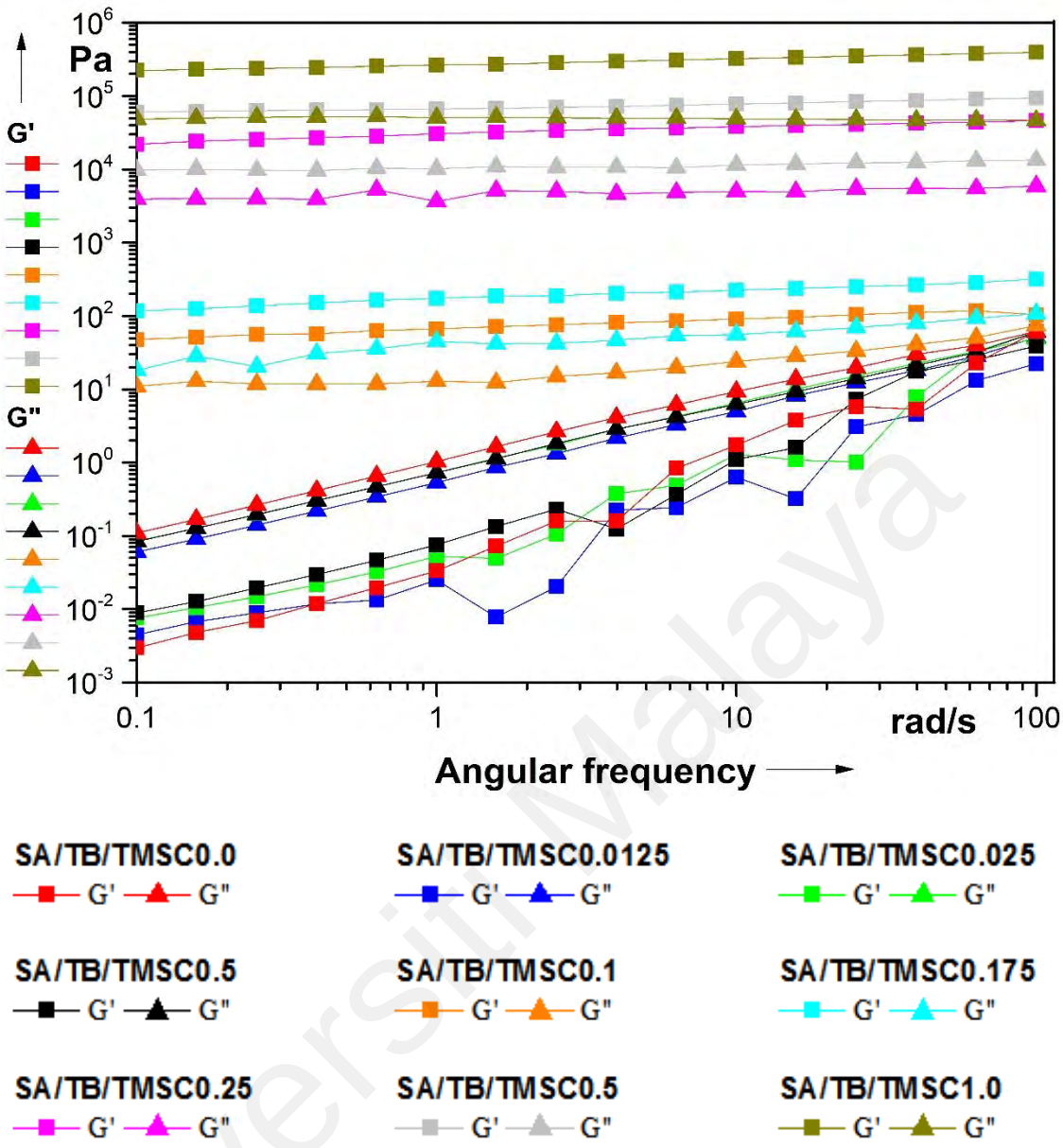

Figure 4.24: Frequency sweep measurements for Tween 80:Brij 35-stabilized oil-in-water emulsions at γ=0.2%.

4.6.3.3 Viscoelastic properties of SA/IL/OMFC based secondary emulsions

Dynamic oscillating measurements for SA/IL/OMFC based secondary emulsions were demonstrated in Figure 4.25. It was observed that G″ with plateau behavior is always dominant over G′ without the appearance of crossover point for all the evaluated SA/IL/OMFC based secondary emulsions regardless of the concentration of MFC. Thus, they manifest predominantly characteristic liquid behavior (T. Sharma et al., 2015). The type of emulsifier employed for stabilizing the O/W emulsions greatly influences the rheological behavior of systems.

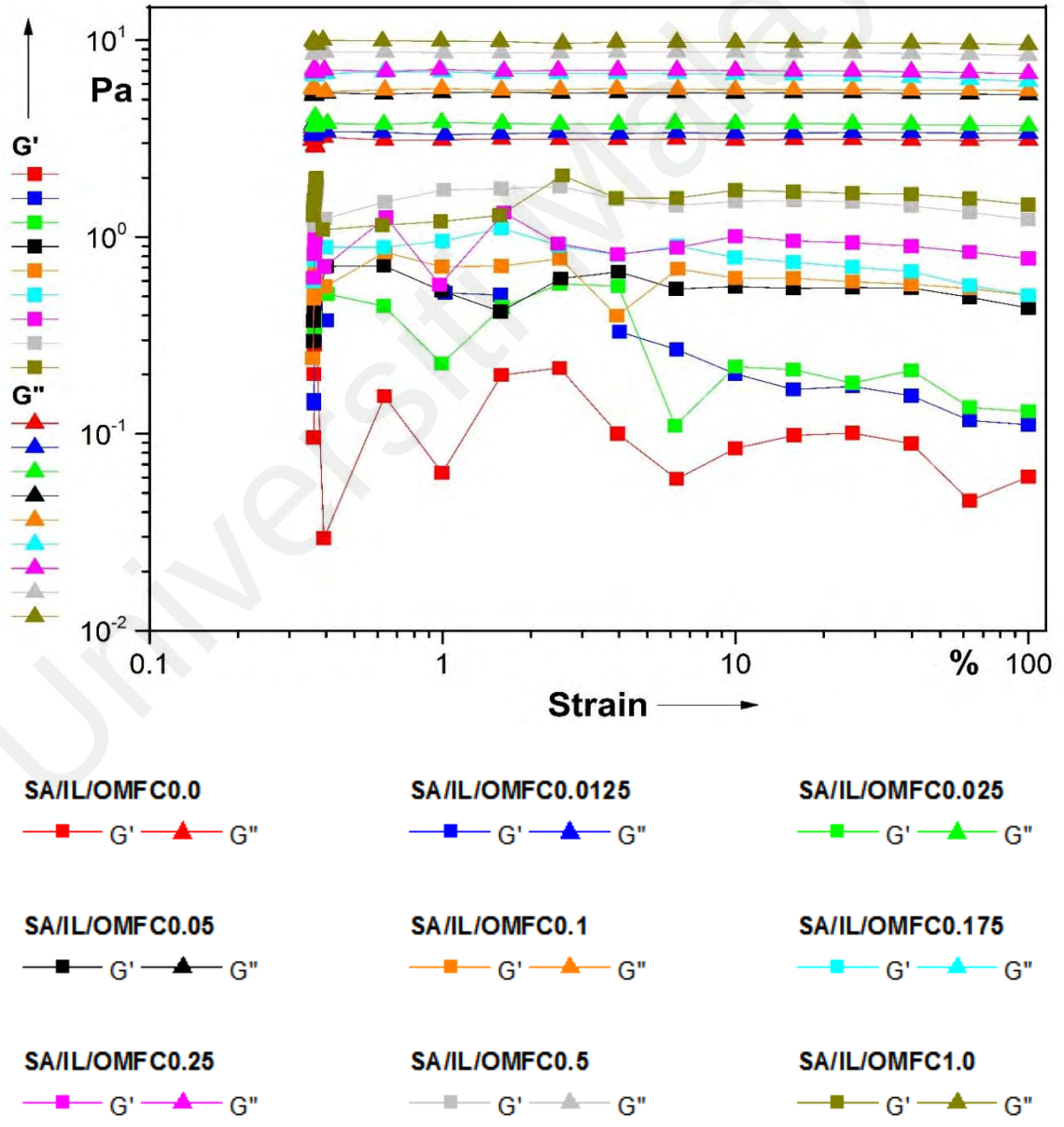

Figure 4.25: Dynamic strain sweep measurements for $C_4mimC_8SO_4$-stabilized emulsions at various concentrations of APS-oxidized microfibrillated celluloses.

All O/W systems employing ionic liquid as surface active agent maintained viscous character, in which both moduli were particularly dependent on frequency and G″ is greater than G′ throughout the entire range of measured frequency (Figure 4.26). Insights into the oscillation rheology measurements that obtained after incorporating MFCs revealed that the concentration of MFCs imparts a trivial effect on the rheological behavior of O/W emulsions.

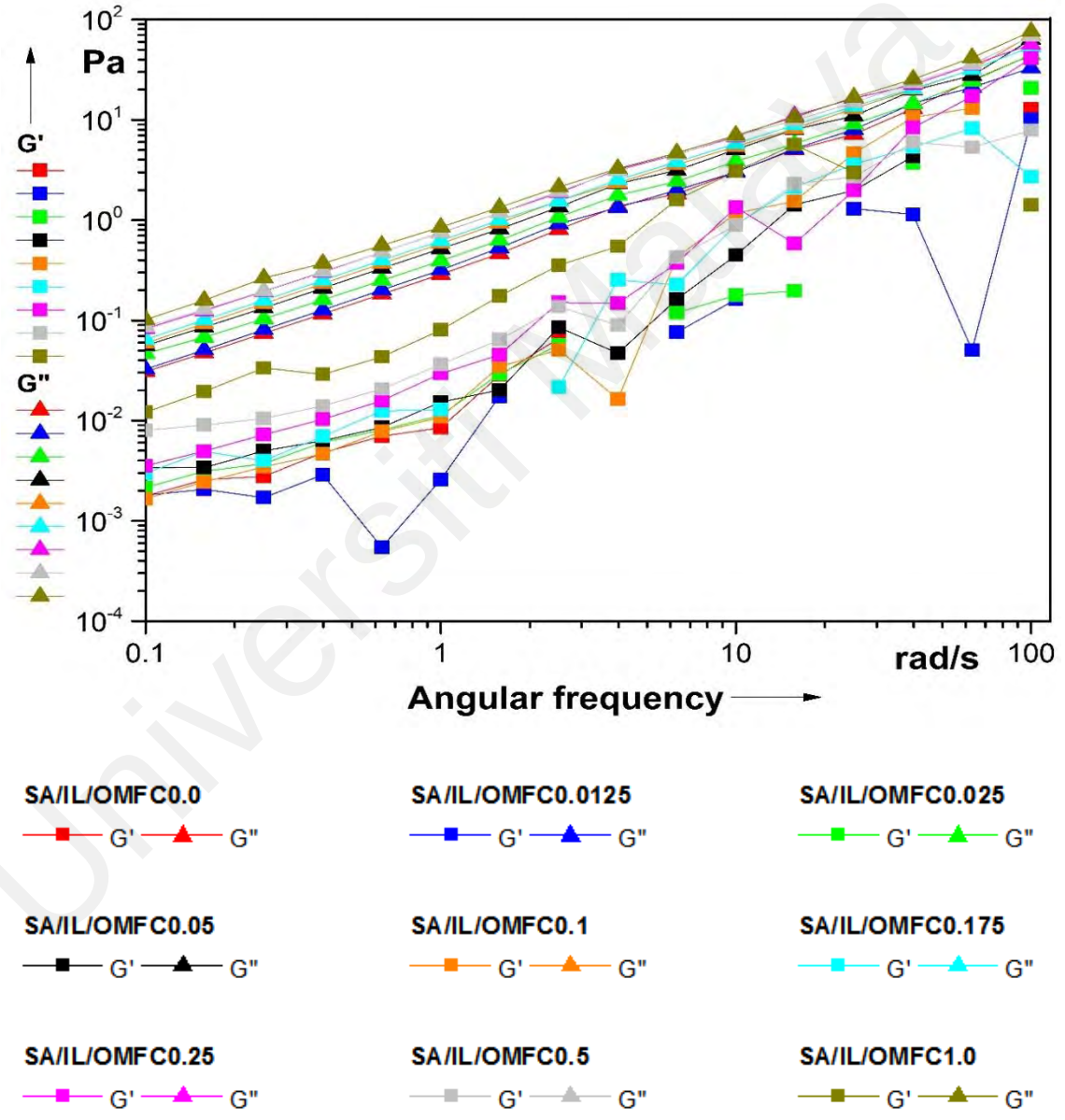

Figure 4.26: Frequency sweep measurements for $C_4mimC_8SO_4$-stabilized oil-in-water emulsions at γ=0.2%.

4.7 Characterizations of vitamin E-loaded alginate microbeads

4.7.1 Fourier transform infrared spectroscopy (FTIR)

FTIR spectra of vitamin E, sodium alginate (SA), APS-oxidized MFCs, TMSC and vitamin E-loaded microbeads were displayed in Figure 4.27. Both SA and MFC exhibited many common peaks in their spectra due to the similar chemical structures of these two biopolymers. FTIR spectra of the APS-oxidized MFCs and SA depicted a dominant and broad absorption band close to 3400 cm^{-1}, which was attributed to the stretching vibration of hydroxyl groups (O–H) and the peak at approximately 2900 cm^{-1} ascribed to methylene group (C-H) stretching vibration (Lin et al., 2011). The peaks at 1626 and 1447 cm^{-1} in the FTIR spectrum of MFC were assigned to the H-O-H stretching vibration of the water molecules absorbed by the biopolymer (1625 cm^{-1}) (Wenshuai ChenHaipeng Yu & Yixing Liu, 2011) and H-C-H and O-C-H in plane bending vibrations (Satyamurthy et al., 2011), respectively. As shown in Figure 4.27(b), the peaks located at 1612, 1420 and 1096 cm^{-1} were corresponded to asymmetrical and symmetrical stretching vibrations of the $–COO^-$ groups and C-O-C (cyclic ether) stretching vibration on the polymeric backbone of SA, respectively (Hua et al., 2010; Lin et al., 2011).

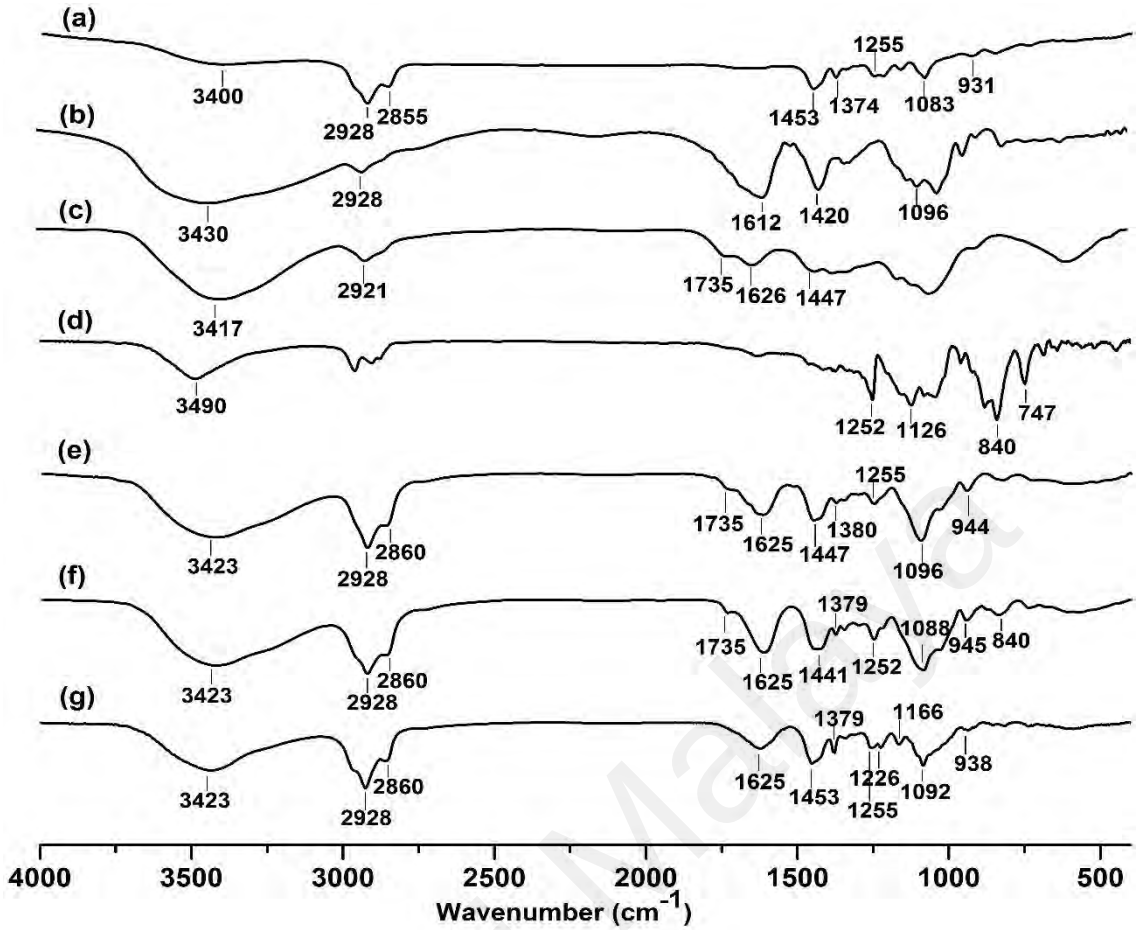

Figure 4.27: FTIR spectra of (a) vitamin E, (b) sodium alginate, (c) APS-oxidized MFCs, (d) TMSC, (e) SA/TB/OMFC0.25, (f) SA/TB/TMSC0.25 and (g) SA/IL/OMFC0.25 microbeads.

The possible interactions in the formulated nanocomposite microbeads encapsulating vitamin E was also examined by FTIR spectroscopy. As compared to the SA spectrum, there was a change of hydroxyl stretching band in all the spectra of vitamin E-loaded microbeads as shown in Figure 4.27 (e), (f) & (g). The shift from 3430 cm^{-1} to lower wavelength at approximately 3423 cm^{-1} indicated the existence of intermolecular hydrogen bonding (X. W. Shi et al., 2005). Meanwhile, the peak of SA at 1612 cm^{-1} was shifted to higher wavenumber in all the spectra of microbeads. A notable shift of $–COO^-$ stretching bands was probably due to the interactions between Ca^{2+} and the $–COO^-$ of alginate via ionic bonding during the crosslinking process (Hua et al., 2010). Our observations resembled the IR spectrum of Ca-crosslinked sodium alginate/cellulose nanocrystals microbeads reported in the previous study (Lin et al., 2011). Furthermore, a

signal at 1735 cm^{-1} was demonstrated in the spectrum of SA/TB/OMFC0.25 microbeads (Figure 4.30 (e)), substantiating the ionic crosslinking between the carboxyl groups of SA and APS-oxidized MFCs with Ca^{2+} (X. W. Shi et al., 2005). Swamy and Yun (2015) also observed a new peak at 1751 cm^{-1} after crosslinked sodium alginate and sodium carboxymethyl cellulose (SA/NaCMC) with trivalent ions. The peak at 1735 cm^{-1} can also be the carboxylic acid groups of APS-derived MFCs (K. Y. Goh et al., 2016).

From the FTIR spectrum of vitamin E, we observed the appearance of absorption band at about 3400 cm^{-1} and prominent peaks at 2928 and 2855 cm^{-1}, assigning to OH stretching, asymmetric and symmetric stretching vibrations of the CH_2 and CH_3, respectively as reported by Man et al. (2005) (Man et al., 2005). Figure 4.27(a) also showed the characteristic peaks of vitamin E at 1453, 1374, 1255, 1083 and 931 cm^{-1}, which attributed to the phenyl skeletal and methyl asymmetric bending (1453 cm^{-1}), methyl symmetric bending, $–CH_2$, plane bending of phenyl and trans $=CH_2$ stretching, respectively (Fathi et al., 2017). These peaks were not shifted significantly in the spectra of vitamin E-loaded microbeads. Evidently, vitamin E has entrapped within microbeads successfully.

In Figure 4.27 (e) and (f), the bands centered at 2928 and 2860 cm^{-1} can also be contributed by the asymmetric (v_{as}) and symmetric (v_s) stretching vibrations of methylene ($-CH_2$) of Tween 80, respectively (Ren et al., 2012). The presence of 1735 cm^{-1} peak in FTIR spectra of SA/TB/OMFC0.25 and SA/TB/TMSC0.25 microbeads was attributed to the C=O stretching of the ester group of Tween 80 (Y. Ma et al., 2011; Ren et al., 2012). The peak at approximate 1088 cm^{-1} originates from C−O stretching of Brij 35 (Muthukumar et al., 2007). In the FTIR spectrum of SA/IL/OMFC0.25 (Figure 4.27(g)), the characteristic peaks of $C_4mimC_8SO_4$ at 1092 and 1226 cm^{-1} were also observed, which are attributed to C−O-SO_3 symmetric stretching and C−O-SO_3 asymmetric stretching

(Kiefer et al., 2007), respectively. Moreover, a ring in-plane asymmetric stretching of $C_4mimC_8SO_4$ due to the C–C stretching, $(N)CH_2$, and $(N)CH_3C$–N stretching contributed to the appearance of peak at 1166 cm^{-1} (Kiefer et al., 2007) as shown in FTIR spectrum of SA/IL/OMFC0.25.

4.7.2 Syneresis test

Syneresis is an undesirable problem encountered in the systems undergoing sol-gel transition, which poses challenge in the fabrication of food grade gels. Syneresis is macroscopically characterized as the time-dependent shrinkage of a gel with concomitant exudation of liquid (Draget et al., 2001). Syneresis degree of a gel indicates its ability to retain its original volume (Nunamaker et al., 2011). Unbound water molecules are expelled from matrix during gelation process that results in the formation of gel with wet surface, which promote spoilage (Somboon et al., 2014).

First, the syneresis degree of SA/TB/OMFC based microbeads at room temperature (21 ºC) for day 1, 3 and 7 were examined (Figure 4.28(a)). Microbeads without APS-oxidized MFCs (SA/TB/OMFC0.0) are more susceptible to syneresis. Guluronate blocks restricted within elastic segments of alginate could interact with divalent calcium ions to form lateral association of junction zones and result in the contraction of the primary network structure (Morch et al., 2007). The addition of appropriate amount of APS-treated MFCs can retard syneresis rate because the hydrophilic MFCs able to retain water molecules by forming hydrogen bonds with them (Chami Khazraji & Robert, 2013). The syneresis rate of alginate microbeads was strongly depended on the MFC concentrations. Upon increasing the concentration of APS-oxidized MFCs, the syneresis rate of the calcium-mediated microbeads was increased markedly. The observed trend stems from the expansion of attachment sites with Ca^{2+} as more carboxyl groups from APS-oxidized MFCs available for the formation of junction zones (Draget et al., 2001; N. Lin et al., 2012). Subsequently, smaller and stronger microbeads with compact networks were obtained and it was accompanied by the contraction of structure. The growth of junction zones becomes primary driving force for the syneresis (Morch et al., 2007; Tarté, 2009). Similar observation was reported in the previous study, whereby the syneresis degree of

Ca-mediated alginate gels reduced after the addition of mechanically-fibrillated or TEMPO-oxidized cellulose nanofibrils (Aarstad et al., 2017).

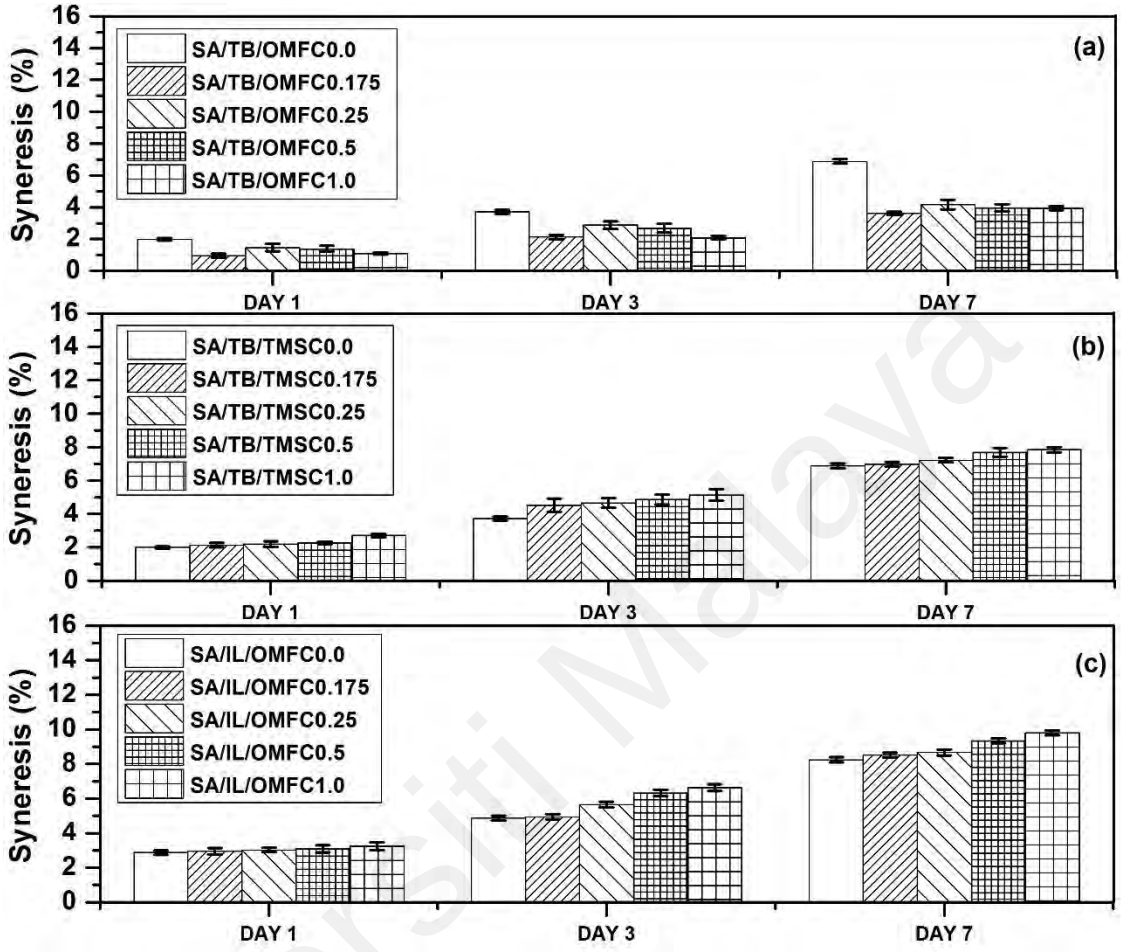

Figure 4.28: Syneresis (%) of (a) SA/TB/OMFC microbeads, (b) SA/TB/TMSC microbeads and (c) SA/IL/OMFC microbeads for day 1, 3 and 7 at room temperature (21 ºC).

According to the literature review, the syneresis degree of pure alginate gels and alginate gels reinforced by silanized hydroxypropyl methyl cellulose (Si-HPMC) was investigated. Pure alginate gels showed high syneresis degree whereby the gels encountered 50% weight loss during the first two days due to the expulsion of water from the gel matrix. The syneresis degree increased with the increasing of crosslinker $CaCO_3$ concentration. This was driven by the increased contraction of gels due to the rise in the number of crosslinks within the alginate matrix. However, syneresis of alginate gels was inhibited after the addition of Si-HPMC. The syneresis of alginate gels reinforced by un-

crosslinked hydroxypropyl methyl cellulose (HPMC) was reduced and it was observed that the weight loss was less than 10% after 20 days of storage (Viguier et al., 2016). In addition, Aarstad et al. (2017) also studied the syneresis of both pure alginate gels and cellulose nanofibrils-reinforced alginate composite gels. This similar observation was reported in which the syneresis reduced relatively for alginate composite gels as compared to pure alginate gels.

We observed that SA/TB/TMSC based microbeads displayed higher degree of syneresis than SA/TB/OMFC based microbeads at room temperature (21 ^{o}C) for all days (Figure 4.28(b)). The addition of TMSC showed adverse effect on the syneresis of the microbeads. This was stem from the non-polar character of TMSC that expelled water molecules from the system, resulting in higher exudation of fluid from matrix. Elevation of TMSC concentration led to increase in the syneresis degree. Whereas, Figure 4.28(c) depicted the syneresis rate of SA/IL/OMFC based microbeads and it was observed to be higher than the corresponding SA/TB/OMFC based microbeads. Since ionic liquid can be easily regenerated in the water, it can be exuded from the matrix together with water during gelation (Paul & Moulik, 2015). With this reason, the weight loss would be higher in the case of SA/IL/OMFC microbeads and resulted in the increased of syneresis (%).

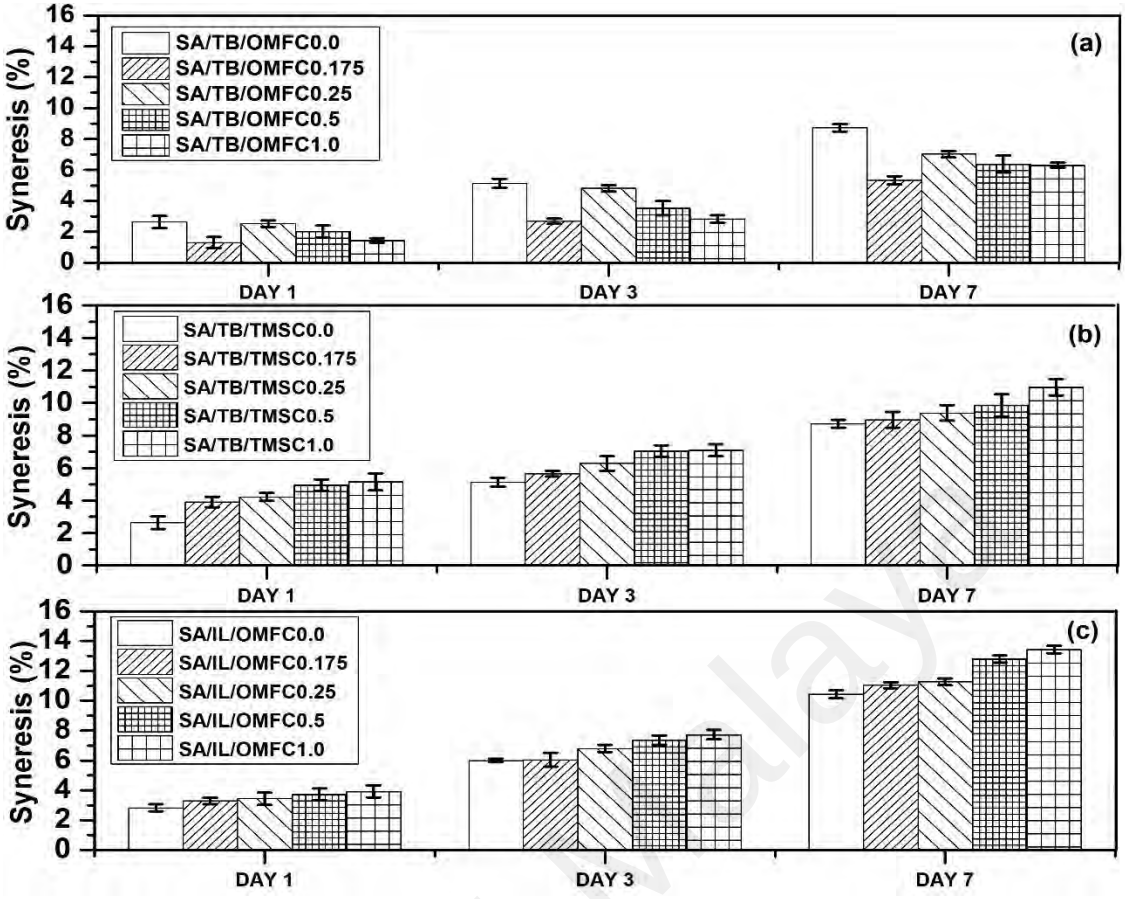

Figure 4.29: Syneresis (%) of (a) SA/TB/OMFC microbeads, (b) SA/TB/TMSC microbeads and (c) SA/IL/OMFC microbeads for day 1, 3 and 7 at 4 ^{o}C.

All the formulated microbeads exhibited higher syneresis degree upon subjecting to refrigerated condition, 4 ^{o}C (Figure 4.29). Under refrigerated condition, cooling treatment enhanced the dewatering process because this condition can lead to the molecular reorganization and tightening of molecular structure (Tarté, 2009). This phenomenon is also common in a gelatinized starch paste. Gelatinized starch containing disaggregated amylose and amylopectin chains undergo reassociation upon cooling to form more ordered structures, leading to syneresis. This process is known as starch retrogradation, becoming the major determinant of its functional properties (Tarté, 2009).

One of the key challenges in this study is that alginate microbeads are susceptible to syneresis due to the contraction of the primary network structure which will eventually result in spoilage. By comparing the formulations SA/TB/OMFC, SA/TB/TMSC, SA/IL/OMFC, the alginate microbeads with Tween 80:Brij 35 and oxidized MFCs

exhibited lowest syneresis degree at room temperature (21 ºC) as oxidized MFCs could retain the water within the microbeads due to the formation of hydrogen bonds. Although the syneresis rate of all the formulations increased when we stored the samples at refrigerated condition (4 ºC), SA/TB/OMFC microbeads exhibited relatively lower syneresis degree as compared to the corresponding SA/TB/TMSC, SA/IL/OMFC microbeads. It is essential to maintain the quality of the microbeads.

4.7.3 Mechanical strength of microbeads

Mechanical strength of hydrogels must be sufficiently high to withstand the high pressure or compression stress that might be encountered *in vivo* (Mørch, 2008). It is also vital to prevent the leakage of drugs before arriving the site of action. Therefore, appropriate mechanical strength is required to maintain physical integrity (Augst et al., 2006). The compressive stress at 85% strain was used to evaluate the compressive strength of the microbeads. As previously mentioned, neat alginate hydrogels exhibit poor mechanical performance that restrained their application as drug carrier (N. Lin et al., 2012). Production of alginate hydrogel beads with favorable mechanical properties is one of the principal goals in the present study and this can be achieved by adding reinforcing agents into alginate matrix (Y. Cheng et al., 2012). According to the previous study, the formation of composites by blending alginate with other biopolymers such as psyllium, pectin and carrageenan was examined to be a successful strategy to enhance the mechanical strength of hydrogel beads (Belscak-Cvitanovic et al., 2015).

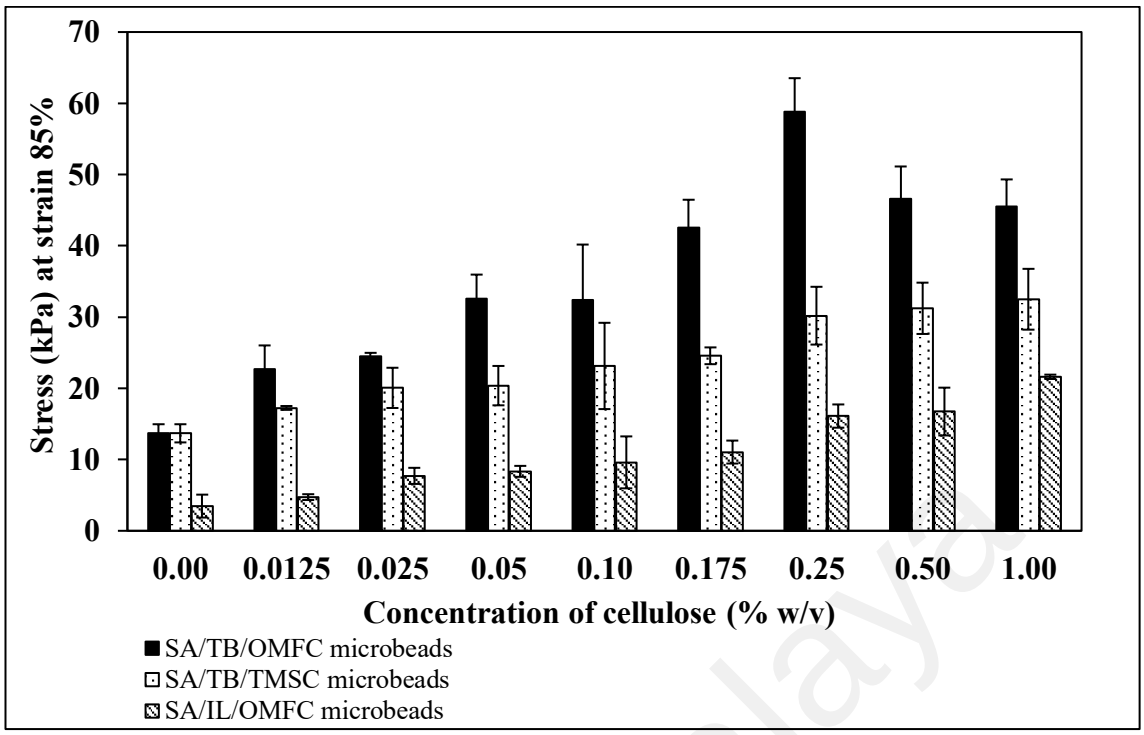

Figure 4.30: Compressive stress of (a) SA/TB/OMFC based microbeads, (b) SA/TB/TMSC based microbeads and (c) SA/IL/OMFC based microbeads at various concentrations of celluloses.

In this study, we examined the influence of two different types of reinforcements (hydrophilic APS-oxidized MFCs and hydrophobic TMSCs) on the mechanical performance of alginate microbeads. The findings demonstrated that the incorporation of cellulose nanoparticles as reinforcements improved the mechanical properties of the alginate-based hydrogels as anticipated. The mechanical properties of the microbeads were primarily affected by the concentration of cellulose nanoparticles added into the microbeads. First, the compressive strengths of SA/TB/OMFC based microbeads were determined and the results displayed in Figure 4.30. The compressive stress of the drug-loaded microbeads at 85% strain increased significantly with increasing of the oxidized MFC concentration. This result indicates that APS-oxidized MFCs involved in the formation of densely packed and three-dimensional matrix structures of hydrogels. In addition, the interactive strengths among oxidized MFC and alginate molecules also contributed to the improvement of the compressive strength of the microbeads. Since both MFC and ALG molecules have strong polar groups, they can interact with each other via

the formation of hydrogen bonds (Y. Cheng et al., 2012; KMa et al., 2012). SA/TB/OMFC0.25 achieved the highest compressive strength. However, the compressive strength was reduced when superfluous nanoparticles were added into microbeads as shown by SA/TB/OMFC0.5 and SA/TB/OMFC1.0. The reinforcing effect was shaded-off due to the self-aggregation of nanoparticles (Ning Lin et al., 2012).

According to the previous study, Onyianta et al. (2018) investigated the influence of various concentrations of carboxymethylated cellulose nanofibrils (CMCNF) and morpholine pre-treated cellulose nanofibrils (MCNF) on compressive modulus of calcium-crosslinked alginate based hydrogels. MCNF was observed to be more effective in improving the compressive strength of alginate hydrogels at the same loadings as compared to CMCNF. The addition of 5 wt. % MCNF increased the compressive modulus by 36% while the incorporation of CMCNF resulted in only 17% increased at the constant concentration of nanofibrils. However, reduction in the compressive modulus was observed when 10 wt. % or 20 wt. % of MCNF were added into the hydrogels. This is because excessive amounts of MCNF led to fibrillar aggregations as well as entanglements with hydrogels, which demonstrated antagonistic effect in reinforcing capacity of nanofibril. Moreover, Thomas et al. (2018) also synthesized rifampicin-loaded calcium crosslinked-alginate hydrogels via ionic gelation with cellulose nanocrystal as reinforcing agent. By using probe sonication, nanoparticles with less than 100 nm were first prepared prior to the formation of hydrogels due to the poor solubility of rifampicin. This approach is beneficial in increasing the cellular uptake as the particles in nanometer scale possess a higher surface area, leading to efficient delivery of a drug (Nasir et al., 2015; Panyam & Labhasetwar, 2003). This was followed by encapsulating the drug-loaded nanoparticles into alginate hydrogels in order to provide sustained release for extended period of time. However, mechanical stability is one of the weaknesses of alginate that restricted its application in drug delivery system. Hence, cellulose

nanocrystals were added to enhance the mechanical properties of alginate-based hydrogels.

Furthermore, N. Lin et al. (2012) also synthesized TEMPO-oxidized cellulose reinforced alginate based sponges. The modified celluloses formed bonds with alginate using carboxyl groups on the surfaces of nanocelluloses induced by TEMPO oxidization. This was subsequently resulted in improving the mechanical strength of alginate based sponges. Neat alginate sponge exhibited low mechanical strength which restricted their applications especially in the biomedical and pharmaceutical field. Conversely, alginate sponges in the presence of unmodified or oxidized celluloses were generally stronger and more robust. The formulation SA/OCN-10 (alginate sponge containing 10 wt. % of TEMPO-oxidized cellulose nanocrystals) showed the highest mechanical strength in which the compressive strength of SA/OCN-10 increased by factors of 2.78, 2.80, and 2.94 at compressive strains of 30%, 50%, and 70%, respectively as compared to neat alginate sponge. Furthermore, the compressive strength of SA/OMFC-30 (alginate sponge containing 10 wt. % of TEMPO-oxidized microfibrillated celluloses) increased by factors of 2.03, 1.79, and 1.68 at compressive strains of 30%, 50%, and 70%, respectively. Oxidized celluloses were observed to be more effective in enhancing the compressive stress of sponges as compared to pristine cellulose nanocrystals, which can be ascribed to the participation of carboxyl groups in forming crosslinking with alginate. Nevertheless, the reinforcing effect was diminished when excessive nanocrystals were added to the sponges attributed to the self-aggregation of nanoparticles.

The weight ratio of cellulose/alginate was the key determinant of the mechanical strength of the hydrogels. Chang et al. (2009) reported that the compressive modulus increased with the increasing of weight ratio of cellulose/alginate. Hence, the results showed that the cellulose plays a significant role in enhancing the mechanical properties

of the resultant hydrogels. Hydrogel with low mechanical strength was obtained when the weight ratio of cellulose/SA is below 5:5 due to the weak interactions. The mechanical properties of alginate-based hydrogels can be tailored by manipulating the concentration of cellulose added into formulation.

Further investigation was conducted to determine the effect of different types of nanoparticles (MFC or TMSC) on the compressive strength of the microbeads. As shown in Figure 4.30, TMSC was employed to stabilize SA/TB/TMSC based microbeads and their compressive strengths were examined. Despite the superior rheological behaviors of secondary emulsions reinforced by TMSCs as previously discussed, the compressive strengths of SA/TB/TMSC based microbeads were lower than SA/TB/OMFC based microbeads. It is noteworthy to highlight that APS-oxidized MFCs exhibit a better reinforcing effect, which ascribed to the participation of carboxyl groups of MFCs in crosslinking together with ALG molecules. The coupling of oxidized MFC and alginate molecules through hydrogen bonds also contributes to the higher compressive strength of SA/TB/OMFC based microbeads (N. Lin et al., 2012). In the contrary, TMSC with -$Si(CH_3)_3$ groups led to reduced prevalence of ionic crosslinking points with Ca^{2+}. Besides, TMSCs lack of OH groups restricted the formation of bonds with ALG molecules, decreasing the interactive strength of the beads. However, the compressive strengths of the SA/TB/TMSC based microbeads were enhanced with the elevating amount of TMSC.

Lastly, the compressive strengths of SA/IL/OMFC based microbeads were relatively low as compared to the corresponding formulations (Figure 4.30). The results indicate that the type of surfactant employed in emulsion stabilization being one of the major factors that determined the mechanical strength of the resultant microbeads. Microbead can be defined as hydrogel matrix in which bioactive materials are finely distributed (Benavides et al., 2016). Premix of both the active ingredient and the polymer solution is

required prior to the microencapsulation (Drusch & Berg, 2008). Hence, the efficiency of emulsifier in stabilizing the vitamin E-loaded emulsions will eventually determine the properties of the resultant microbeads. The emulsifying capacity of $C_4mimC_8SO_4$ is not as effective as Tween 80 and Brij 35. The result was in consistent to the rheological measurement of SA/IL/OMFC based secondary emulsions.

Poor mechanical strength of alginate is one of the major drawbacks that restrained its application as drug carrier, we found that incorporation of nanocelluloses significantly enhanced the mechanical performance of alginate microbeads. Based on the observations, we concluded that the mechanical strength of vitamin E-loaded alginate microbeads increased with increasing the cellulose concentration regardless the type of the nanocelluloses. SA/TB/OMFC0.25 was observed to be the formulation with highest mechanical strength. In addition, the mechanical properties of microbeads were also greatly affected by the type of the emulsifiers used in stabilizing the emulsions prior to the formation of the microbeads. Higher stability emulsions can be obtained by employing Tween 80:Brij 35 as emulsifiers and eventually produced microbeads with higher mechanical strength.

4.7.4 Swelling test

Swelling behavior of microbeads also plays a vital role in determining their practical application as drug delivery vehicle. The microbeads loaded with vitamin E will transit through the gastrointestinal tract after the oral administration of the beads. Prior to the arrival in the intestine, the oral formulation resides in highly acidic condition of stomach for approximately 2 h (F. Kong & Singh, 2008). Since the proposed beads are oral dosage form for vitamin E absorption in the intestine, it is requisite to examine the swelling behaviors of these beads in both the simulated gastric fluid (SGF, pH 1.2 HCl) and simulated intestinal fluid (SIF, pH 7.4 PBS) (J. P. Zhang et al., 2010).

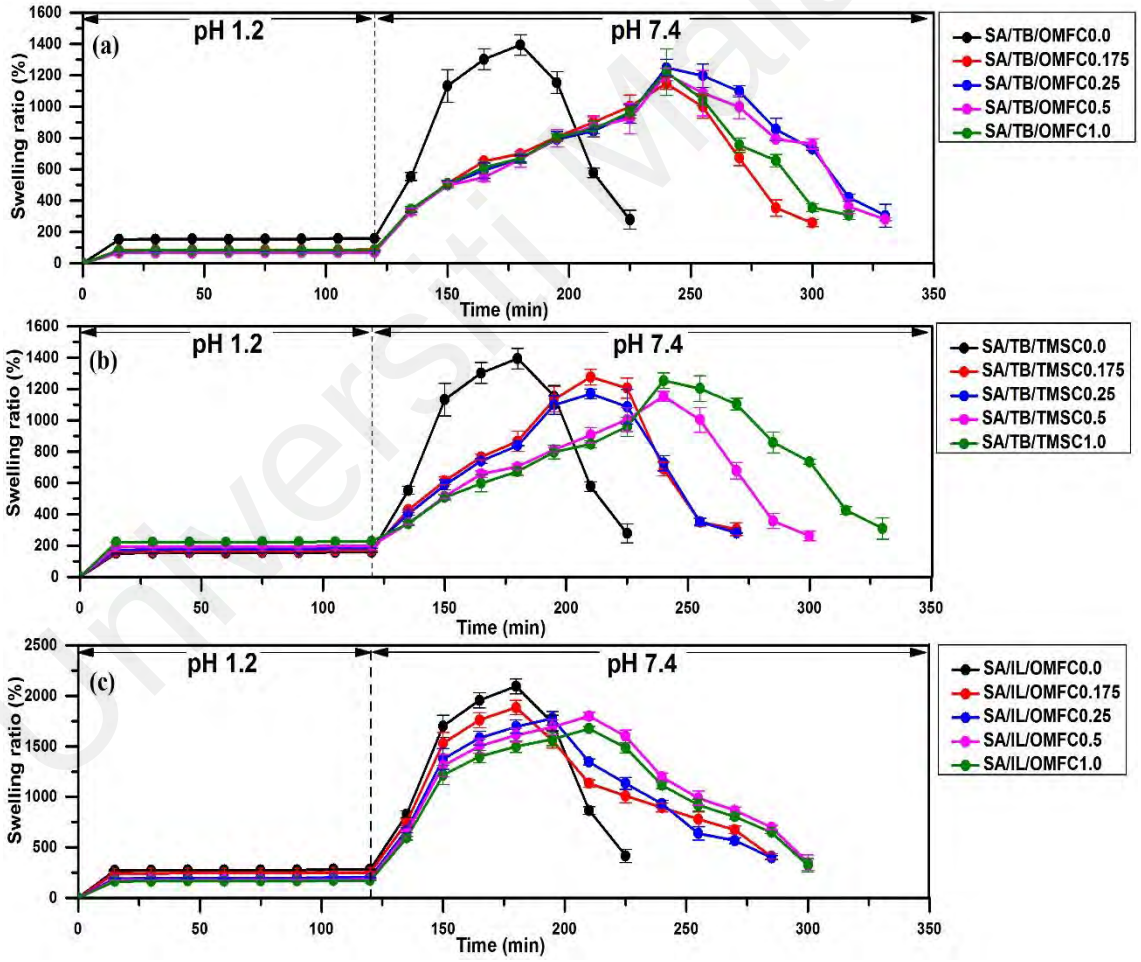

Figure 4.31: Swelling ratio (%) of (a) SA/TB/OMFC, (b) SA/TB/TMSC and (c) SA/IL/OMFC microbeads at pH 1.2 and pH 7.4 at predetermined time.

The swelling degree of the beads in pH 1.2 HCl was low and there was no dissolution of beads occurred in this buffer. According to Reyes-Ortega (2014), the carboxylate groups of alginate is protonized and unionized at low pH and hence the electrostatic repulsions among these groups diminished, leading to volume reduction of the polymer that contains the carboxylate groups. Despite of this, microbeads have still gained some weight due to the hydration of the hydrophilic groups of alginate and APS-oxidized MFC (Hoffman, 2012). Furthermore, alginate is hydrolyzed into more soluble low molecular weight alginic acid when the vitamin E encapsulated microbeads being treated with pH 1.2 HCl. Since the carboxylate groups (COO^- ions) of alginate is unionized at low pH and hence the electrostatic attraction between Ca^{2+} ions and COO^- ions in the "egg-box" junction will be diminished. Therefore, weakly acid-treated beads are loosely crosslinked and the beads may degrade quickly after arriving intestine (S. K. Bajpai & Sharma, 2004). With this reason, the mechanical strength of microbeads must be enhanced in order for them to withstand the hydrolysis in the stomach and allow them to reside in intestine for sufficient time for proper absorption of vitamin E. As shown in Figure 4.31(a), the swelling degree of SA/TB/OMFC based microbeads in pH 1.2 SGF reduced with increasing of MFC contents. However, the swelling degree increased again after the addition of 1.0 % w/v oxidized MFCs (SA/TB/OMFC1.0).

The crosslinked SA/TB/OMFC based microbeads demonstrated obvious elevation of swelling degree when exposed to pH 7.4 SIF. All the microbeads displayed similar swelling and dissolution trends in pH 7.4 SIF. However, the microbeads reinforced with oxidized MFCs required longer time to complete dissolution as compared to neat alginate beads (SA/TB/OMFC0.0), as illustrated in Figure 4.31(a). Slightly alkaline environment led to the ionization of the groups and the generated electrostatic repulsive forces that believed to be the driving force for the swelling of these systems (Chaterji et al., 2007). The swelling curves of microbeads in pH 7.4 PBS buffer were observed to decline after

attaining maximum water uptake indicating the dissolution or degradation of beads. The ion-exchange process between the Ca^{2+} ions present in the "egg-box" junction of polyguluronate units and Na^{+} ions from the phosphate buffer (SIF) is believe to be responsible for swelling and subsequent disintegration of beads. The interactions between Na+ ions and the $–COO^{-}$ ion groups in polyguluronate units are not as strong as divalent ions, Ca^{2+} that minimized the crosslinking and permitted the entry of water molecules into the matrix (S. K. Bajpai & Sharma, 2004; Colinet et al., 2010). J. P. Zhang et al. (2010) also carried similar experiment whereby the group designed SA beads with improved swelling properties by mixing layered double hydroxides (LDHs) into the hydrogel. They investigated the effect of LDHs concentration on the swelling behaviors of SA/LDHs hybrid beads in pH 7.4 PBS and they observed that the dissolution of the beads in alkaline buffer was slower after the inclusion of LDHs.

In the previous study, cellulose nancrystals-reinforced alginate hydrogels prepared by the researchers also exhibited predominantly pH-responsive swelling properties whereby the swelling degree of hydrogels was low at low pH condition while increased drastically at high pH condition. This remarkable characteristic is significant especially for the pharmaceutical formulation in which the intestine is the site of action. Hence, the resultant cellulose nanocrystals-reinforced alginate hydrogels were successfully protected the entrapped rifampicin from the harsh acidic condition in the stomach. The incorporation of cellulose nanocrystals were observed to enhance the stability of hydrogels by extending the drug release up to 12 hours before the degradation of hydrogels. The three-dimensional network of the cellulose nanocrystals interacted with rifampicin and formed entanglements with hydrogels, hindering the burst release of drugs at gastric condition. Sustained release of rifampicin was achieved in this study with the presence of cellulose nanocrystals as reinforcing agents (Thomas et al., 2018).

Furthermore, the swelling profile of SA/TB/TMSC based microbeads (Figure 4.31(b)) also exhibited similar trend as SA/TB/OMFC based microbeads whereby considerably low swelling ratio was observed in pH 1.2 dissolution medium but increased drastically after transferring to pH 7.4 dissolution medium. At pH 1.2 buffer solution, swelling ratio rises with the increasing of TMSC contents that can be ascribed to the structure of TMSC. TMSCs with functional groups of $-Si(CH_3)_3$ are not involving in the formations of three-dimensional networks of microbeads. Besides, lack of OH groups of cellulose derivatives to hydrogen bonds with -OH groups of alginates increased the swelling degree of microbeads (Klebe & Schenectady, 1968). However, increased in the concentration of TMSC strengthens the alginate-based microbeads in pH 7.4 as evidenced by the longer time required to achieve dissolution.

The swelling profile of SA/IL/OMFC based microbeads was displayed in Figure 4.31(c). Higher degree of swelling was apparently observed for SA/IL/OMFC0.0 microbeads. This implies that ionic liquid, $C_4mimC_8SO_4$ employed in the emulsion stabilization influences the swelling properties of the resultant microbeads. Cationic part of ionic liquid, C_4mim^+ tends to repel with the positively charge crosslinking divalent ions (Ca^{2+}) resulted in an elevated swelling degree at pH 1.2 buffer solution (Thakkar et al., 2016). In the contrary, repulsive forces were created among the deprotonated alginate molecules with $-COO^-$ groups and anionic part of ionic liquid, $C_8SO_4^-$ in pH 7.4 buffer solution (Thakkar et al., 2016). However, swelling degree reduced with an increasing of APS-oxidized MFCs.

Since the release profile of vitamin E-loaded microbeads is greatly affected by their swelling properties, it is vital to ensure that the microbeads are protected from the harsh gastric condition and release vitamin E in the intestine which is the site of action. The objective has been achieved in this study whereby the vitamin E-loaded alginate

microbeads remained intact in pH 1.2 simulated gastric fluid but disintegrated in pH 7.4 simulated intestinal fluid due to the chemical structure of alginate. We also observed that the swelling degree reduced with an increasing of APS-oxidized MFCs. In addition, the time for complete disintegration of microbeads in pH 7.4 also longer after the incorporation of APS-oxidized MFCs.

4.8 Alginate-based microbeads for encapsulation of vitamin E

4.8.1 Encapsulation efficiency

Alginate exhibits numerous advantageous properties such as biocompatible, biodegradable and relatively economical, which is a potential candidate in developing excellent drug carrier. Nevertheless, the poor mechanical performance and the stability of neat alginate microbeads which are attributed to their macroporous structure as matrices, resulting in low encapsulation efficiency and burst release of bioactive molecules (George & Abraham, 2006). Hence, APS-oxidized MFCs and TMSCs were adopted as bio-based reinforcing nanofillers to enhance these properties.

The abilities of SA/TB/OMFC based microbeads to entrap vitamin E were evaluated through the determination of encapsulation efficiency, as displayed in Figure 4.32. Encapsulation efficiency reflects the strength of the microbeads as beads with higher mechanical performance can attain more vitamin E after crosslinking process. Encapsulation efficiency % of SA/TB/OMFC0.0 was calculated to be 68.96 ± 1.00%. Results revealed that encapsulation efficiency % was improved after the incorporation of APS-oxidized MFCs. At constant alginate content, the elevation in encapsulation efficiency % was observed upon increasing the concentration of oxidized MFC from 0.0125% to 0.2500 %w/v except for the sample SA/TB/OMFC0.175. SA/TB/OMFC0.25 achieved maximum encapsulation efficiency % of 98.76 ± 0.02%. This observation was in agreement with the mechanical test of microbeads.

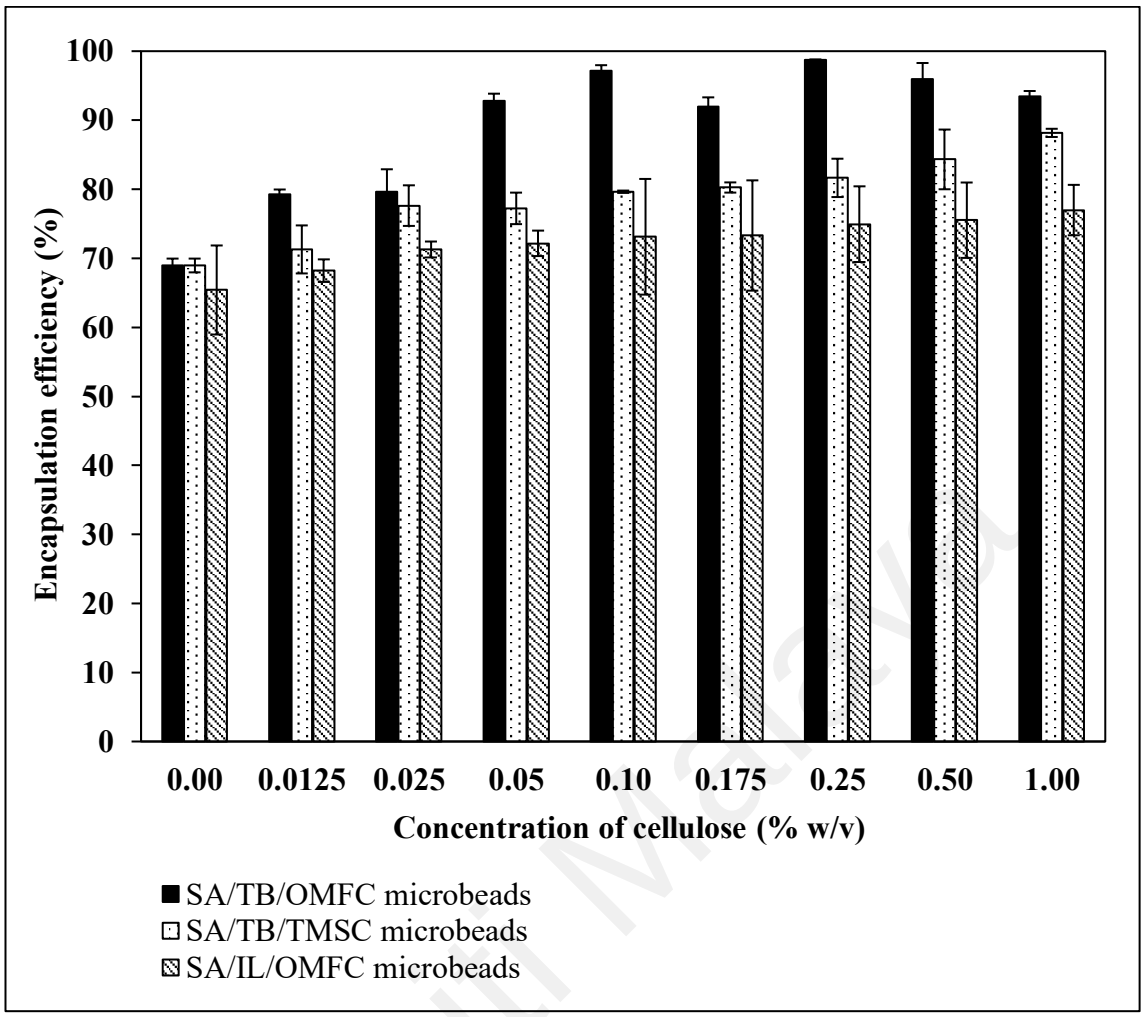

Figure 4.32: Encapsulation efficiency of (a) SA/TB/OMFC based microbeads, (b) SA/TB/TMSC based microbeads and (c) SA/IL/OMFC based microbeads at various concentrations of celluloses.

Owing to the highly porous structure of alginate microbeads, vitamin E can escape through void regions of the polymer network within the beads and result in a low attainment of vitamin E. Conversely, the three-dimensional network structures of the alginate-based microspheres are surrounded by APS-oxidized MFCs that provides a mechanical barrier and reduced leaking of vitamin E (Lin et al., 2011). Both the anionic carboxylic groups of alginate and APS-induced carboxyl groups on MFCs participate in the construction of compact three-dimensional network structure by interacting with bivalent calcium ion to form vitamin E-loaded microbeads (Agarwal et al., 2015). Besides, oxidized MFCs also served as the coupling points with alginate, forming reinforced framework of beads. This plays a fundamental role in enhancing the

mechanical stability of the resulting microbeads, which eventually improved the encapsulation efficiency of microbeads (N. Lin et al., 2012).

However, the vitamin E entrapment capacity slightly lowered when further increased the amount of the oxidized MFCs (0.50 and 1.00% w/v). Encapsulation efficiency % for SA/TB/OMFC0.5 and SA/TB/OMFC1.0 microbeads were calculated to be 95.96 ± 2.33% and 93.44 ± 0.79%, respectively. When superfluous MFCs were introduced into the formation of microbeads, the reinforcing effect of MFCs will be shaded-off due to the self-aggregation of nanoparticles (N. Lin et al., 2012). Agarwal et al. (2015) also obtained similar results while working with calcium alginate-carboxymethyl cellulose (CA-CMC) beads. At constant alginate and crosslinker concentration, CA-CMC blend beads with two different concentrations of CMC (0.5 and 1.0 wt%) were prepared and the encapsulation efficiency of anticancer drug 5-fluorouracil (5-FU) was examined. The encapsulation efficiency % of ALG beads without CMC was found to be 95.93 ± 2.3%. After the addition of 0.5 and 1.0 wt% CMC, encapsulation efficiency % declined to 92.04 ± 1.9 and 88.56 ± 2.7%, respectively.

In the previous study, they also applied the similar approach in fabricating drug delivery system whereby they produced oil-in-water emulsions prior to encapsulation of alfacalcidol into the alginate-based beads. Since alfacalcidol is a hydrophobic drug, it is one of the challenges to entrap hydrophobic drug into alginate due to its hydrophilicity. Hence, they proposed the production of Pickering emulsions containing alfacalcidol using amphiphilic bacterial cellulose nanocrystals (BCNs) as surface active agents and dichloromethane CH_2Cl_2 as the oil phase via ultrasonic dispersion method. They were then well dispersed in alginate solution and drug-loaded alginate composite beads abbreviated as SA/BCNs CBs were synthesized by external gelation using 0.25 M $CaCl_2$ as crosslinking agent. The results obtained showed that the encapsulation efficiency of

alginate composite beads increased with the increasing of bacterial cellulose nanocrystals concentration. Encapsulation efficiency of 54.2%, 80.3%, 89.6% and 91.4% were obtained for SA/BCNs-0.3 CBs, SA/BCNs-0.6 CBs and SA/BCNs-0.9 CBs, respectively. Alginate beads with 0.6 wt% and 0.9 wt% of bacterial cellulose nanocrystals did not show significant difference in encapsulation efficiency. This can be explained by the sufficient coverage of bacterial cellulose nanocrystals at the freshly formed oil-water interface during the preparation of the drug-loaded Pickering emulsions when concentration of cellulose nanocrystals reached up to 0.6 wt%. The addition of excess BCNs might have only trivial effect on the drug-loading capacity of beads (H. Yan et al., 2019).

In addition, Al-Kahtani and Sherigara (2014) also immobilized diclofenac sodium-loaded emulsions stabilized by acrylamide-grafted hydroxyethyl cellulose (AAm-g-HEC) into alginate based microspheres using glutaraldehyde as a crosslinker. The encapsulation efficiency of diclofenac sodium-loaded alginate microspheres were manipulated by the concentrations of AAm-g-HEC as well as the amount of glutaraldehyde used. This rise in encapsulation efficiency from 59% to 63% was observed when the amount of AAm-g-HEC in the matrix was increased from 10 to 30%. Furthermore, the encapsulation efficiency was also affected by the concentration of glutaraldehyde in which the encapsulation efficiency increased when the amount of glutaraldehyde used as crosslinking agent was increased from 3 to 9 ml.

We extend this study by further preparing the SA/TB/TMSC based microbeads via ionotropic gelation encapsulating vitamin E, as a model of hydrophobic natural therapeutics and their loading capabilities of drug were assessed. The encapsulation efficiency % for SA/TB/TMSC based microbeads at various TMSC concentrations was in the range of 68.96 ± 1.00 to 88.16 ± 0.59% as displayed in Figure 4.32. Despite of the general increase in encapsulation efficiency % due to the presence of TMSC, vitamin E

successfully loaded into these beads were not as high as in SA/TB/OMFC based microbeads. This serves as a supplementary evidence for the results obtained during the compressive test. Therefore, we believed that the type of stabilizer (APS-oxidized MFCs or TMSCs) employed in the fabrication of emulsions will eventually affect the encapsulation efficiency of the final microbeads.

Since the hydrophobic TMSC was modified from cellulose by replacing –OH groups with $–Si(CH_3)_3$, the availability of –OH groups to form hydrogen bonds with ALG was reduced (Klebe & Schenectady, 1968). TMSC can adsorb strongly to the oil-water interface together with surfactant to form smaller oil droplets due to its hydrophobicity. Nevertheless, the newly modified TMSC with $–Si(CH_3)_3$ could not involve in the chemical crosslinking with divalent calcium ions. In the previous study, Ibrahim M. El-Sherbiny et al. (2011) developed alginate based microspheres in combination with a hydrophobic poly(d,l-lactic-co-glycolic acid) (PLGA) polymer as a potential carrier for hydrophobic cargo, which is silymarin in this study. The encapsulation efficiency % were calculated to be in the range 71.4 ± 4 to 88.7 ± 2% at different composition ratio of ALG/PLGA. In addition, there was also research conducted to investigate the encapsulation of diclofenac potassium by modified hydrophobic HPMC/ALG based hydrogel beads and the encapsulation efficiency % were observed within the range of 77.9 ± 2.0 to 87.6 ± 1.4% (Ghosal & Ray, 2011).

Conversely, encapsulation efficiency % of SA/IL/OMFC emulsion-laden microbeads were found to be lower at the corresponding concentration of cellulose particles. We suggest that these emulsion formulations were inefficient. The emulsion properties can greatly affect the performance of the resultant microbeads. In the absence of cellulose particles, SA/IL/OMFC based microbeads displayed encapsulation efficiency % lower than SA/TB/OMFC based microbeads. This result revealed that ionic liquid,

$C_4mimC_8SO_4$ is not as effective as Tween 80 and Brij 35 in the emulsion stabilization. This is a complementary evidence for emulsion droplet size results. Consequently, delivery of high amount of drugs within emulsions was not achieved, which in turn results in low encapsulation efficiency % of relative microbeads. The encapsulation efficiency % varied from 65.4 ± 6.4 to 76.9 ± 3.7% (Figure 4.32), being the lowest value obtained for the microbeads with 0 %w/v of APS-oxidized MFCs. Carneiro et al. (2013) also reported that the performance of spray dried powder encapsulating flaxseed oil was affected by the emulsion properties and the selection of polymer wall material. The emulsion using maltodextrin and whey protein concentrate at a 25:75 ratio as encapsulating materials showed poorer emulsion stability, in which the obtained dried powder turned out to exhibit the lowest encapsulation efficiency.

Encapsulation efficiency is one of the criteria that taken into account in the fabrication of effective drug delivery system. Intensive attempts have been carried out in the previous studies to improve the encapsulation efficiency of microbeads. In this study, SA/TB/OMFC0.25 demonstrated highest mechanical strength also observed to have maximum encapsulation efficiency. Hence, we can conclude that encapsulation efficiency is the reflection of mechanical strength of microbeads.

4.8.2 *In vitro* release profile

In order to avoid exposure of vitamin E to harsh environment in stomach, vitamin E has to be protected by a carrier to avoid its release in the stomach. It is desirable that the carrier allows the release of vitamin E in the intestine to promote absorption of vitamin E. The release of vitamin E from microbeads at pH 1.2 followed by a vitamin E-triggered release at pH 7.4 were examined. Results of % cumulative release of vitamin E versus time under simulated gastrointestinal pH fluids for all the studied samples were shown in Figure 4.33, 4.34 & 4.35.

Regardless the concentration of the APS-oxidized MFCs, all the SA/TB/OMFC microbeads evaluated for this study demonstrated similar release pattern with slow release at pH 1.2 and increased release at pH 7.4 (Figure 4.33). Up to 2 h in acidic condition, the vitamin E released from the tested SA/TB/OMFC microbeads was considerably low. It was less than 2.5% of the total encapsulated vitamin E except for the sample of SA/TB/OMFC0.0. The microbeads remained intact after 2 h of incubation in pH 1.2 HCl medium. This result proposed that the formulated microbeads could potentially withstand the low pH environment encountered in the stomach and provide desired protective effects to prevent the leakage of therapeutic agents. This observation was in consistent with previous study, in which they encapsulated fluorescein isothiocyanate conjugated albumin (from bovine, BSA-FITC) within alginate beads, the BSA-FITC exuded from alginate beads was relatively slow and it was about 3.46 ± 1.33% after 3 h incubation in pH 1.2 acidic medium. Furthermore, they also reported that the amount of BSA-FITC released from alginate/carboxymethyl cellulose (CMC) hybrid systems with different ratio of alginate and CMC did not exceed 5% of the total entrapped protein (M. S. Kim et al., 2012).

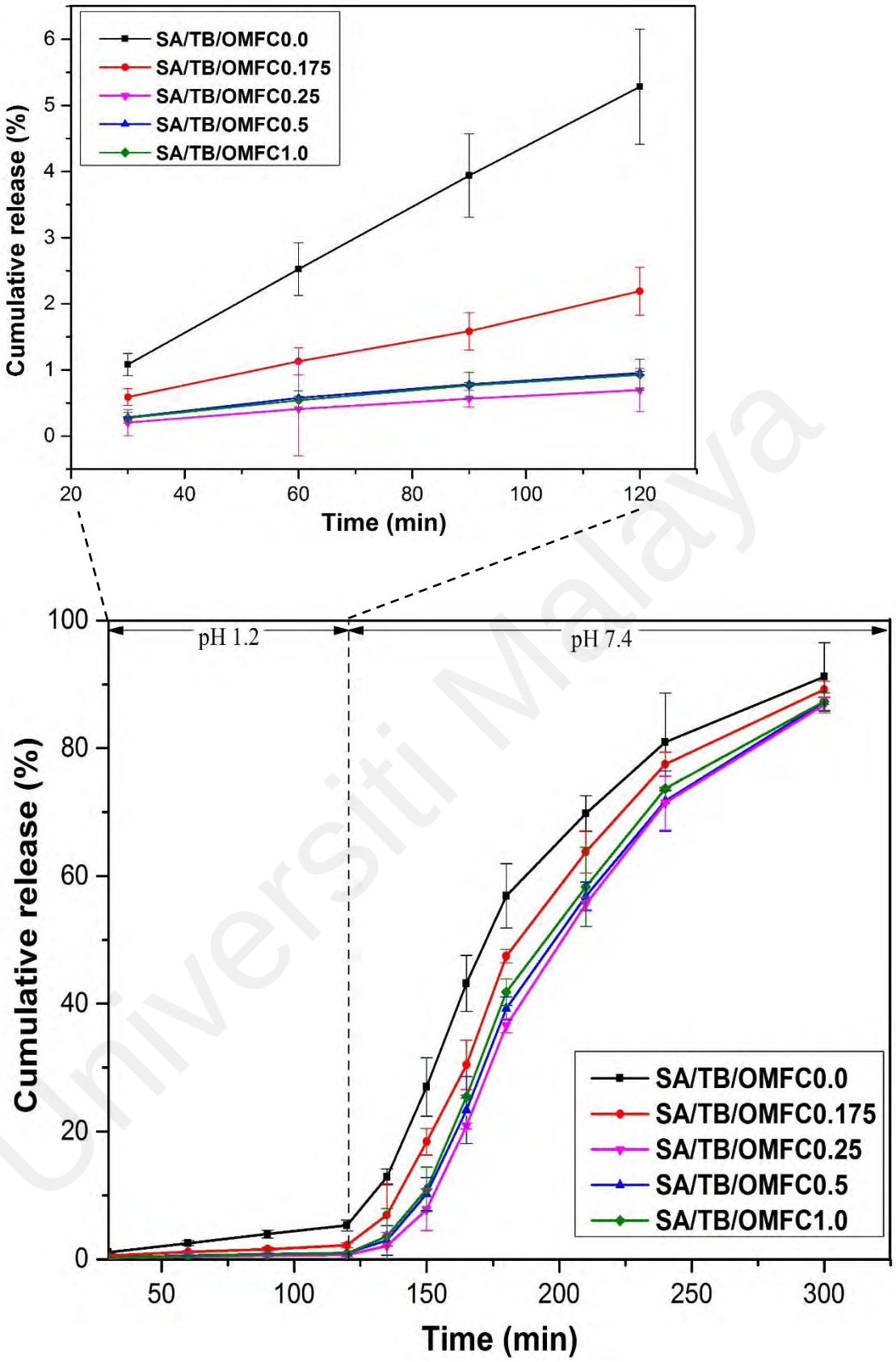

Figure 4.33: Cumulative release of vitamin E from SA/TB/OMFC0.0, SA/TB/OMFC0.175, SA/TB/OMFC0.25, SA/TB/OMFC0.5 and SA/TB/OMFC1.0 microbeads at pH 1.2 HCl and pH 7.4 PBS at predetermined time.

However, the swelling degree of microbeads was higher after transferring them to pH 7.4 dissolution medium and the diffusion rate of vitamin E from the microbeads was elevated. Distinct release behaviors in both pH 1.2 and pH 7.4 media can be explained by the strength of electrostatic interactions between biopolymers at different pH values. Protonation of carboxyl groups of alginate occurred, resulting in minimum swelling degree. Lesser extent of swelling restricted the diffusion of vitamin E through the matrix because more compact three-dimensional network structures are formed (Agnihotri & Aminabhavi, 2005; Y. Qiu & Park, 2001). By increasing pH value to 7.4, carboxyl groups were ionized in this slightly alkaline environment and electrostatic repulsive forces are predominated. Consequently, this results in the swelling and disintegration of microbeads, enabling extended release of vitamin E (Martins et al., 2007; Xing et al., 2003).

SA/TB/OMFC0.0 microbeads without the incorporation of APS-oxidized MFCs released nearly 81% of vitamin E after 4 h of incubation. In the contrary, SA/TB/OMFC0.175, SA/TB/OMFC0.25, SA/TB/OMFC0.5 and SA/TB/OMFC1.0 released 77%, 71%, 72% and 74% of vitamin E, respectively. It is worth noting that the release rate of vitamin E was decreased gradually by increasing APS-oxidized MFC contents in the formulated beads. This is because oxidized MFCs also aided in Ca^{2+} crosslinking together with alginate in the development of compact structure that results in the improvement of vitamin E retention in microbeads (N. Lin et al., 2012). The release studies were consistent with the results obtained in swelling tests. Nevertheless, diffusion of drug through polymeric matrix was greater by increasing the oxidized MFC concentration up to 0.5 %w/v. Addition of excessive APS-oxidized MFCs into the microbeads enhanced the release of therapeutic agents because of the extremely hydrophilic character of oxidized MFCs, promoting the penetration of water molecules into drug-entrapped microbeads and subsequently facilitates the release of vitamin E (Al-

Kahtani & Sherigara, 2014). The result obtained for the present study was in accordance with the previous study whereby they varied the volume ratios of SA and CMC - 2:0, 2:1, 1:1, 1:2 and 0:2 (defined as AL2, A2C1, A1C1, A1C2, and CMC2, respectively) using ferric chloride as crosslinker (M. S. Kim et al., 2012). Release of drug in pH 7.4 medium at 6 h was slower in the SA/CMC blend microbeads as compared to neat SA and CMC beads. They observed that the drug released from A2C1, A1C1, and A1C2 beads after 6 h in the dissolution media were 48.15 ± 7.73%, 42.81 ± 5.81%, and 45.61 ± 6.03%, respectively.

In addition, we also investigate the release profile of SA/TB/TMSC based microbeads and the results were shown in Figure 4.34. Cumulative drug release at pH 1.2 was increased with increasing of concentration of TMSC in the microbeads, with the exception of SA/TB/TMSC0.175 microbeads. Hydrophobic cellulose derivative, TMSC was produced by replacing -OH groups on cellulose backbone with $-Si(CH_3)_3$ groups through silylation (Klebe & Schenectady, 1968). The newly modified hydrophobic TMSC with $–Si(CH_3)_3$ could not involve in the chemical crosslinking with divalent calcium ions. On top of this, the free carboxylate groups of alginates in the system prone to interact with each other via hydrogen bonding. Importantly, they can also form bonds with -OH groups of the sugar moieties as in the case of oxidized MFCs. These hydrogen bonds are responsible in reducing the swelling degree at pH 1.2 (I. M. El-Sherbiny et al., 2010). Subsequently, the migration of drug from microbeads was hampered due to the minimal penetration of fluid (Ghosal & Ray, 2011). However, alginate could not form bonds with TMSC because of its limited -OH groups after modification (Klebe & Schenectady, 1968). Therefore, TMSC did not play a role in declining the swelling degree and the release of drugs.

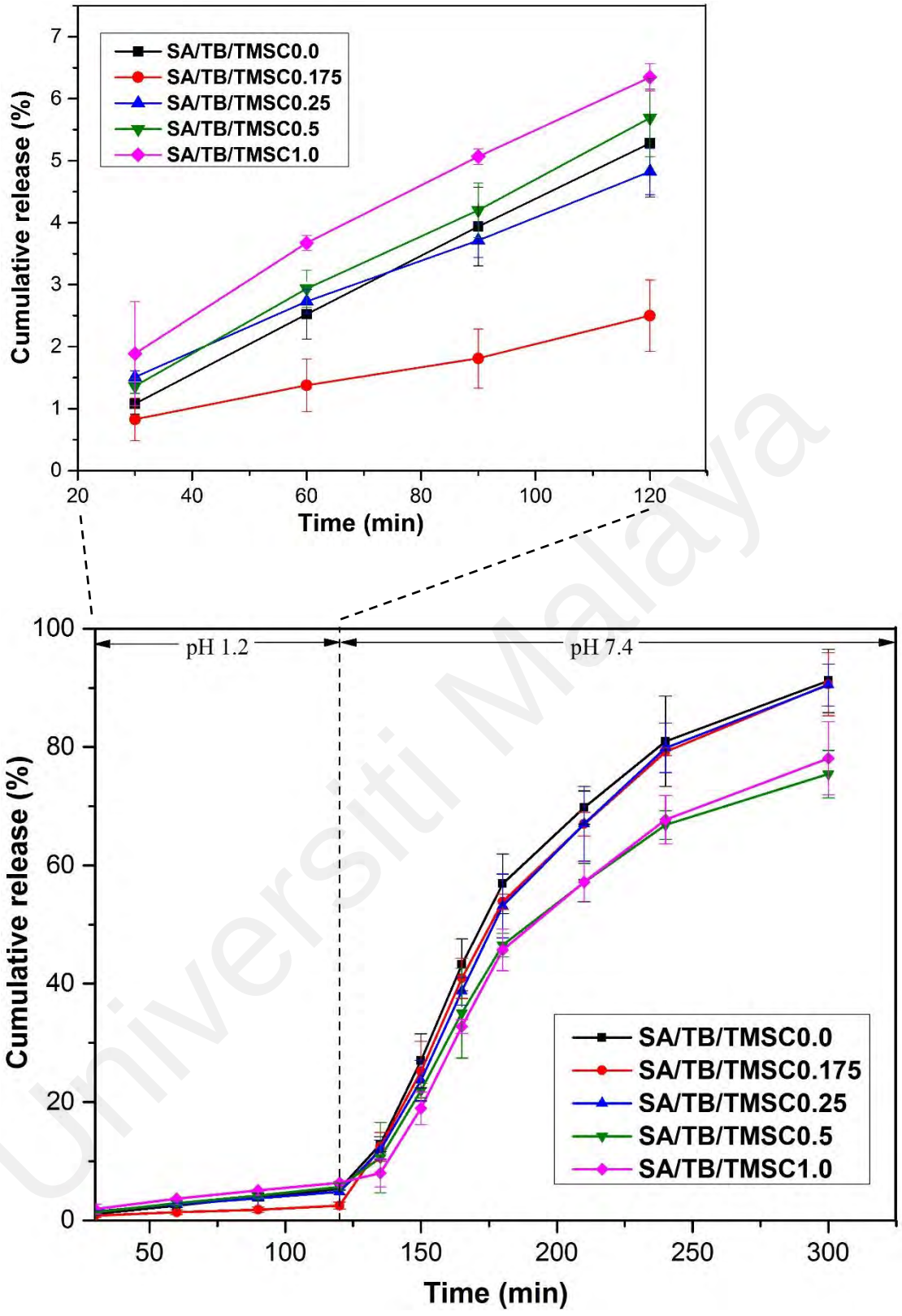

Figure 4.34: Cumulative release of vitamin E from SA/TB/TMSC0.0, SA/TB/TMSC0.175, SA/TB/TMSC0.25, SA/TB/TMSC0.5 and SA/TB/TMSC1.0 microbeads at pH 1.2 HCl and pH 7.4 PBS at predetermined time.

However, the cumulative release profile of SA/TB/TMSC based microbeads in a pH 7.4 simulated intestinal fluid was in contrast to the results obtained in pH 1.2 simulated gastric fluid. Most of the free carboxylic groups of alginates were ionized at pH 7.4, creating strong repulsive forces among themselves. These repulsive forces facilitate the penetration of dissolution fluids, resulting in high swelling degree and consequently increased the release rate of vitamin E (Ghosal & Ray, 2011). In pH 7.4 phosphate buffer saline, the release of drug was slower in the microbeads containing higher concentration of TMSC particles. TMSCs are responsible in minimizing the release rate of vitamin E in simulated intestinal fluid by reducing the swelling of microbeads as evidenced in the swelling test.

As displayed in Figure 4.35, the drug release was anomalous high for SA/IL/OMFC based microbeads at both pH 1.2 and pH 7.4 dissolution media. The type of emulsifier utilized for stabilizing the emulsions is an essential factor that affects the retention release of resultant microbeads. In pH 1.2 simulated gastric fluid, cationic domain of IL, C_4mim^+ acts as counterion resides around oil droplets tend to repel with Ca^{2+} ions and thus resulted in fast release of vitamin E (Thakkar et al., 2016). These extremely strong repulsive forces were large enough to surpass any attractive interactions and *van der Waal* forces in the system. However, oxidized MFCs can aid in reducing the strength of these electrostatic repulsive forces by forming H-bonds with alginate molecules as well by interacting with Ca^{2+} using their $-COO^-$ groups (N. Lin et al., 2012). Therefore, reduction in the drug release was observed upon increasing the concentration of oxidized MFC. As previously discussed, carboxylate groups of alginate molecules will be deprotonated in pH 7.4 simulated intestinal fluid. Hence, anionic alginate molecules formed strong repulsive forces among themselves and also with anionic part of ionic liquid, $C_8SO_4^-$. The release of vitamin E at pH 7.4 was enhanced due to the anionic nature of ionic liquid (Thakkar et al., 2016).

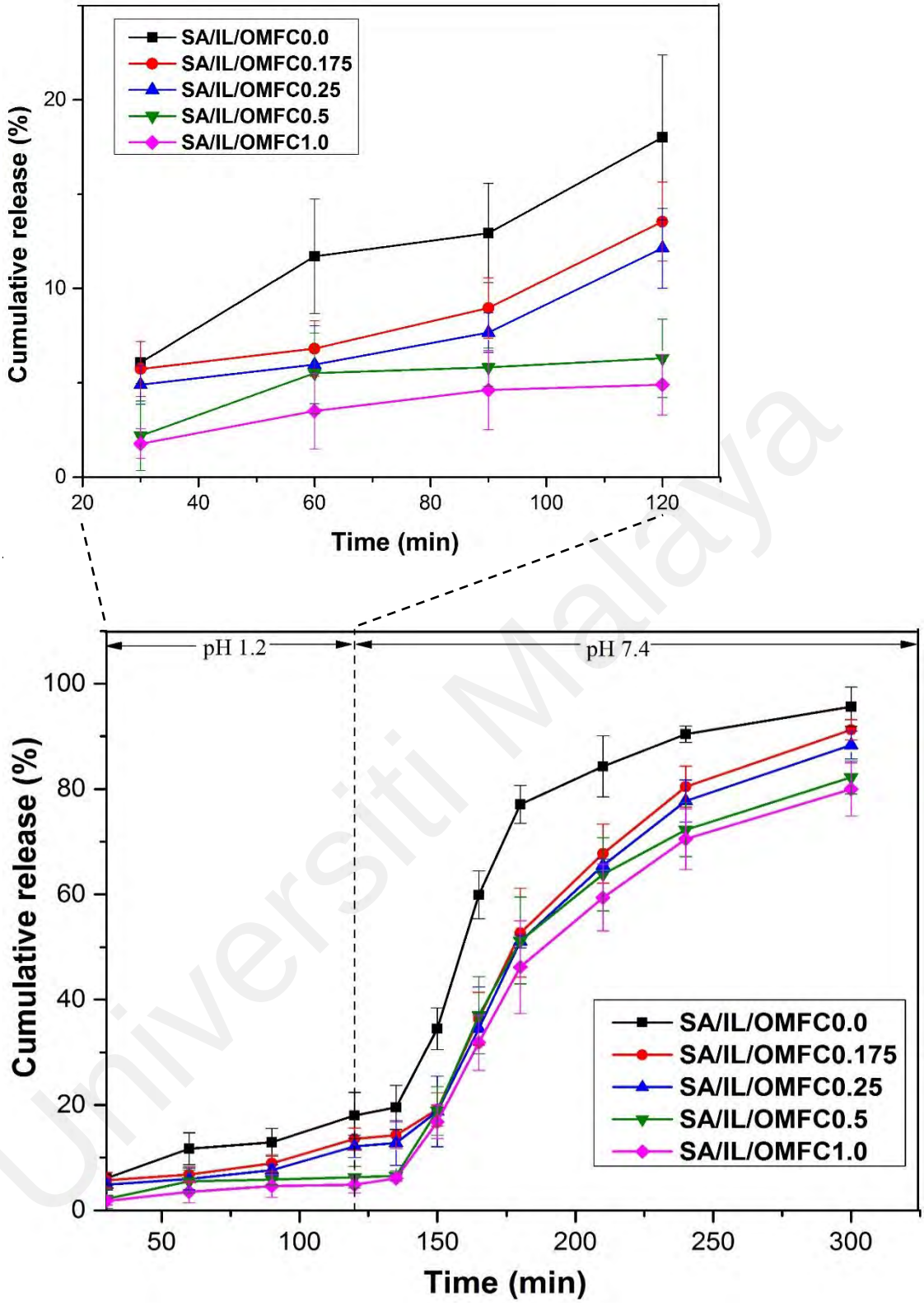

Figure 4.35: Cumulative release of vitamin E from SA/IL/OMFC0.0, SA/IL/OMFC0.175, SA/IL/OMFC0.25, SA/IL/OMFC0.5 and SA/IL/OMFC1.0 microbeads at pH 1.2 HCl and pH 7.4 PBS at predetermined time.

In the development of drug delivery system, we aim to improve patient compliance in which the alginate microbeads produced are pH responsive. The release of vitamin E is responsive to pH change in controlled manner over prolonged period of time. Thus, patient compliance can be enhanced as frequent administration of vitamin E is not required. All the formulations displayed similar pattern in which slow release of vitamin E was observed at pH 1.2 simulated gastric fluid followed by rapid release at pH 7.4 simulated intestinal fluid. However, the swelling of microbeads were retarded by the addition of oxidized MFCs, leading to slow release of vitamin E as MFCs involved in the construction of gel matrix.

4.8.3 Release kinetics mechanisms of microbeads

The release kinetics and mechanisms of vitamin E from alginate-based microbeads were analyzed by fitting the experimental *in vitro* release data to various mathematical models namely the zero order, first order, Higuchi, and Ritger–Peppas models. It gives us ideas on the underlying mechanisms of drug release across the alginate microbeads. This is crucial to predict the way the therapeutic agents will be releasing at the absorption site (Patel et al., 2016). The data was interpreted based on the value of the correlation coefficients (R^2), which obtained from the regression analysis of the plots (Patel et al., 2016). Since all of the tested kinetic models are only valid for the first 60% of the drug release (Unagolla & Jayasuriya, 2018), the values of R^2 were determined by fitting only the initial 60% of *in vitro* release data into each model and the results are presented in Table 4.4 & 4.5.

Table 4.4: Release kinetics of vitamin E from Ca-crosslinked alginate-based microbeads at pH 1.2 buffer solution.

Formulation code	Zero order R^2	First order R^2	Higuchi R^2	Ritger-Peppas	
				R^2	n
SA/TB/OMFC0.0	0.9936	0.9921	0.7563	0.9985	1.1503
SA/TB/OMFC0.175	0.9956	0.9958	0.8117	0.9983	0.9337
SA/TB/OMFC0.25	0.9710	0.9717	0.8628	0.9938	0.8940
SA/TB/OMFC0.5	0.9604	0.9614	0.8700	0.9911	0.8828
SA/TB/OMFC1.0	0.9704	0.9712	0.8630	0.9954	0.8875
SA/TB/TMSC0.175	0.9608	0.9633	0.8632	0.9918	0.7756
SA/TB/TMSC0.25	0.9749	0.9793	0.8689	0.9994	0.8318
SA/TB/TMSC0.5	0.9985	0.9984	0.7961	0.9981	1.0226
SA/TB/TMSC1.0	0.9751	0.9807	0.8646	0.9971	0.8763
SA/IL/OMFC0.0	0.8728	0.9059	0.8800	0.9645	0.7444
SA/IL/OMFC0.175	0.8079	0.8356	0.8072	0.8598	0.5786
SA/IL/OMFC0.25	0.8252	0.8426	0.7790	0.8533	0.6020
SA/IL/OMFC0.5	0.5541	0.5735	0.8068	0.8594	0.7636
SA/IL/OMFC1.0	0.7849	0.7983	0.9004	0.9604	0.7597

Table 4.5: Release kinetics of vitamin E from Ca-crosslinked alginate-based microbeads at pH 7.4 buffer solution.

Formulation code	Zero order R^2	First order R^2	Higuchi R^2	Ritger-Peppas	
				R^2	N
SA/TB/OMFC0.0	0.9964	0.9532	0.7692	0.9994	1.0808
SA/TB/OMFC0.175	0.9476	0.8862	0.6625	0.9991	1.3727
SA/TB/OMFC0.25	0.9079	0.8591	0.6063	0.9866	1.9093
SA/TB/OMFC0.5	0.9325	0.8864	0.6426	0.9871	1.7117
SA/TB/OMFC1.0	0.9381	0.8965	0.6572	0.9853	1.6209
SA/TB/TMSC0.175	0.9958	0.9565	0.7680	0.9988	1.0689
SA/TB/TMSC0.25	0.9973	0.9421	0.7499	0.9978	1.0828
SA/TB/TMSC0.5	0.9508	0.9841	0.8390	0.9852	0.9737
SA/TB/TMSC1.0	0.9672	0.9702	0.7871	0.9832	1.1378
SA/IL/OMFC0.0	0.9748	0.8933	0.7295	0.9797	0.9976
SA/IL/OMFC0.175	0.9507	0.8927	0.7056	0.9199	0.9484
SA/IL/OMFC0.25	0.9558	0.8945	0.7010	0.9454	0.9990
SA/IL/OMFC0.5	0.9422	0.8903	0.6554	0.9975	1.5084
SA/IL/OMFC1.0	0.9658	0.9496	0.7419	0.9810	1.3169

The release mechanism of alginate-based microbeads was determined by Ritger–Peppas model, in which the mode of release was reflected by the diffusional exponent, n. According to Ritger and Peppas (1987), $n = 0.43$ indicates that the drug release system exhibits Fickian diffusion that is diffusion-controlled drug release. The value $0.43 < n < 0.85$ implies that the system is governed by anomalous transport, or drug release that controlled by both diffusion and erosion. When the value $n = 0.85$, it revealed the release system follows case II transport whereby the polymer relaxation responsible for the release of drug. Lastly, $n > 1$ has been regarded as super case II transport also known as erosion-controlled release (Paarakh et al., 2018). Super Case II transport can be the result of plasticization process occurs within the gel matrix, in which minimization of the attractive forces among polymeric chains leads to the increased in the mobility of

macromolecules (Ritger & Peppas, 1987). Relaxation of polymer chains is the drive force for the diffusion process of drugs (Llabot et al., 2004).

The release mechanisms were evaluated at two distinct conditions, which are simulated gastric pH condition (pH 1.2) and simulated intestinal pH condition (pH 7.4). The experimental release data of microbeads at pH 1.2 simulated gastric condition for the formulations SA/TB/OMFC and SA/TB/TMSC at various concentration of cellulose particles were fitted well into Ritger-Peppas model ($R^2 > 0.99$), having n values in the range from 0.78 to 1.15. All these delivery systems follow super case II transport with n values > 0.85. However, the exceptions were observed for samples SA/TB/TMSC0.175 and SA/TB/TMSC0.25, that having n value of 0.78 and 0.83, respectively. This implies the systems followed anomalous transport. After transferring the microbeads to pH 7.4 buffer solution, n > 0.85 was obtained for all the systems and this confirmed the release mechanisms of all the systems were governed by super case II transport. For SA/IL/OMFC systems with varying proportion of APS-oxidized MFCs, the mode of release at pH 1.2 was characterized by anomalous transport with the n values ranging from 0.58 to 0.76. However, the release mechanisms followed super case II transport after transferring to pH 7.4 as reflected by the n values > 0.85 for all the SA/IL/OMFC samples. Hence, release mechanisms of vitamin E are depend on the physicochemical characteristics of the microbeads and the pH condition.

The release kinetics of the samples were evaluated using Ritger-Peppas, zero order, first order and Higuchi models. The goodness of fit for various models is arranged in descending order: Ritger-Peppas > zero-order > first-order > Higuchi. A drug system (or dosage forms) exhibits zero-order release kinetics when it releases the drug in a constantly manner over a period of time (Patel et al., 2016). Moreover, dosage forms that swell and experience slow erosion had been showed to follow first-order release kinetics. Higuchi's

equation was originally introduced to describe drug release manner from thin films. Derivation of Higuchi's equation was based on the assumptions that the drugs are homogenously distributed within the matrix, in which the matrix does not undergo swelling during the drug release (Patel et al., 2016). With this reason, Higuchi model is not applicable to swellable drug delivery systems theoretically. However, this model has been widely used to evaluate the release kinetics of various drug loading systems due to the extreme simplicity of the model (Basak et al., 2008; Carbinatto et al., 2014; G. Yan et al., 2017). The drug release from all the evaluated beads did not conform to Higuchi's equation as shown in Table 4.4 and 4.5.

4.8.4 Drug activity

The interactions between drugs and polymer matrix which might result in the change of chemical structure of drugs could be one of the major problems in the fabrication of drug delivery vehicle. It is vital to ensure that the drug profile remained unchanged before and after the encapsulation into the carrier (Bashir et al., 2016). Therefore, the activity of vitamin E before loading and after released in the dissolution medium (pH 7.4 PBS) was monitored using HPLC. The chromatographic profile of pure vitamin E and in the simulated intestinal medium were recorded and displayed in Figure 4.36. It was observed that there was no significant difference in the chromatography of vitamin E before and after encapsulation. The result indicates that the chemical composition of vitamin E was not affected after entrapment into the alginate matrix. In addition, ^{1}H NMR test was also carried out to confirm the chemical structure of tocotrienol-rich fraction before and after the encapsulation. The atom numbering system used in this study for the NMR assignment of α-tocotrienols was shown in Figure 4.37. The proton assignments of α-tocotrienols in NMR spectra were indicated in Table 4.6. ^{1}H NMR spectra (Figure 4.38) provided information that the vitamin E retained its chemical structure after encapsulation into alginate-based microbeads.

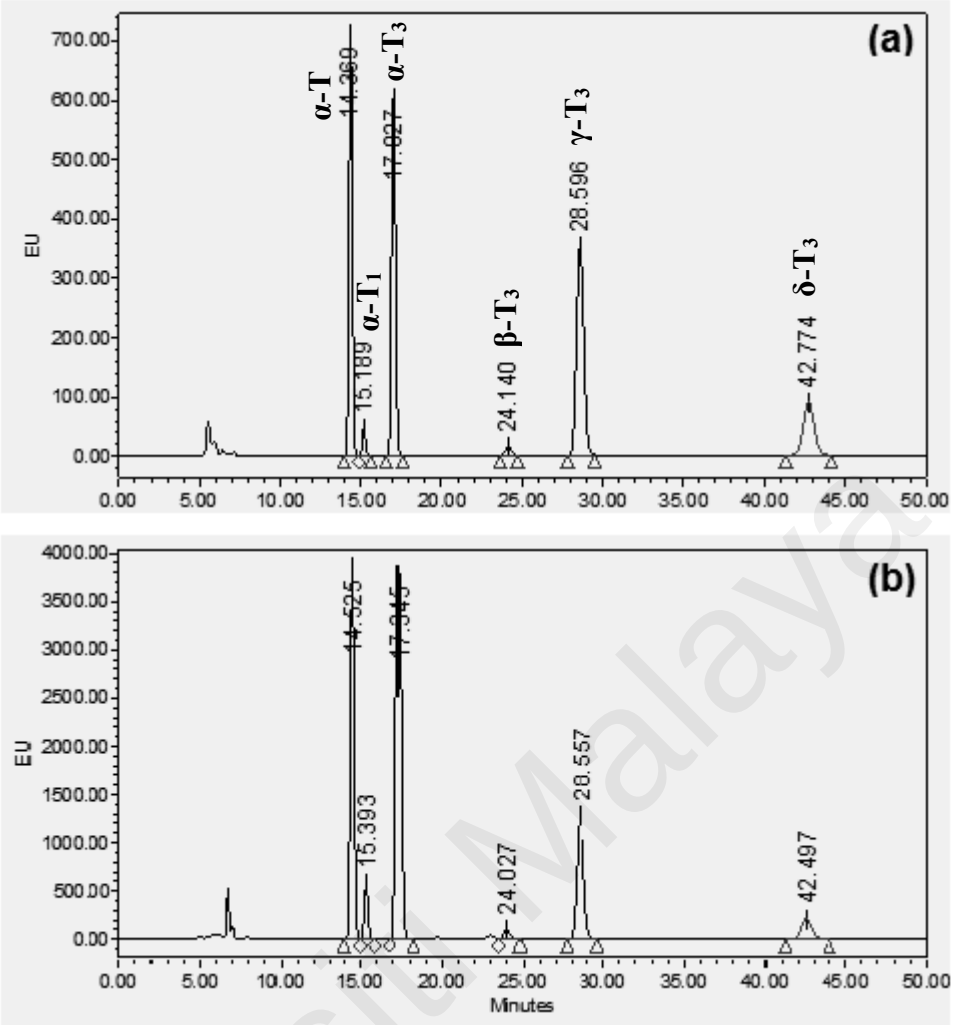

Figure 4.36: Chromatographic profile of (a) pure vitamin E and (b) encapsulated vitamin E that released in the PBS buffer. (α-T: α-tocopherol; α-T_1: α-tocomonoenol; α-T_3: α-tocotrienol; β-T_3: β-tocotrienol; γ-T3: γ-tocotrienol and δ-T_3: δ-tocotrienol).

FTIR spectra of vitamin E-loaded microbeads (Figure 4.27) obtained also provide a supplementary evidence whereby the characteristic peaks of vitamin E were not shifted significantly. Unchanged vitamin E profile after its entrapment within alginate matrix is essential to maintain its nutritional functions. Hence, immobilization of vitamin E into MFC-reinforced alginate microbeads was identified to be a favorable approach.

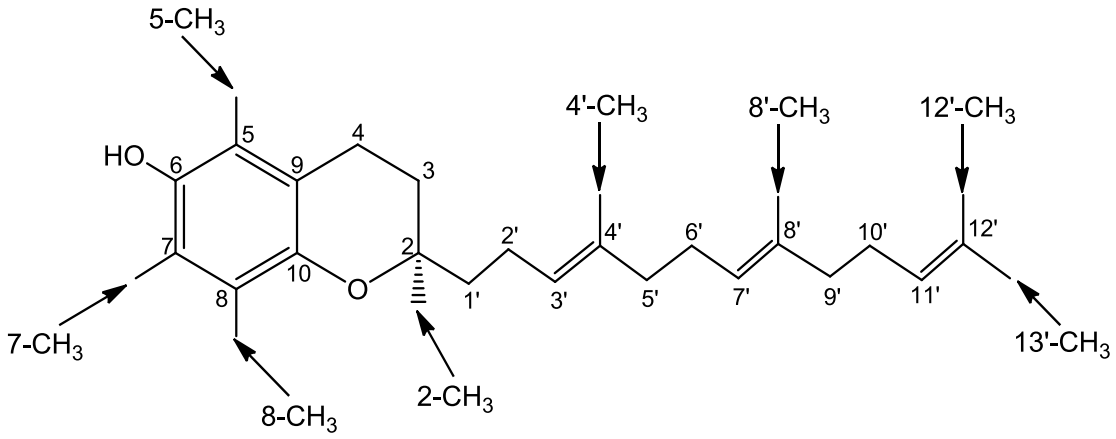

Figure 4.37: Atom numbering system employed in this work for the α-tocotrienols.

Table 4.6: ^{1}H NMR spectral data of vitamin E

Proton	α-T_3
3′, 7′, 11′-CH	5.13, 5.13, 5.10
6-OH	4.23
4-CH_2	2.61
5-CH_3	2.11
7-CH_3	2.15
8-CH_3	2.13
1′, 2′, 5′, 6′, 9′, 10′-CH_2	1.55 – 2.10
3-CH_3	–
13′-CH_3	1.68
4′-CH_3, 8′-CH_3, 12′-CH_3	1.60, 1.60, 1.58
2-CH_3	1.25

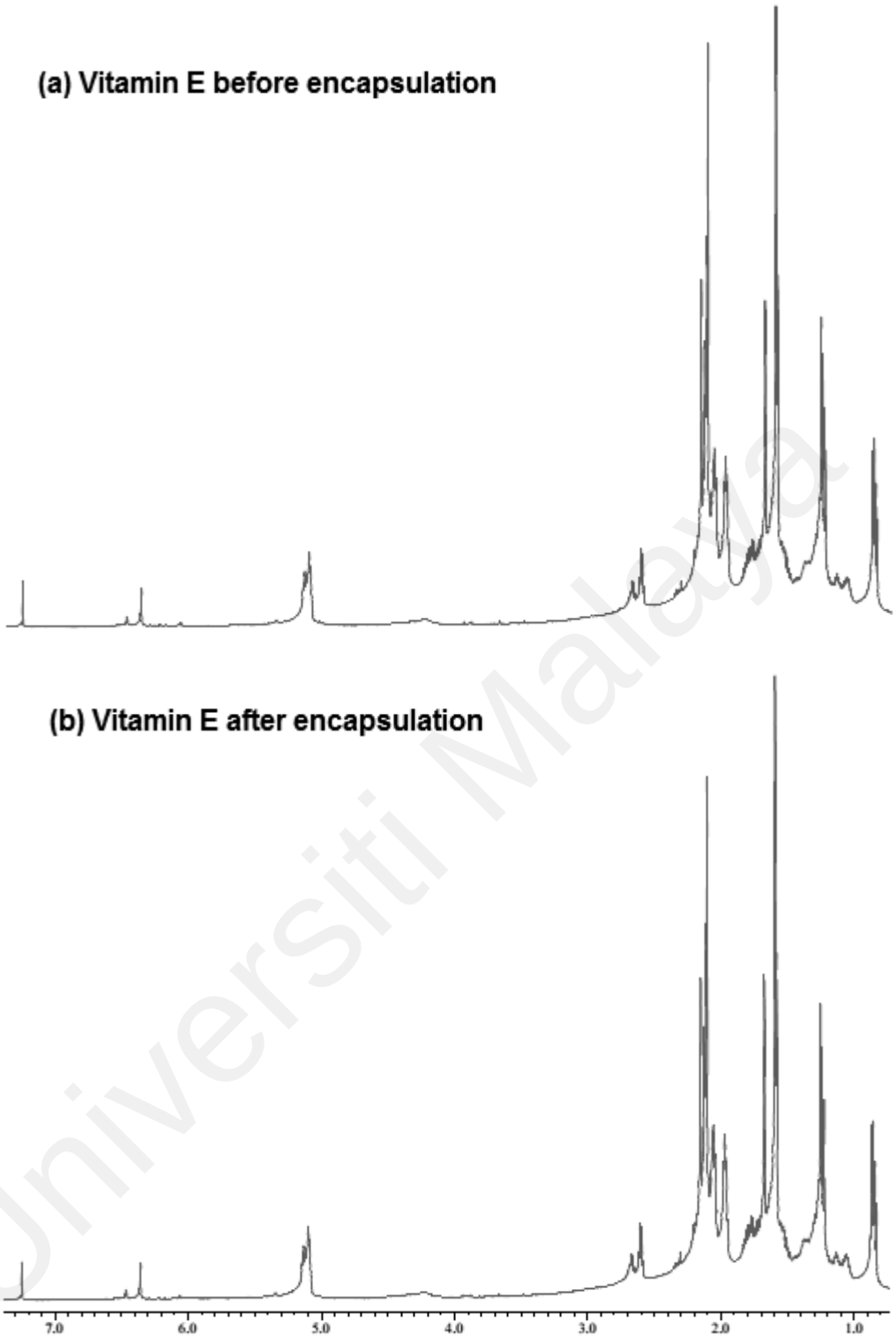

Figure 4.38: ^{1}H NMR spectra of (a) vitamin E before encapsulated and (b) after encapsulated into alginate matrix.

CHAPTER 5: CONCLUSIONS AND RECOMMENDATIONS FOR FUTURE WORK

5.1 Conclusions

With the rise in the demand for the protection of lipophilic therapeutic substances to be taken orally, there is a need for the developments of sophisticated and patient-friendly delivery systems for successful administration. Alginate is a versatile material with intriguing properties such as its biocompatibility and sol-gel transition behavior that allows bioactive materials to be loaded into the gel form and can then be administrated orally. Celluloses are well-known for their excellent mechanical strength, which incorporated into the alginate microbeads as reinforcements.

First, microfibrillated celluloses that exhibited long and network-like structures with an average diameter of 23 nm were individualized from oil palm empty fruit bunches via ammonium persulfate oxidation. APS-derived MFCs are hydrophilic in nature due to the presence of the carboxyl groups, evidenced from the appearance of a characteristic peak at 1735 cm^{-1} in the FTIR spectrum. In addition, we also prepared hydrophobic trimethylsilyl celluloses via silylation using trimethylchlorosilane as a silylating agent. Cellulose nanoparticles with distinct natures were utilized as bio-based nanofillers and their reinforcing effects on the emulsion properties as well as on the performance of microbeads were investigated.

SA/TB/OMFC based secondary O/W emulsions showed the smallest droplet sizes followed by SA/TB/TMSC based emulsions and SA/IL/OMFC based emulsions. The mean droplet diameters of SA/IL/OMFC based secondary emulsions were in micron range, whereas SA/TB/OMFC and SA/TB/TMSC based emulsions were in nanometer scale. Regardless the type of the surface-active agent utilized in the emulsion production, the average droplet diameters of all the evaluated systems increased with the increasing

of cellulose concentration. In addition, APS-treated MFCs tend to increase the viscosities of SA/TB/OMFC and SA/IL/OMFC based secondary emulsions by forming hydrogen bonds with alginate molecules as well as with water molecules in the systems. However, modified TMSCs reduced the viscosities of SA/TB/TMSC systems due to their hydrophobicity.

When sufficient amount of APS-oxidized MFCs (≥ 0.175 % w/v) or TMSCs (≥ 0.1 % w/v) incorporated into Tween 80:Brij 35-stabilized secondary O/W emulsions, the rheological behavior of the emulsions changed from liquid-like to viscoelastic nature. The prominent rheological behavior of SA/TB/TMSC based secondary O/W emulsions was ascribed to the hydrophobicity of TMSCs that allowed them to involve in the emulsion stabilization by anchoring to the freshly formed oil-water interfaces. Conversely, all the studied SA/IL/OMFC based secondary emulsions showed liquid-like behavior and the rheological characteristics were not significantly improved by the presence of oxidized MFCs.

After the prepared vitamin E-loaded emulsions were immobilized into Ca-mediated microbeads via ionotropic gelation. Syneresis of microbeads was examined at both room temperature (21 ºC) and refrigerated condition (4 ºC) by observing the weight loss of microbeads due to the exudation of water. APS-oxidized MFCs reduced the syneresis degree of SA/TB/OMFC based microbeads by forming hydrogen bonds with the water molecules in the systems. However, the incorporation of hydrophobic TMSCs into the systems enhanced the syneresis process due to the repulsions created with the water molecules. Since the ionic liquid can be easily regenerated in the water, it can be exuded from the matrix during the gelation that resulted in the higher weight loss in SA/IL/OMFC based microbeads. Besides, syneresis degree of all the microbeads enhanced in

refrigerated condition (4 ºC), which might be ascribed to the reorganization of the structure.

The emulsion properties were observed to give a big impact on the mechanical strength and the encapsulation efficiency of the resultant microbeads. Mechanical strengths of SA/TB/TMSC based microbeads at various concentrations of TMSCs were anticipated to be higher as compared to SA/TB/OMFC and SA/IL/OMFC due to the outstanding G′ and G″ of their emulsion formulations. However, compressive test results showed that the mechanical strengths of SA/TB/OMFC based microbeads at corresponding cellulose contents were higher than SA/TB/TMSC based microbeads with the highest compressive stress of 58.8 kPa for SA/TB/OMFC0.25. It can be explained by the participation of oxidized MFCs in the formation of three-dimensional networks of microbeads whereby the carboxyl group of oxidized MFCs crosslinked with the divalent ions. This was supported by the encapsulation efficiency results in which SA/TB/OMFC0.25 also demonstrated the highest encapsulation efficiency % of 98.76 ± 0.02%. In the contrary, SA/IL/OMFC based microbeads loading emulsions manifested typical viscous behavior, exhibiting low mechanical strength with considerably low encapsulation efficiency %.

In addition, *in vitro* investigations of vitamin-laden microbeads were conducted in both simulated gastric pH condition (pH 1.2 buffer solution) and simulated intestinal pH condition (pH 7.4 dissolution medium). The results showed that vitamin E was completely protected from acidic condition in stomach by cellulose-reinforced microbeads. However, vitamin E prone to release from the beads in intestinal medium and this allowed for absorption of the therapeutic agent. *In vitro* drug release data of all the evaluated microbeads showed good fitting to Ritger-Peppas model. Hence, the results of the present study highlighted the potential of alginate in synergy with APS-oxidized MFCs as a delivery system for vitamin E with enhanced mechanical strength, higher

encapsulation efficiency and tailored release rate. In this study, we observed that SA/TB/OMFC0.25 was the most optimum formulation for the encapsulation of palm-based vitamin E.

5.2 Future prospective

In the current studies, vitamin E was employed as a model lipophilic substance and several aspects have been considered to assess the performance of alginate-based drug carrier for loading vitamin E. Alginate microbeads with the optimum formulation showed outstanding mechanical strength and high encapsulation efficiency (98.8%) with sustained released of vitamin E. The formulated cellulose-reinforced alginate microbeads can be proposed to encapsulate other lipophilic bioactive materials such as antioxidants, flavors and perfumes. Nevertheless, it is important to translate successful results from the laboratory into clinical application. Therefore, clinical studies are suggested in future works to correlate the physicochemical properties of alginate microbeads with clinical outcomes in the application as food supplement.

Due to the presence of the free carboxyl groups, alginate molecules possess good mucoadhesive property by interacting with mucosal tissues via hydrogen bonds and electrostatic attractions. However, alginate showed mucoadhesive character solely in slightly alkaline physiological fluids condition because only ionized carboxyl groups are able to bind with mucins. Owing to this reason, the mucoadhesive property of alginate is desirable to extend the vitamin E residence time at the adsorption site and to prolong the release of therapeutic agents from drug carrier. Hence, mucoadhesive property of alginate can be investigated in future to examine its effects on the *in vitro* retention release of microbeads.

Apart from microbeads, these composite materials could be formulated into other solid dosage forms such as films, tablets, capsules, softgels as sustained/controlled drug

delivery systems. Furthermore, these cellulose-reinforced alginate microbeads encapsulating vitamin E could potentially develop into cosmetic products such as hand creams, facial creams and body lotions because vitamin E functions as a natural anti-aging nutrient (Shalaka et al., 2009). It could open new opportunities in cosmetics industry, thus, detailed investigations must be conducted to evaluate their application in cosmetic field.

Since the incorporation of cellulose nanoparticles that extracted from oil palm empty fruit bunches as reinforcements were observed to enhance the mechanical strength and the performance of the alginate microbeads as vitamin E carrier. Future research should be carried out to incorporate cellulose nanoparticles that isolated from other natural resources into alginate microbeads and the composites should be evaluated for their mechanical stability, encapsulation efficiency and *in vitro* release profile. Cellulose nanoparticles can be individualized from kenaf, banana, pineapple, coconut and so on.

REFERENCES

Aaen, R., Brodin, F. W., Simon, S., Heggset, E. B., & Syverud, K. (2019). Oil-in-water emulsions stabilized by cellulose nanofibrils—The effects of ionic strength and pH. *Nanomaterials, 9*(2), 259.

Aarstad, O., Heggset, E. B., Pedersen, I. S., Bjørnøy, S. H., Syverud, K., & Strand, B. L. (2017). Mechanical properties of composite hydrogels of alginate and cellulose nanofibrils. *Polymers, 9*(8), 378.

Abdullah, N., & Sulaiman, F. (2013). The oil palm wastes in Malaysia. *Biomass Now-Sustainable Growth and Use, 1*(3), 75-93.

Aben, S., Holtze, C., Tadros, T., & Schurtenberger, P. (2012). Rheological investigations on the creaming of depletion-flocculated emulsions. *Langmuir, 28*(21), 7967-7975.

Abraham, E., Deepa, B., Pothan, L. A., Jacob, M., Thomas, S., Cvelbar, U., & Anandjiwala, R. (2011). Extraction of nanocellulose fibrils from lignocellulosic fibres: A novel approach. *Carbohydrate Polymers, 86*(4), 1468-1475.

Adams, F., Walstra, P., Brooks, B., Richmond, H., Zerfa, M., Bibette, J., Hibberd, D., Robins, M., Weers, J., & Kabalnov, A. (2007). *Modern Aspects of Emulsion Science*: Royal Society of Chemistry.

Agarwal, T., Narayana, S. N., Pal, K., Pramanik, K., Giri, S., & Banerjee, I. (2015). Calcium alginate-carboxymethyl cellulose beads for colon-targeted drug delivery. *International Journal of Biological Macromolecules, 75*, 409-417.

Aggarwal, B. B., Sundaram, C., Prasad, S., & Kannappan, R. (2010). Tocotrienols, the vitamin E of the 21st century: its potential against cancer and other chronic diseases. *Biochemical Pharmacology, 80*(11), 1613-1631.

Agnihotri, S. A., & Aminabhavi, T. M. (2005). Development of novel interpenetrating network gellan gum-poly(vinyl alcohol) hydrogel microspheres for the controlled release of carvedilol. *Drug Development and Industrial Pharmacy, 31*(6), 491-503.

Agüero, L., Zaldivar-Silva, D., Peña, L., & Dias, M. L. (2017). Alginate microparticles as oral colon drug delivery device: A review. *Carbohydrate Polymers, 168*, 32-43.

Ahmadi-Dastgerdi, A., Nasirpour, A., & Rahimi, E. (2015). Physical and rheological properties of oil in water heat stable emulsions made from different stabilizers. *Journal of Food Biosciences and Technology, 5*(1), 45-62.

Ahsan, H., Ahad, A., Iqbal, J., & Siddiqui, W. A. (2014). Pharmacological potential of tocotrienols: a review. *Nutrition & Metabolism, 11*(1), 1-22.

Al-Kahtani, A. A., & Sherigara, B. S. (2014). Controlled release of diclofenac sodium through acrylamide grafted hydroxyethyl cellulose and sodium alginate. *Carbohydrate Polymers, 104*, 151-157.

Alemdar, A., & Sain, M. (2008). Isolation and characterization of nanofibers from agricultural residues: wheat straw and soy hulls. *Bioresource Technology, 99*(6), 1664-1671.

Amin, S., Rajabnezhad, S., & Kohli, K. (2009). Hydrogels as potential drug delivery systems. *Scientific Research and Essays, 4*(11), 1175-1183.

An, H. Z., Helgeson, M. E., & Doyle, P. S. (2012). Nanoemulsion composite microgels for orthogonal encapsulation and release. *Advanced Materials, 24*(28), 3838-3844.

Anghel, N., Dinu, V. M., Verestiuc, L., & Spiridon, I. A. (2021). Transcutaneous drug delivery systems based on collagen/polyurethane composites reinforced with cellulose. *Polymers, 13*(11), 1845.

Angkuratipakorn, T., Sriprai, A., Tantrawong, S., Chaiyasit, W., & Singkhonrat, J. (2017). Fabrication and characterization of rice bran oil-in-water Pickering emulsion stabilized by cellulose nanocrystals. *Colloids and Surfaces A: Physicochemical and Engineering Aspects, 522*, 310-319.

Atsuki, K., & Tomoda, Y. (1926). Studies on seaweeds of Japan I. The chemical constituents of Laminaria. *The Journal of the Society of Chemical Industry, Japan, 29*, 509-517.

Augst, A. D., Kong, H. J., & Mooney, D. J. (2006). Alginate hydrogels as biomaterials. *Macromolecular Bioscience, 6*(8), 623-633.

Aulin, C., Ahola, S., Josefsson, P., Nishino, T., Hirose, Y., sterberg, M., & W gberg, L. (2009). Nanoscale cellulose films with different crystallinities and mesostructures: their surface properties and interaction with water. *Langmuir, 25*(13), 7675-7685.

Azizi Samir, M. A. S., Alloin, F., & Dufresne, A. (2005). Review of recent research into cellulosic whiskers, their properties and their application in nanocomposite field. *Biomacromolecules, 6*(2), 612-626.

Bacelar, A. H., Cengiz, I. F., Silva-Correia, J., Sousa, R. A., Oliveira, J. M., & Reis, R. L. (2017). "Smart" hydrogels in tissue engineering and regenerative medicine applications *Handbook of Intelligent Scaffolds for Tissue Engineering and Regenerative Medicine* (pp. 333-367): Jenny Stanford.

Badwaik, H. R., Kumari, L., Nakhate, K., Verma, V. S., & Sakure, K. (2019). Phytoconstituent plumbagin: Chemical, biotechnological and pharmaceutical aspects. *Studies in Natural Products Chemistry* (Vol. 63, pp. 415-460): Elsevier.

Bajpai, P. (2018). *Biermann's Handbook of Pulp and Paper: Volume 1: Raw Material and Pulp Making*: Elsevier.

Bajpai, S. K., & Sharma, S. (2004). Investigation of swelling/degradation behaviour of alginate beads crosslinked with Ca^{2+} and Ba^{2+} ions. *Reactive and Functional Polymers, 59*(2), 129-140.

Bakar, N. A., Chee, C. Y., Abdullah, L. C., Ratnam, C. T., & Ibrahim, N. A. (2015). Thermal and dynamic mechanical properties of grafted kenaf filled poly (vinyl chloride)/ethylene vinyl acetate composites. *Materials & Design (1980-2015), 65*, 204-211.

Baloch, M. K., & Hameed, G. (2005). Emulsification of oil in water as affected by different parameters. *Journal of Colloid and Interface Science, 285*(2), 804-813.

Barhoumi, Z., Saini, M., Amdouni, N., & Pal, A. (2016). Interaction between amphiphilic ionic liquid 1-butyl-3-methylimidazolium octyl sulfate and anionic polymer of sodium polystyrene sulfonate in aqueous medium. *Chemical Physics Letters, 661*, 173-178.

Basak, S. C., Kumar, K. S., & Ramalingam, M. (2008). Design and release characteristics of sustained release tablet containing metformin HCl. *Revista Brasileira de Ciências Farmacêuticas, 44*(3), 477-483.

Bashir, S., Teo, Y. Y., Ramesh, S., & Ramesh, K. (2016). Synthesis, characterization, properties of N-succinyl chitosan-g-poly (methacrylic acid) hydrogels and in vitro release of theophylline. *Polymer, 92*, 36-49.

Belscak-Cvitanovic, A., Komes, D., Karlovic, S., Djakovic, S., Spoljaric, I., Mrsic, G., & Jezek, D. (2015). Improving the controlled delivery formulations of caffeine in alginate hydrogel beads combined with pectin, carrageenan, chitosan and psyllium. *Food Chemistry, 167*, 378-386.

Benavides, S., Cortés, P., Parada, J., & Franco, W. (2016). Development of alginate microspheres containing thyme essential oil using ionic gelation. *Food Chemistry, 204*, 77-83.

Benhamou, K., Dufresne, A., Magnin, A., Mortha, G., & Kaddami, H. (2014). Control of size and viscoelastic properties of nanofibrillated cellulose from palm tree by varying the TEMPO-mediated oxidation time. *Carbohydrate Polymers, 99*, 74-83.

Besbes, I., Vilar, M. R., & Boufi, S. (2011). Nanofibrillated cellulose from Alfa, Eucalyptus and Pine fibres: Preparation, characteristics and reinforcing potential. *Carbohydrate Polymers, 86*(3), 1198-1206.

Bhowmik, D., Harish, G., Duraivel, S., Kumar, B. P., Raghuvanshi, V., & Kumar, K. S. (2013). Solid dispersion-A Approach to enhance the dissolution rate of poorly water soluble drugs. *The Pharma Innovation, 1*(12, Part A), 24.

Binks, B. P., Desforges, A., & Duff, D. G. (2007). Synergistic stabilization of emulsions by a mixture of surface-active nanoparticles and surfactant. *Langmuir, 23*(3), 1098-1106.

Binks, B. P., Rodrigues, J. A., & Frith, W. J. (2007). Synergistic interaction in emulsions stabilized by a mixture of silica nanoparticles and cationic surfactant. *Langmuir, 23*(7), 3626-3636.

Braccini, I., & Pérez, S. (2001). Molecular basis of Ca^{2+}-induced gelation in alginates and pectins: the egg-box model revisited. *Biomacromolecules, 2*(4), 1089-1096.

Branen, A. L., Davidson, P. M., Salminen, S., & Thorngate, J. (2001). *Food additives*: CRC Press.

Brennecke, J. F., & Maginn, E. J. (2001). Ionic liquids: innovative fluids for chemical processing. *AIChE Journal, 47*(11), 2384-2389.

Brunier, B. l. m., Sheibat-Othman, N., Chniguir, M., Chevalier, Y., & Bourgeat-Lami, E. (2016). Investigation of four different Laponite clays as stabilizers in Pickering emulsion polymerization. *Langmuir, 32*(24), 6046-6057.

Çalış, S., Atar, K. ., Arslan, F. B., Eroğlu, H., & Çapan, Y. (2019). Nanopharmaceuticals as drug-delivery systems: for, against, and current applications *Nanocarriers for Drug Delivery* (pp. 133-154): Elsevier.

Callari, M., De Souza, P. L., Rawal, A., & Stenzel, M. H. (2017). The effect of drug loading on micelle properties: solid-state NMR as a tool to gain structural insight. *Angewandte Chemie International Edition, 56*(29), 8441-8445.

Caló, E., & Khutoryanskiy, V. V. (2015). Biomedical applications of hydrogels: A review of patents and commercial products. *European Polymer Journal, 65*, 252-267.

Canselier, J. P., Delmas, H., Wilhelm, A. M., & Abismaïl, B. (2002). Ultrasound Emulsification—An Overview. *Journal of Dispersion Science and Technology, 23*(1-3), 333-349.

Capron, I., & Cathala, B. (2013). Surfactant-free high internal phase emulsions stabilized by cellulose nanocrystals. *Biomacromolecules, 14*(2), 291-296.

Carbinatto, F. M., de Castro, A. D., Evangelista, R. C., & Cury, B. S. (2014). Insights into the swelling process and drug release mechanisms from cross-linked pectin/high amylose starch matrices. *Asian Journal of Pharmaceutical Sciences, 9*(1), 27-34.

Carneiro, H. C., Tonon, R. V., Grosso, C. R., & Hubinger, M. D. (2013). Encapsulation efficiency and oxidative stability of flaxseed oil microencapsulated by spray drying using different combinations of wall materials. *Journal of Food Engineering, 115*(4), 443-451.

Castro-Guerrero, C. F., & Gray, D. G. (2014). Chiral nematic phase formation by aqueous suspensions of cellulose nanocrystals prepared by oxidation with ammonium persulfate. *Cellulose, 21*(4), 2567-2577.

Cauchetier, E., Deniau, M., Fessi, H., Astier, A., & Paul, M. (2003). Atovaquone-loaded nanocapsules: influence of the nature of the polymer on their in vitro characteristics. *International Journal of Pharmaceutics, 250*(1), 273-281.

Chaemsawang, W., Prasongchean, W., Papadopoulos, K. I., Sukrong, S., Kao, W. J., & Wattanaarsakit, P. (2018). Emulsion cross-linking technique for human fibroblast encapsulation. *International Journal of Biomaterials, 2018*.

Chami Khazraji, A., & Robert, S. (2013). Interaction effects between cellulose and water in nanocrystalline and amorphous regions: A novel approach using molecular modeling. *Journal of Nanomaterials, 2013*, 1-10.

Chandler, D. (2005). Interfaces and the driving force of hydrophobic assembly. *Nature, 437*(7059), 640-647.

Chang, C., Duan, B., & Zhang, L. (2009). Fabrication and characterization of novel macroporous cellulose–alginate hydrogels. *Polymer, 50*(23), 5467-5473.

Chaterji, S., Kwon, I. K., & Park, K. (2007). Smart polymeric gels: redefining the limits of biomedical devices. *Progress in Polymer Science, 32*(8), 1083-1122.

Chee, C. Y., Yong, G. K., Abdullah, L. C., & Nadarajah, K. (2013). Effect of nanosilica and titania on thermal stability of polypropylene/oil palm empty fruit fibre composite. *Journal of Biobased Materials and Bioenergy, 7*(1), 169-174.

Chen, W., Liu, X., Liu, Y., Bang, Y., & Kim, H.-I. (2011). Preparation of O/W Pickering emulsion with oxygen plasma treated carbon nanotubes as surfactants. *Journal of Industrial and Engineering Chemistry, 17*(3), 455-460.

Chen, W., Yu, H., & Liu, Y. (2011). Preparation of millimeter-long cellulose I nanofibers with diameters of 30–80nm from bamboo fibers. *Carbohydrate Polymers, 86*(2), 453-461.

Chen, W., Yu, H., Liu, Y., Chen, P., Zhang, M., & Hai, Y. (2011). Individualization of cellulose nanofibers from wood using high-intensity ultrasonication combined with chemical pretreatments. *Carbohydrate Polymers, 83*(4), 1804-1811.

Cheng, Q., Wang, S., Rials, T. G., & Lee, S.-H. (2007). Physical and mechanical properties of polyvinyl alcohol and polypropylene composite materials reinforced with fibril aggregates isolated from regenerated cellulose fibers. *Cellulose, 14*(6), 593-602.

Cheng, Y., Lu, L., Zhang, W., Shi, J., & Cao, Y. (2012). Reinforced low density alginate-based aerogels: Preparation, hydrophobic modification and characterization. *Carbohydrate Polymers, 88*(3), 1093-1099.

Cherian, B. M., Leão, A. L., de Souza, S. F., Costa, L. M. M., de Olyveira, G. M., Kottaisamy, M., Nagarajan, E. R., & Thomas, S. (2011). Cellulose nanocomposites with nanofibres isolated from pineapple leaf fibers for medical applications. *Carbohydrate Polymers, 86*(4), 1790-1798.

Cherian, B. M., Leão, A. L., de Souza, S. F., Thomas, S., Pothan, L. A., & Kottaisamy, M. (2010). Isolation of nanocellulose from pineapple leaf fibres by steam explosion. *Carbohydrate Polymers, 81*(3), 720-725.

Cherian, B. M., Pothan, L. A., Nguyen-Chung, T., Mennig, G. n., Kottaisamy, M., & Thomas, S. (2008). A novel method for the synthesis of cellulose nanofibril whiskers from banana fibers and characterization. *Journal of Agricultural and Food Chemistry, 56*(14), 5617-5627.

Chevalier, Y., & Bolzinger, M.-A. (2013). Emulsions stabilized with solid nanoparticles: Pickering emulsions. *Colloids and Surfaces A: Physicochemical and Engineering Aspects, 439*, 23-34.

Ching, Y. C., Rahman, A., Ching, K. Y., Sukiman, N. L., & Cheng, H. C. (2015). Preparation and characterization of polyvinyl alcohol-based composite reinforced with nanocellulose and nanosilica. *BioResources, 10*(2), 3364-3377.

Choudhary, S., Reck, J. M., Carr, A. J., & Bhatia, S. R. (2018). Hydrophobically modified alginate for extended release of pharmaceuticals. *Polymers for Advanced Technologies, 29*(1), 198-204.

Christensen, B. (2011). Alginates as biomaterials in tissue engineering. *Carbohydrate Chemistry: Chemical and Biological Approaches, 37*, 227-258.

Chuang, J.-J., Huang, Y.-Y., Lo, S.-H., Hsu, T.-F., Huang, W.-Y., Huang, S.-L., & Lin, Y.-S. (2017). Effects of pH on the shape of alginate particles and its release behavior. *International Journal of Polymer Science, 2017*.

Coburn, J., Gibson, M., Bandalini, P. A., Laird, C., Mao, H.-Q., Moroni, L., Seliktar, D., & Elisseeff, J. (2011). Biomimetics of the extracellular matrix: an integrated three-dimensional fiber-hydrogel composite for cartilage tissue engineering. *Smart Structures and Systems, 7*(3), 213.

Colinet, I., Dulong, V., Mocanu, G., Picton, L., & Le Cerf, D. (2010). Effect of chitosan coating on the swelling and controlled release of a poorly water-soluble drug from an amphiphilic and pH-sensitive hydrogel. *International Journal of Biological Macromolecules, 47*(2), 120-125.

Costa, C., Medronho, B., Filipe, A., Mira, I., Lindman, B., Edlund, H., & Norgren, M. (2019). Emulsion formation and stabilization by biomolecules: The leading role of cellulose. *Polymers, 11*(10), 1570.

Cummins, H. Z. (2007). Liquid, glass, gel: The phases of colloidal Laponite. *Journal of Non-Crystalline Solids, 353*(41-43), 3891-3905.

Daik, R., Bidol, S., & Abdullah, I. (2007). Effect of molecular weight on the droplet size and rheological properties of liquid natural rubber emulsion. *Malaysian Polymer Journal, 2*(1), 29-38.

Dapčević Hadnađev, T., Dokić, P., Krstonošić, V., & Hadnađev, M. (2013). Influence of oil phase concentration on droplet size distribution and stability of oil-in-water emulsions. *European Journal of Lipid Science and Technology, 115*(3), 313-321.

Dave, N., & Joshi, T. (2017). A concise review on surfactants and its significance. *International Jurnal of Applied Chemistry, 13*(3), 663672.

de Vos, P., Faas, M. M., Strand, B., & Calafiore, R. (2006). Alginate-based microcapsules for immunoisolation of pancreatic islets. *Biomaterials, 27*(32), 5603-5617.

del Valle, L. J., Díaz, A., & Puiggalí, J. (2017). Hydrogels for biomedical applications: cellulose, chitosan, and protein/peptide derivatives. *Gels, 3*(3), 27.

Derkach, S. R. (2009). Rheology of emulsions. *Advances in colloid and interface science, 151*(1-2), 1-23.

Desfrançois, C., Auzély, R., & Texier, I. (2018). Lipid nanoparticles and their hydrogel composites for drug delivery: a review. *Pharmaceuticals, 11*(4), 118.

Desrumaux, A., & Marcand, J. (2002). Formation of sunflower oil emulsions stabilized by whey proteins with high-pressure homogenization (up to 350 MPa): effect of pressure on emulsion characteristics. *International Journal of Food Science & Technology, 37*(3), 263-269.

Ding, Z., Jiang, Y., & Liu, X. (2018). Nanoemulsions-based drug delivery for brain tumors. *Nanotechnology-based targeted drug delivery systems for brain tumors* (pp. 327-358): Elsevier.

Dobler, D., Schmidts, T., Klingenhöfer, I., & Runkel, F. (2013). Ionic liquids as ingredients in topical drug delivery systems. *International Journal of Pharmaceutics, 441*(1-2), 620-627.

Donati, I., & Paoletti, S. (2009). Material properties of alginates. *Alginates: Biology and applications* (pp. 1-53): Springer.

Dong, H., Strawhecker, K. E., Snyder, J. F., Orlicki, J. A., Reiner, R. S., & Rudie, A. W. (2012). Cellulose nanocrystals as a reinforcing material for electrospun poly (methyl methacrylate) fibers: Formation, properties and nanomechanical characterization. *Carbohydrate Polymers, 87*(4), 2488-2495.

Dong, X. M., Revol, J.-F., & Gray, D. G. (1998). Effect of microcrystallite preparation conditions on the formation of colloid crystals of cellulose. *Cellulose, 5*(1), 19-32.

Draget, K. I. (2009). Alginates *Handbook of Hydrocolloids (Second Edition)* (pp. 807-828): Elsevier.

Draget, K. I., Gåserød, O., Aune, I., Andersen, P. O., Storbakken, B., Stokke, B. T., & Smidsrød, O. (2001). Effects of molecular weight and elastic segment flexibility on syneresis in Ca-alginate gels. *Food Hydrocolloids, 15*(4), 485-490.

Draget, K. I., Moe, S., Skjåk-Bræk, G., Alginates Smidsrød, O., Stephen, A., Phillips, G., & Williams, P. (2006). Food polysaccharides and their applications. *CRC Press, Boca Raton*, 289-234.

Drusch, S., & Berg, S. (2008). Extractable oil in microcapsules prepared by spray-drying: Localisation, determination and impact on oxidative stability. *Food Chemistry, 109*(1), 17-24.

Edlund, U., & Albertsson, A.-C. (2003). Polyesters based on diacid monomers. *Advanced Drug Delivery Reviews, 55*(4), 585-609.

El-Say, K. M. (2016). Maximizing the encapsulation efficiency and the bioavailability of controlled-release cetirizine microspheres using Draper–Lin small composite design. *Drug Design, Development and Therapy, 10*, 825.

El-Sherbiny, I. M., Abdel-Bary, E. M., & Harding, D. R. K. (2010). Preparation andin vitroevaluation of new pH-sensitive hydrogel beads for oral delivery of protein drugs. *Journal of Applied Polymer Science, 115*(5), 2828-2837.

El-Sherbiny, I. M., Abdel-Mogib, M., Dawidar, A.-A. M., Elsayed, A., & Smyth, H. D. C. (2011). Biodegradable pH-responsive alginate-poly (lactic-co-glycolic acid) nano/micro hydrogel matrices for oral delivery of silymarin. *Carbohydrate Polymers, 83*(3), 1345-1354.

Elanthikkal, S., Gopalakrishnapanicker, U., Varghese, S., & Guthrie, J. T. (2010). Cellulose microfibres produced from banana plant wastes: Isolation and characterization. *Carbohydrate Polymers, 80*(3), 852-859.

Eral, H. B., L pez-Mejías, V., O'Mahony, M., Trout, B. L., Myerson, A. S., & Doyle, P. S. (2014). Biocompatible alginate microgel particles as heteronucleants and encapsulating vehicles for hydrophilic and hydrophobic drugs. *Crystal Growth & Design, 14*(4), 2073-2082.

Evans, H. M., & Bishop, K. S. (1922). On the existence of a hitherto unrecognized dietary factor essential for reproduction. *Science, 56*(1458), 650-651.

Fahma, F., Iwamoto, S., Hori, N., Iwata, T., & Takemura, A. (2010). Isolation, preparation, and characterization of nanofibers from oil palm empty-fruit-bunch (OPEFB). *Cellulose, 17*(5), 977-985.

Fatah, I., Khalil, H., Hossain, M., Aziz, A., Davoudpour, Y., Dungani, R., & Bhat, A. (2014). Exploration of a chemo-mechanical technique for the isolation of nanofibrillated cellulosic fiber from oil palm empty fruit bunch as a reinforcing agent in composites materials. *Polymers, 6*(10), 2611-2624.

Fathi, M., Nasrabadi, M. N., & Varshosaz, J. (2017). Characteristics of vitamin E-loaded nanofibres from dextran. *International Journal of Food Properties, 20*(11), 2665-2674.

Ferrer, A., Filpponen, I., Rodriguez, A., Laine, J., & Rojas, O. J. (2012). Valorization of residual empty palm fruit bunch fibers (EPFBF) by microfluidization: production of nanofibrillated cellulose and EPFBF nanopaper. *Bioresource Technology, 125*, 249-255.

Fischer, F., & Dörfel, H. (1955). Die polyuronsäuren der braunalgen (Kohlenhydrate der Algen I). *Hoppe-Seyler´ s Zeitschrift für physiologische Chemie, 302*(1-2), 186-203.

Fujii, S., Okada, M., & Furuzono, T. (2007). Hydroxyapatite nanoparticles as stimulus-responsive particulate emulsifiers and building block for porous materials. *Journal of Colloid and Interface Science, 315*(1), 287-296.

Fujii, S., Okada, M., Sawa, H., Furuzono, T., & Nakamura, Y. (2009). Hydroxyapatite nanoparticles as particulate emulsifier: fabrication of hydroxyapatite-coated biodegradable microspheres. *Langmuir, 25*(17), 9759-9766.

Gaikwad, S. G., & Pandit, A. B. (2008). Ultrasound emulsification: effect of ultrasonic and physicochemical properties on dispersed phase volume and droplet size. *Ultrasonics Sonochemistry, 15*(4), 554-563.

George, M., & Abraham, T. E. (2006). Polyionic hydrocolloids for the intestinal delivery of protein drugs: alginate and chitosan--a review. *Journal of Controlled Release, 114*(1), 1-14.

Gheorghita Puscaselu, R., Lobiuc, A., Dimian, M., & Covasa, M. (2020). Alginate: From food industry to biomedical applications and management of metabolic disorders. *Polymers, 12*(10), 2417.

Ghosal, K., & Ray, S. D. (2011). Alginate/hydrophobic HPMC (60M) particulate systems: New matrix for site-specific and controlled drug delivery. *Brazilian Journal of Pharmaceutical Sciences, 47*(4), 833-844.

Goh, K. Y., Ching, Y. C., Chuah, C. H., Abdullah, L. C., & Liou, N.-S. (2016). Individualization of microfibrillated celluloses from oil palm empty fruit bunch: comparative studies between acid hydrolysis and ammonium persulfate oxidation. *Cellulose, 23*(1), 379-390.

Goh, P. S., Ng, M. H., Choo, Y. M., Amru, N. B., & Chuah, C. H. (2015). Production of nanoemulsions from palm-based tocotrienol rich fraction by microfluidization. *Molecules, 20*(11), 19936-19946.

Gombotz, W. R., & Wee, S. F. (2012). Protein release from alginate matrices. *Advanced Drug Delivery Reviews, 64*, 194-205.

Gou, M., Li, X., Dai, M., Gong, C., Wang, X., Xie, Y., Deng, H., Chen, L., Zhao, X., & Qian, Z. (2008). A novel injectable local hydrophobic drug delivery system: Biodegradable nanoparticles in thermo-sensitive hydrogel. *International Journal of Pharmaceutics, 359*(1), 228-233.

GR, D. (2015). Microemulsions: platform for improvement of solubility and dissolution of poorly soluble drugs. *Asian Journal of Pharmaceutical and Clinical Research, 8*(5), 7-17.

Griffin, W. C. (1949). Classification of surface-active agents by" HLB". *Journal of the Society of Cosmetics Chemists, 1*, 311-326.

Gu, D., O'Connor, A. J., GH Qiao, G., & Ladewig, K. (2017). Hydrogels with smart systems for delivery of hydrophobic drugs. *Expert Opinion on Drug Delivery, 14*(7), 879-895.

Guillot, S., Bergaya, F., de Azevedo, C., Warmont, F., & Tranchant, J.-F. (2009). Internally structured pickering emulsions stabilized by clay mineral particles. *Journal of Colloid and Interface Science, 333*(2), 563-569.

Habibi, Y. (2014). Key advances in the chemical modification of nanocelluloses. *Chemical Society Reviews, 43*(5), 1519-1542.

Habibi, Y., Lucia, L. A., & Rojas, O. J. (2010). Cellulose nanocrystals: chemistry, self-assembly, and applications. *Chemical Reviews, 110*(6), 3479-3500.

Haniffa, M. A. C. M., Ching, Y. C., Chuah, C. H., Ching, K. Y., Nazri, N., Abdullah, L. C., & Nai-Shang, L. (2017). Effect of TEMPO-oxidization and rapid cooling on thermo-structural properties of nanocellulose. *Carbohydrate Polymers, 173*, 91-99.

Hariyadi, D. M., & Islam, N. (2020). Current status of alginate in drug delivery. *Advances in Pharmacological and Pharmaceutical Sciences, 2020*.

Hashtjin, A. M., & Abbasi, S. (2015). Optimization of ultrasonic emulsification conditions for the production of orange peel essential oil nanoemulsions. *Journal of Food Science and Technology, 52*(5), 2679-2689.

Hatanaka, J., Chikamori, H., Sato, H., Uchida, S., Debari, K., Onoue, S., & Yamada, S. (2010). Physicochemical and pharmacological characterization of alpha-tocopherol-loaded nano-emulsion system. *International Journal of Pharmaceutics, 396*(1-2), 188-193.

Haug, A., & Larsen, B. (1966). *A study on the constitution of alginic acid by partial acid hydrolysis.* Paper presented at the Proceedings of the Fifth International Seaweed Symposium, Halifax, August 25–28, 1965.

Haug, A., Larsen, B., & Smidsrød, O. (1974). Uronic acid sequence in alginate from different sources. *Carbohydrate Research, 32*(2), 217-225.

Haug, A., & Smidsrød, O. (1967). Strontium–calcium selectivity of alginates. *Nature, 215*(5102), 757.

Hermes, M., & Clegg, P. S. (2013). Yielding and flow of concentrated Pickering emulsions. *Soft Matter, 9*(31), 7568-7575.

Hoare, T. R., & Kohane, D. S. (2008). Hydrogels in drug delivery: Progress and challenges. *Polymer, 49*(8), 1993-2007.

Hoffman, A. S. (2012). Hydrogels for biomedical applications. *Advanced Drug Delivery Reviews, 64*, 18-23.

Hogan, S. A., McNamee, B. F., O'Riordan, E. D., & O'Sullivan, M. (2001). Emulsification and microencapsulation properties of sodium caseinate/carbohydrate blends. *International Dairy Journal, 11*(3), 137-144.

HPS, A. K., Saurabh, C. K., Adnan, A., Fazita, M. N., Syakir, M., Davoudpour, Y., Rafatullah, M., Abdullah, C., Haafiz, M., & Dungani, R. (2016). A review on

chitosan-cellulose blends and nanocellulose reinforced chitosan biocomposites: Properties and their applications. *Carbohydrate Polymers, 150*, 216-226.

Hua, S., Ma, H., Li, X., Yang, H., & Wang, A. (2010). pH-sensitive sodium alginate/poly(vinyl alcohol) hydrogel beads prepared by combined Ca^{2+} crosslinking and freeze-thawing cycles for controlled release of diclofenac sodium. *International Journal of Biological Macromolecules, 46*(5), 517-523.

Huang, Z.-M., Zhang, Y.-Z., Kotaki, M., & Ramakrishna, S. (2003). A review on polymer nanofibers by electrospinning and their applications in nanocomposites. *Composites Science and Technology, 63*(15), 2223-2253.

Hubbe, M. A., Rojas, O. J., Lucia, L. A., & Sain, M. (2008). Cellulosic nanocomposites: a review. *BioResources, 3*(3), 929-980.

Hult, E.-L., Larsson, P., & Iversen, T. (2001). Cellulose fibril aggregation—an inherent property of kraft pulps. *Polymer, 42*(8), 3309-3314.

Hunter, R. J. (2013). *Zeta potential in colloid science: principles and applications* (Vol. 2): Academic press.

Im, J. S., Kim, S. J., Kang, P. H., & Lee, Y.-S. (2009). The improved electrical conductivity of carbon nanofibers by fluorinated MWCNTs. *Journal of Industrial and Engineering Chemistry, 15*(5), 699-702.

Irías-Mata, A., Sus, N., Flory, S., Stock, D., Woerner, D., Podszun, M., & Frank, J. (2018). α-Tocopherol transfer protein does not regulate the cellular uptake and intracellular distribution of α-and γ-tocopherols and-tocotrienols in cultured liver cells. *Redox biology, 19*, 28-36.

Isogai, A., Saito, T., & Fukuzumi, H. (2011). TEMPO-oxidized cellulose nanofibers. *Nanoscale, 3*(1), 71-85.

Jackson, J. K., Letchford, K., Wasserman, B. Z., Ye, L., Hamad, W. Y., & Burt, H. M. (2011). The use of nanocrystalline cellulose for the binding and controlled release of drugs. *International Journal of Nanomedicine, 6*, 321-330.

Jacob, S., Nair, A. B., Shah, J., Sreeharsha, N., Gupta, S., & Shinu, P. (2021). Emerging role of hydrogels in drug delivery systems, tissue engineering and wound management. *Pharmaceutics, 13*(3), 357.

Jafari, S. M., Assadpoor, E., He, Y., & Bhandari, B. (2008a). Encapsulation efficiency of food flavours and oils during spray drying. *Drying Technology, 26*(7), 816-835.

Jafari, S. M., Assadpoor, E., He, Y., & Bhandari, B. (2008b). Re-coalescence of emulsion droplets during high-energy emulsification. *Food Hydrocolloids, 22*(7), 1191-1202.

Jafari, S. M., He, Y., & Bhandari, B. (2006). Optimization of nano-emulsions production by microfluidization. *European Food Research and Technology, 225*(5-6), 733-741.

Jafari, S. M., He, Y., & Bhandari, B. (2007a). Effectiveness of encapsulating biopolymers to produce sub-micron emulsions by high energy emulsification techniques. *Food Research International, 40*(7), 862-873.

Jafari, S. M., He, Y., & Bhandari, B. (2007b). Production of sub-micron emulsions by ultrasound and microfluidization techniques. *Journal of Food Engineering, 82*(4), 478-488.

Jagadeesan, D., Nasimova, I., Gourevich, I., Starodubtsev, S., & Kumacheva, E. (2011). Microgels for the encapsulation and stimulus‐responsive release of molecules with distinct polarities. *Macromolecular Bioscience, 11*(7), 889-896.

Jankauskaitė, V., Balčiūnaitienė, A., Alexandrova, R., Buškuvienė, N., & Žukienė, K. (2020). Effect of cellulose microfiber silylation procedures on the properties and antibacterial activity of polydimethylsiloxane. *Coatings, 10*(6), 567.

Jeong, B., Bae, Y. H., & Kim, S. W. (2000). Drug release from biodegradable injectable thermosensitive hydrogel of PEG–PLGA–PEG triblock copolymers. *Journal of Controlled Release, 63*(1), 155-163.

Jialal, I., & Devaraj, S. (2005). Scientific evidence to support a vitamin E and heart disease health claim: research needs. *The Journal of Nutrition, 135*(2), 348-353.

Jiang, J., Oberdörster, G., & Biswas, P. (2009). Characterization of size, surface charge, and agglomeration state of nanoparticle dispersions for toxicological studies. *Journal of Nanoparticle Research, 11*(1), 77-89.

Jiang, M., Hong, Y., Gu, Z., Cheng, L., Li, Z., & Li, C. (2019). Preparation of a starch-based carrier for oral delivery of Vitamin E to the small intestine. *Food Hydrocolloids, 91*, 26-33.

Jim nez Saelices, C., & Capron, I. (2018). Design of Pickering micro-and nanoemulsions based on the structural characteristics of nanocelluloses. *Biomacromolecules, 19*(2), 460-469.

John, M. J., & Anandjiwala, R. D. (2008). Recent developments in chemical modification and characterization of natural fiber-reinforced composites. *Polymer Composites, 29*(2), 187-207.

John, M. J., & Anandjiwala, R. D. (2008). Recent developments in chemical modification and characterization of natural fiber-reinforced composites. *Polymer Composites, 29*(2), 187-207.

Johnson, B., Bauer, J., Niedermaier, D. J., Crone, W., & Beebe, D. (2004). Experimental techniques for mechanical characterization of hydrogels at the microscale. *Experimental Mechanics, 44*(1), 21.

Jonoobi, M., Khazaeian, A., Tahir, P. M., Azry, S. S., & Oksman, K. (2011). Characteristics of cellulose nanofibers isolated from rubberwood and empty fruit bunches of oil palm using chemo-mechanical process. *Cellulose, 18*(4), 1085-1095.

Joscelyne, S. M., & Trägårdh, G. (2000). Membrane emulsification - a literature review. *Journal of Membrane Science, 169*(1), 107-117.

Joshi, B., & Joshi, A. (2019). Ultrasound-based drug delivery systems. *Bioelectronics and Medical Devices*, 241-260.

Kalashnikova, I., Bizot, H., Cathala, B., & Capron, I. (2012). Modulation of cellulose nanocrystals amphiphilic properties to stabilize oil/water interface. *Biomacromolecules, 13*(1), 267-275.

Kalia, S., Dufresne, A., Cherian, B. M., Kaith, B. S., Avérous, L., Njuguna, J., & Nassiopoulos, E. (2011). Cellulose-based bio- and nanocomposites: A review. *International Journal of Polymer Science, 2011*, 1-35.

Kalia, S., Kaith, B., & Kaur, I. (2011). *Cellulose fibers: bio-and nano-polymer composites: green chemistry and technology*: Springer Science & Business Media.

Kaltsa, O., Gatsi, I., Yanniotis, S., & Mandala, I. (2014). Influence of ultrasonication parameters on physical characteristics of olive oil model emulsions containing xanthan. *Food and Bioprocess Technology, 7*(7), 2038-2049.

Kang-Mieler, J. J., Dosmar, E., Liu, W., & Mieler, W. F. (2017). Extended ocular drug delivery systems for the anterior and posterior segments: biomaterial options and applications. *Expert Opinion on Drug Delivery, 14*(5), 611-620.

Kargar, M., Fayazmanesh, K., Alavi, M., Spyropoulos, F., & Norton, I. T. (2012). Investigation into the potential ability of Pickering emulsions (food-grade particles) to enhance the oxidative stability of oil-in-water emulsions. *Journal of Colloid and Interface Science, 366*(1), 209-215.

Kargarzadeh, H., Ahmad, I., Abdullah, I., Dufresne, A., Zainudin, S. Y., & Sheltami, R. M. (2012). Effects of hydrolysis conditions on the morphology, crystallinity, and thermal stability of cellulose nanocrystals extracted from kenaf bast fibers. *Cellulose, 19*(3), 855-866.

Katepalli, H. (2014). *Formation and stability of emulsions: Effect of surfactant-particle interactions and particle shape.* University of Rhode Island.

Katepalli, H., & Bose, A. (2014). Response of surfactant stabilized oil-in-water emulsions to the addition of particles in an aqueous suspension. *Langmuir, 30*(43), 12736-12742.

Kentish, S., Wooster, T. J., Ashokkumar, M., Balachandran, S., Mawson, R., & Simons, L. (2008). The use of ultrasonics for nanoemulsion preparation. *Innovative Food Science & Emerging Technologies, 9*(2), 170-175.

Khanna, S., Roy, S., Ryu, H., Bahadduri, P., Swaan, P. W., Ratan, R. R., & Sen, C. K. (2003). Molecular basis of vitamin E action tocotrienol modulates 12-lipoxygenase, a key mediator of glutamate-induced neurodegeneration. *Journal of Biological Chemistry, 278*(44), 43508-43515.

Kharkwal, H., & Janaswamy, S. (2016). *Natural Polymers for Drug Delivery*: CABI.

Khayata, N., Abdelwahed, W., Chehna, M. F., Charcosset, C., & Fessi, H. (2012). Preparation of vitamin E loaded nanocapsules by the nanoprecipitation method: from laboratory scale to large scale using a membrane contactor. *International Journal of Pharmaceutics, 423*(2), 419-427.

Kiefer, J., Fries, J., & Leipertz, A. (2007). Experimental vibrational study of imidazolium-based ionic liquids: Raman and infrared spectra of 1-ethyl-3-methylimidazolium bis (trifluoromethylsulfonyl) imide and 1-ethyl-3-methylimidazolium ethylsulfate. *Applied Spectroscopy, 61*(12), 1306-1311.

Kim, D.-Y., Nishiyama, Y., Wada, M., & Kuga, S. (2001). High-yield carbonization of cellulose by sulfuric acid impregnation. *Cellulose, 8*(1), 29-33.

Kim, M. S., Park, S. J., Gu, B. K., & Kim, C.-H. (2012). Ionically crosslinked alginate–carboxymethyl cellulose beads for the delivery of protein therapeutics. *Applied Surface Science, 262*, 28-33.

Kim, Y. J., Park, H. G., Yang, Y. L., Yoon, Y., Kim, S., & Oh, E. (2005). Multifunctional drug delivery system using starch-alginate beads for controlled release. *Biological and Pharmaceutical Bulletin, 28*(2), 394-397.

Klebe, J. F., & Schenectady, N. Y. (1968). Process for producing soluble trimethylsilylated cellulose: US Patents.

KMa, M., TMb, P. K., & Bc, B. S. (2012). Formulation and evaluation of dexibuprofen alginate–clay composite microbeads for oral controlled drug delivery. *Asian Journal of Pharmaceutical Sciences, 7*(1), 28-39.

Köhler, S., Liebert, T., & Heinze, T. (2008). Interactions of ionic liquids with polysaccharides. VI. Pure cellulose nanoparticles from trimethylsilyl cellulose synthesized in ionic liquids. *Journal of Polymer Science Part A: Polymer Chemistry, 46*(12), 4070-4080.

Kong, F., & Singh, R. (2008). Disintegration of solid foods in human stomach. *Journal of Food Science, 73*(5), R67-R80.

Kong, H. J., Smith, M. K., & Mooney, D. J. (2003). Designing alginate hydrogels to maintain viability of immobilized cells. *Biomaterials, 24*(22), 4023-4029.

Koroleva, M., Nagovitsina, T., & Yurtov, E. (2018). Nanoemulsions stabilized by non-ionic surfactants: stability and degradation mechanisms. *Physical Chemistry Chemical Physics, 20*(15), 10369-10377.

Kostag, M., Köhler, S., Liebert, T., & Heinze, T. (2010). Pure cellulose nanoparticles from trimethylsilyl cellulose. *Macromolecular Symposia, 294*(2), 96-106.

Kronberg, B., & Lindman, B. (2003). *Surfactants and polymers in aqueous solution*: John Wiley & Sons Ltd., Chichester.

Kumar, A., & Han, S. S. (2017). PVA-based hydrogels for tissue engineering: A review. *International Journal of Polymeric Materials and Polymeric Biomaterials, 66*(4), 159-182.

Kumar, A., Park, B. J., Tu, F., & Lee, D. (2013). Amphiphilic Janus particles at fluid interfaces. *Soft Matter, 9*(29), 6604-6617.

Kumar, G. P., & Rajeshwarrao, P. (2011). Nonionic surfactant vesicular systems for effective drug delivery—an overview. *Acta Pharmaceutica Sinica B, 1*(4), 208-219.

Kunz, W., Zemb, T., & Harrar, A. (2012). Using ionic liquids to formulate microemulsions: Current state of affairs. *Current Opinion in Colloid & Interface Science, 17*(4), 205-211.

Kuo, C. K., & Ma, P. X. (2001). Ionically crosslinked alginate hydrogels as scaffolds for tissue engineering: Part 1. Structure, gelation rate and mechanical properties. *Biomaterials, 22*(6), 511-521.

Lacík, I. (2006). Polymer chemistry in diabetes treatment by encapsulated islets of Langerhans: review to 2006. *Australian Journal of Chemistry, 59*(8), 508-524.

Ladhe, A. R., & Bhattacharyya, D. (2009). Adsorption of ethoxylated nonionic surfactants from siloxane-based solvent and aqueous systems: Use of qcm and model polymeric surfaces. *Chemical Engineering Communications, 196*(7), 872-889.

Ladhe, A. R., Radomyselski, A., & Bhattacharyya, D. (2006). Ethoxylated nonionic surfactants in hydrophobic solvent: Interaction with aqueous and membrane-immobilized poly (acrylic acid). *Langmuir, 22*(2), 615-621.

Lam, E., Leung, A. C. W., Liu, Y., Majid, E., Hrapovic, S., Male, K. B., & Luong, J. H. T. (2012). Green strategy guided by raman spectroscopy for the synthesis of ammonium carboxylated nanocrystalline cellulose and the recovery of byproducts. *ACS Sustainable Chemistry & Engineering, 1*(2), 278-283.

Lam, S., Velikov, K. P., & Velev, O. D. (2014). Pickering stabilization of foams and emulsions with particles of biological origin. *Current Opinion in Colloid & Interface Science, 19*(5), 490-500.

Laouini, A., Fessi, H., & Charcosset, C. (2012). Membrane emulsification: A promising alternative for vitamin E encapsulation within nano-emulsion. *Journal of Membrane Science, 423-424*, 85-96.

Larrañeta, E., Stewart, S., Ervine, M., Al-Kasasbeh, R., & Donnelly, R. (2018). Hydrogels for hydrophobic drug delivery. Classification, synthesis and applications. *Journal of Functional Biomaterials, 9*(1), 13.

Lavoine, N., Desloges, I., Dufresne, A., & Bras, J. (2012). Microfibrillated cellulose–Its barrier properties and applications in cellulosic materials: A review. *Carbohydrate Polymers, 90*(2), 735-764.

Lavoine, N., Tabary, N., Desloges, I., Martel, B., & Bras, J. (2014). Controlled release of chlorhexidine digluconate using β-cyclodextrin and microfibrillated cellulose. *Colloids and Surfaces B: Biointerfaces, 121*, 196-205.

Law, K.-N., Daud, W. R. W., & Ghazali, A. (2007). Morphological and chemical nature of fiber strands of oil palm empty-fruit-bunch (OPEFB). *BioResources, 2*(3), 351-362.

Lee, I.-M., Cook, N. R., Gaziano, J. M., Gordon, D., Ridker, P. M., Manson, J. E., Hennekens, C. H., & Buring, J. E. (2005). Vitamin E in the primary prevention of cardiovascular disease and cancer: the Women's Health Study: a randomized controlled trial. *Jama, 294*(1), 56-65.

Lee, K. Y., & Mooney, D. J. (2012). Alginate: properties and biomedical applications. *Progress in Polymer Science, 37*(1), 106-126.

Leonard, S. W., Paterson, E., Atkinson, J. K., Ramakrishnan, R., Cross, C. E., & Traber, M. G. (2005). Studies in humans using deuterium-labeled α-and γ-tocopherols demonstrate faster plasma γ-tocopherol disappearance and greater γ-metabolite production. *Free Radical Biology and Medicine, 38*(7), 857-866.

Leong, T. S., Wooster, T. J., Kentish, S. E., & Ashokkumar, M. (2009). Minimising oil droplet size using ultrasonic emulsification. *Ultrasonics Sonochemistry, 16*(6), 721-727.

Leung, A. C., Hrapovic, S., Lam, E., Liu, Y., Male, K. B., Mahmoud, K. A., & Luong, J. H. (2011). Characteristics and properties of carboxylated cellulose nanocrystals prepared from a novel one-step procedure. *Small, 7*(3), 302-305.

Li, J., & Mooney, D. J. (2016). Designing hydrogels for controlled drug delivery. *Nature Reviews Materials, 1*(12), 16071.

Li, R., Fei, J., Cai, Y., Li, Y., Feng, J., & Yao, J. (2009). Cellulose whiskers extracted from mulberry: A novel biomass production. *Carbohydrate Polymers, 76*(1), 94-99.

Liang, F., Shen, K., Qu, X., Zhang, C., Wang, Q., Li, J., Liu, J., & Yang, Z. (2011). Inorganic janus nanosheets. *Angewandte Chemie International Edition, 50*(10), 2379-2382.

Lin, N., Bruzzese, C., & Dufresne, A. (2012). TEMPO-oxidized nanocellulose participating as crosslinking aid for alginate-based sponges. *ACS Applied Materials & Interfaces, 4*(9), 4948-4959.

Lin, N., Huang, J., Chang, P. R., Feng, L., & Yu, J. (2011). Effect of polysaccharide nanocrystals on structure, properties, and drug release kinetics of alginate-based microspheres. *Colloids and Surfaces B: Biointerfaces, 85*(2), 270-279.

Llabot, J. M., Manzo, R. H., & Allemandi, D. A. (2004). Drug release from carbomer: carbomer sodium salt matrices with potential use as mucoadhesive drug delivery system. *International Journal of Pharmaceutics, 276*(1-2), 59-66.

Lu, P., & Hsieh, Y.-L. (2010). Preparation and properties of cellulose nanocrystals: Rods, spheres, and network. *Carbohydrate Polymers, 82*(2), 329-336.

Lu, P., & Hsieh, Y.-L. (2012). Preparation and characterization of cellulose nanocrystals from rice straw. *Carbohydrate Polymers, 87*(1), 564-573.

Łuczak, J., Hupka, J., Thöming, J., & Jungnickel, C. (2008). Self-organization of imidazolium ionic liquids in aqueous solution. *Colloids and Surfaces A: Physicochemical and Engineering Aspects, 329*(3), 125-133.

Lynd, L. R., Weimer, P. J., Van Zyl, W. H., & Pretorius, I. S. (2002). Microbial cellulose utilization: fundamentals and biotechnology. *Microbiology and Molecular Biology Reviews, 66*(3), 506-577.

Ma, P. X., & Elisseeff, J. (2005). *Scaffolding in tissue engineering*: CRC press.

Ma, Y., Zheng, Y., Zeng, X., Jiang, L., Chen, H., Liu, R., Huang, L., & Mei, L. (2011). Novel docetaxel-loaded nanoparticles based on PCL-Tween 80 copolymer for cancer treatment. *International Journal of Nanomedicine, 6*, 2679.

Mahdi Jafari, S., He, Y., & Bhandari, B. (2006). Nano-emulsion production by sonication and microfluidization - a comparison. *International Journal of Food Properties, 9*(3), 475-485.

Mahmoud, K. A., Male, K. B., Hrapovic, S., & Luong, J. H. (2009). Cellulose nanocrystal/gold nanoparticle composite as a matrix for enzyme immobilization. *ACS Applied Materials & Interfaces, 1*(7), 1383-1386.

Malekghasemi, S., Kahveci, E., & Duman, M. (2016). Rapid and alternative fabrication method for microfluidic paper based analytical devices. *Talanta, 159*, 401-411.

Man, Y. C., Ammawath, W., & Mirghani, M. E. S. (2005). Determining α-tocopherol in refined bleached and deodorized palm olein by Fourier transform infrared spectroscopy. *Food Chemistry, 90*(1), 323-327.

Mandal, A., & Chakrabarty, D. (2011). Isolation of nanocellulose from waste sugarcane bagasse (SCB) and its characterization. *Carbohydrate Polymers, 86*(3), 1291-1299.

Maphosa, Y., & Jideani, V. A. (2018). Factors affecting the stability of emulsions stabilised by biopolymers. *Science and Technology Behind Nanoemulsions*, 65.

Martin, C., Aibani, N., Callan, J. F., & Callan, B. (2016). Recent advances in amphiphilic polymers for simultaneous delivery of hydrophobic and hydrophilic drugs. *Therapeutic Delivery, 7*(1), 15-31.

Martínez-Sanz, M., Lopez-Rubio, A., & Lagaron, J. M. (2011). Optimization of the nanofabrication by acid hydrolysis of bacterial cellulose nanowhiskers. *Carbohydrate Polymers, 85*(1), 228-236.

Martins, S., Sarmento, B., Souto, E. B., & Ferreira, D. C. (2007). Insulin-loaded alginate microspheres for oral delivery - effect of polysaccharide reinforcement on

physicochemical properties and release profile. *Carbohydrate Polymers, 69*(4), 725-731.

Mason, T., Wilking, J., Meleson, K., Chang, C., & Graves, S. (2006). Nanoemulsions: formation, structure, and physical properties. *Journal of Physics: Condensed Matter, 18*(41), R635.

McClements, D. (2000). Comments on viscosity enhancement and depletion flocculation by polysaccharides. *Food Hydrocolloids, 14*(2), 173-177.

McClements, D. J. (2004). Protein-stabilized emulsions. *Current Opinion in Colloid & Interface Science, 9*(5), 305-313.

McClements, D. J. (2011). Edible nanoemulsions: fabrication, properties, and functional performance. *Soft Matter, 7*(6), 2297-2316.

McClements, D. J. (2012a). Crystals and crystallization in oil-in-water emulsions: Implications for emulsion-based delivery systems. *Advances in Colloid and Interface Science, 174*, 1-30.

McClements, D. J. (2012b). Nanoemulsions versus microemulsions: terminology, differences, and similarities. *Soft Matter, 8*(6), 1719-1729.

McClements, D. J. (2015). *Food emulsions: principles, practices, and techniques*: CRC press.

McClements, D. J., Decker, E. A., Park, Y., & Weiss, J. (2009). Structural design principles for delivery of bioactive components in nutraceuticals and functional foods. *Critical Reviews in Food Science and Nutrition, 49*(6), 577-606.

McClements, D. J., & Gumus, C. E. (2016). Natural emulsifiers—Biosurfactants, phospholipids, biopolymers, and colloidal particles: Molecular and physicochemical basis of functional performance. *Advances in Colloid and Interface Science, 234*, 3-26.

Moakes, R. J. A., Sullo, A., & Norton, I. T. (2015). Preparation and rheological properties of whey protein emulsion fluid gels. *RSC Advances, 5*(75), 60786-60795.

Mohamad Haafiz, M. K., Eichhorn, S. J., Hassan, A., & Jawaid, M. (2013). Isolation and characterization of microcrystalline cellulose from oil palm biomass residue. *Carbohydrate Polymers, 93*(2), 628-634.

Mollakhalili Meybodi, N., Mohammadifar, M. A., & Naseri, A. (2014). Effective factors on the stability of oil-in-water emulsion based beverage: a review. *Journal of Food Quality and Hazards Control, 1*(3), 67-71.

Moniruzzaman, M., Kamiya, N., & Goto, M. (2010). Ionic liquid based microemulsion with pharmaceutically accepted components: Formulation and potential applications. *Journal of Colloid and Interface Science, 352*(1), 136-142.

Moniruzzaman, M., Tahara, Y., Tamura, M., Kamiya, N., & Goto, M. (2010). Ionic liquid-assisted transdermal delivery of sparingly soluble drugs. *Chemical Communications, 46*(9), 1452-1454.

Montanucci, P., Terenzi, S., Santi, C., Pennoni, I., Bini, V., Pescara, T., Basta, G., & Calafiore, R. (2015). Insights in behavior of variably formulated alginate-based microcapsules for cell transplantation. *BioMed Research International, 2015*.

Moon, R. J., Martini, A., Nairn, J., Simonsen, J., & Youngblood, J. (2011). Cellulose nanomaterials review: structure, properties and nanocomposites. *Chemical Society Reviews, 40*(7), 3941-3994.

Morán, J. I., Alvarez, V. A., Cyras, V. P., & Vázquez, A. (2007). Extraction of cellulose and preparation of nanocellulose from sisal fibers. *Cellulose, 15*(1), 149-159.

Mørch, Y. (2008). Novel alginate microcapsules for cell therapy. *Department of Biotechnology*.

Morch, Y. A., Donati, I., Strand, B. L., & Skjak-Braek, G. (2007). Molecular engineering as an approach to design new functional properties of alginate. *Biomacromolecules, 8*(9), 2809-2814.

Mormann, W., & Wezstein, M. (2009). Trimethylsilylation of cellulose in ionic liquids. *Macromolecular Bioscience, 9*(4), 369-375.

Muñoz-Bonilla, A., Echeverría, C., Sonseca, Á., Arrieta, M. P., & Fernández-García, M. (2019). Polymeric materials: Surfaces, interfaces and bioapplications. *Materials, 12*(8), 1312.

Murray, B. S., Durga, K., Yusoff, A., & Stoyanov, S. D. (2011). Stabilization of foams and emulsions by mixtures of surface active food-grade particles and proteins. *Food Hydrocolloids, 25*(4), 627-638.

Murshid, N., & Wang, X. (2017). Hydrophobic effect of alkyl groups stabilizing self-assembled colloids in water. The *Journal of Physical Chemistry B, 121*(25), 6280-6285.

Muthukumar, N., Maruthamuthu, S., & Palaniswamy, N. (2007). Role of cationic and nonionic surfactants on biocidal efficiency in diesel-water interface. *Colloids and Surfaces B: Biointerfaces, 57*(2), 152-160.

Nasir, A., Kausar, A., & Younus, A. (2015). A review on preparation, properties and applications of polymeric nanoparticle-based materials. *Polymer-Plastics Technology and Engineering, 54*(4), 325-341.

Nciri, H., Huang, N., Rosilio, V., Trabelsi-Ayadi, M., Benna-Zayani, M., & Grossiord, J.-L. (2010). Rheological studies in the bulk and at the interface of Pickering oil/water emulsions. *Rheologica Acta, 49*(9), 961-969.

Newton, A., Kaur, B., Indana, V., & Rajesh, K. (2014). Chronotherapeutic drug delivery of pectin vs. guar gum, xanthan gum controlled release colon targeted directly

compressed propranolol hcl matrix tab-lets. *SAJ Pharmacy and Pharmacology, 1*(201), 2375-2262.2371.

Ng, B. F., Xiong, J. W., & Wan, M. P. (2017). Application of acoustic agglomeration to enhance air filtration efficiency in air-conditioning and mechanical ventilation (ACMV) systems. *PloS One, 12*(6), e0178851.

Nguyen, H. D., Mai, T. T. T., Nguyen, N. B., Dang, T. D., Le, M. L. P., & Dang, T. T. (2013). A novel method for preparing microfibrillated cellulose from bamboo fibers. *Advances in Natural Sciences: Nanoscience and Nanotechnology, 4*(1), 015016.

Nguyen, T. N., Tran, V.-T., Duan, W., Tran, P. H., & Tran, T. T. (2017). Nanoprecipitation for poorly water-soluble drugs. *Current Drug Metabolism, 18*(11), 1000-1015.

Niknam, S. M., Escudero, I., & Benito, J. M. (2020). Formulation and preparation of water-In-oil-In-water emulsions loaded with a phenolic-rich Inner aqueous phase by application of high energy emulsification methods. *Foods, 9*(10), 1411.

Nokhodchi, A., Raja, S., Patel, P., & Asare-Addo, K. (2012). The role of oral controlled release matrix tablets in drug delivery systems. *Bioimpacts, 2*(4), 175-187.

Nunamaker, E. A., Otto, K. J., & Kipke, D. R. (2011). Investigation of the material properties of alginate for the development of hydrogel repair of dura mater. *Journal of the Mechanical Behavior of Biomedical Materials, 4*(1), 16-33.

O'Byrne, D., Grundy, S., Packer, L., Devaraj, S., Baldenius, K., Hoppe, P., Kraemer, K., Jialal, I., & Traber, M. (2000). Studies of LDL oxidation following α-, γ-, or δ-tocotrienyl acetate supplementation of hypercholesterolemic humans. *Free Radical Biology and Medicine, 29*(9), 834-845.

Odriozola-Serrano, I., Oms-Oliu, G., & Martin-Belloso, O. (2014). Nanoemulsion-based delivery systems to improve functionality of lipophilic components. *Frontier Nutrition, 1*, 24.

Okada, M., Maeda, H., Fujii, S., Nakamura, Y., & Furuzono, T. (2012). Formation of Pickering emulsions stabilized via interaction between nanoparticles dispersed in aqueous phase and polymer end groups dissolved in oil phase. *Langmuir, 28*(25), 9405-9412.

Olsson, R. T., Kraemer, R., Lopez-Rubio, A., Torres-Giner, S., Ocio, M. a. J., & Lagar n, J. M. a. (2010). Extraction of microfibrils from bacterial cellulose networks for electrospinning of anisotropic biohybrid fiber yarns. *Macromolecules, 43*(9), 4201-4209.

Onyianta, A. J., Castellano, M., Dorris, M., Williams, R. L., & Vicini, S. (2018). The effects of morpholine pre-treated and carboxymethylated cellulose nanofibrils on the properties of alginate-based hydrogels. *Carbohydrate Polymers, 198*, 320-327.

Ooi, S. Y., Ahmad, I., & Amin, M. C. I. M. (2016). Cellulose nanocrystals extracted from rice husks as a reinforcing material in gelatin hydrogels for use in controlled drug delivery systems. *Industrial Crops and Products, 93*, 227-234.

Pääkkö, M., Vapaavuori, J., Silvennoinen, R., Kosonen, H., Ankerfors, M., Lindström, T., Berglund, L. A., & Ikkala, O. (2008). Long and entangled native cellulose I nanofibers allow flexible aerogels and hierarchically porous templates for functionalities. *Soft Matter, 4*(12), 2492-2499.

Paarakh, M. P., Jose, P. A., Setty, C., & Peter, G. (2018). Release kinetics–concepts and applications. *International Journal of Pharmacy Research & Technology, 8*(1), 12-20.

Pallandre, S., Decker, E. A., & McClements, D. J. (2007). Improvement of stability of oil-in-water emulsions containing caseinate-coated droplets by addition of sodium alginate. *Journal of Food Science, 72*(9), E518-524.

Panyam, J., & Labhasetwar, V. (2003). Biodegradable nanoparticles for drug and gene delivery to cells and tissue. *Advanced Drug Delivery Reviews, 55*(3), 329-347.

Panyam, J., Williams, D., Dash, A., Leslie ‐ Pelecky, D., & Labhasetwar, V. (2004). Solid-state solubility influences encapsulation and release of hydrophobic drugs from PLGA/PLA nanoparticles. *Journal of Pharmaceutical Sciences, 93*(7), 1804-1814.

Papich, M. G., & Martinez, M. N. (2015). Applying biopharmaceutical classification system (BCS) criteria to predict oral absorption of drugs in dogs: challenges and pitfalls. *The AAPS Journal, 17*(4), 948-964.

Paques, J. P., van der Linden, E., van Rijn, C. J., & Sagis, L. M. (2014). Preparation methods of alginate nanoparticles. *Advances in Colloid and Interface Science, 209*, 163-171.

Patel, N., Lalwani, D., Gollmer, S., Injeti, E., Sari, Y., & Nesamony, J. (2016). Development and evaluation of a calcium alginate based oral ceftriaxone sodium formulation. *Progress in Biomaterials, 5*(2), 117-133.

Pathak, V. M. (2018). *Handbook of research on microbial tools for environmental waste management*: IGI Global.

Patil, N., Wadd, N., & Thorat, S. (2017). Microspheres: A Novel drug delivery system. *American Journal of Pharmtech Research, 10*(2), 287-301

Paul, B. K., & Moulik, S. P. (2015). *Ionic liquid-based surfactant science: formulation, characterization, and applications*: John Wiley & Sons.

Peppas, N., Bures, P., Leobandung, W., & Ichikawa, H. (2000). Hydrogels in pharmaceutical formulations. *European Journal of Pharmaceutics and Biopharmaceutics, 50*(1), 27-46.

Pereira, A. L. S., do Nascimento, D. M., Morais, J. P. S., Vasconcelos, N. F., Feitosa, J. P., Brígida, A. I. S., & Rosa, M. d. F. (2014). Improvement of polyvinyl alcohol

properties by adding nanocrystalline cellulose isolated from banana pseudostems. *Carbohydrate Polymers, 112*, 165-172.

Pereira, L., & Cotas, J. (2020). Introductory Chapter: Alginates-A General Overview. *Alginates-Recent Uses of This Natural Polymer*. London, United Kingdom.

Pernak, J., Sobaszkiewicz, K., & Mirska, I. (2003). Anti-microbial activities of ionic liquids. *Green Chemistry, 5*(1), 52-56.

Peters, I. R., Majumdar, S., & Jaeger, H. M. (2016). Direct observation of dynamic shear jamming in dense suspensions. *Nature, 532*(7598), 214-217.

Phillips, G. O., & Williams, P. A. (2009). *Gums and stabilisers for the food industry 12*: Royal Society of Chemistry.

Pichot, R. (2012). *Stability and characterisation of emulsions in the presence of colloidal particles and surfactants.* University of Birmingham.

Pichot, R., Spyropoulos, F., & Norton, I. (2009). Mixed-emulsifier stabilised emulsions: Investigation of the effect of monoolein and hydrophilic silica particle mixtures on the stability against coalescence. *Journal of Colloid and Interface Science, 329*(2), 284-291.

Pichot, R., Spyropoulos, F., & Norton, I. T. (2010). O/W emulsions stabilised by both low molecular weight surfactants and colloidal particles: The effect of surfactant type and concentration. *Journal of Colloid and Interface Science, 352*(1), 128-135.

Pickering, S. U. (1907). CXCVI.—emulsions. *Journal of the Chemical Society, Transactions, 91*, 2001-2021.

Pillai, J. J., Thulasidasan, A. K. T., Anto, R. J., Chithralekha, D. N., Narayanan, A., & Kumar, G. S. V. (2014). Folic acid conjugated cross-linked acrylic polymer (FA-CLAP) hydrogel for site specific delivery of hydrophobic drugs to cancer cells. *Journal of Nanobiotechnology, 12*(1), 25.

Pillai, O., & Panchagnula, R. (2001). Polymers in drug delivery. *Current Opinion in Chemical Biology, 5*(4), 447-451.

Pongsawatmanit, R., Harnsilawat, T., & McClements, D. J. (2006). Influence of alginate, pH and ultrasound treatment on palm oil-in-water emulsions stabilized by β-lactoglobulin. *Colloids and Surfaces A: Physicochemical and Engineering Aspects, 287*(1-3), 59-67.

Pourjavadi, A., Amin, S. S., & Hosseini, S. H. (2018). Delivery of hydrophobic anticancer drugs by hydrophobically modified alginate based magnetic nanocarrier. *Industrial & Engineering Chemistry Research, 57*(3), 822-832.

Puspasari, T., Pradeep, N., & Peinemann, K.-V. (2015). Crosslinked cellulose thin film composite nanofiltration membranes with zero salt rejection. *Journal of Membrane Science, 491*, 132-137.

Qin, Z.-Y., Tong, G., Chin, Y. F., & Zhou, J.-C. (2011). Preparation of ultrasonic-assisted high carboxylate content cellulose nanocrystals by TEMPO oxidation. *BioResources, 6*(2), 1136-1146.

Qiu, Y., & Park, K. (2001). Environment-sensitive hydrogels for drug delivery. *Advanced Drug Delivery Reviews, 53*(3), 321-339.

Qiu, Z., & Texter, J. (2008). Ionic liquids in microemulsions. *Current Opinion in Colloid & Interface Science, 13*(4), 252-262.

Qua, E., Hornsby, P., Sharma, H., & Lyons, G. (2011). Preparation and characterisation of cellulose nanofibres. *Journal of Materials Science, 46*(18), 6029-6045.

Quiñones, J. P., Gothelf, K. V., Kjems, J., Caballero, Á. M. H., Schmidt, C., & Covas, C. P. (2013). N,O6-partially acetylated chitosan nanoparticles hydrophobically-modified for controlled release of steroids and vitamin E. *Carbohydrate Polymers, 91*(1), 143-151.

Rajpurohit, H., Sharma, P., Sharma, S., & Bhandari, A. (2010). Polymers for colon targeted drug delivery. *Indian Journal of Pharmaceutical Sciences, 72*(6), 689.

Ramanavicius, S., Jagminas, A., & Ramanavicius, A. (2021). Advances in molecularly imprinted polymers based affinity sensors. *Polymers, 13*(6), 974.

Rao, J., & McClements, D. J. (2012). Food-grade microemulsions and nanoemulsions: Role of oil phase composition on formation and stability. *Food Hydrocolloids, 29*(2), 326-334.

Ratner, B. D., Hoffman, A. S., Schoen, F. J., & Lemons, J. E. (2004). *Biomaterials science: an introduction to materials in medicine*: Elsevier.

Reger, M., Sekine, T., & Hoffmann, H. (2012). Pickering emulsions stabilized by amphiphile covered clays. *Colloids and Surfaces A: Physicochemical and Engineering Aspects, 413*, 25-32.

Reger, M., Sekine, T., Okamoto, T., Watanabe, K., & Hoffmann, H. (2011). Pickering emulsions stabilized by novel clay–hydrophobin synergism. *Soft Matter, 7*(22), 11021.

Rehm, B. H. (2009). *Alginates: biology and applications* (Vol. 13): Springer.

Rein, D. M., Khalfin, R., & Cohen, Y. (2012). Cellulose as a novel amphiphilic coating for oil-in-water and water-in-oil dispersions. *Journal of Colloid and Interface Science, 386*(1), 456-463.

Ren, W., Tian, G., Jian, S., Gu, Z., Zhou, L., Yan, L., Jin, S., Yin, W., & Zhao, Y. (2012). TWEEN coated NaYF 4: Yb, Er/NaYF4 core/shell upconversion nanoparticles for bioimaging and drug delivery. *Rsc Advances, 2*(18), 7037-7041.

Reyes-Ortega, F. (2014). pH-responsive polymers: properties, synthesis and applications. *Smart Polymers and their Applications* 45-92.

Ribeiro, A. J., Neufeld, R. J., Arnaud, P., & Chaumeil, J. C. (1999). Microencapsulation of lipophilic drugs in chitosan-coated alginate microspheres. *International Journal of Pharmaceutics, 187*(1), 115-123.

Ritger, P. L., & Peppas, N. A. (1987). A simple equation for description of solute release II. Fickian and anomalous release from swellable devices. *Journal of Controlled Release, 5*(1), 37-42.

Robitaille, R., Leblond, F. A., Bourgeois, Y., Henley, N., Loignon, M., & Hallé, J. P. (2000). Studies on small (< 350 μ m) alginate-poly-L-lysine microcapsules. V. Determination of carbohydrate and protein permeation through microcapsules by reverse-size exclusion chromatography. *Journal of Biomedical Materials Research: An Official Journal of The Society for Biomaterials, The Japanese Society for Biomaterials, and The Australian Society for Biomaterials and the Korean Society for Biomaterials, 50*(3), 420-427.

Roff, W. J., & Scott, J. R. (2013). *Fibres, films, plastics and rubbers: a handbook of common polymers*: Elsevier.

Rojas, O., Tiersch, B., Frasca, S., Wollenberger, U., & Koetz, J. (2010). A new type of microemulsion consisting of two halogen-free ionic liquids and one oil component. *Colloids and Surfaces A: Physicochemical and Engineering Aspects, 369*(1-3), 82-87.

Roman, M., & Winter, W. T. (2004). Effect of sulfate groups from sulfuric acid hydrolysis on the thermal degradation behavior of bacterial cellulose. *Biomacromolecules, 5*(5), 1671-1677.

Rosazley, R., Shazana, M., Izzati, M., Fareezal, A., Rushdan, I., & Ainun, Z. (2016). Characterization of nanofibrillated cellulose produced from oil palm empty fruit bunch fibers (OPEFB) using ultrasound. *Journal of Contemporary Issues and Thought, 6*(28-35), 29.

Rosen, M. J., & Kunjappu, J. T. (2012). *Surfactants and interfacial phenomena*: John Wiley & Sons.

Rubentheren, V., Ward, T. A., Chee, C. Y., & Nair, P. (2015). Physical and chemical reinforcement of chitosan film using nanocrystalline cellulose and tannic acid. *Cellulose, 22*(4), 2529-2541.

Ruvinov, E., Leor, J., & Cohen, S. (2010). The effects of controlled HGF delivery from an affinity-binding alginate biomaterial on angiogenesis and blood perfusion in a hindlimb ischemia model. *Biomaterials, 31*(16), 4573-4582.

Sachan, N. K., Pushkar, S., Jha, A., & Bhattcharya, A. (2009). Sodium alginate: the wonder polymer for controlled drug delivery. *Journal of Pharmacy Research, 2*(8), 1191-1199.

Sahil, K., Akanksha, M., Premjeet, S., Bilandi, A., & Kapoor, B. (2011). Microsphere: A review. *International Journal of Research in Pharmacy and Chemistry, 1*(4), 1184-1198.

Sain, M., & Panthapulakkal, S. (2006). Bioprocess preparation of wheat straw fibers and their characterization. *Industrial Crops and Products, 23*(1), 1-8.

Saito, T., Nishiyama, Y., Putaux, J.-L., Vignon, M., & Isogai, A. (2006). Homogeneous suspensions of individualized microfibrils from TEMPO-catalyzed oxidation of native cellulose. *Biomacromolecules, 7*(6), 1687-1691.

Saito, T., Shibata, I., Isogai, A., Suguri, N., & Sumikawa, N. (2005). Distribution of carboxylate groups introduced into cotton linters by the TEMPO-mediated oxidation. *Carbohydrate Polymers, 61*(4), 414-419.

Salaün, F., Butstraen, C., & Devaux, E. (2018). Sol-gel microencapsulation based on Pickering emulsion. *Science and Technology Behind Nanoemulsions*, 43.

Salmieri, S., Khan, R. A., Safrany, A., & Lacroix, M. (2015). Gamma rays-induced 2-hydroxyethyl methacrylate graft copolymerization on methylcellulose-based films: structure analysis and physicochemical properties. *Industrial Crops and Products, 70*, 64-71.

Sampath, U. T. M., Ching, Y. C., Chuah, C. H., Singh, R., & Lin, P.-C. (2017). Preparation and characterization of nanocellulose reinforced semi-interpenetrating polymer network of chitosan hydrogel. *Cellulose, 24*(5), 2215-2228.

Sanfeld, A., & Steinchen, A. (2008). Emulsions stability, from dilute to dense emulsions—role of drops deformation. *Advances in Colloid and Interface Science, 140*(1), 1-65.

Satyamurthy, P., Jain, P., Balasubramanya, R. H., & Vigneshwaran, N. (2011). Preparation and characterization of cellulose nanowhiskers from cotton fibres by controlled microbial hydrolysis. *Carbohydrate Polymers, 83*(1), 122-129.

Schmidt, E., & Vocke, F. (1926). Zur Kenntnis der Polyglykuronsäuren (I.). *Berichte der deutschen chemischen Gesellschaft (A and B Series), 59*(7), 1585-1588.

Segale, L., Giovannelli, L., Mannina, P., & Pattarino, F. (2016). Calcium alginate and calcium alginate-chitosan beads containing celecoxib solubilized in a self-emulsifying phase. *Scientifica, 2016*.

Sehaqui, H., Allais, M., Zhou, Q., & Berglund, L. A. (2011). Wood cellulose biocomposites with fibrous structures at micro-and nanoscale. *Composites Science and Technology, 71*(3), 382-387.

Selamat, S. N., Muhamad, I. I., Idham, Z., & Pae, N. (2018). Retention of alpha-tocopherol and antioxidant activity of encapsulated palm mixed Vitamin E in formulated blends. *MOJ Food Processing & Technology, 6*(3).

Sen, C. K., Khanna, S., & Roy, S. (2006). Tocotrienols: Vitamin E beyond tocopherols. *Life Sciences, 78*(18), 2088-2098.

Shah, R., Eldridge, D., Palombo, E., & Harding, I. (2014). Optimisation and stability assessment of solid lipid nanoparticles using particle size and zeta potential. *Journal of Physical Science, 25*(1).

Shalaka, D., Naik, S., Amruta, A., & Parimal, K. (2009). Vitamin E loaded pectin alginate microspheres for cosmetic application. *Journal of Pharmacy Research Vol, 2*(6).

Shan, Y., Yu, C., Yang, J., Dong, Q., Fan, X., & Qiu, J. (2015). Thermodynamically stable pickering emulsion configured with carbon-nanotube-bridged nanosheet-shaped layered double hydroxide for selective oxidation of benzyl alcohol. *ACS Applied Materials & Interfaces, 7*(22), 12203-12209.

Sharma, N., Purwar, N., & Gupta, P. C. (2015). Microspheres as drug carriers for controlled drug delivery: A review. *International Journal of Pharmaceutical Sciences and Research, 6*(11), 4579.

Sharma, T., Kumar, G. S., Chon, B. H., & Sangwai, J. S. (2014). Viscosity of the oil-in-water Pickering emulsion stabilized by surfactant-polymer and nanoparticle-surfactant-polymer system. *Korea-Australia Rheology Journal, 26*(4), 377-387.

Sharma, T., Kumar, G. S., & Sangwai, J. S. (2015). Viscoelastic properties of oil-in-water (o/w) pickering emulsion stabilized by surfactant–polymer and nanoparticle–surfactant–polymer systems. *Industrial & Engineering Chemistry Research, 54*(5), 1576-1584.

Sheikhi, A., Hayashi, J., Eichenbaum, J., Gutin, M., Kuntjoro, N., Khorsandi, D., & Khademhosseini, A. (2019). Recent advances in nanoengineering cellulose for cargo delivery. *Journal of Controlled Release, 294*, 53-76.

Shi, X., Zheng, Y., Wang, G., Lin, Q., & Fan, J. (2014). pH-and electro-response characteristics of bacterial cellulose nanofiber/sodium alginate hybrid hydrogels for dual controlled drug delivery. *RSC Advances, 4*(87), 47056-47065.

Shi, X. W., Du, Y. M., Sun, L. P., Yang, J. H., Wang, X. H., & Su, X. L. (2005). Ionically crosslinked alginate/carboxymethyl chitin beads for oral delivery of protein drugs. *Macromolecular Bioscience, 5*(9), 881-889.

Shin, J.-W., Jeun, J.-P., & Kang, P.-H. (2009). Fabrication and characterization of the mechanical properties of multi-walled carbon nanotube-reinforced epoxy resins by e-beam irradiation. *Journal of Industrial and Engineering Chemistry, 15*(4), 555-560.

Shin, S., Park, S., Park, M., Jeong, E., Na, K., Youn, H. J., & Hyun, J. (2017). Cellulose nanofibers for the enhancement of printability of low viscosity gelatin derivatives. *BioResources, 12*(2), 2941-2954.

Sikorski, P., Mo, F., Skjåk-Bræk, G., & Stokke, B. T. (2007). Evidence for egg-box-compatible interactions in calcium-alginate gels from fiber X-ray diffraction. *Biomacromolecules, 8*(7), 2098-2103.

Silvério, H. A., Neto, W. P. F., & Pasquini, D. (2013). Effect of incorporating cellulose nanocrystals from corncob on the tensile, thermal and barrier properties of poly (vinyl alcohol) nanocomposites. *Journal of Nanomaterials, 2013*, 74.

Singh, J., Kaur, K., & Kumar, P. (2018). Optimizing microencapsulation of α-tocopherol with pectin and sodium alginate. *Journal of Food Science and Technology, 55*(9), 3625-3631.

Sinsuebpol, C., & Changsan, N. (2020). Effects of ultrasonic operating parameters and emulsifier system on sacha inchi oil nanoemulsion characteristics. *Journal of Oleo Science*, ess19193.

Siqueira, G., Bras, J., & Dufresne, A. (2010). Cellulosic bionanocomposites: a review of preparation, properties and applications. *Polymers, 2*(4), 728-765.

Siró, I., & Plackett, D. (2010). Microfibrillated cellulose and new nanocomposite materials: a review. *Cellulose, 17*(3), 459-494.

Smirnova, N., & Safonova, E. (2010). Ionic liquids as surfactants. *Russian Journal of Physical Chemistry A, 84*(10), 1695-1704.

Somboon, N., Karrila, T., Kaewmanee, T., & Karrila, S. (2014). Properties of gels from mixed agar and fish gelatin. *International Food Research Journal, 21*(2).

Song, N., Wang, A.-j., Li, J.-m., Zhu, Z., Shi, H., Ma, X.-l., & Sun, D. (2018). Study on influencing factors of Pickering emulsions stabilized by hydroxyapatite nanoparticles with nonionic surfactants. *Soft Matter, 14*(19), 3889-3901.

Spence, K. L., Venditti, R. A., Rojas, O. J., Habibi, Y., & Pawlak, J. J. (2011). A comparative study of energy consumption and physical properties of microfibrillated cellulose produced by different processing methods. *Cellulose, 18*(4), 1097-1111.

Spyropoulosa, F., Hancocks, R. D., & Norton, I. T. (2011). Food-grade emulsions prepared by membrane emulsification techniques. *Procedia Food Science, 1*, 920-926. doi: 10.1016/j.profoo.2011.09.139

Stanford, E. (1881). British patent 142: London.

Steiner, M. (1993). Vitamin E: more than an antioxidant. *Clinical Cardiology, 16*(S1), 16-18.

Sullivan, A. P., & Kilpatrick, P. K. (2002). The effects of inorganic solid particles on water and crude oil emulsion stability. *Industrial & Engineering Chemistry Research, 41*(14), 3389-3404.

Sun, J., & Tan, H. (2013). Alginate-based biomaterials for regenerative medicine applications. *Materials, 6*(4), 1285-1309.

Sun, R., Tomkinson, J., Wang, Y., & Xiao, B. (2000). Physico-chemical and structural characterization of hemicelluloses from wheat straw by alkaline peroxide extraction. *Polymer, 41*(7), 2647-2656.

Swamy, B. Y., & Yun, Y. S. (2015). In vitro release of metformin from iron (III) cross-linked alginate-carboxymethyl cellulose hydrogel beads. *International Journal of Biological Macromolecules, 77*, 114-119.

Tadros, T. (2013). *Encyclopedia of Colloid and Interface Science*: Springer.

Tadros, T. F. (2005). Surfactants in nano-emulsions. *Applied Surfactants: Principles and Applications. Wiley-VCH Verlag GmbH & Co. Weinheim*, 285-308.

Tadros, T. F. (2013). *Emulsion formation and stability*: John Wiley & Sons.

Taherpour, A., & Hashemi, A. (2018). A novel formulation of the pickering emulsion stabilized with silica nanoparticles and its thermal resistance at high temperatures. *Journal of Dispersion Science and Technology, 39*(12), 1710-1720.

Takei, T., Yoshihara, R., Danjo, S., Fukuhara, Y., Evans, C., Tomimatsu, R., Ohzuno, Y., & Yoshida, M. (2020). Hydrophobically-modified gelatin hydrogel as a carrier for charged hydrophilic drugs and hydrophobic drugs. *International Journal of Biological Macromolecules, 149*, 140-147.

Tan, C., & Nakajima, M. (2005). β-Carotene nanodispersions: preparation, characterization and stability evaluation. *Food Chemistry, 92*(4), 661-671.

Tan, P. Y., Tan, T. B., Chang, H. W., Tey, B. T., Chan, E. S., Lai, O. M., Baharin, B. S., Nehdi, I. A., & Tan, C. P. (2018). Effects of storage and yogurt matrix on the stability of tocotrienols encapsulated in chitosan-alginate microcapsules. *Food Chemistry, 241*, 79-85.

Tan, S., Lopez, H. A., Cai, C. W., & Zhang, Y. (2004). Optical trapping of single-walled carbon nanotubes. *Nano Letters, 4*(8), 1415-1419.

Tarigan, J. B., Kaban, J., & Zulmi, R. (2018). Microencapsulation of vitamin E from palm fatty acid distillate with galactomannan and gum acacia using spray drying method. *IOP Conference Series: Materials Science and Engineering 309*(1), 012095.

Tarté, R. (2009). *Ingredients in meat products: properties, functionality and applications*: Springer Science & Business Media.

TD Tran, T., & HL Tran, P. (2017). Perspectives on strategies using swellable polymers in solid dispersions for controlled drug release. *Current Pharmaceutical Design, 23*(11), 1639-1648.

Terasawa, Y., Ladha, Z., Leonard, S. W., Morrow, J. D., Newland, D., Sanan, D., Packer, L., Traber, M. G., & Farese, R. V. (2000). Increased atherosclerosis in hyperlipidemic mice deficient in α-tocopherol transfer protein and vitamin E. *Proceedings of the National Academy of Sciences, 97*(25), 13830-13834.

Terentis, A. C., Thomas, S. R., Burr, J. A., Liebler, D. C., & Stocker, R. (2002). Vitamin E oxidation in human atherosclerotic lesions. *Circulation Research, 90*(3), 333-339.

Thakkar, K., Bharatiya, B., Aswal, V. K., & Bahadur, P. (2016). Aggregation of 1-alkyl-3-methylimidazolium octylsulphate ionic liquids and their interaction with Triton X-100 micelles. *RSC Advances, 6*(84), 80585-80594.

Thakur, V. K., & Thakur, M. K. (2018). *Functional Biopolymers*: Springer.

Thomas, D., Latha, M., & Thomas, K. K. (2018). Synthesis and in vitro evaluation of alginate-cellulose nanocrystal hybrid nanoparticles for the controlled oral delivery of rifampicin. *Journal of Drug Delivery Science and Technology, 46*, 392-399.

Tønnesen, H. H., & Karlsen, J. (2002). Alginate in drug delivery systems. *Drug Development and Industrial Pharmacy, 28*(6), 621-630.

Traber, M. G., & Atkinson, J. (2007). Vitamin E, antioxidant and nothing more. *Free Radical Biology and Medicine, 43*(1), 4-15.

Traber, M. G., & Stevens, J. F. (2011). Vitamins C and E: beneficial effects from a mechanistic perspective. *Free Radical Biology and Medicine, 51*(5), 1000-1013.

Tran, T. T.-D., Tran, P. H.-L., & Lee, B.-J. (2009). Dissolution-modulating mechanism of alkalizers and polymers in a nanoemulsifying solid dispersion containing ionizable and poorly water-soluble drug. *European Journal of Pharmaceutics and Biopharmaceutics, 72*(1), 83-90.

Treesuppharat, W., Rojanapanthu, P., Siangsanoh, C., Manuspiya, H., & Ummartyotin, S. (2017). Synthesis and characterization of bacterial cellulose and gelatin-based hydrogel composites for drug-delivery systems. *Biotechnology Reports, 15*, 84-91.

Tsai, S.-W., Yu, D.-S., Tsao, S.-W., & Hsu, F.-Y. (2013). Hyaluronan–cisplatin conjugate nanoparticles embedded in Eudragit S100-coated pectin/alginate microbeads for colon drug delivery. *International Journal of Nanomedicine, 8*, 2399.

Turbak, A. F., Snyder, F. W., & Sandberg, K. R. (1983). Microfibrillated cellulose, a new cellulose product: properties, uses, and commercial potential. *Journal of Applied Polymer Science, 37*(9), 815-827.

Uchegbu, I. F., Schätzlein, A. G., Cheng, W. P., & Lalatsa, A. (2013). *Fundamentals of pharmaceutical nanoscience*: Springer.

Udeni Gunathilake, T. M. S., Ching, Y. C., & Chuah, C. H. (2017). Enhancement of curcumin bioavailability using nanocellulose reinforced chitosan hydrogel. *Polymers, 9*(2), 64.

Ullah, F., Othman, M. B. H., Javed, F., Ahmad, Z., & Akil, H. M. (2015). Classification, processing and application of hydrogels: A review. *Materials Science and Engineering: C, 57*, 414-433.

Unagolla, J. M., & Jayasuriya, A. C. (2018). Drug transport mechanisms and in vitro release kinetics of vancomycin encapsulated chitosan-alginate polyelectrolyte microparticles as a controlled drug delivery system. *European Journal of Pharmaceutical Sciences, 114*, 199-209.

Upston, J. M., Kritharides, L., & Stocker, R. (2003). The role of vitamin E in atherosclerosis. *Progress in Lipid Research, 42*(5), 405-422.

Urban, K., Wagner, G., Schaffner, D., Röglin, D., & Ulrich, J. (2006). Rotor-Stator and Disc Systems for Emulsification Processes. *Chemical Engineering & Technology, 29*(1), 24-31.

Viguier, A., Boyer, C., Chassenieux, C., Benyahia, L., Guicheux, J., Weiss, P., Rethore, G., & Nicolai, T. (2016). Interpenetrated Si-HPMC/alginate hydrogels as a potential scaffold for human tissue regeneration. *Journal of Materials Science: Materials in Medicine, 27*(5), 99.

Walstra, P. (2002). *Physical chemistry of foods*: CRC Press.

Wang, N., Ding, E., & Cheng, R. (2007). Thermal degradation behaviors of spherical cellulose nanocrystals with sulfate groups. *Polymer, 48*(12), 3486-3493.

Wei, Z., Wang, C., Liu, H., Zou, S., & Tong, Z. (2012). Facile fabrication of biocompatible PLGA drug-carrying microspheres by O/W pickering emulsions. *Colloids and Surfaces B: Biointerfaces, 91*, 97-105.

Wen, C., Yuan, Q., Liang, H., & Vriesekoop, F. (2014). Preparation and stabilization of d-limonene Pickering emulsions by cellulose nanocrystals. *Carbohydrate Polymers, 112*, 695-700.

Winuprasith, T., & Suphantharika, M. (2015). Properties and stability of oil-in-water emulsions stabilized by microfibrillated cellulose from mangosteen rind. *Food Hydrocolloids, 43*, 690-699.

Wong, T. W. (2011). Alginate graft copolymers and alginate-co-excipient physical mixture in oral drug delivery. *Journal of Pharmacy and Pharmacology, 63*(12), 1497-1512.

Wooster, T. J., Golding, M., & Sanguansri, P. (2008). Impact of oil type on nanoemulsion formation and Ostwald ripening stability. *Langmuir, 24*(22), 12758-12765.

Wu, M., Ni, C., Yao, B., Zhu, C., Huang, B., & Zhang, L. (2013). Covalently cross-linked and hydrophobically modified alginic acid hydrogels and their application as drug carriers. *Polymer Engineering & Science, 53*(8), 1583-1589.

Wu, X., Moon, R. J., & Martini, A. (2013). Crystalline cellulose elastic modulus predicted by atomistic models of uniform deformation and nanoscale indentation. *Cellulose, 20*(1), 43-55.

Xhanari, K., Syverud, K., & Stenius, P. (2011). Emulsions stabilized by microfibrillated cellulose: the effect of hydrophobization, concentration and O/W ratio. *Journal of Dispersion Science and Technology, 32*(3), 447-452.

Xiao, J., Li, C., & Huang, Q. (2015). Kafirin nanoparticle-stabilized Pickering emulsions as oral delivery vehicles: Physicochemical stability and in vitro digestion profile. *Journal of Agricultural and Food Chemistry, 63*(47), 10263-10270.

Xiao, J., Shi, C., Li, Y., Pan, Y., & Huang, Q. (2017). Pickering emulsions immobilized within hydrogel matrix with enhanced resistance against harsh processing conditions and sequential digestion. *Food Hydrocolloids, 62*, 35-42.

Xie, Y., Aillon, K. L., Cai, S., Christian, J. M., Davies, N. M., Berkland, C. J., & Forrest, M. L. (2010). Pulmonary delivery of cisplatin–hyaluronan conjugates via endotracheal instillation for the treatment of lung cancer. *International Journal of Pharmaceutics, 392*(1-2), 156-163.

Xing, L., Dawei, C., Liping, X., & Rongqing, Z. (2003). Oral colon-specific drug delivery for bee venom peptide: development of a coated calcium alginate gel beads-entrapped liposome. *Journal of Controlled Release, 93*(3), 293-300.

Yan, G., Sun, W., Pei, Y., Yang, Z., Wang, X., Sun, Y., Yang, S., & Pan, J. (2017). A novel release kinetics evaluation of Chinese compound medicine: Application of the xCELLigence RTCA system to determine the release characteristics of Sedum sarmentosum compound sustained-release pellets. *Saudi Pharmaceutical Journal, 26*(3), 445-451.

Yan, H., Chen, X., Feng, M., Shi, Z., Zhang, W., Wang, Y., Ke, C., & Lin, Q. (2019). Entrapment of bacterial cellulose nanocrystals stabilized Pickering emulsions droplets in alginate beads for hydrophobic drug delivery. *Colloids and Surfaces B: Biointerfaces, 177*, 112-120.

Yang, H., Yan, R., Chen, H., Lee, D. H., & Zheng, C. (2007). Characteristics of hemicellulose, cellulose and lignin pyrolysis. *Fuel, 86*(12-13), 1781-1788.

Yang, Y., Fang, Z., Chen, X., Zhang, W., Xie, Y., Chen, Y., Liu, Z., & Yuan, W. (2017). An overview of Pickering emulsions: solid-particle materials, classification, morphology, and applications. *Frontiers in Pharmacology, 8*, 287.

Yang, Y., & McClements, D. J. (2013). Encapsulation of vitamin E in edible emulsions fabricated using a natural surfactant. *Food Hydrocolloids, 30*(2), 712-720.

Yesiltas, B., García-Moreno, P. J., Sørensen, A.-D. M., & Jacobsen, C. (2017). Physical and oxidative stability of high fat fish oil-in-water emulsions stabilized with combinations of sodium caseinate and sodium alginate. *European Journal of Lipid Science and Technology, 119*(11), 1600484.

Yokota, T., Igarashi, K., Uchihara, T., Jishage, K.-i., Tomita, H., Inaba, A., Li, Y., Arita, M., Suzuki, H., & Mizusawa, H. (2001). Delayed-onset ataxia in mice lacking α-tocopherol transfer protein: model for neuronal degeneration caused by chronic oxidative stress. *Proceedings of the National Academy of Sciences, 98*(26), 15185-15190.

Yong, C. K., Ching, Y. C., Chuah, C. H., & Liou, N.-S. (2015). Effect of fiber orientation on mechanical properties of kenaf-reinforced polymer composite. *BioResources, 10*(2), 2597-2608.

Yue, Y., Han, J., Han, G., French, A. D., Qi, Y., & Wu, Q. (2016). Cellulose nanofibers reinforced sodium alginate-polyvinyl alcohol hydrogels: Core-shell structure formation and property characterization. *Carbohydrate Polymers, 147*, 155-164.

Zafeiri, I., Horridge, C., Tripodi, E., & Spyropoulos, F. (2017). Emulsions Co-Stabilised by Edible Pickering Particles and Surfactants: The Effect of HLB Value. *Colloid and Interface Science Communications*(17), 5-9.

Zhang, J., Ge, D., Wang, X., Wang, W., Cui, D., Yuan, G., Wang, K., & Zhang, W. (2021). Influence of surfactant and weak-alkali concentrations on the stability of o/w emulsion in an alkali-surfactant–polymer compound system. *ACS Omega, 6*(7), 5001-5008.

Zhang, J. P., Wang, Q., Xie, X. L., Li, X., & Wang, A. Q. (2010). Preparation and swelling properties of pH-sensitive sodium alginate/layered double hydroxides hybrid beads for controlled release of diclofenac sodium. *Journal of Biomedical Materials Research B Applied Biomaterials, 92*(1), 205-214.

Zhang, N., Hu, X., Guan, P., Du, C., Li, J., Qian, L., Zhang, X., Ding, S., & Li, B. (2017). Preparation of protein imprinted microspheres using amphiphilic ionic liquid as stabilizer and emulsifier via miniemulsion polymerization. *Chemical Engineering Journal, 317*, 356-367.

Zhang, R., & Somasundaran, P. (2006). Advances in adsorption of surfactants and their mixtures at solid/solution interfaces. *Advances in Colloid Interface Science, 123-126*, 213-229.

Zhang, Y. H., & Lynd, L. R. (2004). Toward an aggregated understanding of enzymatic hydrolysis of cellulose: noncomplexed cellulase systems. *Biotechnology Bioengeering, 88*(7), 797-824.

Zhang, Y. H. P., & Lynd, L. R. (2004). Toward an aggregated understanding of enzymatic hydrolysis of cellulose: noncomplexed cellulase systems. *Biotechnology and Bioengineering, 88*(7), 797-824.

Zhao, J., Zhang, W., Zhang, X., Zhang, X., Lu, C., & Deng, Y. (2013). Extraction of cellulose nanofibrils from dry softwood pulp using high shear homogenization. *Carbohydrate Polymers, 97*(2), 695-702.

Zhu, D., Wei, L., Wang, B., & Feng, Y. (2014). Aqueous hybrids of silica nanoparticles and hydrophobically associating hydrolyzed polyacrylamide used for eor in high-temperature and high-salinity reservoirs. *Energies, 7*(6), 3858-3871.

Ziani, K., Fang, Y., & McClements, D. J. (2012). Encapsulation of functional lipophilic components in surfactant-based colloidal delivery systems: vitamin E, vitamin D, and lemon oil. *Food Chemistry, 134*(2), 1106-1112.

Zimmermann, T., Bordeanu, N., & Strub, E. (2010). Properties of nanofibrillated cellulose from different raw materials and its reinforcement potential. *Carbohydrate Polymers, 79*(4), 1086-1093.